PHD

Active Seat Suspensions for Automotive Applications

Alfadhli, Abdulaziz

Award date:
2018

Awarding institution:
University of Bath

Active Seat Suspensions for Automotive Applications

Abdulaziz Alfadhli

A thesis summited for the degree of Doctor Philosophy

Department of Mechanical Engineering

University of Bath

January 2018

COPYRIGHT

To

Souls of My Mother and Father,

My Wife,

and

My Children.

Abstract

Vehicle drivers are exposed daily to harmful low-frequency vertical vibration over the frequency range of 1-20 Hz. This reduces ride comfort and safety as well as possibly causing long-term harmful effects on human health in the form of lower back pain and driver fatigue. Accordingly, intensive work has been undertaken in this field on active seat suspension systems that have superior performance over a wide frequency range compared with passive and semi-active systems. One of the main features of these systems is the control strategy that is used to generate the demand control force and whilst many control strategies have been investigated in this area; their practical implementation is challenging as they require unavailable or expensive system states. Hence, in this thesis, a novel and cost-effective strategy has been developed that uses measurable and inexpensive displacement and velocity preview information from the vehicle suspension. In addition to these practical advantages, employing a prior knowledge of the disturbance in the control strategy increases the ability of the active seat to react rapidly to disturbances and hence provides a supplementary improvement to the vibration attenuation performance.

The potential application of this strategy for an active seat suspension is investigated through both simulation and experimental tests. Firstly, for simplicity, the control force is defined from this suspension preview information based upon a linear control approach, with optimum gains using an integrated simulation model of a linear quarter vehicle model (QvM) and one degree of freedom of seat suspension. These gains are obtained off-line by optimising ride comfort in terms of the vertical Seat Effective Amplitude Transmissibility (SEAT) factor using a genetic algorithm (GA) and considering the physical constraints on both the limited seat suspension travel and actuator force capacity. The experimental tests are performed using a prototype active seat suspension installed on a multi-axis simulation table (MAST), which has been developed to mimic the dynamic motion of the sprung mass of the (QvM) through the principle of hardware-in-loop (HIL) simulation. Moreover, the experimental test rig is used to estimate the characteristics of a passive seat suspension as well as the driver's body model.

The 'preview' control strategy is examined according to the ISO 2631-1 standard, in both the frequency and time domains, under a range of operating conditions, including different road profiles and vehicle speeds. Both simulation and experimental results reveal that, in

comparison with a passive seat suspension, employing this strategy for the active seat system significantly improves ride comfort, especially over the HBSF range (4-8 Hz). Also, experimental tests demonstrate that combining both the preview information with the vehicle body and seat acceleration feedback states provides further improvement in the vibration attenuation level, achieving up to a 19.5 dB reduction over the HBSF range.

The linear control approach cannot always satisfy the physical constraints over a range of operating conditions and thus, to overcome this fault, a fuzzy logic controller (FLC) is selected. Accordingly, two novel and cost-effective FLCs are designed and optimised using the Particle Swarming Optimisation (PSO) algorithm. The feedforward fuzzy logic controller (FF-FLC) uses similar preview information as in the linear control approach, while the feedforward/feedback controller (FFFB-FLC) utilises a combination of both the preview information with seat suspension deflection and velocity feedback states. Once again, the simulation and experimental results confirm the effectiveness of these strategies for attenuating the vertical vibration, especially over the HBSF range, in which the FFFB-FLC provides the best performance as well as the highest robustness level at a variety of different driver weights and vehicle speeds.

The application of the preview enhanced controller for an active seat suspension in a full vehicle model has been investigated in the simulation. Accordingly, three FLCs strategies, namely, front-left suspension (FLS-FLC), front-axle (FA-FLC) and four wheels (4W-FLC), have been developed based upon which vehicle suspension or/ suspensions are used to acquire the preview information. The former involves utilising suspension displacement and velocity preview information from the vehicle suspension nearest to the driver's seat. The FA-FLC uses similar preview information, but from the front-left and front-right suspensions, whilst the 4W-FLC controller employs similar preview information from all the vehicle suspensions. Numerical results show that the proposed controllers are very useful in attenuating the vertical acceleration at the driver's seat compared with a passive alternative. The 4W-FLC provides the best vibration attenuation performance, independent of the vehicle speed. Finally, to reduce the implementation cost of this controller, a practical alternative has been developed that requires less measured preview information. In conclusion, using the preview information enhanced controller for an active seat suspension provides a practical and cost-effective system that improves ride comfort and reduces driver fatigue.

Keywords*: active seat suspension, preview controller, genetic algorithm, quarter vehicle model, hardware-in-the-loop simulation, fuzzy logic control, feedforward-feedback control.*

Acknowledgements

I would like to sincerely thank my supervisors, **Dr. Jos Darling and Dr. Andrew Hillis**, for their most excellent support, encouragement, and much-respected enthusiasm towards the field. Special thanks to Dr. Jos Darling, your support and endless help during each stage of this research have always been the motivation for me to improve my academic skills and to successfully complete this work.

I am grateful to thank the Centre for Power Transmission and Motion Control (CPTMC) at the University of Bath. Many thanks go to **Mr. Vijay Rajput** for his technical support and substantial help in performing experimental tests. I also would like to thank **Martin Goater, Graham Rattley**, **John Robbins** and the Technical Service staff for their technical support.

It is an honour for me to thank Kuwait Government, especially my sponsor the Public Authority for Applied Education and Training (PAAET). This work would not have been possible without their financial support.

Also, I would like to thank my external and internal examiners, **Dr. Ya Hunag** from the University of Portsmouth and **Dr. Jonathan du Bois** for their effort and helpful feedback in improving the quality of this thesis.

I express my grateful thank my best friend **Mustafa Thega** for his assistance and support.

Finally, I am deeply grateful for the love and inspiration provided by my wife **Athari**. Your endless support, patience, and encouragement have been my most precious tools for facing the challenges I have encountered throughout my nascent career. Special thanks also go to my family and my children, for their assistance and patience while I have been away from them for the last four years.

Publications

Part of the study presented in this thesis has already been published and can be found in:

1) Alfadhli A, Darling J and Hillis AJ (2017) The control of an active seat with vehicle suspension preview information. Journal of Vibration and Control: 1–15.

2) Darling J, Hillis A, Alfadhli AEHE, et al. (2016) Hardware-in-the-Loop (HIL) Simulation of a Quarter Vehicle Model using a Multi-axis Simulation Table (MAST). In: Bath/ASME FPMC 2016, University of Bath.

3) A. Alfadhli, J. Darling, A.J. Hillis, the Control of an Active Seat Suspension Using an Optimised Fuzzy Logic Controller, Based on Preview Information from a Full Vehicle Model, *Vibration*. 1 **2018**, 3. doi: 10.3390/vibration1010003.

4) Alfadhli A, Darling J, Hillis AJ. An Active Seat Controller with Vehicle Suspension Feedforward and Feedback States: An Experimental Study. Appl Sci; 8. Epub ahead of print 2018. DOI: 10.3390/app8040603.

Contents

List of Tables

List of Figures

Nomenclature

Abbreviations

4W	Four wheel
4W-FLC	Four wheel fuzzy logic controller
ACGIH	American Conference of Government Industrial Hygienists
DOFs	Degrees of freedom
FA	Front axle
FA-FLC	Front axle fuzzy logic controller
FFFB-FLC	Feedforward-feedback fuzzy logic control
FF-FLC	Feedforward fuzzy logic control
FLC	Fuzzy logic controller
FLS	Front left suspension
FLS-FLC	Front left suspension fuzzy logic controller
FvM	Full vehicle model
GA	Genetic algorithm
HBSF	Human body sensitive frequency range (4-8 Hz)
HIL	Hardware-in-the-loop simulation
MAST	Multi-axis simulation table
MF	Membership function
P4W-FLC	Practical four wheel fuzzy logic controller
PSD	Power spectral density
PSO	Particle swarming optimisation
QvM	Quarter vehicle model
RB	Rule base
RMS	Root mean square
SEAT	Seat Effective Amplitude Transmissibility factor
TLVs	Threshold limit values
ISO	International standard organization

Symbols

Symbol	Description	Unit
a_w	Frequency-weighted RMS acceleration	m/s2 (RMS)
W_i	Frequency-weighting value at the centre frequency	--------
f_i	One-third octave frequency	Hz
$x(t)$	State-space vector	--------
C_{max}	Maximum damping coefficient	N.s/m
C_{min}	Minimum damping coefficient	N.s/m
C_{sa}	Semi-active damping coefficient	N.s/m
α	Tuning parameter	
$(\ddot{x}_{s,w})_{rms}$	Weighted root mean square of the vertical sprung mass acceleration	m/s2
$(\ddot{x}_{se,w})_{rms}$	Weighted root mean square of the vertical seat acceleration	m/s2
$(x_{se} - x_s)_{max}$	Maximum seat stroke	m
$(x_{se} - x_s)_{min}$	Minimum seat stroke	m
$\hat{G_m}$	Estimated dynamics of the MAST	-
$\dot{x}_{rel}$	Relative velocity of the vehicle suspension	m/s
$\ddot{x}_s$	Vertical acceleration of the sprung mass	m/s^2
$\ddot{x}_{se}$	Vertical acceleration of the seat	m/s^2
$\ddot{x}_{us}$	Vertical acceleration of the usprung mass	m/s^2
D_{sij}	Vehicle suspension displacement $i\ and\ j = 1, 2$	m
F_a	Actuator control force	N
F_s	Vehicle suspension dynamic force	N
F_{se}	Seat suspension dynamic force	N
I_{sx}	Moment of inertia in the longitudinal direction	kg.m^2
I_{sy}	Moment of inertia in the lateral direction	kg.m^2
R_x	Lateral distance from the driver's seat to C.G	m
R_y	Longitudinal distance from the driver's to C.G	m
V_{sij}	Vehicle suspension velocity , $i\ and\ j = 1, 2$	m/s
V_o	Forward vehicle speed	km/h

D_{sij}	Vehicle suspension displacement , $i\ and\ j = 1, 2$	m
c_s	Damping coefficient of the vehicle suspension	N.s/m
c_{se}	Damping coefficient of the seat suspension	N.s/m
k_s	Stiffness of the vehicle suspension	N/m
k_{se}	Stiffness of the seat suspension	N/m
k_t	Stiffness of the tyre	N/m
m_s	Sprung mass in the QvM	kg
m_{se}	Mass of the seat	kg
m_{us}	Unsprung mass in the QvM	kg
m_b	Human body mass	kg
k_b	Human body spring rate	N/m
c_b	Damping coefficient of human body	N.s/m
q_j $(i = odd)$	Optimum gain of the vehicle suspension velocity	N.s/m
q_j $(j = even)$	Optimum gain of the vehicle suspension displacement	N/m
r_1	Optimum gain of the sprung mass acceleration state (Controller A2)	N.s²/m
r_2	Optimum gain of the seat acceleration state (Controller A3)	N.s²/m
r_3	Optimum gain of the sprung mass acceleration state (Controller A4)	N.s²/m
r_4	Optimum gain of the seat acceleration state (Controller A4)	N.s²/m
r_5	Optimum gain of the relative velocity of the seat suspension (Controller A5)	N.s/m
r_6	Optimum gain of the relative displacement of the seat suspension (Controller A5)	N/m
x_r	Road profile displacement	m
$x_{se,max}$	maximum allowable seat stroke	m
$x_{se,min}$	minimum allowable seat stroke	m
x_{se}	vertical displacement of the seat	m
x_{us}	vertical displacement of the usprung mass	m
$\ddot{\theta}$	Pitch angular acceleration	rad/s²
φ_n	random phase angle between $(0, 2\ \pi)$	radian
$\ddot{\phi}$	Roll angular acceleration	rad/s²
A	Controller strategy	-----

J	final optimization objective function	-----
L	length of the road segment (random road profile)	m
N	limit of the frequency range (random road profile)	--------
PG	Penalty function	--------
R	Dry friction force limit	N
S	Scaling factor	--------
a	height of the bump road profile	mm
b	Full vehicle model	-------
f	optimization objective function	-------
$f(V_s)$	Dry friction force (full vehicle model)	N
$g(1)$	seat stroke constraints	------
$g(2)$	actuator capacity force constraints	------
l	length of the bump road profile	m
ε	Viscous band	m/s
θ	Pitch rotation angle	rad
f_n	Cut-off frequency	Hz
ϕ	Roll rotation angle	rad

Chapter 1
Introduction

1.1 Problem definition

Vehicle drivers are daily exposed to low-frequency vibration transmitted to the driver's seat caused by road roughness, transmitted through the vehicle suspension and body. This type of vibration is considered a risk factor for human health as it matches many of the human body parts' natural frequencies. This reduces ride quality and safety as well as possibly yielding long-term harmful effects on human health, mainly in the form of lower back pain and driver fatigue. Consequently, an intensive amount of work has been carried out to overcome this problem, in particular, with regards to vehicle suspensions. Despite the complexity and high cost of vehicle suspensions, they generally remain ineffective in attenuating this type of vibration, as there is a trade-off between improving ride comfort and road handling. Seat suspensions are simple, practical and cost-effective devices that are employed in vehicles to improve ride comfort and reduce vibration linked health risks, by directly attenuating the transmitted vertical vibration at the seat. Generally, seat suspension systems can be classified into: passive, semi-active and active systems. The main elements of the passive system consist of a spring and damper with fixed properties. However, despite these systems being simple and inexpensive, they have a limited vibration attenuation performance, and there is always a compromise between improving ride comfort and retaining satisfactory seat suspension travel. Also, they cannot guarantee optimum performance, because they are not robust to variations in working conditions, such as the driver's weight, disturbance type, or vehicle speed. Alternatively, semi-active seat suspensions provide better vibration attenuation performance compared with passive alternatives, because the suspension characteristics (spring and/or damper) can be adjusted using a control strategy with minimal power consumption. However, their performance is still compromised, because they can only dissipate energy from the system. Moreover, they require special active devices that can rapidly modulate rapidly the suspension characteristics [1]. Conversely, active seat

suspensions are able to both dissipate and add energy to/from the system by applying an external force from an actuator based upon a control strategy. This actuator can be placed in parallel with a passive suspension system and may be hydraulic, pneumatic or electromagnetic in design. Hence, these systems provide a superior vibration attenuation performance over a wide frequency range and can be a potential solution for improving ride comfort and protecting the driver from harmful low-frequency vertical vibration.

Many aspects need to be addressed when designing an active seat suspension, such as the selection of sensors and actuators, power supply and control strategy [2]. In addition, to make the practical application of these systems feasible the cost of both the instrumentation and actuators has to be considered. Moreover, the control strategy employed to produce the required control force based upon system states, significantly influences the performance of these systems. Many control techniques have been investigated and applied in the literature, such as classical, optimal, robust, adaptive, intelligent and preview control as will be discussed in detail in chapter 2. Despite the fact that many of these strategies have shown significant improvement in the ride comfort through simulation, their practical implementation is challenging, because they depend on employing inaccessible or difficult and/or expensive system states, such as the absolute velocity of the occupant or the seat. Consequently, this significant shortcoming motivates to develop a reliable control strategy for an active seat suspension that utilises only the available and inexpensive system states. Moreover, it is believed that the application of the 'preview' or feed-forward control for an active vehicle suspension or active seat suspension is a promising control approach that can provide a significant improvement in vibration attenuation [3].

To deal with the aforementioned limitations as well as gaining the benefits of including preview information, a novel control strategy for an active seat suspension, based on the preview control concept is developed and investigated in this thesis. Unlike the conventional preview control concept applied to a vehicle suspension, this strategy involves employing measurable and inexpensive preview information from the vehicle suspension dynamics to control the active seat suspension. It should be noted that, to the knowledge of the researcher, this approach has not been previously investigated and thus it provides an interesting research topic to be explored. It is anticipated that the outcomes of this work will significantly help in

the commercial development of actively controlled seat suspension systems for vehicles, especially those pertaining to the off-road vehicle industry.

1.2 Research objectives

The main aim of this research is to develop a reliable and economic active seat suspension for automotive applications that can attenuate the harmful low-frequency vertical vibration in the frequency range of 1-20 Hz that is caused by road disturbances transmitted through the vehicle suspension and vehicle body. This will be achieved through the development of a reliable and cost-effective control strategy that utilises measurable and inexpensive preview information from the vehicle suspension as well as taking into account the physical limitations in both the seat suspension travel and actuator force. Furthermore, this strategy has to be robust to variations in operating conditions such as road disturbance type and frequency content, driver's weight and vehicle speed. The performance of this strategy will be investigated and evaluated through both simulation and experimental studies. This will be accomplished through the pursuit the following objectives:

1) To develop a control strategy based on a linear control approach that employs measurable and inexpensive preview information from the vehicle suspension of a (QvM) and satisfies the necessary physical system constraints.
2) To develop a test rig for experimental evaluation purposes, involving a hardware-in-the-loop (HIL) simulation technique.
3) To evaluate the performance of this strategy through both simulation and experimental tests under different operating conditions, including a range of road disturbances types and driving characteristics.
4) To investigate the capability of this strategy to satisfy the necessary physical system constraints over different operating conditions and develop the controller accordingly.
5) To examine the application of the preview information controller concept to a full vehicle model.

1.3 Thesis structure

This thesis is organised into nine further chapters, and a brief description of these chapters is presented in this section.

Chapter 2 presents a literature review of whole body vibrations (WBV) and their effects on human health, comfort and activities as well as the response of the human body to WBV and its measurement techniques. Different vibration attenuation techniques including passive, semi-active and active systems are described and compared to highlight their advantages and limitations. Finally, a brief literature review of control strategies that have been applied to semi-active and active suspension systems is provided.

Chapter 3 describes assessment and analysis methods for evaluating the performance of a seat suspension system regarding improving ride comfort based on the ISO 2631-1 standard. In addition, the analytical generation of common road disturbances, namely random and bump road profiles, is presented.

Chapter 4 presents a comparative simulation study of some fundamental control strategies that are applied for semi-active and active seat suspensions with a passive seat suspension system using a linear quarter vehicle model (QvM) and a single degree of freedom seat suspension model.

Chapter 5 describes the experimental test rig and setup needed to investigate the performance of the developed active controlled seat suspension. Also, it provides the development and validation of the Multi Axis Simulation Table (MAST) to mimic the sprung mass motion of a quarter vehicle model (QvM) using the hardware-in-the-loop (HIL) technique and the inverse estimated dynamics of the MAST.

In Chapter 6, a novel and reliable control strategy for an active seat suspension that attenuates the harmful low-frequency vertical vibration at the driver's seat is developed. This strategy employs measurable preview information from the vehicle suspension based upon a linear control approach, using an integrated model of a QvM and 1 DOF seat suspension. The performance of an active seat suspension utilising this strategy is examined and compared to a passive alternative through simulation and experimental tests under different working conditions.

Chapter 7 investigates the effectiveness of novel control strategies for an active seat suspension that applies preview information (feedforward) states from the vehicle suspension together with measurable and inexpensive feedback system states. The performance of these strategies in improving ride quality is examined through laboratory tests in both the frequency and time domains, with a range of different vehicle speeds and road disturbances.

Chapter 8 presents the design and evaluation of two optimal fuzzy logic (FL) controllers for an active seat suspension to ensure that necessary practical constraints on the seat suspension travel and the actuator force capacity are met. The developed controllers apply similar preview information as in the linear control approach as well as measurable and available feedback states from the seat suspension. The knowledge base of the FLC structure, including the rule base (RB) and fuzzification process, is sequentially optimised using the Particle Swarm Optimisation (PSO) algorithm. The theoretical design and performance assessment of these FLCs through simulation studies using different road disturbances are presented, including their robustness to changes in both the driver's weight and vehicle speed. Then, they are implemented and examined in real time.

Chapter 9 investigates the application of the preview control approach for an active seat suspension in a full vehicle model using a FLC. Accordingly, three FL control strategies that use measurable and low-cost preview information from the vehicle suspension states are designed and optimised, namely: front-left (FLS-FLC), front axle (FA-FLC) and four wheel (4W-FLC). The performance of these strategies is examined through simulation using different road disturbances at a range of forward vehicle speeds. Finally, in chapter 10, conclusions from this work are summarised and recommendations for future work are presented.

Chapter 2
Literature Review

This chapter presents a background and literature review relating to this research. It starts with a description of whole body vibration (WBV) and its effects on the human health as well as highlighting the associated influencing factors, including vibration direction and vibration frequency. Then, the response of the human body to WBV and available measurement methods are described. It followed by a description of suspension systems including passive, semi-active and active together with a consideration of their main advantages and drawbacks. Finally, control strategies found in the literature and their application to semi-active and active suspension systems are discussed.

2.1 Whole body vibration and its effects on the human body

Whole body vibration (WBV) is that transmitted to the human body through direct or indirect contact with a vibrating surface, commonly when sitting or standing. Generally, WBV is considered as an occupational risk factor that affects human health and safety [4–8]. Palmer et al. highlighted how approximately 9 million people in the UK are exposed to WBV when they use private or public transport (cars, vans, buses, trains, and or motorcycles) [9]. In terms of modes of transport, it has been reported that light cars and vans, as well as heavy forklift trucks, lorries, tractors, buses and loaders, are the primary sources of WBV [9]. Drivers of off-road vehicles, industrial trucks and buses as well as crane-operators, crews on ships and helicopters are exposed to particularly high levels of WBV [10–13]. It has been claimed that occupational WBV in the UK could be responsible for more than 500,000 lower back pain (LBP) cases [14]. In addition, it has been estimated that up to 7% of all workers in Europe, U.S.A. and Canada are frequently exposed to unsafe WBV [4]. According to data from national surveys

in Germany, Spain, France and Finland, WBV can affect any of the aforementioned mobile machine operators [15].

Many studies have reported that WBV causes damage to the human spinal system and can cause various musculoskeletal diseases, including lower-back pain (LBP) [5,16,17], early degeneration of the lumbar spinal system and herniated lumbar discs, all of which are strongly related to exposure to WVB for long periods [18]. Also, a study conducted by Seidel [19] has shown that the health of pregnant females is under risk when exposed to WBV. Whilst drivers of regular vehicles are exposed to lower levels of WBV compared to those in off-road vehicles or operating heavy machinery, several studies have shown that the phenomenon can also affect their health [20–22].

Paddan and Griffin [23] estimated the level of WBV for 100 different vehicles based on International Standard ISO 2631-1 [24] and British Standard [11] procedures. Figure 2-1 shows the median values of root mean square (RMS) acceleration using ISO 2631-1 and RMS equivalent acceleration using BS 6841 for the 100 different vehicles utilised in that study. For most of the vehicles the estimated vibration magnitude was higher than 0.47 m/s^2 RMS, which corresponds to the lower boundary of the health guidance caution zone of 8 hours exposure within a 24 hour period, according to the standard ISO 2631-1.

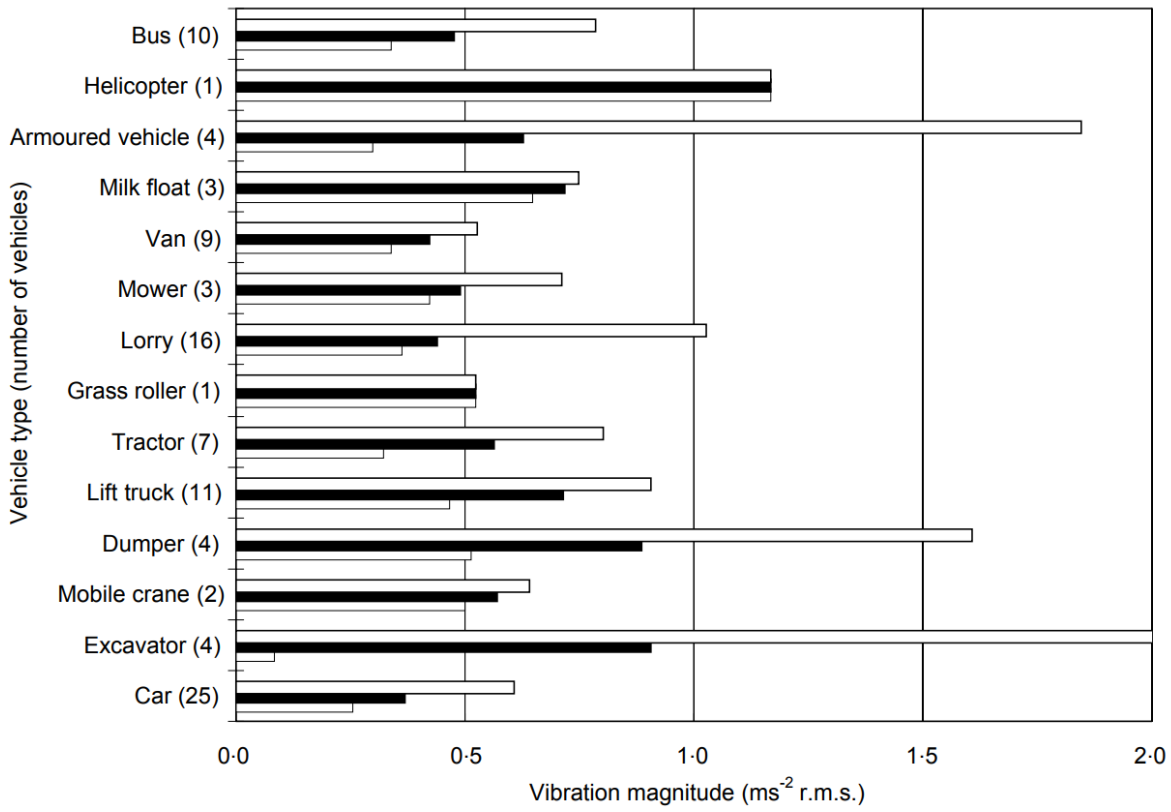

Figure 2-1: Median values of RMS acceleration using ISO 2631-1 and BS 6841 for different vehicles [23]

The effects of WBV can be classified into three categories [25]:

1) Interference with comfort;

2) Interference with activities;

3) Interference with health;

According to Smith and Leggat [13], those relating to health can be classified into two main groups, severe and continuing health effects, as described in Figure 2-2, depending on the degree of physiological changes in the human body that result from exposure to WBV. Acute health effects refer to short periods of exposure to WBV, which usually do not lead to significant physiological changes in the human body and most of the impact can be eliminated by removing the source of the vibration. In contrast, chronic health effects are associated with long periods of frequent exposure to WBV and can result in permanent physiological changes to the human body [13].

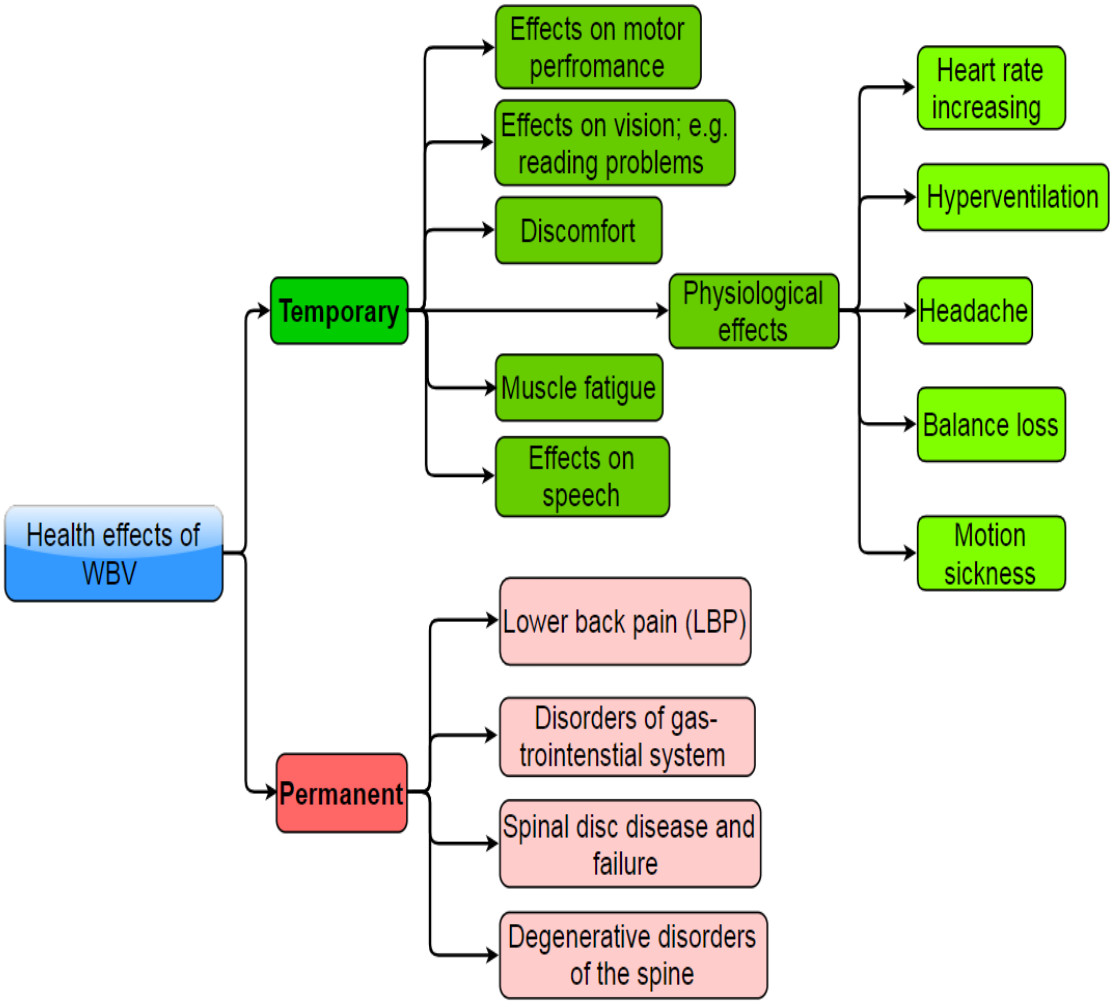

Figure 2-2: Effects of WBV on human health: adapted from [13]

Generally, WBV is related to frequencies between 0.5 and 100 Hz, with peak acceleration magnitudes of approximately 0.01 and 10 m/s². Its effects on the human body significantly depends on both its characteristics (direction of vibration and frequency level) and body state (posture and direction of body) [25]. Despite the fact that a unique human resonance is impossible to define owing to the different physical characteristics within the human body parts, such as mass and density, WBV mostly affects the human body over a frequency range between 0.5 Hz and 80 Hz [13].

Due to the variation of the human body parts, inaccurate human biomechanical models and the difficulty of reaching many parts of the human body [26], different resonant frequencies for the relevant parts have been introduced in the literature, as listed in Table 2-1. Clearly, it can be seen that the whole body has different resonant frequencies depending on the posture and the direction of vibration. Also, Table 2-1 shows that the resonant frequency range for the

majority of the human body parts is between 2 and 20 Hz. The frequency of the WBV excitation plays a significant role in determining the effects of WBV on the human body. In addition, human responses to WBV are frequency dependent and according to Anna, [27] the frequency ranges can be classified into three main groups: low, medium and high frequency, as presented in Table 2-2. Apparently, the highest level of health effects of WBV on the human body relates to the medium frequency range (2-20 Hz).

Table 2-1: Resonant frequencies of the human body [26]

Category	Resonant frequency range (Hz)
Whole body	
Vertical sitting	4-6
Vertical standing	6-15
Horizontal on a rigid slab Longitudinal	1-3.5
Head	8-40
Eyes	12-17
Face and Jaws	4-27
Throat	6-27
Chest	2-12
Lumbar portion of the spinal column	4-14
Shoulders	4-8
Lungs	4-8
Abdomen	4-12
Hands and feet	2-8
Arms with hands	20-70

Table 2-2: Effect of WBV frequency on human response [27]

Frequency Category	Frequency (Hz)	Symptoms
Low (< 2 Hz)	< 0.5	Motion sickness
Medium (2-20 Hz)	4 -10	Discomfort
		Abdominal pain
		Influence on breathing
		Muscle contraction
	5-7	Chest pain
	13-20	Head symptoms
		Influence on speech
	10-18	Urge to urinate
High (> 20 Hz)	20-23	Increased muscle tone
	>= 1000	Damage to tissue

2.2 Response of the human body to WBV

Understanding the responses of the human body exposed to vibration is a crucial aspect not only for optimising the design of a vehicle seat suspension, but also for analysing the effects of WBV on the human body. Consequently, many researchers have studied the biodynamic responses of the human body exposed to vibration both experimentally and analytically. The experimental studies can be categorised into two groups based on the test samples used in the experiments [28]. The first group typically used animals, human corpses and dummies to avoid damage to humans. The second worked with live humans in order to measure their kinetic responses through assessments [28]. Both methods require much time and effort [29]. Not only this, but experiments that expose the human body to vibration are restricted to

protect health, as well as being costly [30]. Moreover, the biodynamic responses of the human body are different compared to those of animals or dummies and consequently, the accuracy of measuring biodynamic responses in this way would be limited [31].

The biodynamic response of the human body exposed to vibration can be evaluated using frequency response transfer functions. There are three main functions: driving-point mechanical impedance (DPMI), apparent mass mechanical impedance (APMI) and transmissibility of driving-point motion to a segment on the body, such as seat to head transmissibility (STHT), as illustrated in Figure 2-3. The first two functions (DPMI and APMI) correspond to the relation between the excited forces and the resulting motion of the body in terms of displacement, velocity, or acceleration at the driving point. The DPMI represents the movement of the body due to a force at a given frequency which is given by the frequency response of the ratio between the excitation force to the resulting velocity at the driving point. The AMPI is akin to the DPMI; however, it associates the excitation force with the resultant acceleration at the driving point.[32], whilst, motion through the body is dealt with by the transmissibility [31]. Experimental measurements of these transfer functions have shown that for a seated human exposed to vertical vibration, there is a primary resonance frequency in the range of 4-6 Hz. Also, a second primary resonance was found in the frequency range of 8-12 Hz [33].

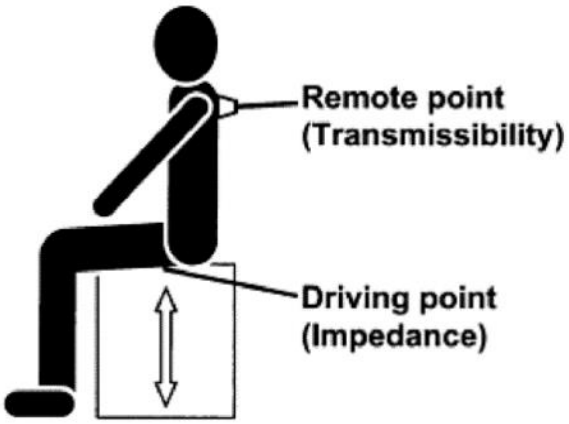

Figure 2-3 Definition of transmissibility and mechanical impedance [31]

2.2.1 Transmissibility

The transmissibility transfer function is concerned with the amount of vibration energy that is transferred from the source of the vibration (seat) to a specific point on the subject (the human body) as a function of frequency. Mathematically, it is represented by the magnitude ratio and phase angle. Measurements of transmissibility are used to determine the resonant frequencies of different human body parts as well as the damping characteristics of each part [31]. Also, the value of the phase angle in transmissibility offers valuable information about the relative motion between the two points as mentioned earlier.

Many experiments have been conducted to measure transmissibility through the human body. Figures 2.4 and 2.5 show the transmissibility of vertical vibration from a vibration table to different parts of seated and standing human subjects, respectively. It is clear from these figures that the human body is sensitive to vertical vibrations in a frequency range (HBSF) of about 2-8 Hz regardless of the posture situation. However, the resonant frequency of the head is somewhat higher in the seated position. Also, a second resonant frequency for the head is shown at about 21 Hz in the standing case, which was not found in the seated case.

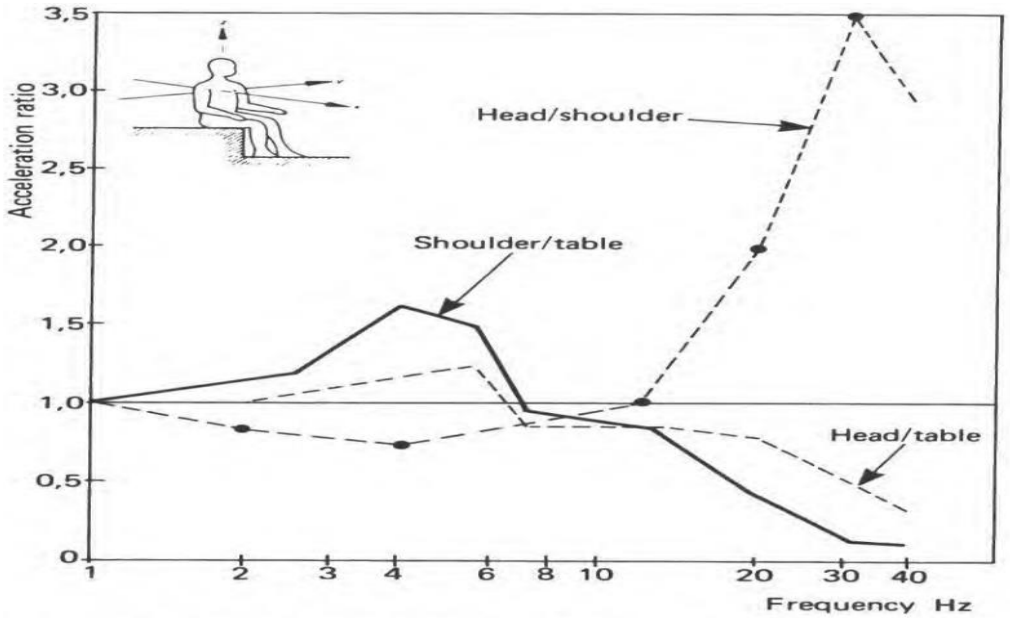

Figure 2-4: Variation of vertical vibration transmissibility from a table to different parts of a seated human subject with frequency [34]

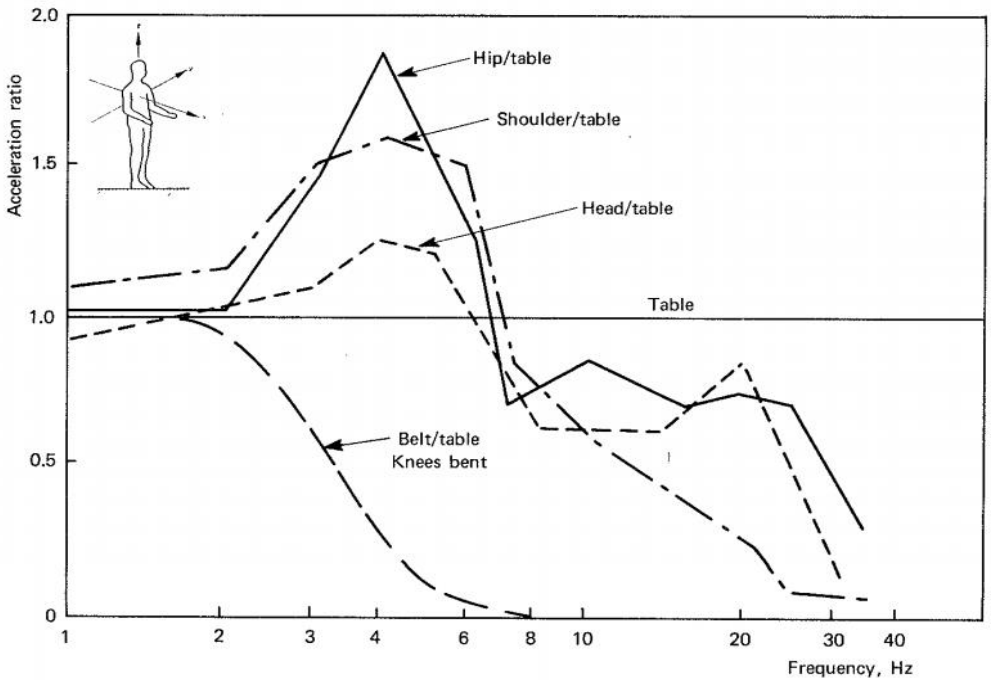

Figure 2-5: Variation of vertical vibration transmissibility from a table to different parts of a standing human subject with frequency [34]

Rakheja et al. [35] reviewed and synthesised measured datasets of biodynamic responses of the seated and standing human body exposed to whole body vibration. Various datasets were used, including driving-point biodynamic responses of a seated person exposed to vertical, fore-aft and lateral vibration, with and without back support. The seat-to-head vibration transmissibility (STHT) of the seated human in vertical vibration datasets was also included. According to the analysis, the STHT datasets show a primary resonant frequency over a frequency range of 4-6 Hz, while some others recommend a second resonance frequency above 8 Hz. Furthermore, several studies were found to have shown, not only that posture affects the biodynamic responses of the seated human body, but also backrest support. For example, Cho and Yoon [36] measured the acceleration transmissibility of 10 seated human subjects at different locations (the floor, hip surface, back surface and head). These measurements were collected while the subjects were exposed to random vertical vibration with and without backrest support. Figure 2-6 illustrates the measured transmissibilities (magnitude ratio and phase) between the hip surface and the floor (H_{1e}) as well as between the head and floor (H_{3e}), both with and without a backrest. The influence of backrest support can be seen on both transmissibility magnitudes, especially over the resonant frequency range. Specifically, the

principle frequency is increased by approximately 20% with backrest support compared to without it [36]. In addition, the magnitude of the head transmissibility with backrest support is larger than that without it.

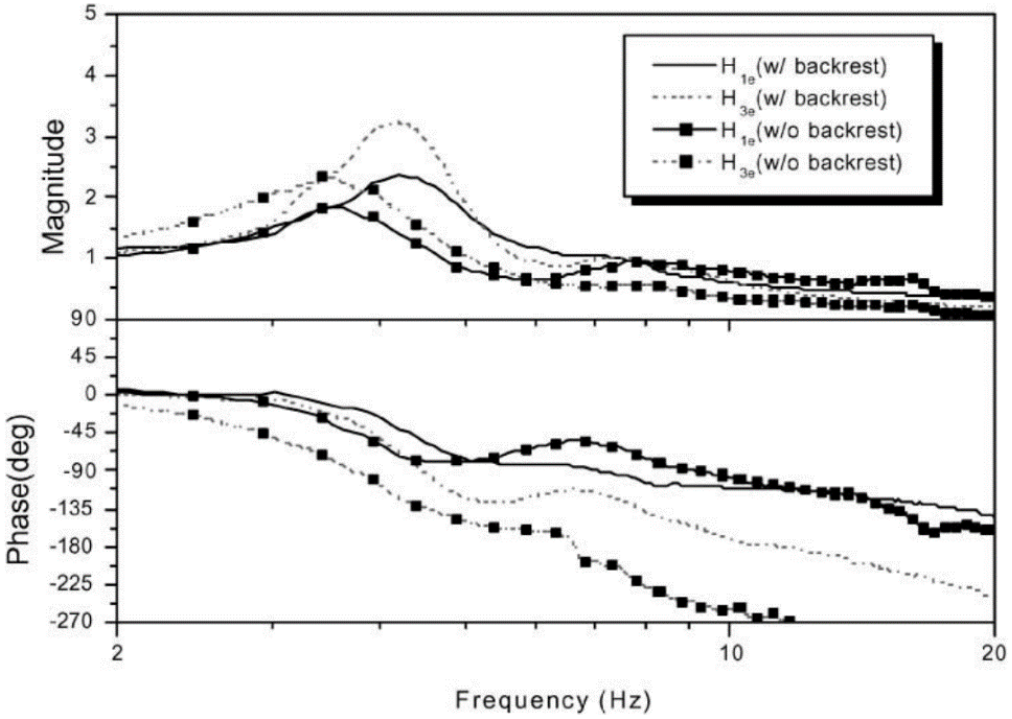

Figure 2-6: Effects of the backrest on the vibration transmissibility [36]

In a moving vehicle, the main sources of the vehicle body vibrations are as a result of road irregularities, aerodynamics forces and powertrain systems including the engine [37,38]. However, the vertical vibrations induced in the vehicle body whilst passing over uneven road surfaces are of a high magnitude and low-frequency range usually less than 12 Hz [39]. Indeed, according to Griffin [25], a seated person in a vehicle is typically exposed to vibrations with a dominant frequency of less than 20 Hz. Hence, much attention has to be given to isolating the driver from this type of vibration as it contains frequencies to which the human body is most sensitive (HBSF).

2.3 Seat Effective Amplitude Transmissibility (SEAT) factor

The vehicle seat dynamics is another factor that contributes to the transmitted vibration to the human body [25]. WBV can be amplified or attenuated depending on these dynamics [23] and

hence, evaluating the performance of a seat to reduce vibration is a crucial issue. The seat effective amplitude transmissibility (SEAT) factor is one of the most widely used methods to evaluate the seat vibration attenuation efficiency [40–47]. It is defined as the ratio between the measured vertical acceleration at the seat surface and that at the seat base [25]. The measured vibration can be expressed by either the frequency-weighted root mean square value (RMS) acceleration or the vibration dose value (VDV). The selection of a suitable measurement method depends on the nature of the vibration exposure and working conditions. The VDV method is mostly used in the case of shock excitation events. However, before calculating either the frequency-weighted RMS acceleration or VDV values, the RMS acceleration should be weighted according to a frequency weighting function that takes consideration the sensitivity of the human body to vibration in exposure direction [47]. This can be either W_k shown in ISO 2631-1 or W_b provided by BS 6841 standard. The former was originally devised as the human tolerance limit regarding whole body vibration by [48], while the involved using equivalent comfort contours for its derivation [49]. Despite this, both are very similar, in particular, for frequencies between 4 and 20 Hz, as illustrated in Figure 2-7. However, the ISO 2631-1 was selected in this thesis because it is the most frequently applied standard in this field.

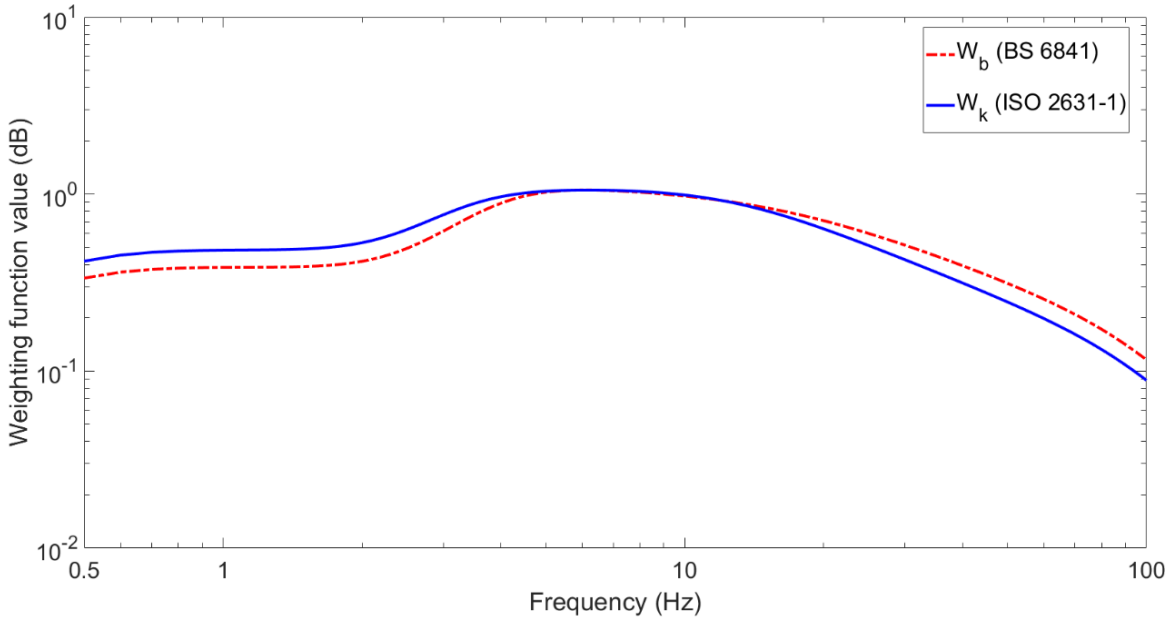

Figure 2-7: Comparison between vertical vibration weighting functions W_k (ISO 2631-1) and W_b (BS 6841)

When the SEAT value is equal to unity, this means that the seat has transmitted the whole vibration from its base to its surface, whereas when this value is greater than unity, this indicates that the seat amplifies the transmitted vibration. Consequently, many studies have involved experimentally measuring the SEAT factor of different seats, including using different vehicles. Figures 2.7 (a) and (b) show the transmissibilities of six different passive truck suspension seats as well as the SEAT values in the vertical and fore-and-aft axis, respectively. It is clear that all the tested seats amplify the vibration around the resonant frequency and attenuate the vibration for frequencies approximately above 3 Hz. Also, most of the suspension seats have a SEAT value less than 100 %.

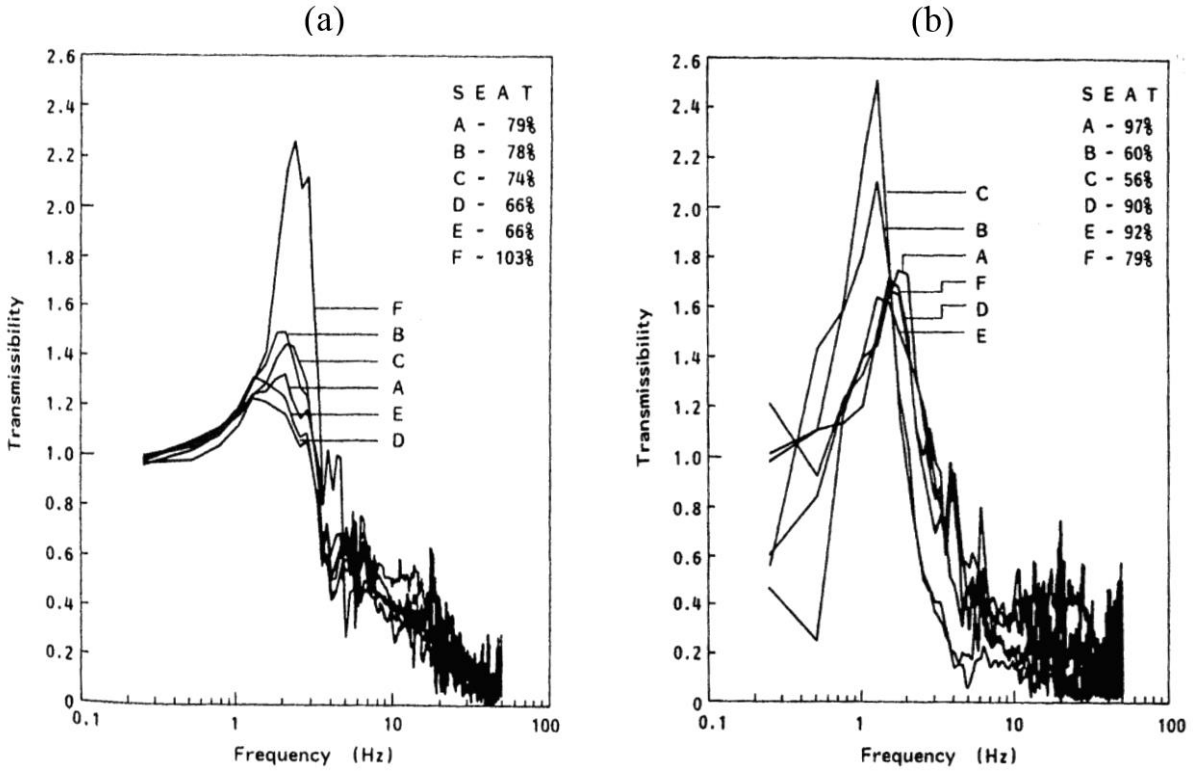

Figure 2-8: Transmissibilities of six truck suspension seats: a) Vertical axis and b) Fore-and-aft axis [50] cited in [25]

The performance of eleven different suspension seats that are widely used in fork-lift trucks, agricultural tractors and lorries was investigated by Burdorf and Swuste [51] using a laboratory and 24 vehicle-seat field measurement combinations exposed to vertical vibration. The field measurements showed that the vertical vibration was reduced in only approximately 70 % of the 24 vehicle-seat combinations. Moreover, significant variations in the seat transmissibility were measured with the same seat and different vehicles. In an extensive

study [52], evaluated the vibration isolation efficiency of 67 conventional and 33 suspension seats as found in various working vehicles, using a SEAT factor that was obtained from both the RMS and the VDV acceleration, whilst being exposed to vertical vibration. They reported that the medium SEAT value of suspension seats was only slightly lower than that of conventional non-suspensions seats and that some seats failed to attenuate WBV. The effectiveness of air suspension seats in isolating WBV in three different buses commonly used on long urban routes was investigated experimentally by [53]. In this study, the SEAT factor was used to compare the performance of the air seat suspension WBV isolation of each bus. A variation in SEAT value between all types of buses was found in which the air suspension seat can attenuate up to 25 % of the WBV. The authors attributed the variation in the SEAT values among the different buses as a discrepancy between the seat and bus suspension.

The vibration attenuation of different cab seats mounted in 22 U.S. locomotives operating on normal working conditions was investigated in [54] and it was found that the mean seat transmissibility ratios were greater than one for all measured axes x, y and z. However, despite the age or the type of the seat (cushion or suspension), none was able to attenuate the vertical vibration. Blood et al. [55] compared the performances of mechanical suspension and air suspension seats installed in forklift trucks vehicles in terms of their capacity to reduce vertical vibration. They concluded that the WBV was significantly reduced when the suspension air is used specifically at low frequency, which contradicts the outcome of the study carried out by Burdorf and Swuste [51]. Also, Blood et al. showed that the performance of mechanical suspension seats in attenuating WBV is dependent on the load upon the seat, such that the performance increases as the driver's weight is increased. However, this dependency on weight was not reported for the air suspension seat type. Blood et al. [56] compared the WBV attenuation of three different seats installed in metropolitan buses and driven over widely used roads, using the standard evaluation methods recommended in ISO 2631-1, including root mean square average vibration and VDV. It was found that none of the tested seats attenuated WBV over all road types. However, it was concluded that the peak vibration transmitted to the driver increased as the amount of silicone foam within the seat is increased. In a recent study, Blood et al. [57] compared the performance of three different suspension seats, namely an air-ride bus seat, an air-ride-truck seat and an electromagnetically active (EM-

active) seat. They found that the vibration transmissibility was significantly reduced when the EM-active seat was used.

Moreover, they stated that the seat suspension design plays a major role in attenuating WBV transmitted to vehicle drivers. Furthermore, [58] evaluated the WBV attenuation performance of three air-seat suspensions implemented in trucks when driving over different road types. Through his study, it was found that the attenuation performance of all seats is sensitive to road surface profile.

2.4 Seat end-stop impacts

The performance of a seat suspension in attenuating vibration is limited by the constraint associated with restricted travel suspension, for which it is essential to maintain the driver within the control area of vehicle instruments, such as the steering wheel and/or pedal. Most suspension seats comprise a low stiffness suspension that increases vibration attenuation but results in a large dynamic deflection when exposed to shocks or vibration of high magnitude and low frequency [59]. This large dynamic deflection may result in metal to metal contact as the seat suspension reaches its maximum travel. Hence, a high impact on the seat will be produced, which will result in a high level of vibration being transmitted to the driver. These severe impacts may affect the health of the human body more than that of uneven road vibration [31]. This type of impact is called 'end-stop impact' and to overcome its severe impact rubber buffers are often installed within the suspension seats. Despite the rubber buffers reducing the hardness of the end-stop impact, the driver is still exposed to a high level of acceleration when the end-stop impact arises [60]. High suspension stiffness may be used with the suspension seat to prevent considerable suspension travel but this leads to a trade-off in the passive suspension seat design, between isolating the driver from high levels of acceleration and severe shocks. Studies have been conducted to overcome this trade-off design criterion either by optimising the damping material of the rubber buffers or, using semi-active or active control technology. For example, Rebelle [61] carried out a study to find the optimum characteristics of the bottom end-stop buffers of a compact suspension seat used in fork lift trucks. It was shown that the acceleration peaks, resulting from a real field excitation input,

were reduced by more than 70 % when the optimised characteristics of the bottom-end stop buffers are used instead of the nominal end-stop buffers.

2.5 Classification of vibration isolation methods

This section presents the classification of different suspension systems and their main features. The classifications are based on power consumption, controllability range and the available bandwidth of each system. Also, the main advantages and disadvantages of each are presented. Specifically, the characteristics of three primary suspension systems, namely passive, semi-active and active, are described and compared. The objective is to consider the overall performance of each system, thereby identifying an appropriate seat suspension system that improves ride comfort.

2.5.1 Classification of suspension systems

Suspension systems can be classified according to the amount of energy required to complete their function and there are three main types, as described below.

2.5.1.1 Passive suspension system

A passive suspension system consists of a spring to store vibration energy and a damper (shock absorber) to dissipate the stored energy, as shown in Figure 2-9 (a). The characteristics of the passive suspension elements (stiffness and damper) are fixed, and thus it does not require energy to complete its function although its vibration attenuation performance is limited. In the case of a passive seat suspension, the vertical vibration is amplified at the natural frequency of the seat when using low damping. On the other hand, isolation of the vertical vibration is degraded at frequencies higher than the natural frequency when deploying high damping.

Reducing the natural frequency of the seat suspension by using a softer spring is not a suitable solution, because this will result in a significant suspension deflection and hence, physical suspension travel, which leads to severe end-stop impacts. Thu, a trade-off between attenuating the vibration around the natural frequency of the seat and at higher frequencies, as well as shocks, becomes apparent. Indeed, the isolation performance is sensitive to changes

in the driver's weight, type of excitation, or the individual characteristics of the suspension seat elements. Consequently, it is beneficial to design a seat suspension that can overcome these limitations, and actively controlled devices are one option.

However, during the last two decades, a new concept has been introduced in the literature to enhance the isolation performance of passive isolation systems. This system is called '' high-static-low dynamic-stiffness'' (HSLDS) or vibration isolation systems with quasi-zero stiffness. The systems offer together a high static stiffness to limit a large static displacement but with a low dynamic stiffness. The low dynamic stiffness reduces the natural frequency of the isolated system which is usually achieved by combining a positive stiffness with a negative stiffness [62]. Consequently, the isolation bandwidth of the system is extended which improves the vibration attenuation performance without any additional power. Therefore, this topic has been attracted by many researchers both theoretically experimentally [63–66]. Although these studies prove the effectiveness of HSLDS systems in improving the vibration attenuation performance, the stiffness nonlinearity could induce jump phenomenon near the resonant frequency which deteriorates system stability as well as it has a relatively large peak amplitude near the resonant frequency [65]. Moreover, the design and fabrication process of HSLDS systems is complicated, the practical implementation is challenging and the isolation performance is sensitive to parameters deviation [67].

2.5.1.2 Semi-active suspension systems

In a semi-active suspension system, the fixed spring and/or damper are replaced with an adjustable spring and/or damper along with a controller, as shown Figure 2-9 (c). The modulation of the damping rate is usually used and can be easily applied utilising different variable damper devices in which the damping rate is modulated rapidly, based on the working conditions of the suspension, through a control algorithm. These dampers can be realised using either oil hydraulics and controllable valves or by deploying magnetorheological (MR) dampers or electrorheological (ER) ones [68].

The power consumption of this system is relatively small and serves to modulate the damping as well as being safe and cost-effective. However, the main drawback of semi-active suspension is that the isolation performance is still limited. This is because the damping force

can only be generated in the opposite direction to the suspension motion and thus, it can just dissipate energy from the system, as illustrated in Table 2-3.

In contrast, semi-active suspensions with variable stiffness rate are more challenging [69] and have physical limitations, such as changing the natural frequency of the suspension system or the static position of the suspended mass. In addition to implementation complications and the high cost of these semi-active suspensions, they have a limited control bandwidth and require substantial energy to change the stiffness rate [70].

2.5.1.3 Adaptive suspension systems

These suspension systems are originally passive, but their suspension parameters (spring and damper) can be changed based on the operating conditions, and hence, improves the suspension performance. This adaptation can be achieved either manually by the driver or automatically via a control system. The characteristics of this system, such as the damper, can be adjustable manually by the driver or automatically by a control system. However, manual adjustment is inefficient, because of the slow response reaction of the driver compared to the rapid changes in operating conditions encountered from road conditions, such as potholes or turns (Braun et al., 2002). Moreover, the performance of these systems is less than that of semi-active systems due to their small control bandwidth range, which is less than 1 Hz [71].

2.5.1.4 Active suspension systems

For active suspension systems, the control of the system is achieved by replacing the passive elements (spring and damper) wholly or partially by an actuator that generates an external force, as shown Figure 2-9 (b). In contrast, to the passive and semi-active suspension systems, which are only able to dissipate energy from the system, it can add energy to the suspension system or remove it independently of the suspension velocity or displacement direction [72]. Consequently, a greater controllability is possible together with the potential of high bandwidth, as given Table 2-3 and shown in Figure 2-10. The disadvantages of this approach are that the external force requires a high level of external energy as well as an expensive actuator. In addition to these shortcomings, the system is less safe than other control systems, because producing external control forces can make it unstable [37,68] and this has to be considered during the design process. Moreover, designing an active suspension system is a

complicated process as some important issues need to be considered, such as the choice of sensors and actuators, weight constraints, power supplies, closed-loop performance and the failure algorithm [2].

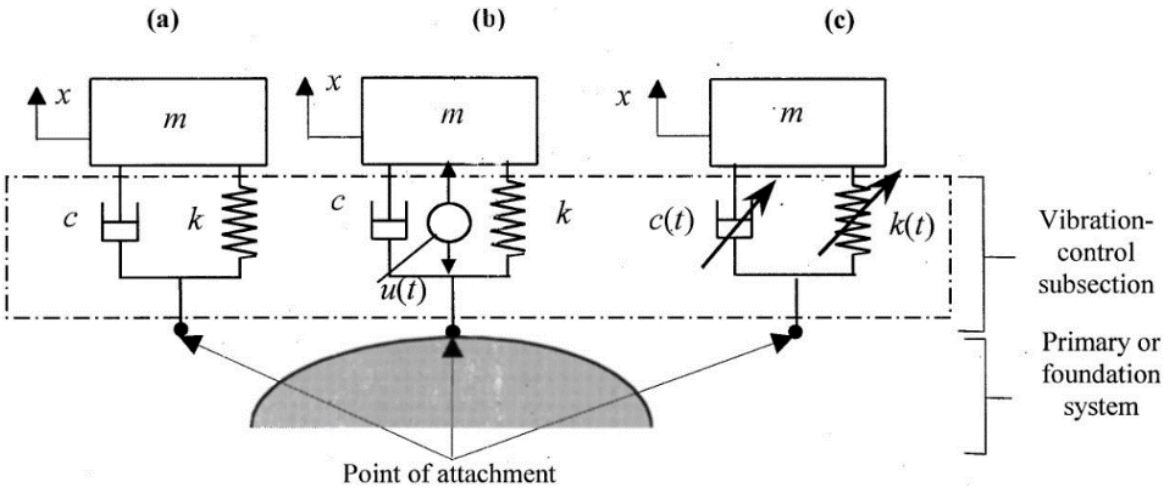

Figure 2-9: Schematic diagram of the main suspension systems: (a) passive; (b) active and (c) semi-active [73]

Table 2-3: Comparison of different suspension systems [68]

System class	Control range (spring)	Control range (damper)	Control bandwidth	Power request	Control variable
Passive	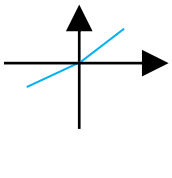	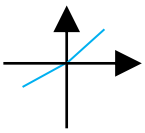	------	------	------
Semi-active	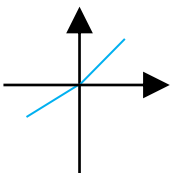	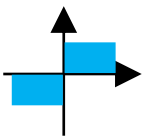	30-40 Hz	Small	C (damping ratio)
Active		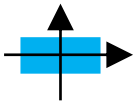	20-30 Hz	High	F(force)

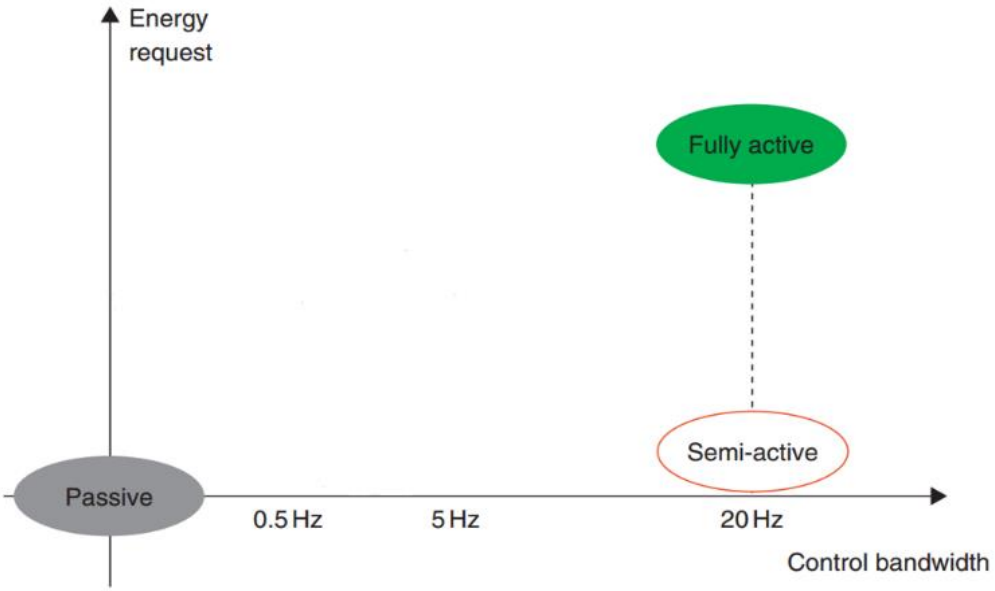

Figure 2-10: Classification of suspension systems based on control bandwidth range and energy required [68]

Whatever the type of the suspension system, it can be implemented either for a vehicle suspension (primary suspension) or a seat suspension. However, active seat suspensions are low-cost, less sophisticated and require less construction effort than vehicle suspensions [74]. Thus, the abovementioned drawbacks of active suspension systems are more associated with vehicle suspension, especially, the power consumption issue. In the case of a seat suspension, the power consumption is much lower when compared to that of a vehicle suspension. This is because the overall weight of a seat and a driver is much less than that of the vehicle body and consequently, less energy is required to control vibrations. Accordingly, less expensive and complicated active system components, including actuators, sensory systems and hardware, can be used and this reduces the practical implementation challenges of the active system for seat suspensions. Moreover, unlike vehicle suspensions, improving ride comfort using active seat suspensions does not influence the vehicle road handling performance and hence this reduces the controller complexity and effort. Not only this but in many off-road and heavy-duty vehicles, seat suspensions are often the only available technique that can be used to attenuate vertical vibration [75]. Therefore, an active seat suspension technique is selected in this thesis to improve ride comfort.

Intensive studies have been carried out in this area, as given in a review paper [76]. Indeed, active seat suspensions have found commercial applications in the automotive industry, such

as the Grammer Maximo Evolution Active seat provided by TEK Seating, as shown Figure 2-11. Recently, Bose also presented a new active suspension seat for trucks, as shown Figure 2-12. According to Bose, the system generates the required control forces within milliseconds using a linear electromagnetic actuator that is capable of working over a wide range of both driver weight and frequency.

Figure 2-11: Grammer Maximo Evolution Active seat [77]

Figure 2-12: Bose active seat system [78]

2.6 Control algorithm methods

The control strategy is considered as the brain of semi-active or active suspension systems, which can be applied into two scenarios. The first approach utilises a control strategy to generate the required control force through an actuator device while assuming ideal characteristics of the actuator. Whilst the second, uses a control strategy, as an inner control loop, to control an actuator device in order to track a required control force. Control strategies for the first scenario can be classified by the type of measurements or system states that are used to provide the control action namely, feedback, feedforward and feedforward-feedback approaches, as illustrated Figure 2-13. Simply, the feedback control uses error states between the output of a system and a desired reference to achieve its control function, whereas the feedforward approach utilises measurements either from disturbances acting on the system or from a desired reference but not error signals. The feedback-feedforward control employs both feedback and feedforward signals. The main advantages and limitations of each approach are summarised in Table 2-4. In addition to this classification, control strategies can also be categorised into five main groups: classical control, optimal control, robust control, adaptive control and intelligent control [79]. The following sections provide a brief review of these approaches and their application to semi-active and active suspension systems.

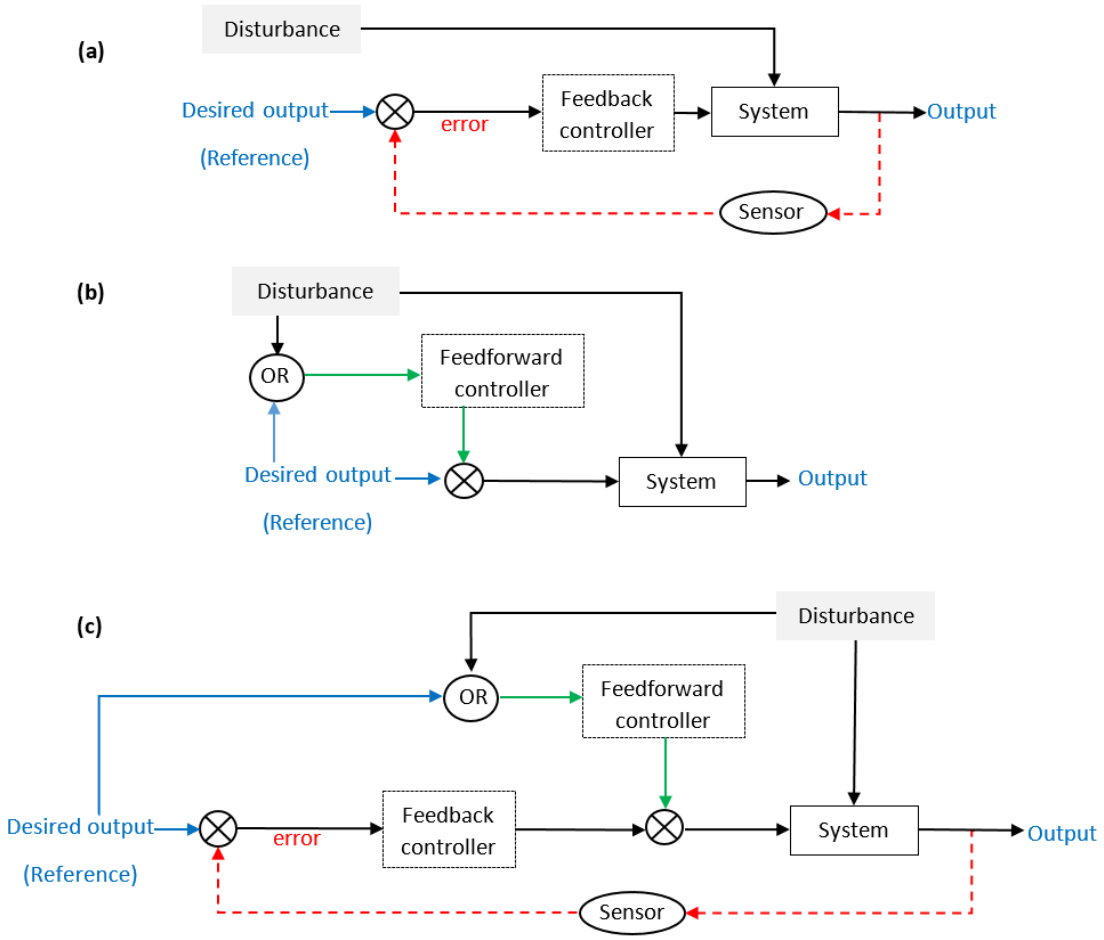

Figure 2-13: Control strategy classification: (a) Feedback control, (b) Feedforward control and (c) Feedforward-feedback control

Table 2-4: Comparison between the feedback and feedforward control approaches (adapted from [80])

Control approach	Advantages	Disadvantages
Feedback	• The control action is independent of the type and source of the disturbance. • Does not require an accurate mathematical model of the system.	• A large frequent disturbance may lead to an unstable system. • Control action of measurable disturbances cannot be obtained. • Does not provide control action until disturbances take action on the system. • On-line variable measurements from the system may be difficult to obtain.
Feedforward	• Provides control action before disturbances act on the system. • Offers control of the action of measurable and known disturbances.	• Not suitable for unviable on-line disturbance measurements (e.g. random excitation) • Requires an approximated mathematical model of the system.

2.6.1 Classical control

2.6.1.1 Proportional-integral-derivative (PID) controller

The operation of these controllers is based on using a feedback error signal, between the actual output and the desired reference, as well as the integration and derivation of this error signal with gains designed to minimise this error [79]. Due to its simplicity and effectiveness it is has been applied in many industrial applications. However, it is based on the assumption that the system is linear and neither its performance nor stability can be guaranteed under parameter or model uncertainties.

2.6.1.2 Skyhook control

Skyhook control was first introduced by Karnopp et al. [81]. The basic idea of this algorithm is to reduce the vibration of the suspended mass by connecting it to a fictitious sky frame through a damper. Figure 2-14 (a) illustrates a single degree of freedom system incorporated with a skyhook damper.

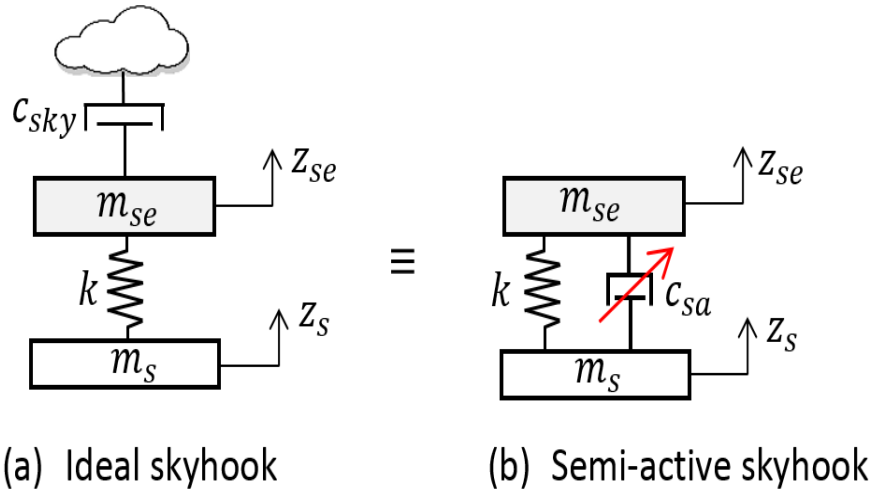

Figure 2-14: Skyhook seat suspension configuration: (a) Ideal skyhook and (b) semi-active skyhook

Practically, it is not possible to construct the ideal skyhook. Hence, an equivalent semi-active damper system is assumed to emulate the performance, as shown in Figure 2-14 (b), in which the skyhook damper is replaced by a semi-active damper connected between the isolated mass and the base. Whilst this control law has been quantified in the literature for a semi-active suspension system, it can be applied for an active system through an active actuator in which the active force is proportional to the absolute velocity of the isolated mass [82,83].

Many studies have been conducted to explore the performance of a skyhook in attenuating vibration both theoretically and experimentally, such as [84–86]. In [84], three semi-active control schemes, including skyhook, groundhook and hybrid, were experimentally studied using a quarter-car model that was integrated with an MR damper. It was shown that the skyhook scheme efficiently reduces the sprung mass acceleration, which results in improved ride comfort. In contrast, the groundhook scheme significantly reduces the acceleration of the unsprung mass. This decreases the fluctuation in the dynamic load of the tire, which leads to improved vehicle handling performance and a reduction road damage [74].The hybrid control

performance lies somewhere between the performance of a skyhook or groundhook depending on the gain value that biases its performance towards one or the other.

Despite the skyhook algorithm having been proven to isolate the mass system significantly from transmitted vibration, it has some drawbacks. Firstly, switching between high and low damping levels generates a sharp change in the damping force, and thus discontinuities are introduced. Consequently, this will provide a severe change in the suspended mass acceleration and jerk leading to compromised vibration isolation. To overcome this problem, Ahmadian et al. [87] developed the classical skyhook algorithm through two alternative methods. These were theoretically and experimentally analysed, with the results showing that they can reduce high jerk levels. In addition, Miller (1990), cited in [88], introduced a strategy to minimise jerk based on decreasing the generated damping force.

Secondly, the implementation of a skyhook in a real seat suspension requires the measurement of the absolute velocity of the suspended mass, and this is very difficult and costly to achieve for a moving vehicle. Alanoly and Sankar [89] modified the concept of the skyhook algorithm, such that it only requires the relative displacement and velocity across the suspension with a continuous damping force. However, the necessary damping force could not be provided by the damper [88]. Also, Shen et al. [90] modified the switching law of the skyhook algorithm by using the jerk measurement of the suspended mass instead of the absolute velocity, while [91] proposed a switching control algorithm denoted acceleration-driven damper (ADD) to improve ride quality. This ADD algorithm has the same concept as the classical skyhook, but the switching law is based on the suspended mass acceleration and hence it can be easily applied in practice although the switching law could result in a chattering problem and affect the closed-loop performance [92].

2.6.2 Optimal control

Optimal control is based on optimising the system state variables to improve a specific performance index under some constraints [93]. The most common form of this technique is the Linear Quadratic Regulator (LQR), for which it is assumed that all system states are measurable and hence, this makes its real application difficult if not impossible. To overcome this drawback, an observer, such as a Kalman filter can be used to estimate the unavailable states, such as in the Linear Quadratic Gaussian (LGR) approach. Whilst this approach would

seem to be more practical than LQR, it increases the complexity of the system and also the state estimators require an accurate plant model [94]. Further details about the application of optimal control in active suspension systems are given in [95–98].

2.6.3 Robust control

The main purpose of these control strategies is to maintain a good system performance and stability over a range of system parameters uncertainties [79]. The most common techniques used to design a robust control are H∞ and sliding mode control (SMC), where the latter is mainly used for controlling nonlinear systems. Many studies investigating the application of these strategies for semi-active suspension systems have been carried out [75,99–101] and active suspension systems [102–106].

However, these strategies have some inherent drawbacks. For instance, the H∞ controller is both mathematically complicated and requires an accurate plant model [107]. Moreover, Sliding Mode Controllers induce chattering that results from rapid switching in the control output to achieve a desired sliding mode and are sensitive to noise within measurements and thus practical implementation has been limited [108].

2.6.4 Adaptive control

This type of algorithm is usually employed to control nonlinear systems with unknown or time-varying parameters. The controller parameters are attuned automatically over time such that they compensate for variations in the system performance associated with changing system parameters [109,110]. Generally, adaptive control algorithms can be classified into two methods: direct and indirect. In the direct method, also referred to as model-reference adaptive, the error between the output of a reference system model and the actual output is utilised directly to adjust the controller parameters. By contrast, in the indirect method, also referred to as self-tuning, the adaptation consists of two stages. The first estimates the system plant parameters based on measurements of the inputs and outputs to the plant. These updated plant parameters are used in the second stage to adjust the controller parameters [110].

Despite, the model-reference adaptive technique requiring less computational time compared to self-tuning, the system stability is guaranteed only for small adaptation gains and it is only

applicable for systems with minimum phase (all poles and zeros are in the lift side of the s-plane in the Laplace domain). Also, it requires some knowledge about the plant system, such the order of the plant [111].

Highly nonlinear and complex systems can be controlled using the self-tuning adaptive control, but this requires relatively high computational time and system stability cannot be guaranteed [112]. Much research has been undertaken on active suspensions with adaptive controllers [113–115] and other studies in a review paper conducted by [109]. However, the application of such controllers has not been limited to active systems, and it has also been extended to semi-active suspensions [116–119]. Yi and Song [120] proposed an adaptive skyhook control scheme with a road detection algorithm to select the optimal damping gains based on the frequency content of the road input. The adaptive skyhook control law was numerically and experimentally compared to the conventional skyhook and passive suspension systems using simulation and a quarter-car test rig in both the time and frequency domains. It was found that the proposed control scheme improves the ride comfort and road holding. However, the road detection algorithm is difficult to apply practically.

Feedforward has been widely applied to cancel disturbance with narrowband frequency ranges. For example, a Least-Mean-Square (LMS) algorithm was utilised as an adaptive feedforward control in many active noise and vibration cancelations systems (ANVCs). In a recent study, Gan [121] developed an active suspension seat to attenuate periodic disturbances using an adaptive filtered-x LMS (FXLMS) algorithm. This algorithm was confirmed theoretically and experimentally to attenuate vibration at the seat when excited by periodic disturbances. This algorithm has also been applied to control active engine mounts [39]. Wu and Chen [122] experimentally studied a hybrid controller consisting of an adaptive feedforward FXLMS with an H∞ feedback controller to reduce vibration at the driver's seat, which was excited by small amplitudes of vibration. Even though the proposed controller succeeds in reducing vibration at specific frequency ranges, it amplifies vibration at other frequency ranges, which means it is not applicable for a broadband vibration disturbance and is computationally intensive [109]. In addition to this, the control performance depends on the algorithm convergence speed, which is affected by the type of vibration and operating conditions of the system [122]. Kawana and Shimogo [97] conducted theoretical and experimental studies on an active seat suspension for a heavy duty truck seat to reduce the

driver vertical acceleration, which included a dummy and a live human. The active seat suspension controller was designed using optimum linear theory, based on feedback and feedforward state variables, while the active force was obtained using an electric servomotor and ballscrew mechanism. Despite the active controller improving the riding quality, it was not compared to other passive or semi-active seat suspensions nor was it tested under different road conditions. Besides, the experimental results were in disagreement with those obtained from simulation.

2.6.5 Intelligent controllers (ICs)

These are based on using algorithms that follow the performance of intelligent biological systems, such as the human brain [123]. The main algorithms associated with this type of controller are fuzzy logic (FLC) and artificial neural network (ANNC) controllers. FLC involves attaching an input to an output based on the logical thinking of the human brain using a set of logical rules [124], while ANNCs emulate the intelligent learning process of the brain using previous information. ICs have been applied widely in active vibration systems as witnessed by the references given in the review papers [108,109]. In addition to active systems, these methods have also been applied in semi-active suspensions [125–127]. In Avdagic et al. [125] a FLC and an ANNC were studied in simulation and experimental environments, with the aim being to reduce the vertical vibration of the driver's seat of an off-road vehicle. The first study was conducted using an FLC to modulate the stiffness of the air spring of a seat suspension, whilst in the second, ANNC was used to adjust the seat suspension damper. The results showed that both FLC and ANNC can reduce the vertical seat acceleration. However, the experimental results were not in agreement with simulation. Also, the results were not compared with either a passive system or other simple control algorithms. Moreover, the seat deflection was not considered for either study, and according to the authors, the spring force is limited by the direction of the velocity of the spring bellows.

Generally speaking, IC controllers are efficient for handling complex and nonlinear plant systems and different types of disturbances. Nevertheless, they have some drawbacks, such as the control performance using FLC depending on the number of logical rules, which are not guaranteed as being coherent, while using ANNCs rely on the accuracy and availability of the

training set data. Overall, clear stability analysis of these methods is not feasible, and they require relatively intensive computational time [128].

To overcome the weakness of each IC strategy, many studies have investigated a combination of these strategies, as in a comprehensive review paper given by [108] or with classical and modern control laws, such as in [129,130,130–136].

2.6.6 Preview control

Most of the aforementioned control algorithms used in active or semi-active suspension systems are based on employing the dynamic response changes of the vehicle that results from road disturbances to cancel the effect of these. However, in this approach, the controller is activated only after a road disturbance has already acted on the vehicle and thus this increases the effort of the controller to attenuate the effects of this disturbance on the system.

In a preview controller, prior knowledge of the road disturbance is utilised in the control strategy as illustrated in Figure 2-15, which prepares it to cancel the effect of this disturbance on the vehicle in a more appropriate time. That is, this can compensate for the controller and actuator delay times as well as reducing the power consumption, the feedback information and the complexity, thus potentially improving the suspension performance [137–139].

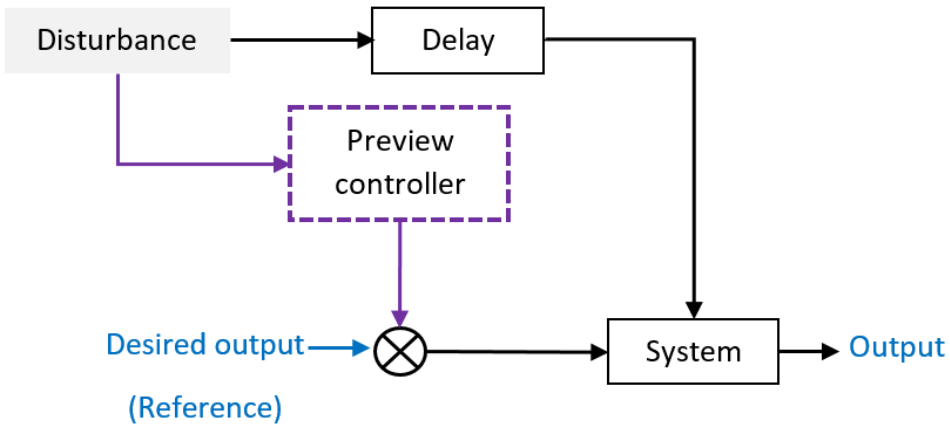

Figure 2-15: Preview control configuration

It was Bender [140], who first presented the concept of preview information in vehicle suspensions using a single degree of freedom model, arguing that the employment of such information in the control strategy can efficiently improve suspension performance. There are

two approaches to preview control based upon the way in which preview information is obtained: "look ahead'' and "wheelbase''. In the first scenario, the preview information from the road profile is sensed and used by the controller of the active suspension. These sensors are mounted at the front of the vehicle body, as illustrated in Figure 2-16 and hence, the preview information is available for both the front and rear active suspensions. The types of sensors used in this field can be ultrasonic, optical or radar technology [74]. This approach has been investigated in many theoretical studies in the literature. For example, Thompson et al. [141] researched the application of a preview controller for an active suspension system using optimal control theory and a quarter vehicle model. Hac [142] proposed a linear preview controller for an active suspension with minimal preview information, considering measurement errors. The simulation results indicated that involving preview information offers significant improvements in all features of suspension performance and dramatically reduces power consumption. Soliman and Colar [143] applied look-ahead preview control for a semi-active vehicle suspension using a quarter vehicle model. Interestingly, they concluded that the performance achieved by a preview semi-active suspension is better than that of a fully active suspension without preview. Kim et al. [144] proposed a preview active suspension based on a full vehicle model and real road profiles extracted from a road sensing system, whilst El Madany et al. [145] investigated the application of stochastic optimal control with preview information for an active suspension using a two-degrees of freedom vehicle model, considering integral constraints. Intensive studies have been conducted in this area, which can be found in the literature and a review paper presented by Arunachalam et al. [138]. Theoretical studies have indicated the potential benefits of including preview information using the look-ahead concept for an active suspension and a few experimental studies have also been carried out. For example, Langlois et al. [146] tested a preview control active suspension system for an off-road military vehicle using an ultrasonic height sensor and a minor improvement in the RMS body acceleration was achieved when compared with a non-preview alternative. In another study, Nagiri et al. [147] investigated a hydro-pneumatic preview active suspension with a contactless optical sensor for a vehicle using the Skyhook approach and a virtual vehicle model to compensate for the actuator and computational time delays. The experimental results, when driving over a rough random road, showed that the

look-ahead preview active suspension significantly improved the ride comfort, especially over the human sensitivity range (1- 8 Hz) when compared to an active system without preview. Akbari et al. [148] applied multi-objective look-ahead preview control for an active suspension using a quarter vehicle model test rig, whilst the look-ahead preview information was virtually generated in simulation at an advanced time including measurement noise. The experimental results showed that only minor improvements in the ride comfort could be gained with preview information when compared with a non-preview active system.

The real implementation of a look-ahead preview scenario is challenging, as it requires an expensive and accurate sensor system as well as complicated algorithms in order to characterise different road profiles accurately, whilst taking into account the amount of preview information, vehicle speed, road conditions and measurement noise [137–139,149]. Moreover, inaccurate preview information can significantly influence handling and hence vehicle stability [137,149].

According to [3], Nissan applied look-ahead preview control in their vehicles in 1990, using a 'super supersonic' suspension with ultrasonic sensors to provide preview information. Similarly, Mercedes, in their S-Class, in 2013, deployed 'magic body control' and a 3-D stereo camera for sensing preview information.

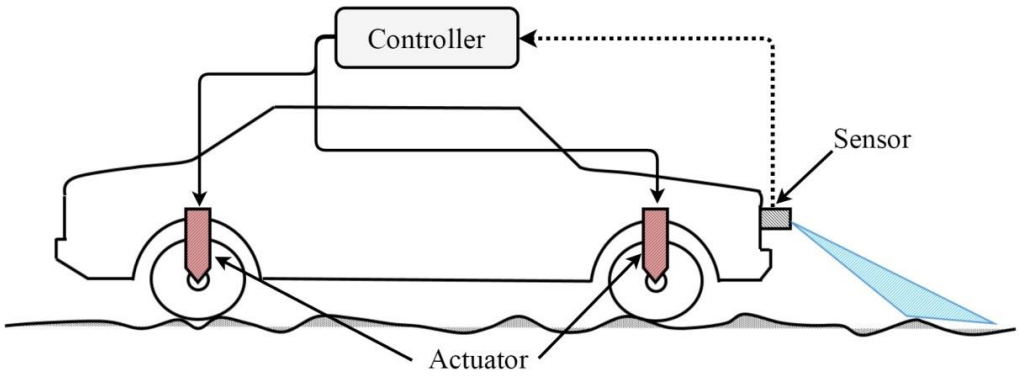

Figure 2-16: Look ahead preview control for vehicle suspension

2.6.6.1 Wheel-base preview control

In wheelbase preview control, the preview information is directly detected from the dynamic changes of the front axle and utilised in the control of the rear active suspension, as shown in Figure 2-17. This concept is based on the assumption that the road profile at the rear wheels is at variance to that at the front wheels by only a time delay, which depends on the vehicle

wheelbase and its velocity. Intensive studies have been carried out based on using wheelbase preview control. For example, [150] considered an active suspension with wheelbase preview control based on LQR, assuming the availability of all state variables. Pilbeam and Sharp [151], designed a wheelbase preview controller using the LQR theory for a slow-active suspension, based on a half-vehicle model and considered the influence of the preview information weight on improving system performance. Roh and Park [152] developed a wheelbase preview for an active suspension based on a state feedback controller incorporated with a Kalman-Bucy filter. The numerical results, using a half-vehicle model, showed that significant improvement in the suspension performance can be achieved with preview information, but that this depends on accurate road models. Kitching et al. [153] tested a prototype semi-active suspension for a heavy vehicle, incorporating the wheelbase preview principle using two-DOF hardware-in-the-loop simulation technology. However, the theoretical improvements achieved by the preview control were not obtained through experimental tests.

ElMadany et al. [154] investigated both the look-ahead and wheelbase preview concepts for a slow active suspension based on optimal control theory, using a half-vehicle model. They concluded that the wheelbase offers a significant improvement in the rear slow active suspension at low vehicle speeds, while combining both preview scenarios offers substantial improvements in all features of the slow active suspension. A wheelbase preview controller based on optimal control theory and a full vehicle model for a slow active suspension was investigated in [155]. The simulation results showed the benefits of including wheelbase preview information in slow active suspension performance. Li et al. [149] studied a wheel-base preview control for an active vehicle suspension using a multi-objective control strategy and a half-vehicle model. The effect of preview information weight on improving the suspension performance was also investigated.

Whilst wheelbase preview control provides an opportunity to improve the suspension performance at the rear axle as well as being cost-effective and realisable compared with look ahead alternatives [149], it has some drawbacks. The preview information is only accessible to control the rear suspension and the road profiles at the front and rear axles cannot always be assumed to be identical, especially during cornering [137]. Moreover, the benefits of including preview information are diminished when driving at moderate and high vehicle speeds [154,156], when the delay time between the front and rear axles becomes shorter.

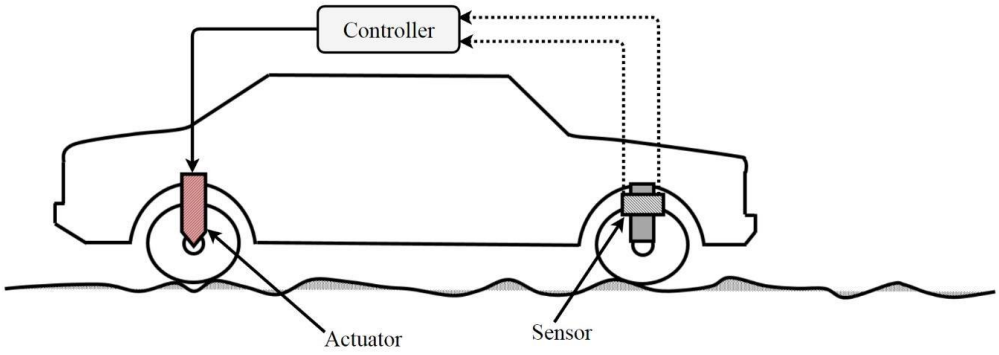

Figure 2-17: Wheelbase preview control for vehicle suspension

2.7 Evolutionary algorithms (EAs) optimisation

Classical optimisation problems, such as linear programming and dynamic programming cannot deal with large-scale optimisation tasks with non-linear objective functions and /or constraints. Also, they usually cannot ensure to find a global optimum solution as well as requiring gradient information of the objective function, which can be either unavailable or needs a considerable processing time to obtain it [157]. To deal with these challenges, evolutionary algorithms (EAs) are introduced which are stochastic optimisation techniques that work similar to natural biological evolution and/or the social behaviour of species [158]. There are many types of EAs such as, genetic algorithms (GAs), particle swarm algorithm (PSO), ant-colony algorithm (AN) and shuffled frog leaping. However, in this thesis, only the first two algorithms, namely GA and PSO, are considered as they are widely used in this field, with the following subsections giving a brief introduction to each technique.

2.7.1 Genetic Algorithm (GA)

A genetic algorithm (GA) is a stochastic optimization technique, which was first developed by Holland [159] , based on the natural rules of selection and genetics [160]. The concept of a GA is based merely on evaluating different sets of solutions (chromosomes) for the desired optimisation problem, called population, in the search space using a fitness function (objective function) at each iteration (generation). Each chromosome in the population consists of genes

which denote the design variables of the desired optimisation problem. These chromosomes are modified towards the optimum solution during each iteration (generation), starting from randomly generated chromosomes. This modification is based on applying genetic operators known as selection, crossover, and mutation, as presented in The first operator is responsible for transferring valuable information from the current generation to the next one through selecting the most effective chromosomes that are most improving the desired fitness function, while neglecting others without affecting the size of the population [161]. The purpose of the crossover operator is to produce new chromosomes (feasible solutions) from the currently selected solutions through cutting these solutions at an arbitrary genes position and swapping between these genes [162]. After that, to ensure some diversity in the population, the mutation operator creates new solutions by changing the value of a gene in a randomly selected chromosome based on a mutation rate. Unlike classical optimisation techniques such as linear programming, a GA does not depend on gradient information and thus, can deal with complex optimisation problems that involve nonlinear objective functions and/or constraints as well as being able to handle different types of design variables, both continuous and discrete [163]. This algorithm has been extensively employed in the academic sector in various research fields, including different configuration of vehicle and seat suspension systems (passive, semi-active, and active) [131,133,164]. It can search randomly over a wide range of feasible solutions and thus, can offer a near-global optimum solution [131,165–167]. The performance of the GA is affected by four parameters: the population size, crossover rate, number of generations and mutation rate. The chance of obtaining a global optimum solution is increased when large population size and number of generations are used. However, this raises the computational time, especially in the case of large-scale problems. Usually the value of the crossover rate is between 0.6 and 1.0, while the mutation rate is chosen to be less than 0.1 [158]. More detailed information about GAs can be found in many textbooks, such as [168,169].

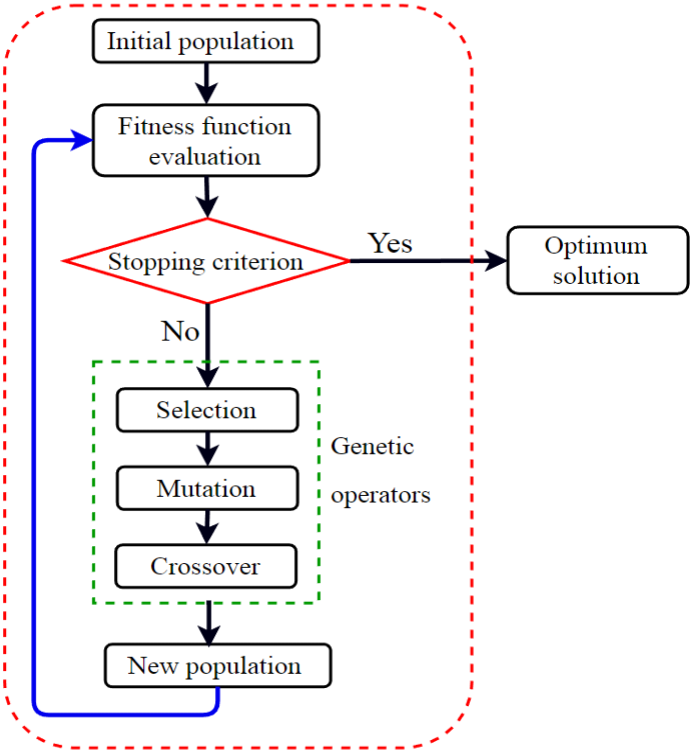

Figure 2-18: Genetic algorithm flowchart

2.7.2 Particle swarm optimisation (PSO)

PSO, which was first proposed by Kennedy and Eberhard [170], is an evolutionary optimisation method that is based on the behaviour of animals, such as birds flocking and fish schooling to creating swarms towards food sources [171].

For a given optimisation problem with M design variables, suppose that there is a swarm with n particles, then, at a given instant of time each particle has a position vector, $X_i(t) = [x_{i1}(t), x_{i2}(t), \dots\dots, x_{iM}(t)]$, of size M [172], which represents a candidate solution to the optimisation problem. Initially, the position and velocity vectors of each particle are randomly generated in the searching space. Later, the position and velocity vectors of each particle are updated based on the best previous position P_{best} of this particle, and the global best position that corresponds to the best position obtained by all the particles in the swarm, G_{best}.The mathematical equations for updating the velocity and position of the *ith* element of each particle are given as follows [173] and a flowchart of the PSO process is presented in Figure 2-19:

$$v_i^{t+1} = wv_i^t + c_1 r_1 \left(P_{best_i}{}^t - x_i^t\right) + c_2 r_2 \left(G_{best_i}{}^t - x_i^t\right) \quad \textbf{(3-1)}$$

$$x_i^{t+1} = x_i^t + v_i^{t+1} \quad \textbf{(3-2)}$$

Where, w is the inertia weight, as proposed by Shi and Eberhart [174] in order to improve the convergence rate of the algorithm and it has a value in the range [0.8 1.2]. The constants c_1 and c_2 are the cognitive and social factors, respectively while r_1 and r_2 are random numbers between 0, and 1). The values c_1 and c_2 are usually chosen to be less than 2.0. Further details about the PSO can be found in [171,175].

Similar to the GA the PSO does not require gradient information corresponding to the objective function, but the latter technique is simple and can be easily applied. Moreover, its convergence characteristics are stable, computationally efficient and it requires less adjusting of parameters, compared to other evolutionary optimisation algorithms [171,173,176]. In sum, PSO is an effective tool for an optimisation problem with a relatively large number of design variables, such as when optimising the structure of an FLC.

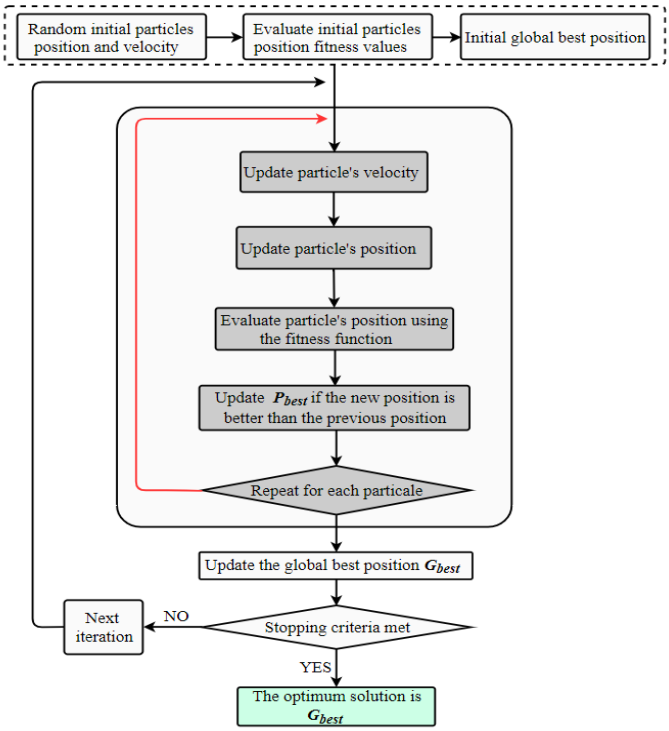

Figure 2-19: Flowchart of the PSO algorithm adapted from [173]

2.8 State Measurement and Estimation

Despite the fact that many of the aforementioned Active Vibration Control (AVC) strategies having shown high performance through simulation, their practical implementation is a challenge. For instance, some of the strategies require online measurements of all the state variables, which increases the number of sensors and hence, the cost and system complexity [177]. Moreover, some states are difficult to obtain, such as the absolute velocity of the seat or the driver, as in the case of the well-known classical Skyhook algorithm [178]. Many researchers have attempted to solve this problem by assuming that the system states (velocities and displacements) can be obtained by numerically integrating the measured acceleration signals. In practice, noise and signal offsets can result in inaccurate states and compromised controllers [179]. In other studies, it has been argued that the state variables can be estimated using an observer, but this increases the complexity of the system, and also the state estimators require an accurate plant model [94].

Consequently, it is an important issue from both a cost and reliability point of view to develop an active seat suspension that utilises a control strategy requiring only accessible and inexpensive system states, whilst taking into account the restrictions on both the allowable seat suspension travel and actuator force capacity. Moreover, it should be robust to changes in operating conditions mainly the driver's weight and vehicle speed. These issues make the design of a reliable and robust active seat suspension a challenging problem, which the current research is aimed at solving.

Based on the above literature review, for this thesis, the benefits of employing preview information to control an active seat suspension are investigated. To overcome the drawbacks of the aforementioned preview information concepts, a novel preview information scenario similar to the wheelbase preview is developed here. With this approach, the required preview information is directly obtained from the vehicle dynamics based upon available states that can be measured reliably and cheaply. Moreover, this preview information (feedforward) is combined along with available and inexpensive feedback states in the control strategy of the active seat suspension, hence improving the ride comfort of the driver.

2.9 Conclusions

Low-frequency vertical vibration, transmitted to the driver's seat from road roughness through the vehicle body is an occupational risk factor that affects human health and safety. Different suspension systems can be used to overcome this, including passive, semi-active, and active. Among these, active suspensions provide the best performance improvement in ride comfort over a wide frequency range. Nevertheless, its practical application to a vehicle suspension is limited because of high energy consumption, complexity and cost. Alternatively, active seat suspensions are more reliable, practical and less complicated systems that directly attenuate this vibration without deteriorating handling performance. However, the control strategy used to modulate the control force plays an important role in their performance and many strategies found in the literature are challenging to implement in a practical system successfully.

In summary, the main aim of this research is to develop a novel, reliable and cost-effective active seat suspension that employs measurable and inexpensive preview information states from the vehicle suspension. Further details of this principle are provided in chapter 6.

Chapter 3
Performance Evaluation Methods of Seat Suspension Systems

This chapter presents and explains the available numerical quantities found in the literature that are used to evaluate and analyse the performance of a seat suspension system regarding improving ride quality and the procedures to obtain them. Also, generation of artificial road disturbances including random and bump road profiles are also provided.

3.1 Introduction

The main objective of an active seat suspension is to provide a more comfortable environment for an occupant (driver) through reducing the transmitted vibration to the driver's seat from the vehicle body and hence, improving ride quality. Accordingly, performance evaluation methods are essential for evaluating and analysing the performance of such a system [180]. The effects of WBV on a seated occupant depends on many factors such as vibration magnitude and direction, the frequency content and exposure duration [25] and, hence the assessment is not straightforward. Moreover, assessing ride comfort of a seated occupant can be performed either qualitatively or quantitatively [181]. The first approach is based on using the knowledge, skills and experience of expert drivers to evaluate the ride quality, which requires a massive effort and much time as well as being expensive. While the second pertains to using some ride comfort assessment criteria suggested in the standard ISO 2631-1, such as vibration dose value (VDV), frequency-weighted root mean square (RMS) acceleration a_w and the Seat Effective Amplitude Transmissibility (SEAT) factor. In this thesis, the lattermost, which correspond to the vibration isolation performance of a seat suspension and the frequency-weighted root mean square (RMS) acceleration value a_w are considered. However, the following sections give brief descriptions for each of them.

3.2 Methods for evaluating WBV effects

3.2.1 The frequency-weighted root mean square (RMS) acceleration a_w

While many measures can be used to evaluate ride comfort, such as velocity, acceleration and jerk time histories or in terms of their RMS values, the ISO 2631-1, much of the literature has suggested acceleration magnitude with appropriate frequency weighting filters to assess ride quality [181]. Accordingly, the frequency-weighted RMS acceleration value a_w is deemed here as being an essential quantity for the analysing the effects of WBV in terms of comfort, health and perception, as suggested by the standard ISO 2631-1 [182]. The frequency-weighted RMS acceleration value a_w can be expressed mathematically as follows:

$$a_w = \left[\sum_i (W_i\, a_i)^2\right]^{\frac{1}{2}} \quad \textbf{(3-1)}$$

where W_i is the frequency-weighting at the centre frequency f_i of one-third octave frequency bands and a_i is the corresponding RMS acceleration value which can be obtained using the following mathematical formula [181] :

$$a_i = \sqrt{\int_{f_{li}}^{f_{ui}} S_y(f)df} \quad \textbf{(3-2)}$$

where S_y is the power spectral density function of the acceleration time data, whilst f_{li} and f_{ui} are the lower and upper limits of *i-th* one-third octave frequency band, respectively, which can be obtained as follows:

$$f_{li} = 0.891\, f_i \quad \textbf{(3-3)}$$

$$f_{ui} = 1.21\, f_i \quad \textbf{(3-4)}$$

The total value of the frequency-weighted RMS acceleration value in the three principle translation axis (X, Y and Z) coordinates is given by:

$$a_v = \sqrt{\left(k_x^2 a_{wx}^2 + k_y^2 a_{wy}^2 + k_z^2 a_{wz}^2\right)} \quad \textbf{(3-5)}$$

where $k_x = 1.4$, $k_y = 1.4$ and $k_z = 1.0$ are multiplying factors for each axis as suggested by the ISO 2631-1 standard. However, in this thesis only the vertical vibration is considered; thus the total value of the frequency-weighted RMS acceleration a_v value is identical to the frequency-weighted RMS acceleration in the vertical direction a_{wz}. Hence Eqn. (3-5) is rewritten as follows:

$$a_v = \sqrt{k_x^2 a_{wz}^2} = a_{wz} = a_w \quad \textbf{(3-6)}$$

The frequency weighting function (filter) in the vertical direction W_k considers the human body sensitivity frequency range when exposed to the vertical vibration in which the human body is most sensitive to vertical vibration energy over a frequency range of 4-8 Hz. The ISO 2631-1 standard provides mathematical formulae to design the frequency weighting function (filter) in the vertical direction W_k for seated posture, as given in Annex A of the ISO 2631-1 standard. Figure 3-1 illustrates the magnitude (dB) of the W_k over a one-third octave frequency band in which more weighting values are given over the human body sensitivity frequency range.

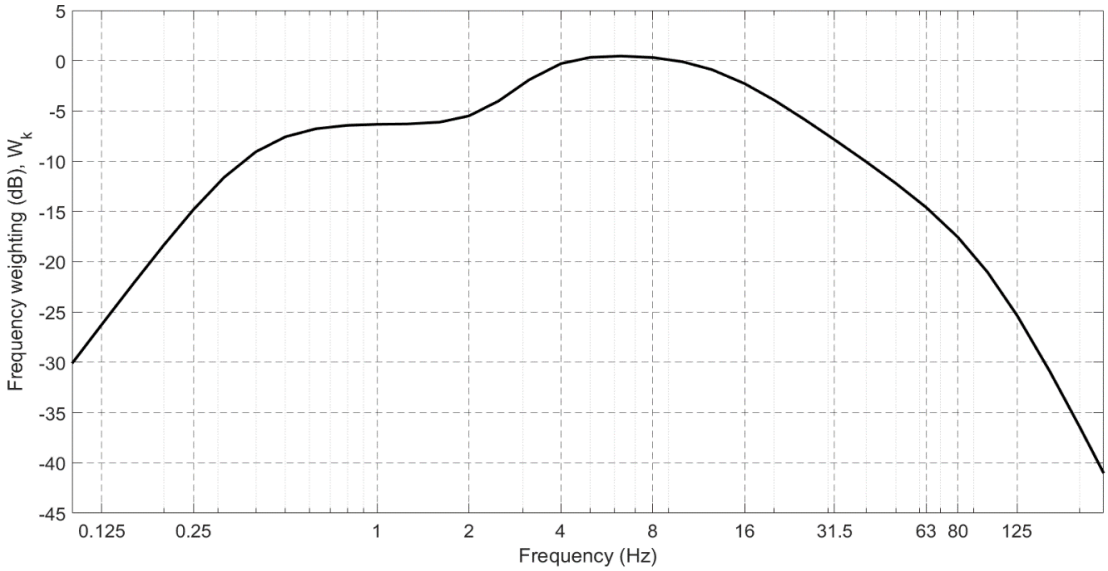

Figure 3-1: Frequency weighting curve for the vertical direction based on ISO 2631-1

Also, the ISO 2631-1 standard provides approximated levels of comfort associated with vibration environments based on the total value of the frequency-weighted RMS acceleration

a_v as listed in Table 3-1, which can also be used to judge the effectiveness of a seat suspension system.

Table 3-1: Uncomfortable reactions level to vibration magnitudes (ISO 2631-1)

Level of uncomfortable	Frequency-weighted RMS acceleration a_v (m/s^2) range
Extremely uncomfortable	> 2.0
Very uncomfortable	1.25-2.5
Uncomfortable	0.8-1.6
Fairly uncomfortable	0.5-1.0
A little uncomfortable	0.315-0.63
Not uncomfortable	< 0.315

3.2.2 WVB exposure threshold limit values (TLVs)

The American Conference of Governmental Industrial Hygienists (ACGIH) [183] have suggested threshold limit values (TLVs) for exposures based on the ISO 2631-1standard [184], which refers to the approximated guidelines for safe zones levels of occupational exposure duration to WBV without affecting health [185]. These limit values related the acceleration magnitude regarding RMS value to exposure duration and frequency content. Figure 3-2 shows the suggested TLVs in the vertical direction in which they indicate that the magnitude of the acceleration regarding the RMS value is inversely related to the exposure time. Also, it shows that the acceleration magnitudes at the human body sensitive frequency range (4-8 Hz) are more significant than other frequencies. However, to use this chart for assessing a seat suspension system, the individual frequency-weighted RMS seat acceleration value $a_{w,RMS}$ at each centre frequency of the one-third octave bands has to be determined. The $a_{w,RMS}$ can be expressed mathematically as follows [186]:

$$a_{w,RMS}(N) = \sqrt{\int_{f_{li}}^{f_{ui}} W_k(f) S_y(f)\, df} \qquad \textbf{(3-7)}$$

where N = 1, 2, 3, ……, 20 is the index for the centre frequency of the one-third octave bands.

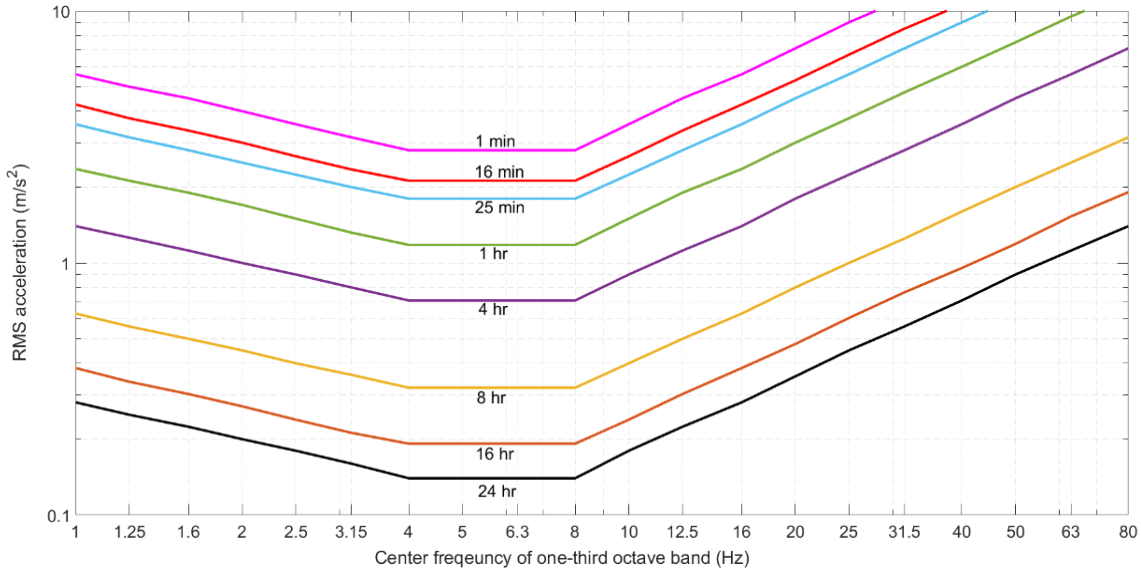

Figure 3-2: Exposure TLVs in the vertical direction (adapted from Finucane, 2010)

3.2.3 The Seat Effective Amplitude Transmissibility (SEAT) factor

The SEAT factor can be expressed mathematically as follows:

$$SEAT = \frac{(\ddot{x}_{se,w})_{rms}}{(\ddot{x}_{s,w})_{rms}} \qquad \textbf{(3-8)}$$

Where $(\ddot{x}_{se,w})_{rms}$ is the frequency-weighted RMS of the seat acceleration in the vertical direction and $(\ddot{x}_{s,w})_{rms}$ is the frequency-weighted RMS of the seat's base (chaises) also in the vertical direction. When the SEAT value is equal to one, this means that the seat transmits all its vibration from its base to its surface, whereas when this value is greater than unity, this indicates that the seat amplifies the transmitted vibration. However, it should be mentioned that the poor ride comfort, low back pain or fatigue cannot be directly quantified from the

SEAT factor, but it does provide a qualitative indicator of increased or decreased risk regarding such adverse effects.

Figure 3-3 presents the flowchart of the numerical methods used in this thesis to assess the ride comfort performance of a seat suspension system in the vertical direction. It starts by obtaining the acceleration time response at the seat's surface and base from either simulation or experimental tests. These values are transformed into the frequency domain using the FFT technique to obtain the corresponding PSD values. These are used to calculate the RMS and the frequency-weighted RMS acceleration values at the centre frequency of the one-third octave bands. Finally, these values are used to determine the total weighted-frequency RMS and the SEAT factor.

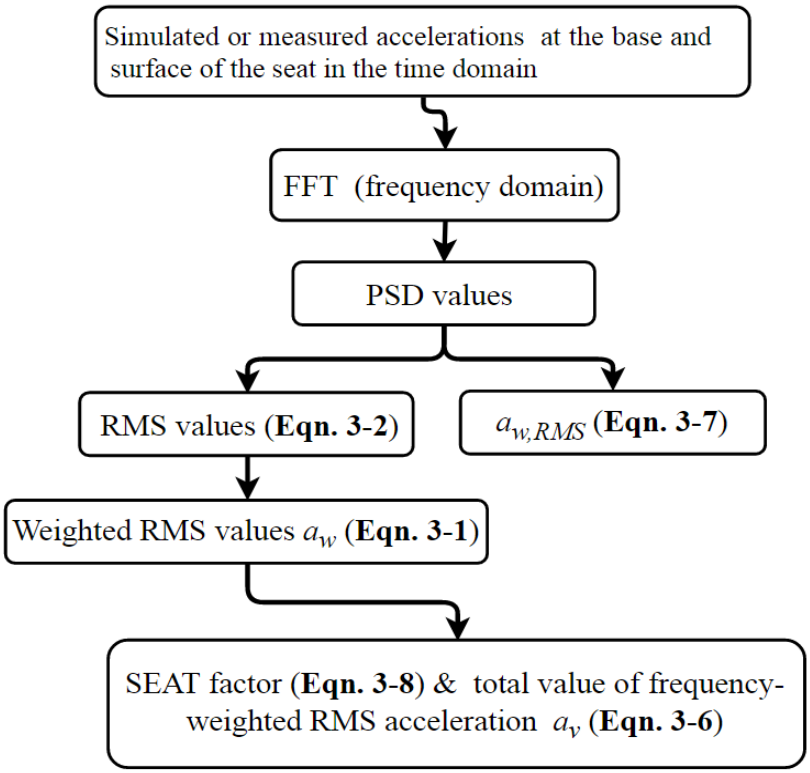

Figure 3-3: Flowchart of quantitative performance evaluation methods of a seat suspension system

3.3 Road profile generation

3.3.1 Random road profile

The main source of transmitted vibrations for vehicle drivers is from road disturbances through the vehicle body (chassis) and afterwards the driver's seat. Hence, to evaluate a seat suspension system with suppression those vibrations either in simulation or even in a laboratory environment, a technique is required to generate such road disturbances analytically. Whilst, harmonic waves or the step function can be easily employed in this case; they are inefficient for mimicking actual road conditions [187]. However, a random road profile can be a proper selection, as most of road disturbance profiles are random and they include the human body sensitive frequency range. To generate a random road profile, the road displacement profile can be represented by a power spectral density (PSD) function. This depends on the measurements of the surface profile for a reference plane [188]. The ISO 8608 (ISO 8608:1995) proposes an approximated formula to obtain the PSD function of the road roughness as follows:

$$\Phi(\Omega) = \Phi(\Omega_0)\left(\frac{\Omega}{\Omega_0}\right)^{-w} \quad \textbf{(3-9)}$$

where $\Omega = \frac{2\pi}{L}$ (rad/m) is the angular spatial frequency, L is the wavelength and w is the waviness, which has a value of 2 for most of the roads. $\Phi(\Omega_0)$ is the reference PSD value for a given road class at the reference angular spatial frequency $\Omega_0 = 1$ (rand/m). The reference values of the PSD at $\Omega_0 = 1$ (rand/m) in the longitudinal direction (vertical direction) for different road classes are given by ISO 8608 as presented in Table 3-2 and illustrated in Figure 3-4, in which the road is categorised by eight classes from A to H. However, in the case of using a linear suspension model, only road classes from A to E can be utilised to excite the model [187]. However, at low spatial frequency Eqn. (3-9) tends to infinity, so that it is modified as follows [188]:

$$\Phi(\Omega) = \begin{cases} \Phi(\Omega_0)\,\Omega_1^{-2} & ,for\ 0 \le \Omega \le \Omega_1 \\ \Phi(\Omega_0)\left(\frac{\Omega}{\Omega_0}\right)^{-2} & ,for\ \Omega_1 < \Omega \le \Omega_N \\ 0 & ,for\ \Omega > \Omega_N \end{cases} \quad \textbf{(3-10)}$$

Table 3-2: Road roughness values for different classes [188]

Road class	Degree of roughness $\Phi(\Omega_0)$ $(10^{-6}\ m^3)$ for $\Omega_0 = 1\ rad/m$		
	Lower limit	Geometric mean	Upper limit
A (very good)	----------	1	2
B (good)	2	4	8
C (average)	8	16	32
D (poor)	32	64	128
E (very poor)	128	256	512
F	512	1,024	2,048
G	2,048	4,096	8,192
H	8,192	16,384	32,768

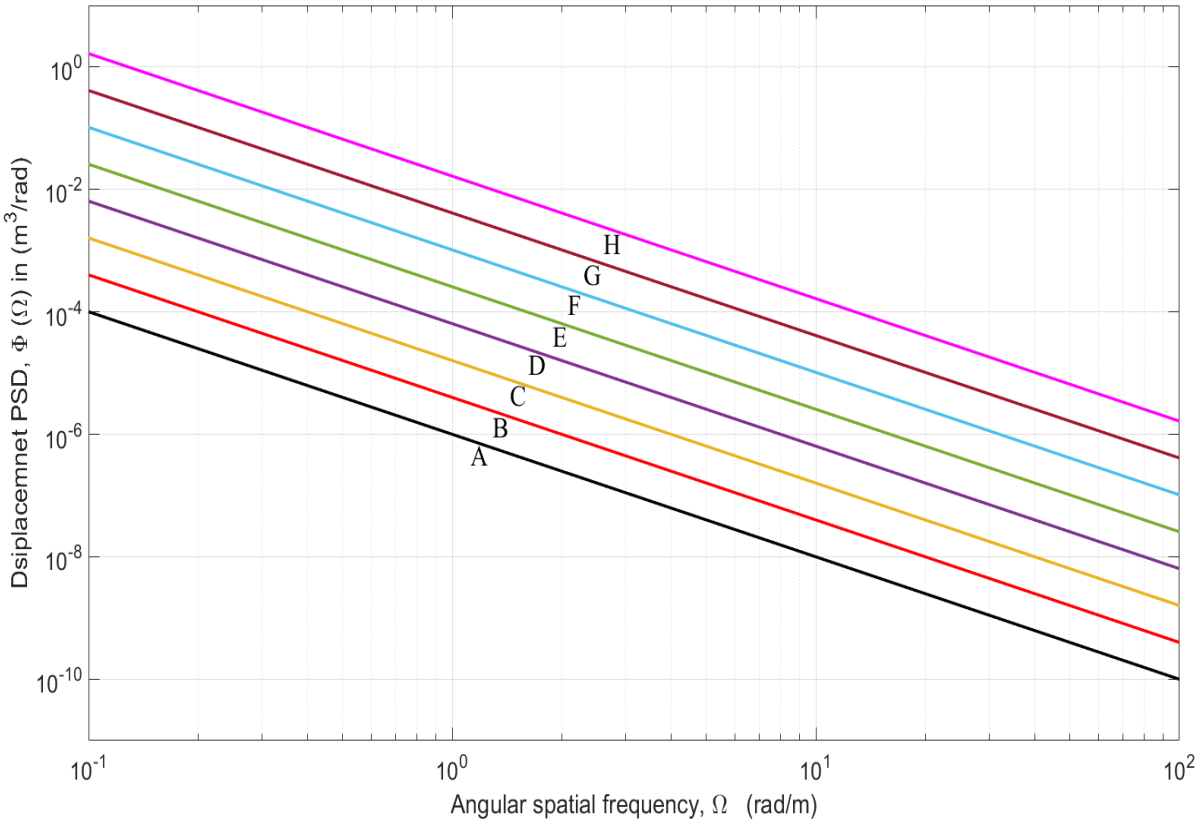

Figure 3-4: Road PSD classes (adapted from Tyan et al., 2009)

The values of Ω_1 and Ω_N are suggested by the ISO 8606 to be 0.02π (rad/m) and 6π (rad/m), respectively [188] which covers a wavelength band of (0.333-100 m). When the vehicle is traveling over a specified road segment of length L and constant velocity V, then the random road profile as a function of a travelled path s, can be approximated using a superposition of N ($\rightarrow \infty$) sine waves as follows:

$$x_r(s) = \sum_{n=1}^{N} A_n \, sin(\Omega_n s - \varphi_n) \qquad \textbf{(3-11)}$$

where the amplitudes A_n are given by:

$$A_n = \sqrt{\Phi(\Omega_n) \, \frac{\Delta\Omega}{\pi}} \qquad \textbf{(3-12)}$$

where $\Delta\Omega = \frac{\Omega_N - \Omega_1}{N-1}$ and φ_n is a random phase angle between $(0, 2\,\pi)$. The term $\Omega\, s$ in Eqn. (3-11) is equivalent to:

$$\Omega\, s = \frac{2\,\pi}{\lambda}\, s = \frac{2\,\pi}{\lambda}\, V\, t = \omega\, t \qquad \textbf{(3-13)}$$

in which λ is the wavelength and ω (rad/sec) is the angular frequency in the time domain. From Eqns. (11) and (13) the road profile in the time domain is given as follows:

$$x_r(t) = \sum_{n=1}^{N} A_n \, sin(n\omega_o t - \varphi_n) \qquad \textbf{(3-14)}$$

where $\omega_0 = V\,\Delta\Omega$ (rad/sec) is the fundamental temporal frequency in the time domain. Figure 3-5 shows an example of a generated random road profile of class E (very poor) in the time domain and vehicle speed of 40 and 100 km/h using Eqn. (3-14), while the corresponding PSDs are presented in Figure 3-6.

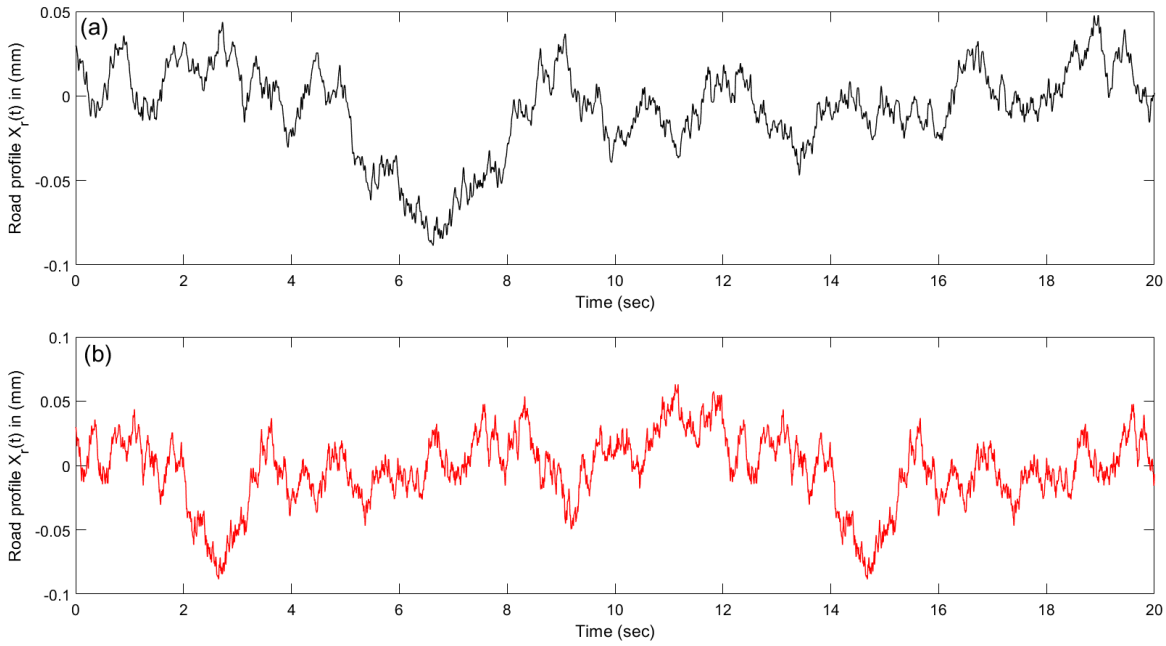

Figure 3-5: Example of random road profiles of class E at vehicle speeds of (a) 40 km/h and (b) 100 km/h

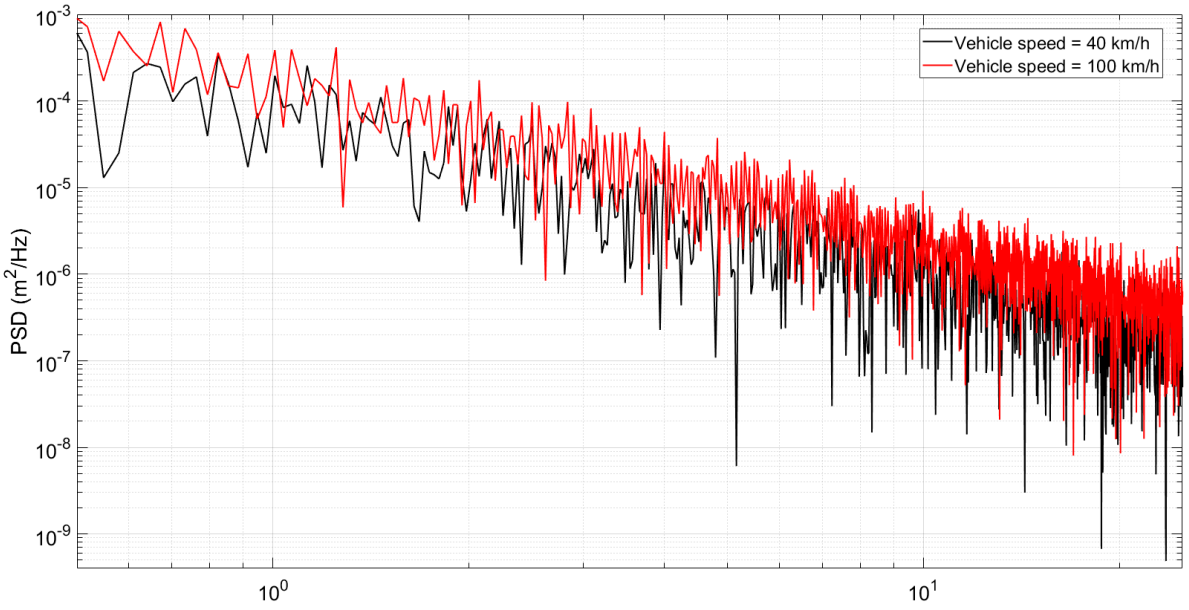

Figure 3-6: PSD of generated random road profiles of class E at vehicle speeds of 40 and 100 km/h

3.3.2 Bump road profile

Although the random road described previously being sufficient to cover most road profiles, it is not enough to represent shock events, such as a pothole or a bump road profile. These

disturbances are characterised as discrete events of relatively high magnitude and short duration [189]. Hence, in this thesis, this type of road disturbances is also considered to analyse the transient response of a seat suspension as well as generate excitations that are sufficient for studying the effect of end-stop impacts. Despite, there being many mathematical formulas used to represent this type of road profile, there is no standard one. In this work, two formulae have been used to generate such a road profile. The first, which is only depends on the bump height, can be expressed mathematically as follows [190]:

$$x_r(t) = \begin{cases} a(1 - cos(8\,\pi\,t))/2 & ; \quad 0.5 \le t \le 0.75 \\ 0 & ; \quad t > 0.75 \end{cases} \qquad \textbf{(3-15)}$$

where, a denotes the bump height. The second one considers the effect of vehicle speed and is given mathematically as follows [191]:

$$x_r(t) = \begin{cases} \frac{a}{2}\left(1 - cos\left(\frac{2\pi V}{l}\,t\right)\right) & , 0 \le t \le \frac{l}{V} \\ 0 & , t > \frac{l}{V} \end{cases} \qquad \textbf{(3-16)}$$

where l is the length of the bump.

3.4 Conclusions

The weighted-frequency RMS acceleration and SEAT factor are sufficient quantitative measures for evaluating and characterising a driver's seat suspension system performance for improving ride quality and reducing WBV when the vehicle is exposed to vertical vibration. This is because they consider the acceleration magnitude and frequency content of the transmitted vibration as well as the seat vibration isolation efficiency. Hence, they are used to evaluate and compare different developed active seat suspension systems in this thesis. In addition, a random road profile can be a proper road input, as most of road disturbance profiles are random and also they contain the frequencies in which the human body is most sensitive to vertical vibration.

Chapter 4
Simulation Studies of Seat Suspension Systems

This chapter describes simulating and characterising the performance of different seat suspension systems based on the numerical quantities that are explained in the previous chapter and studying strengths and weaknesses. These include passive, semi-active and active seat suspension systems that are controlled by classical control algorithms. For simplicity, the simulations were performed using a linear quarter vehicle model (QvM) with 2 DOFs and a 1 DOF lumped-spring-mass seat suspension model, in both frequency and time domains including different working conditions and road profiles.

4.1 Introduction

To gain sufficient understanding and to explore the weaknesses and strengths of semi-active and active seat suspension control algorithms, this chapter presents a simulation analysis and performance evaluation of some well-known classical control strategies including:

- Two versions of skyhook (SH), namely, 2-states and linear.
- Acceleration Driven Damper (ADD).
- Linear quadratic regulator (LQR) controller

The first two approaches that are found in the literature deployed for a semi-active seat suspension while the linear quadratic regulator (LQR) controller is utilised to control the active seat suspension. The simulation was accomplished using an integrated linear mathematical model of quarter vehicle model (QvM) and seat suspension with a 1DOF in MATLAB and Simulink environments. The simulation was performed in both the frequency and time domains, with outcomes being compared with a passive seat suspension. The analysis in the time domain involves different excitation inputs, including bump and random road profiles across different vehicle speeds. Finally, the simulated results are analysed, discussed and conclusions are oulined.

4.2 Simulation models

To illustrate the features and evaluate the performance of the passive, semi-active and active seat suspension systems, mathematical models for the vehicle and the seat suspension are required. The vehicle is represented by a linear quarter vehicle model (QvM) with 2 DOFs. This model has been widely used in the literature as it is simple and can capture adequate information concerning the vertical motion of the vehicle [131,192]. For simplicity, the seat suspension and the human body are assumed to be a 1 DOF linear lumped spring-damper-mass system Figure 4-1 (a) shows the passive seat suspension configuration integrated with a QvM model, in which m_{se}, m_s and m_{us} are the combined seat and driver mass, the sprung mass and the unsprung mass, respectively. The displacements of the corresponding masses in the vertical direction are x_{se}, x_s and x_{us} , respectively, while x_r is the road excitation displacement. The stiffness and damping of the seat suspension are k_{se} and c_{se}, respectively, while k_s and c_s are those of the vehicle suspension. The tyre dynamics are represented only by a stiffness k_t, as the tyre damping can be neglected. Assuming linear characteristics for both the seat and vehicle suspensions, the equations of motion of the passive system are derived as:

$$m_{se}\ddot{x}_{se} = -\,c_{se}\,(\dot{x}_{se} - \dot{x}_s) - \,k_{se}\,(x_{se} - x_s) \tag{4-1}$$

$$m_s\ddot{x}_s = \,c_{se}\,(\dot{x}_{se} - \dot{x}_s) + \,k_{se}\,(x_{se} - x_s) - \,c_s\,(\dot{x}_s - \dot{x}_{us}) - \,k_s\,(x_s - x_{us}) \tag{4-2}$$

$$m_{us}\ddot{x}_{us} = \,c_s\,(\dot{x}_s - \dot{x}_{us}) + \,k_s\,(x_s - x_{us}) - \,k_t\,(x_{us} - x_r) \tag{4-3}$$

In the case of the semi-active seat suspension the fixed damping coefficient $\boldsymbol{c_{se}}$ is replaced with an adjustable damping coefficient c_{sa} , as shown in Figure 4-1 (b). Whilst in the case of active seat suspension, as presented in Figure 4-1 (c), Eqns. (4-1) and (4-2) are rewritten to include the actuator control force F_a , as follows:

$$m_{se}\ddot{x}_{se} = -\,c_{se}\,(\dot{x}_{se} - \dot{x}_s) - \,k_{se}\,(x_{se} - x_s) + F_a \tag{4-4}$$

$$m_s\ddot{x}_s = c_{se}\,(\dot{x}_{se} - \dot{x}_s) + k_{se}\,(x_{se} - x_s) - c_s\,(\dot{x}_s - \dot{x}_{us}) - k_s\,(x_s - x_{us}) - F_a \quad \textbf{(4-5)}$$

Assume the state space variables vector is as follows:

$$x(t) = [x_1(t) \quad x_2(t) \quad x_3(t) \quad x_4(t) \quad x_5(t) \quad x_6(t)\,]^T$$

where $x_1(t) = x_{se}(t) - x_s(t)$ represents the seat suspension deflection, $x_2(t) = \dot{x}_{se}(t)$ represents the seat velocity, $x_3(t) = x_s(t) - x_{us}(t)$ represents the vehicle suspension deflection, $x_4(t) = \dot{x}_s(t)$ represents the sprung mass (vehicle chaises) velocity, $x_5(t) = x_{us}(t) - x_r(t)$, and $x_6(t) = \dot{x}_{us}(t)$ represents the unsprung mass velocity. Then, the dynamic Eqns. (4-3 to 4-5) can be expressed in a state-space formula as follows:

$$\dot{x}(t) = A\,x(t) + B\,u(t) + L\,\dot{x}_r(t) \quad \textbf{(4-6)}$$

$$y = C\,x(t) + D\,u(t) \quad \textbf{(4-7)}$$

where $u(t) = F_a(t)$ and the matrices A, B and L are defined for the passive seat suspension case as follows:

$$A = \begin{bmatrix} 0 & 1 & 0 & -1 & 0 & 0 \\ \frac{-k_{se}}{m_{se}} & \frac{-C_{se}}{m_{se}} & 0 & \frac{C_{se}}{m_{se}} & 0 & 0 \\ 0 & 0 & 0 & 1 & 0 & -1 \\ \frac{k_{se}}{m_s} & \frac{C_{se}}{m_s} & \frac{-k_s}{m_s} & \frac{(C_{se}+C_s)}{m_s} & 0 & \frac{C_s}{m_s} \\ 0 & 0 & 0 & 0 & 0 & 1 \\ 0 & 0 & \frac{k_s}{m_{us}} & \frac{C_s}{m_{us}} & \frac{k_t}{m_{us}} & \frac{-C_s}{m_{us}} \end{bmatrix}; \quad \textbf{(4-8)}$$

$$L = \begin{bmatrix} 0 \\ 0 \\ 0 \\ 0 \\ -1 \\ 0 \end{bmatrix}; \quad B = \begin{bmatrix} 0 \\ 0 \\ 0 \\ 0 \\ 0 \\ 0 \end{bmatrix}$$

where for the semi-active system case the matrix A becomes:

$$A = \begin{bmatrix} 0 & 1 & 0 & -1 & 0 & 0 \\ \frac{-k_{se}}{m_{se}} & \frac{-C_{sa}}{m_{se}} & 0 & \frac{C_{sa}}{m_{se}} & 0 & 0 \\ 0 & 0 & 0 & 1 & 0 & -1 \\ \frac{k_{se}}{m_s} & \frac{C_{sa}}{m_s} & \frac{-k_s}{m_s} & \frac{(C_{sa}+C_s)}{m_s} & 0 & \frac{C_s}{m_s} \\ 0 & 0 & 0 & 0 & 0 & 1 \\ 0 & 0 & \frac{k_s}{m_{us}} & \frac{C_s}{m_{us}} & \frac{k_t}{m_{us}} & \frac{-C_s}{m_{us}} \end{bmatrix} \quad \textbf{(4-9)}$$

, and for the active system the matrices A and B become:

$$A = \begin{bmatrix} 0 & 1 & 0 & -1 & 0 & 0 \\ \frac{-k_{se}}{m_{se}} & \frac{-C_{se}}{m_{se}} & 0 & \frac{C_{se}}{m_{se}} & 0 & 0 \\ 0 & 0 & 0 & 1 & 0 & -1 \\ \frac{k_{se}}{m_s} & \frac{C_{se}}{m_s} & \frac{-k_s}{m_s} & \frac{(C_{se}+C_s)}{m_s} & 0 & \frac{C_s}{m_s} \\ 0 & 0 & 0 & 0 & 0 & 1 \\ 0 & 0 & \frac{k_s}{m_{us}} & \frac{C_s}{m_{us}} & \frac{k_t}{m_{us}} & \frac{-C_s}{m_{us}} \end{bmatrix}; \quad \textbf{(4-10)}$$

$$B = \begin{bmatrix} 0 \\ \frac{1}{m_{se}} \\ 0 \\ \frac{-1}{m_s} \\ 0 \\ 0 \end{bmatrix}$$

The output state variables y are the seat acceleration and the seat suspension travel, hence the matrices C and D are given as:

$$C = \begin{bmatrix} \frac{-k_{se}}{m_{se}} & \frac{-C_{se}}{m_{se}} & 0 & \frac{C_{se}}{m_{se}} & 0 & 0 \\ 1 & 0 & 0 & 0 & 0 & 0 \end{bmatrix}$$

$$D = \begin{bmatrix} \frac{1}{m_{se}} & 0 & 0 & 0 & 0 & 0 \\ 0 & 0 & 0 & 0 & 0 & 0 \end{bmatrix} \quad \textbf{(4-11)}$$

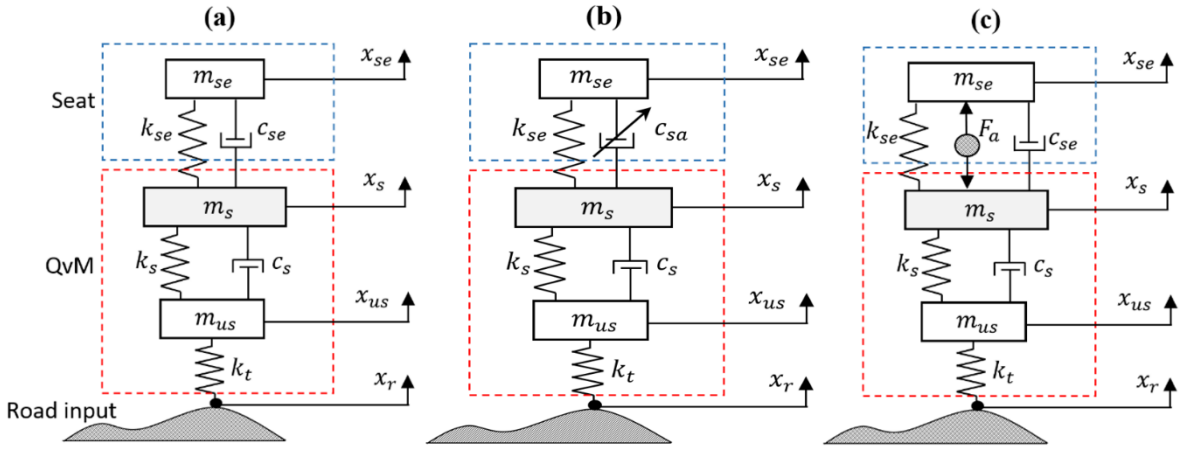

Figure 4-1: QvM and 1 DOF seat suspension model: (a) Passive, (b) semi-active and (c) active

4.2.1 Semi-active seat suspension algorithms

Three semi-active seat suspension systems are used to analysis the characterises of a semi-active seat suspension system, these being based on using different control approaches in which the damping coefficient value is adjustable, namely, two versions of the classical semi-active controller skyhook (2-states and linear) and acceleration- driven damper (ADD). The mathematical formula of the adjustable damper coefficient c_{sa} for each of these approaches are given in Table 4-1.

Table 4-1: Mathematical formula of classical semi-active control algorithms [180]

Algorithm	Mathematical Formula
2- states skyhook	$C_{sa} = \begin{cases} c_{max} \; ; \; \dot{x}_{se}(\dot{x}_{se} - \dot{x}_s) > 0 \\ c_{min} \; ; \; \dot{x}_{se}(\dot{x}_{se} - \dot{x}_s) \leq 0 \end{cases}$ where $c_{max} = c_{sky}$
Skyhook-linear	$C_{sa} = \begin{cases} \dfrac{\alpha c_{max}(\dot{x}_{se} - \dot{x}_s) + (1-\alpha)c_{max}\dot{x}_{se}}{(\dot{x}_{se} - \dot{x}_s)} \; ; \; \dot{x}_{se}(\dot{x}_{se} - \dot{x}_s) > 0 \\ c_{min} \; ; \; \dot{x}_{se}(\dot{x}_{se} - \dot{x}_s) \leq 0 \end{cases}$
Acceleration driven damper (ADD)	$C_{sa} = \begin{cases} c_{max} \; ; \; \ddot{x}_{se}(\dot{x}_{se} - \dot{x}_s) > 0 \\ c_{min} \; ; \; \ddot{x}_{se}(\dot{x}_{se} - \dot{x}_s) \leq 0 \end{cases}$

where, α in the Skyhook-linear is a tuning parameter in the range of (0,1) and when $\boldsymbol{\alpha}$ is set to unity, the Skyhook-linear will be identical to the 2-states skyhook algorithm. It should be noted that for simulation this parameter was selected as 0.70 [180].

4.2.2 LQR (Linear quadratic regulator)

Whilst there are many control approaches that can be applied to study active seat suspension, the linear quadratic regulator (LQR) has been selected here as it is considered one of the classical control approaches [123] for linear multiinput-multioutput (MIMO) time-invariant systems and it is easy to design . The main idea of LQR, is to obtain an optimal solution that minimises a quadratic continuous-time cost function that satisfies the system specifications. In the case of seat suspension, the two important design criteria are minimising the seat acceleration, while keeping the seat suspension travel and actuator force capacity within their limits. Consequently, the cost function can be written as:

$$J = \int_0^\infty [\rho_1 \ddot{x}_{se}^2 + \rho_2 (x_{se} - x_s)^2 + \rho_3 u^2 \,] dt \qquad \textbf{(4-12)}$$

where, ρ_1, ρ_2 and ρ_3 represent weighting coefficients of the seat acceleration, seat travel suspension and the control force, respectively, with these weights being selected based on the

design specification of the system. Recalling the state variables x_1 to x_6 defined in section 2.4, this gives:

$x_{se} - x_s = x_1$ and $x_2 = \dot{x}_{se}$, therefore:

$\dot{x}_2 = \ddot{x}_{se}$

Using equation (4-4), it gives:

$$\ddot{x}_{se} = -\frac{1}{m_{se}}[c_{se}(\dot{x}_{se} - \dot{x}_s) + k_{se}(x_{se} - x_s)] + \frac{1}{m_{se}}F_a$$

Therefore,

$$\dot{x}_2 = -\frac{1}{m_{se}}[c_{se}(x_2 - x_4) + k_{se}x_1] + \frac{1}{m_{se}}F_a \qquad \textbf{(4-13)}$$

Equation (4-12), can be rewritten as follows:

$$J = \int_0^\infty \left[\rho_1\left[-\frac{1}{m_{se}}[c_{se}(x_2 - x_4) + k_{se}x_1] + \frac{1}{m_{se}}F_a\right]^2 + \rho_2 x_1^2 + \rho_3 u^2\right]dt \qquad \textbf{(4-14)}$$

Eqn. (4-14) can be rewritten in a more general form as follows:

$$J = \int_0^\infty [x^T Q x + 2\, x^T N u + u^T R u]dt \qquad \textbf{(4-15)}$$

where,

$$Q = \begin{bmatrix} \rho_1\left(\frac{k_{se}}{m_{se}}\right)^2 + \rho_2 & \rho_1\frac{k_{se}C_{se}}{m_{se}^2} & 0 & -\rho_1\frac{k_{se}C_{se}}{m_{se}^2} & 0 & 0 \\ \rho_1\frac{k_{se}C_{se}}{m_{se}^2} & \rho_1\left(\frac{C_{se}}{m_{se}}\right)^2 & 0 & -\rho_1\left(\frac{C_{se}}{m_{se}}\right)^2 & 0 & 0 \\ 0 & 0 & 0 & 0 & 0 & 0 \\ -\rho_1\frac{k_{se}C_{se}}{m_{se}^2} & -\rho_1\left(\frac{C_{se}}{m_{se}}\right)^2 & 0 & \rho_1\left(\frac{C_{se}}{m_{se}}\right)^2 & 0 & 0 \\ 0 & 0 & 0 & 0 & 0 & 0 \\ 0 & 0 & 0 & 0 & 0 & 0 \end{bmatrix}; N = \begin{bmatrix} \rho_1\frac{k_{se}}{m_{se}^2} \\ -\rho_1\frac{C_{se}}{m_{se}^2} \\ 0 \\ -\rho_1\frac{C_{se}}{m_{se}^2} \\ 0 \\ 0 \end{bmatrix}$$

$; R = \left(\frac{\rho_1}{m_{se}^2} + \rho_3\right)$

And the active control force is given by:

$$F_a(t) = -K\, x(t) \qquad \textbf{(4-16)}$$

where K is a gain matrix given by [123] :

$$K = R^{-1} B^T S \quad \textbf{(4-17)}$$

In which S is a symmetric positive semidefinite matrix that represents the solution of the following Riccati equation:

$$SA + A^T S + C^T C - SB\, R^{-1} B^T S = 0 \quad \textbf{(4-18)}$$

4.3 Simulation results

The numerical values used to simulate the passive system are listed in Table 4-2. The maximum and minimum damping coefficients (c_{max} and c_{min}) were assumed as being 50% and 200% of the nominal damping coefficient C_{se}, respectively. Also, the weighting coefficients ρ_1, ρ_2 and ρ_3 for the LQR controller were assumed as being 1, 0.5 and $1x10^{-5}$, respectively. The integrated model was modelled in Simulink -MATLAB and the optimum feedback gain K was obtained using the LQR MATLAB code as:

$$K = [-2.43 \times 10^4 \quad -54.71 \quad 1.55 \times 10^3 \quad 336.032 \quad 4.076 \times 10^3 \quad -2.89]$$

The following subsections provide a comparison between the performances of passive, semi-active and active seat suspensions in attenuating the seat vertical acceleration in both the frequency and time domains, under different road excitations, including bump and random road profiles.

Table 4-2: QvM and passive seat suspension simulation parameters

Parameter	Value	unit
m_s	250	kg
m_{us}	20	kg
C_s	1500	kN.s/m
k_s	10.0	kN/m
k_t	180.0	kN/m
m_{se}	70.0	kg
C_{se}	830.0	kN/m
k_{se}	31.0	kN/m

4.3.1 Frequency response analysis

Figure 4-2 compares the simulated frequency response of the seat acceleration transmissibility of the semi-active and active controlled seat suspensions, with respect to the sprung mass of the QvM (chassis), with a passive system using soft (c_{min}) and hard (c_{max}) damping values, over low-frequency range (1-20 Hz). It can be clearly observed that the passive seat suspension with the hard damping is efficient in reducing the seat acceleration over low-frequency range, partially around the seat resonant frequency as well as the seat suspension travel as shown in Figure 4-2. However, at higher frequencies its performance in attenuating vibration is deteriorating and soft damping is preferable, but this is at the cost of providing a large seat suspension travel, as presented Figure 4-3. Hence, a trade-off arises between isolating vibration at low frequency and high frequency simultaneously, while not deteriorating the seat suspension deflection. Semi-active and active controlled seat suspensions perform better than the passive system in attenuating the seat acceleration, especially over the human body sensitive frequency (HBSF) range (4-8 Hz), where both ADD semi-active and LQR active seat suspensions show the best levels of vibration reduction. However, the SH 2-states and SH linear provides almost identical results, while the ADD is very similar to the passive system over a frequency range of less than 4 Hz.

In general, the LQR active seat suspension delivers the best performance in vibration attenuation over a wide frequency range, especially over the human body sensitivity frequency range. However, this is at the cost of deteriorating the seat suspension travel compared to the passive system, as illustrated in Figure 4-2 where the ADD semi-active seat suspension shows the worst deterioration level.

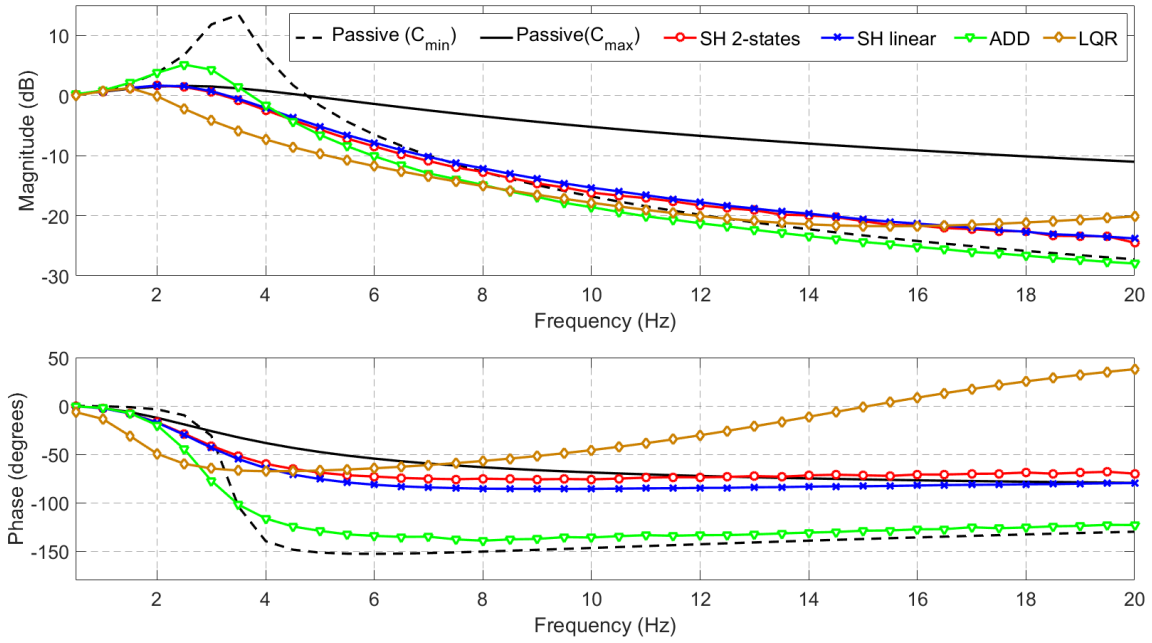

Figure 4-2: Frequency response of the seat acceleration using different seat suspension configurations

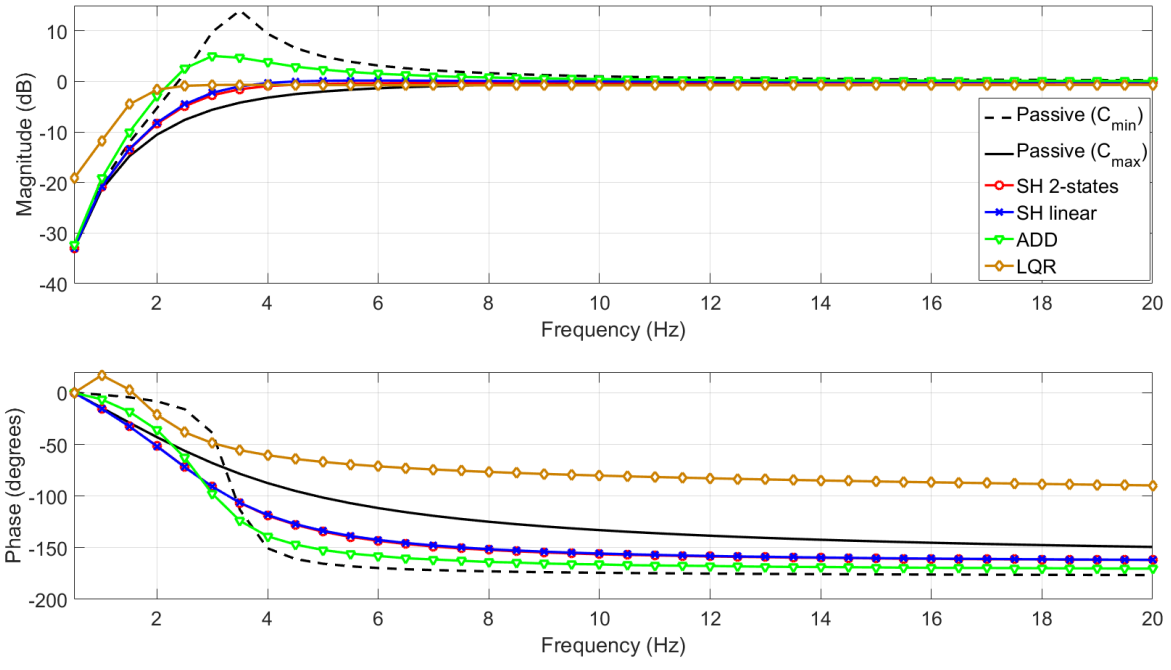

Figure 4-3: Frequency response of the seat suspension travel using different seat suspension configurations

4.3.2 Time response analysis

4.3.2.1 Random road input

In this section, the aforementioned controlled and passive seat suspensions are analysed and evaluated in the time domain when the QvM model is excited by two types of road profiles, namely, bump and random profiles. For the case of the random road profile, a random road profile of PSD roughness of class E (very poor road), as described previously in chapter 3, with a vehicle speed of 60 km/h, as shown in Figure 4-3 was used to excite the QvM. However, the simulation was carried out under different vehicle speeds (20, 40, 60, 80 and 100 km/h).

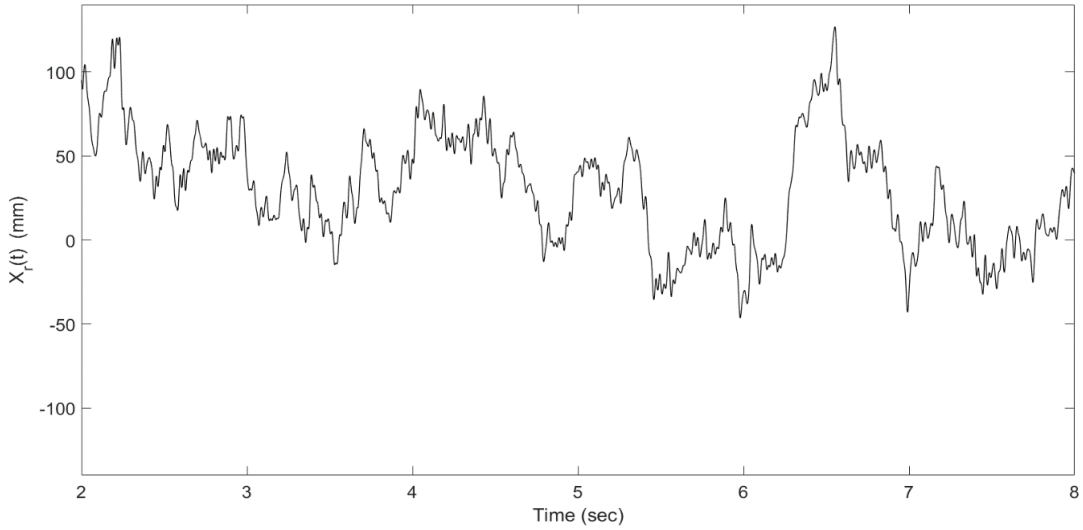

Figure 4-4: Random road profile at a vehicle speed of 60 km/h

For the sake of brevity, the time responses in terms of the seat acceleration and seat suspension travel are shown only for the vehicle speed of 60 km/h, as illustrated in Figures 4.5 and 4.6.
It is clear from Figure 4-5 that both skyhook semi-active seat strategies slightly reduce both the seat acceleration and seat suspension travel when compared to the passive system. This is due to the passivity constraint regarding the semi-active suspension configuration where the controller can only dissipate energy from the system. However, the SH 2-states produces sharp acceleration due to rapid switching between the high and low damping coefficient values as illustrated in Figures 4.7 (a) and (b).

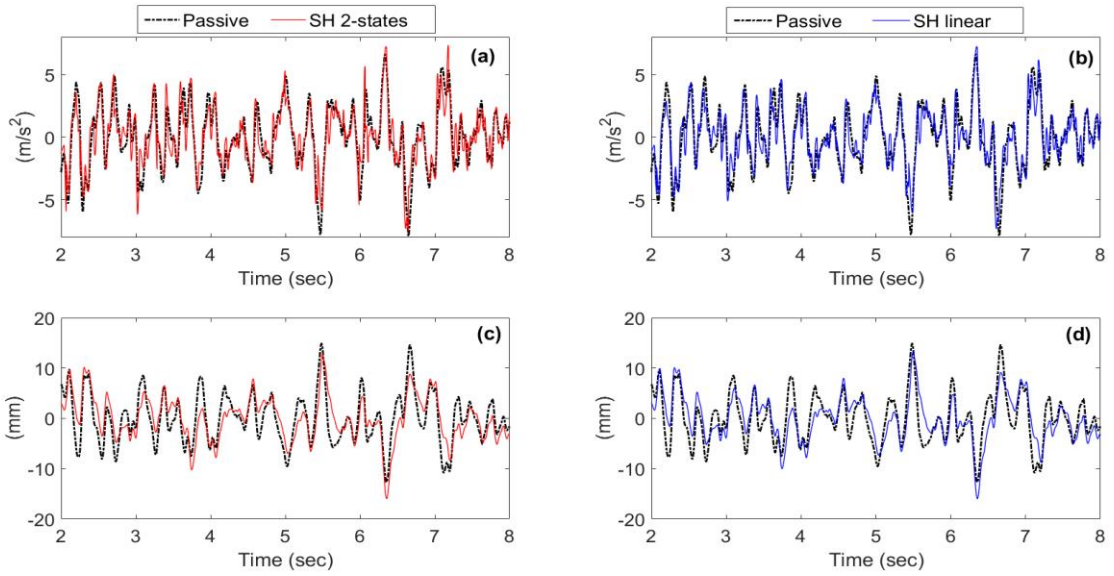

Figure 4-5: Time responses of the seat suspension displacement for the passive and semi-active seat suspensions under random road excitation

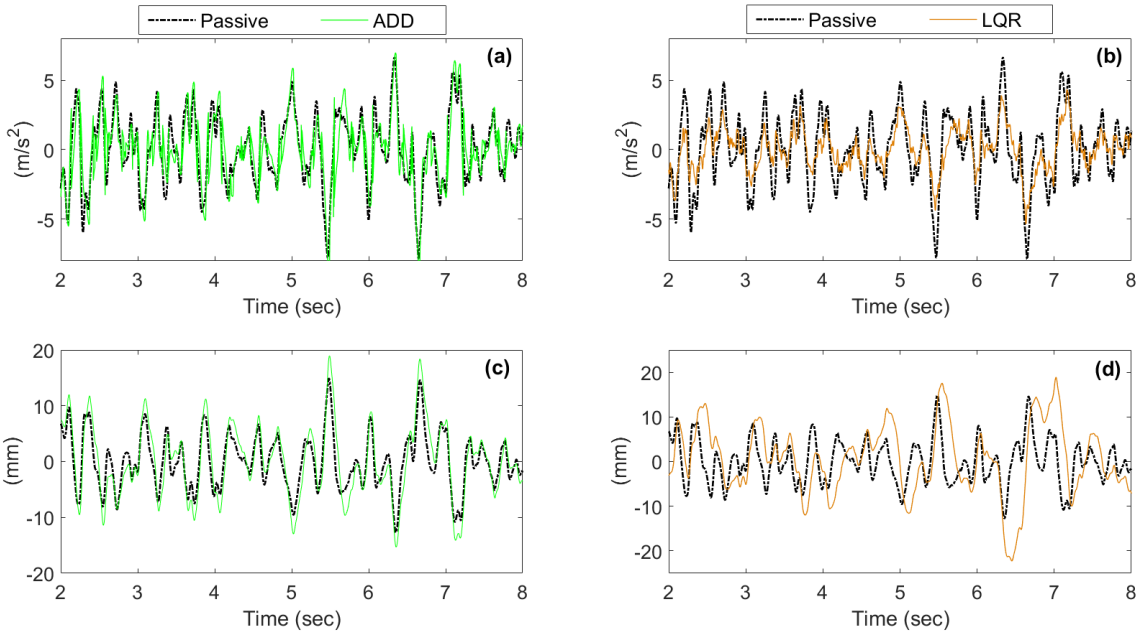

Figure 4-6: Time responses of the seat acceleration for the passive, ADD semi-active and LQR active seat suspensions under random road excitation

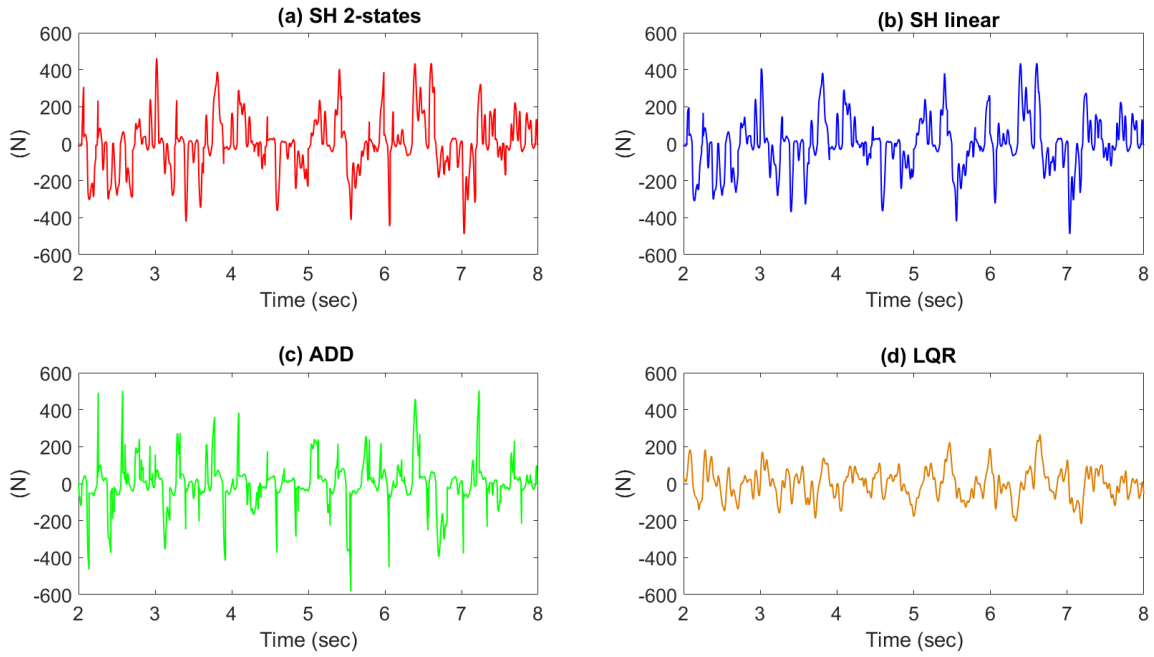

Figure 4-7: Time responses of the demand force for the semi-active and active seat suspensions

Moreover, the attenuation level of these strategies is limited to narrowband frequency range less than 5 Hz, as shown in Figures 4.8 (a) and (b), where the PSD of these systems becomes worse than the passive system in the higher frequency range.

The semi-active seat suspension using the ADD strategy shows a little improvement in reducing the seat acceleration compared to the passive system as shown in Figure 4.8 (c), however, this improvement is at the cost of increasing the seat suspension travel as illustrated in Figure 6. Not only this, but also, the seat acceleration attenuation performance is limited to a narrowband frequency range, as shown in Figure 4.8 (c), in which the PSD of the ADD semi-active suspension is higher than that of the passive system at low (< 3 Hz) and high frequency (> 9 Hz). This is due to the switching law that utilises the seat acceleration, which results in a chattering problem [180]. On the other hand, the LQR active seat suspension provides superior vibration attenuation when compared to the passive system with reasonable seat suspension travel and actuator force as shown in Figure 4.6 (b) and Figure 4.7 (b) Figure, respectively. Moreover, the PSD of the LQR active suspension is lower than that of the passive system over the whole frequency range of interest, as presented in Figure 4.8 (d).

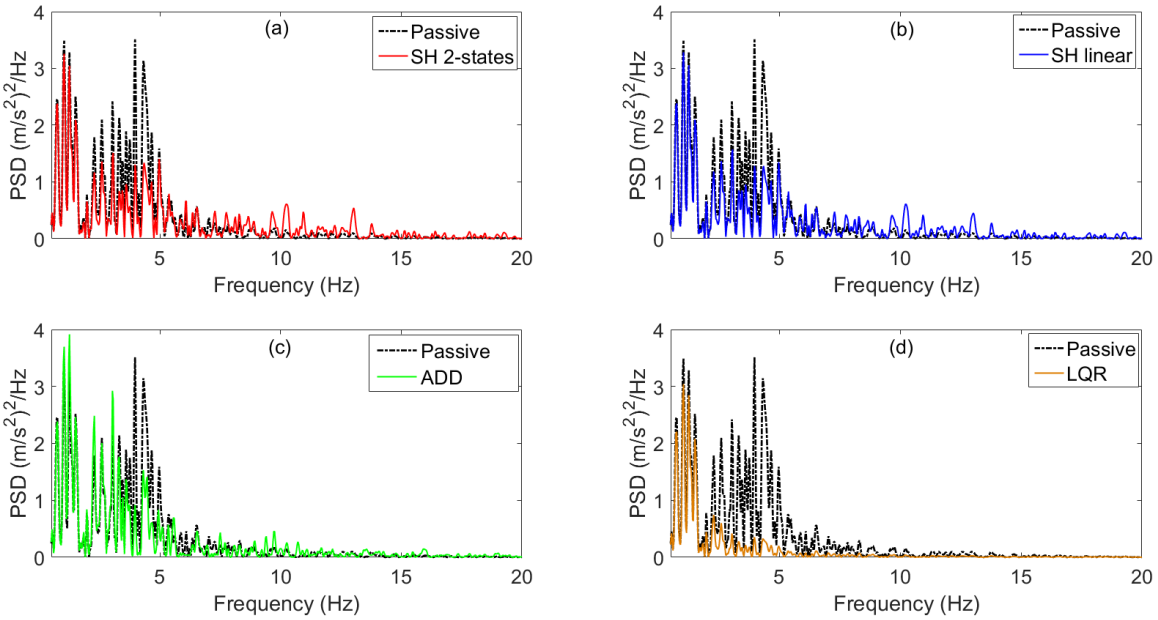

Figure 4-8: PSDs of the seat acceleration for the semi-active and active seat suspensions under random road excitation

Furthermore, the SEAT factor values of the semi-active and active seat suspension systems under different vehicle speeds are compared to the passive seat suspension, as presented in Figure 4-9. It can be seen that the semi-active seat suspensions slightly reduce the SEAT factor compared to the passive one, while it is significantly reduced with the LQR active seat suspension, regardless of the vehicle speed, where the percentage improvements are almost 50 %.

Figure 4-9 also shows the frequency-weighted RMS seat acceleration. Once again, the LQR active seat suspension has much lower frequency-weighted RMS seat acceleration compared to that of the passive system, with ≥ 50 % improvement across the range of vehicle speeds. However, the semi-active seat suspensions have somewhat lower frequency-weighted RMS seat acceleration compared to the passive system. Moreover, at intermediate and high vehicle speeds the passive and semi-active seat suspension systems, often provide ''very uncomfortable'' ride quality level according to the ISO 2631-1 standard.

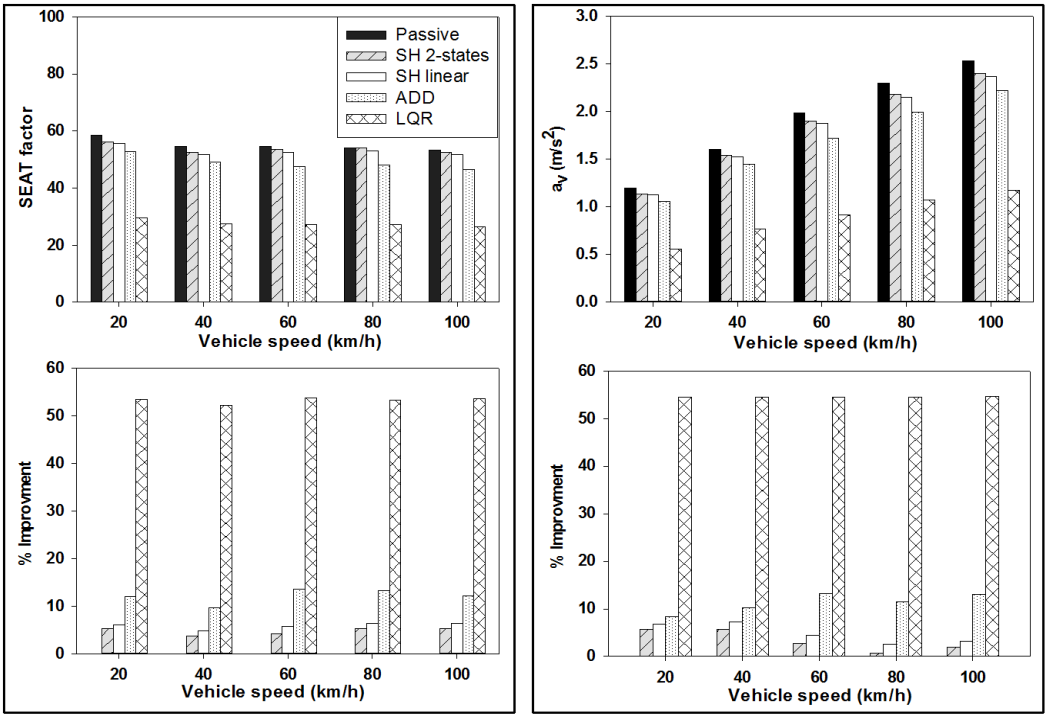

Figure 4-9: Performance assessment of semi-active and active seat suspension configurations under different vehicle speeds

Adaptation of a seat suspension system to the uncertainties in the system parameters and working conditions plays a vital role in performance evaluation of such a system. However, the driver's weight and the vehicle speed corresponding to the most system parameters and working conditions variations. Consequently, the sensitivity of passive, semi-active and active seat suspensions to these factors is evaluated in terms of the SEAT factor. Because the driver's weight is assumed to be implicitly included within the seat mass $\boldsymbol{m_{se}}$, then the variation in his/her weight is obtained by changing the value of the seat mass. Moreover, due to the nature of the random road profile, the simulations were repeated five times for 20 seconds, and the mean values were then taken. Figure 4-10 presents the sensitivity maps of the SEAT factor for the different seat suspension configurations regarding the variation of the driver's weight and vehicle speeds. It is notable that the isolation of the transmitted vibration achieved by the passive system is highly sensitive to both changes in the driver's weight and vehicle speed. Moreover, light drivers are exposed to more vibration energy than heavy ones, regardless of the vehicle speed. Comparable results are shown within the semi-active seat suspensions, but with less transmitted vibration energy, while conversely, the LQR active seat suspension is slightly sensitive to variation in both the driver's weight and vehicle speed.

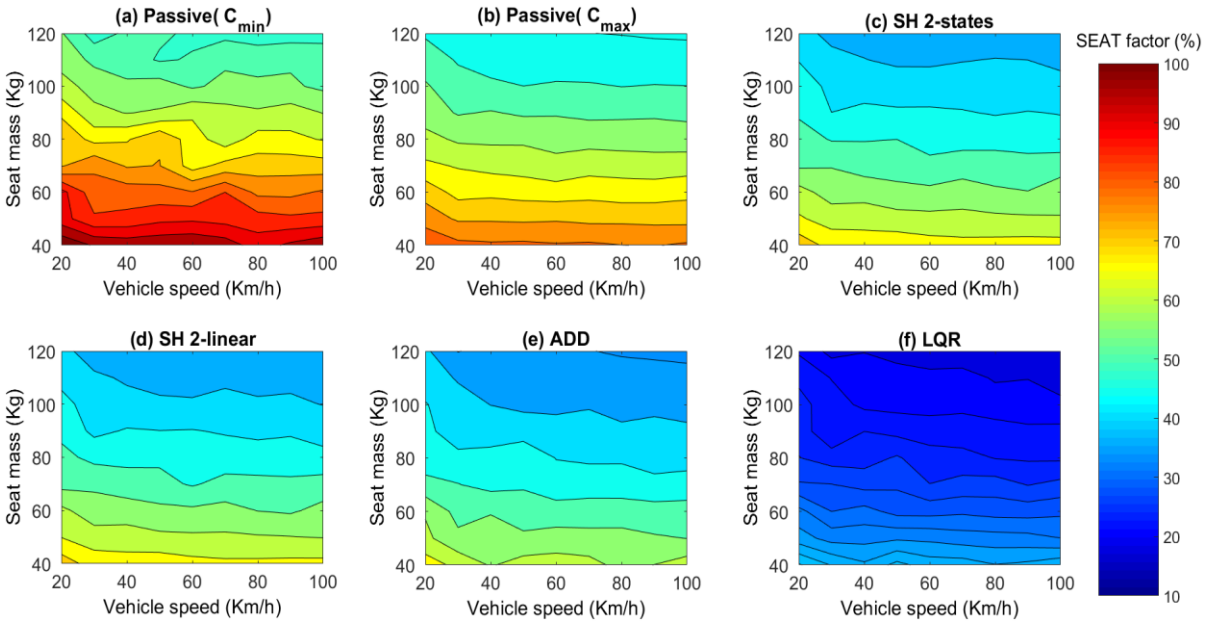

Figure 4-10: Sensitivity of the SEAT factor to seat mass and vehicle speed variations for passive, semi-active and active seat suspension systems

4.3.2.2 Bump road input

In addition to the random road, a bump road profile is also used to excite the QvM, as presented in Figure 4-11. The time responses of the semi-active and active seat suspensions are compared with those of the passive system in terms of the seat acceleration and seat suspension travel, as shown in Figure 4-12, while a comparison regarding the RMS values of both seat acceleration and seat suspension travel is presented in Table 4-3. It can be observed that the semi-active skyhook approaches provide a good vibration reduction while decreasing the seat suspension travel, but, the SH 2-states generates sharp seat acceleration. Moreover, due to the chattering problem within the ADD approach its performance in reducing the seat acceleration is deteriorated and become worse than that of the passive system. In contrast, the LQR active seat suspension provides the best vibration attenuation level when compared with both the passive and semi-active seat suspension systems with a reasonable increase in the seat suspension travel. Figure 4-13 compares the PSD of the semi-active and active seat suspension systems with that of the passive system. It reveals, once again, the greater effectiveness of the LQR active seat suspension in improving the vibration attenuation level over a wide frequency range when compared to both passive and semi-active systems.

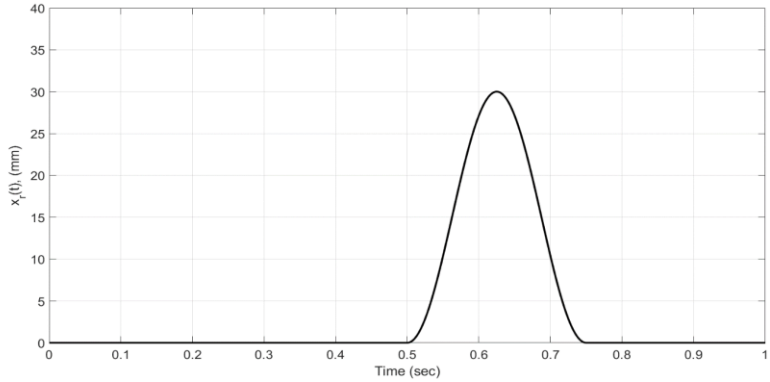

Figure 4-11: Bump road profile

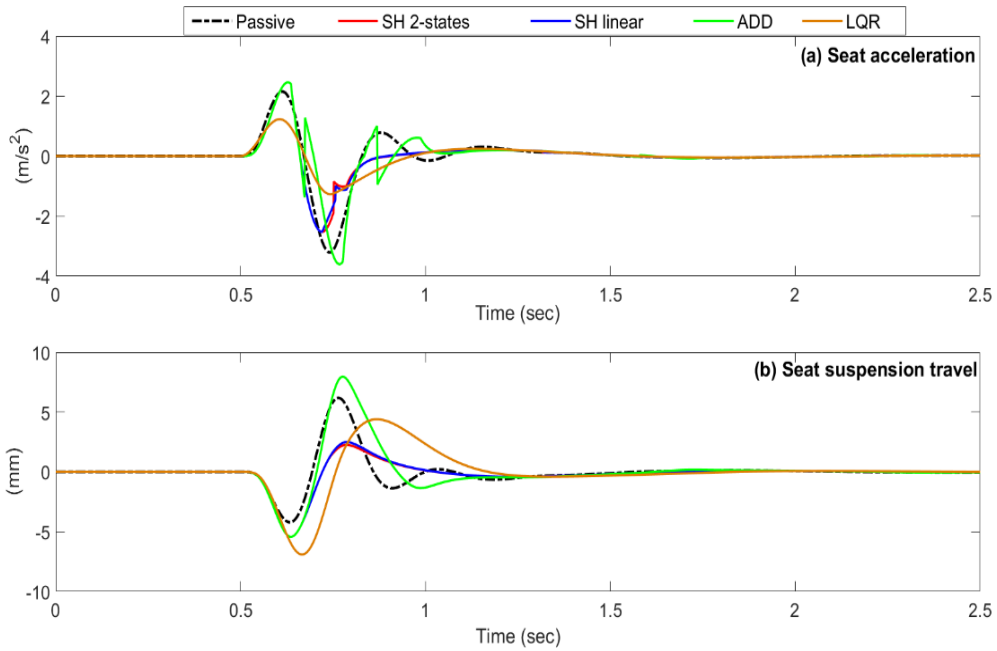

Figure 4-12: Time responses of the passive, semi-active and active seat suspensions under bump road excitation: (a) seat acceleration and (b) seat suspension travel

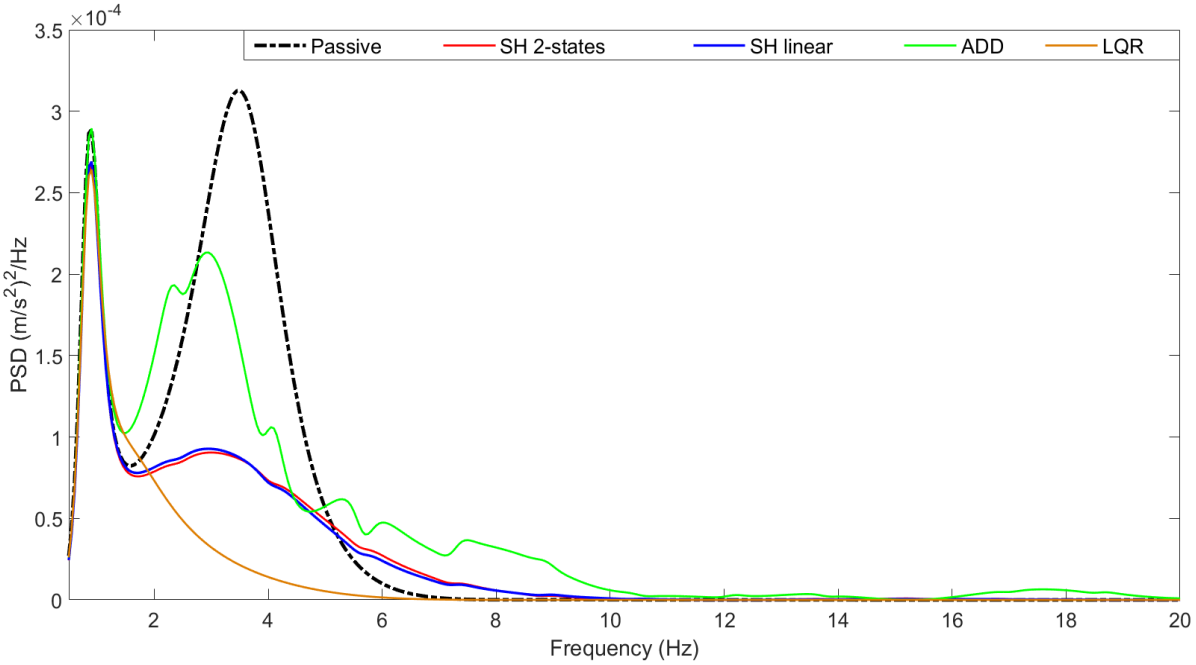

Figure 4-13: PSDs of the seat acceleration for passive, semi-active and active seat suspensions under bump road excitation

Table 4-3: Time responses of passive, semi-active and active seat suspensions under a bump road profile

Control strategy	Seat acceleration		Seat suspension travel	
	RMS (m/s²)	% improvements	RMS (mm)	% increase
Passive	0.329	----------	0.652	----------
SH 2-states	0.273	16.90	0.527	-19.20
SH linear	0.271	17.51	0.536	-17.71
ADD	0.327	0.54	0.884	35.71
LQR	0.172	47.62	0.875	34.30

4.4 Conclusions

In this chapter, comparative studies of some basic semi-active and active control strategies used to attenuate the vertical vibration of the driver's seat have been presented through simulation and compared to a passive seat suspension system. It can be concluded from the above analysis, that the performance of the passive seat suspension is limited to a narrowband frequency range and there is a trade-off between reducing the seat acceleration at the resonant frequency and higher frequencies as well as the performance is neither robust to the driver's weight nor vehicle speed. Moreover, the performance of semi-active seat suspensions in reducing the seat acceleration is limited due to the passivity constraint, where they can only dissipate energy from the system. Conversely, active seat suspension with an LQR controller shows superior performance in attenuating vibrations over a broadband frequency range and different road conditions with reasonable seat suspension travel and actuator force. This significantly improves ride quality and therefore, in this thesis the active seat suspension type will be the main focus.

In addition to the low improvement in ride quality that accomplished by semi-active seat suspensions, the real implementation of both the SH 2-states and SH linear semi-active system is either very difficult or expensive as they require the measurement of the seat's absolute velocity. On the other hand, the ADD semi-active seat suspension can be easily applied in real-time as it acquires accessible and low-cost measurements. Nonetheless, it produces significant seat suspension travel and a chattering problem which deteriorates its performance.

Moreover, the real application of the LQR active seat suspension is impractical as it requires full system state measurements in which some of these states are difficult to be measured, such as the absolute velocity states. Hence, this increases the sensor numbers and the implementation cost.

Chapter 5
Experimental Rig Development

5.1 Introduction

Validation and evaluation of control strategies for an active seat suspension through experimental tests are essential issues, for which a test rig is required. This rig consists of three main parts: a physical active seat suspension, a multi-axis simulation table (MAST) to excite this seat and a dummy representing a seated occupant. This chapter presents and describes the experimental components and setup that are required to investigate the performance of the developed active seat suspension. Also, the development and validation of the Multi- axis simulation Table (MAST) to emulate the sprung mass motion of a Quarter Vehicle Model (QvM) using the hardware-in-the-loop (HIL) approach is outlined.

5.2 Experimental setup

5.2.1 Multi-axis simulation table (MAST)

Figure 5-1 presents the MAST which was produced by Instron Structural Testing Systems. It is a six-degree-of-freedom platform table, which can be moved according to Cartesian co-ordinates with three translation motions in the longitudinal (X), lateral (Y) and vertical (Z) directions as well as the pitch, yaw and roll directions. Also, it can provide any combination of these motions simultaneously in terms of position command signals, such as random and harmonic inputs. The specifications of the MAST are listed in Table 5-1.

Table 5-1: MAST specifications [193]

Parameter	Value	Unit
Actuator stroke	±75	mm
Longitudina1 actuator load rating	33	kN
Maximum working frequency	50	Hz
Oil supply flow	1651	l/min
Oil supply pressure	280	bar
Other actuators load rating	25	kN
Peak acceleration (max payload 450 kg) – (vertical, lateral, longitudinal)	(8, 5, 3)	m/s
Peak velocity (no payload) – (vertical, lateral, longitudinal)	(1.5, 1.25, 1)	m/s
Servo-valve rated flow Q_{rated} (70 bar pressure drop ΔP_{rated})	65	l/min

5.2.2 Accelerometers and the data acquisition system

Single-axis piezoresistive accelerometers of type Entran, EGGS-D1CM-25 were used to measure the required acceleration at different locations including the MAST platform and the active seat's pan in the vertical direction. The measured acceleration signals were sampled and acquired with an xPC Target system using an NI PCI-6229 data acquisition card. This card was also used to command external signals to the MAST rig from a Simulink model. During all the tests conducted in this thesis, the measured acceleration data were sampled using a sampling frequency of 10 kHz. In addition, to eliminate measurement noise and remove high-frequency content they were filtered using a low-pass filter with a cut-off frequency of 250 Hz which is more than ten times the maximum frequency of interest (20 Hz).

Also, power spectral density (PSD) was used to perform spectral analysis of the measured acceleration time data in the frequency domain. However, to estimate the PSD from the acceleration time data, a window of the "Hanning" type with an overlap of 50 % is used, as

this provides a reasonable frequency resolution and an acceptable amplitude accuracy [74] [74].

5.2.3 Excitation signal types

To examine the performance of an active seat suspension system, it should be evaluated in both frequency and time domains using different types of excitations. In addition to the two broadband random and single bump road profiles that have been described previously in chapter 3, a sinusoidal excitation signal is also considered in order to obtain the frequency response. The excitations signal types and their specifications are summarised in Table 5-2.

Table 5-2: Excitation signal types specifications

Criterion	Signal type		
	Sinusoidal	Broadband random	Single bump
Purpose	Frequency response	Time response, SEAT factor and PSDs	Analysis of the transient time response and shock events
Specification	Frequency range from 0.5 Hz up to 20 Hz with a step of 0.5 Hz	A wavelength band of (0.333-100 m)	Equations **(3-17**) and (**3-18**)
Method	A sinusoidal wave with- a fixed amplitude -in the range from 1 mm to 5 mm.	Using equation (**3-16**). For experimental tests, the road roughness ($\Phi(\Omega_0)$) was limited to $40 \times 10^{-6}\ m^3$.	Using equations **(3-17**) and (**3-18**)
Measurement duration	10 seconds	20 seconds	10 seconds

5.2.4 Test dummy

The dynamic response of the human body is best described by a complex nonlinear system that significantly changes from one person to another [25]. To avoid health and safety problems, a test dummy was used to emulate the dynamic response of a seated human. This dummy, developed by Gan [121] consisted of three main parts, namely, the head, upper torso and lower torso, including the pelvis and thighs and has a total weight of 542 N. It was previously proven by Gan [121] through experimental tests, that it can reasonably characterise the behaviour of a seated occupant. This dummy was sat on the active seat suspension regarding which neither the influence of contact between the hands and steering wheel or the feet and the platform was considered. Also, to ensure that it did not move away during the tests, it was secured using a standard car seatbelt.

5.2.5 Active seat suspension prototype

Figure 5-2 shows a schematic diagram of an active vibration seat suspension developed by Gan [121] at the University of Bath, which consists of two main parts: a passive suspension and an active actuation system. An Elka-stage-5 bicycle shock absorber was used as a passive suspension system, which consists of an adaptable damper and a coil spring. The passive suspension unit is linked to the seat pan through a two-bar lever mechanism, which works together with the passive suspension unit to hold the static load of the seat pan and an occupant. The rear of the seat's pan is connected on both sides to linear rails through linear carriages to permit heave motion of the seat pan relative to the seat's frame. Two end stops, upper and lower, were used to limit the vertical stroke of the seat pan relative to the seat's frame to be within a range of ± 22.5 mm. In addition, to provide some rotation motion of the seat pan relative to the seat's frame, the linear carriages were linked to the seat pan through ball bearings.

The active actuating system consists of two identical XTA-3806 electromagnetic linear actuators. These are mounted at the front and rear of the seat pan with an individual peak force of 1,120 N. The detailed specifications of these actuators are presented in Table 5-3. Also, these actuators are provided with a linear encoder of a resolution of 558 counts/mm, which can be used to measure the seat suspension stroke. The linear actuators are controlled using a

Xenus XTL amplifier provided by Copley Controls, from which three digital signals A, B and Z are acquired, where signals A and B are used to indicate the position and direction of motion, respectively, while signal Z denotes the reference signal. These signals are connected to the NI PCI-6229 data acquisition card, as shown in Figure 5-3 and the incremental encoder block PCI-6229 in Simulink is used to convert them into analogue signals.

Table 5-3: XTA-3806 electromagnetic linear actuator specifications [121]

Parameter	Value	Unit
Allowable stroke	±30	mm
Continuous stall force	1.68	kN
Force constant	78.9	N/Arms
Forcer mass (excluding thrust and cables)	3.75	kg
Maximum speed	3.8	m/s
Peak acceleration	313	m/s^2
Peak force	1.116	kN
Thrust rod mass/metre	8.3	kg/m

The test dummy is mounted onto the active seat suspension by a regular seat belt, while the active seat is rigidly fixed on the MAST platform. It should be noted that whilst the seat can move in heave and pitch, in this work, the focus is only on the vertical motion of the seat and the pitch axis was locked. Figure 5-4 provides an outline of the experimental apparatus and setup, while further details about the seat structure and design can be found in the thesis of Gan [121].

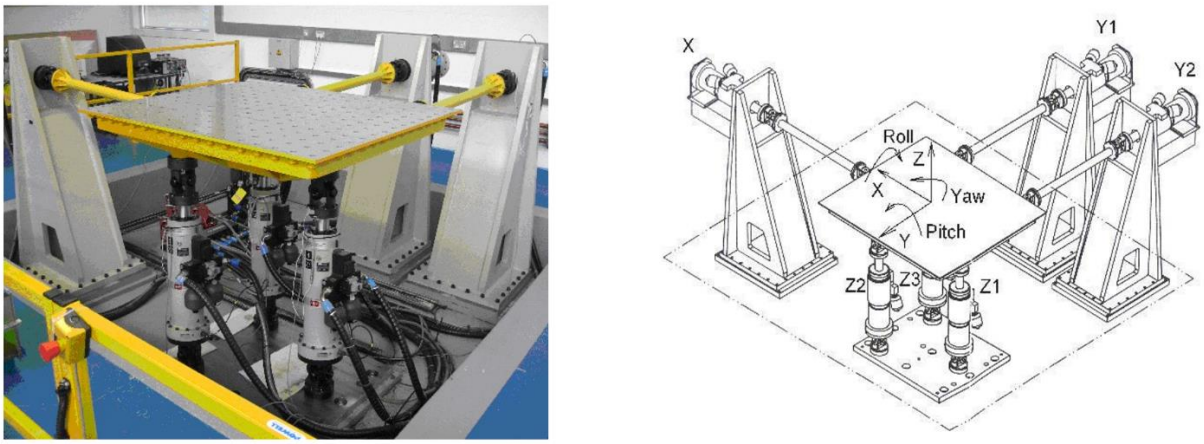

Figure 5-1: A schematic view of the MAST [194]

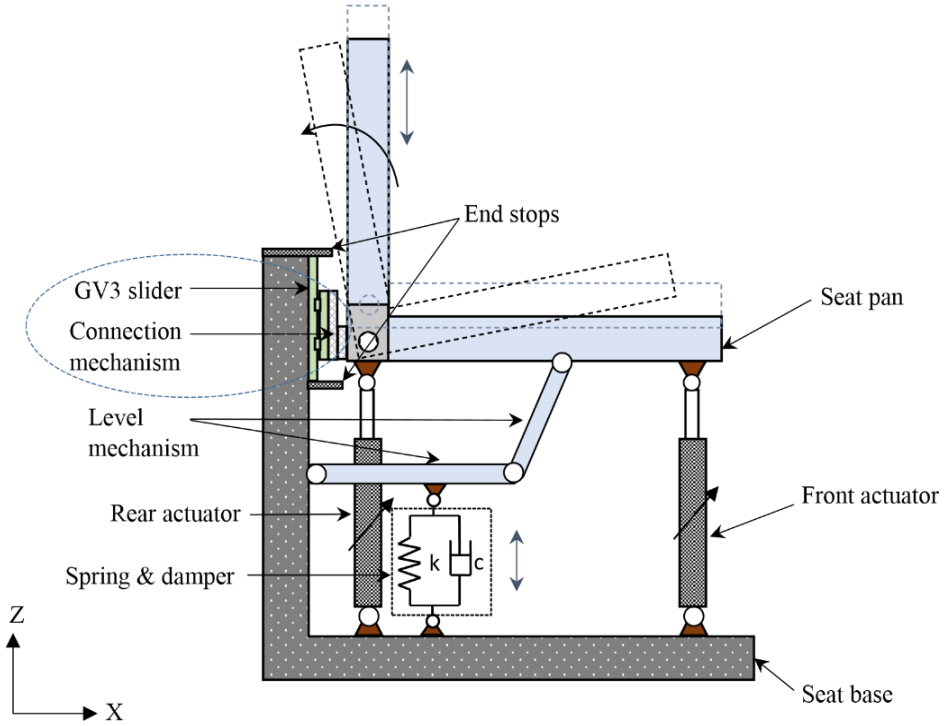

Figure 5-2: Schematic diagram of the active seat suspension [121]

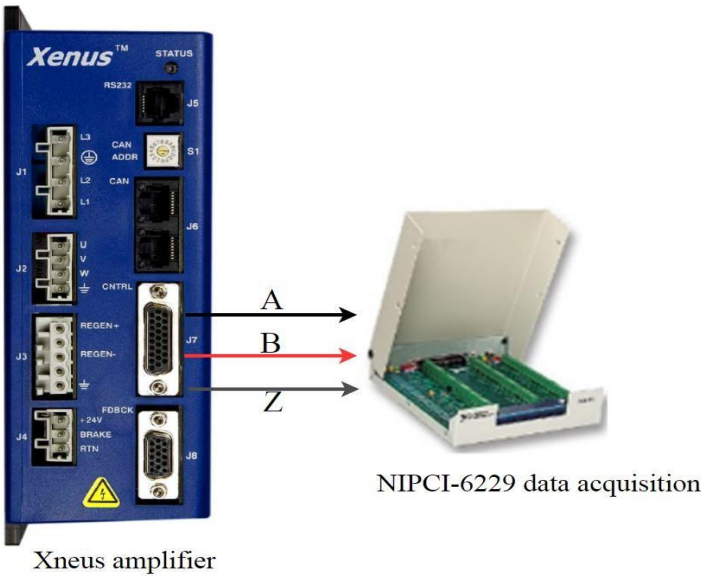

Figure 5-3: Linear actuator controller and an NI PCI-6229 data acquisition card

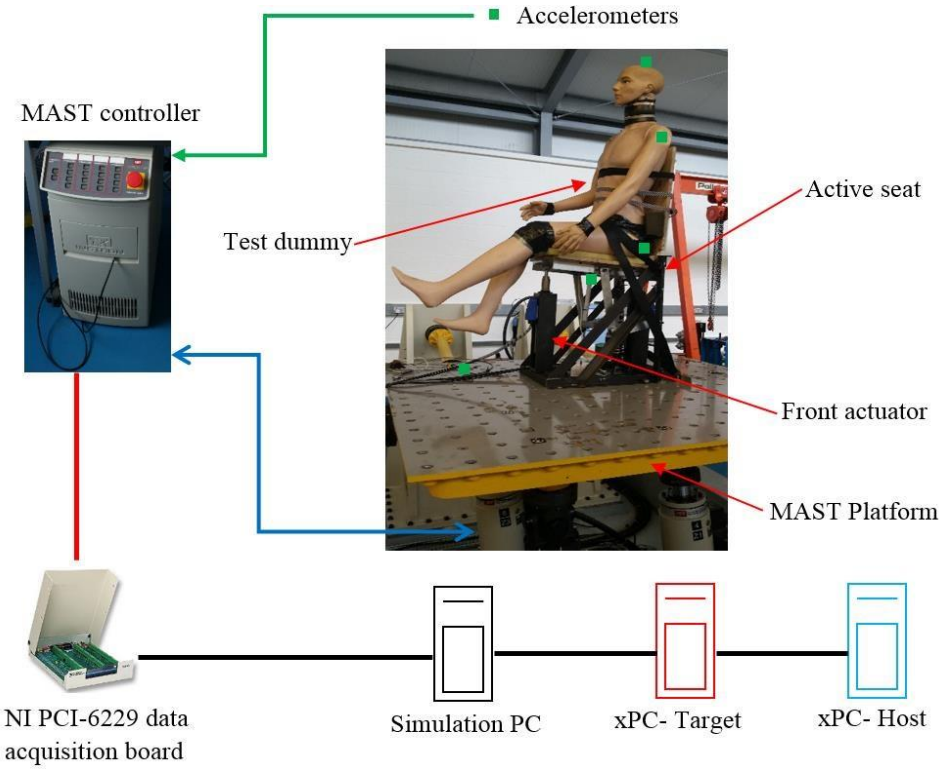

Figure 5-4: Experimental apparatus and setup

5.2.6 Modification of the current active seat suspension

The vertical translation of the seat pan was achieved through a linear bearing mounted on the support structure. Previous, significant use of the rig had resulted in wear and increased friction, so a redesign was undertaken for this project. To provide more robustness and less friction of the translation motion of the seat pan the previous linear slider mechanism was replaced by GV3 linear guidance purchased from HepcoMotion as illustrated in Figure 5-5. Moreover, a slider connection mechanism was built to assemble the GV3 with the active seat suspension, as shown in Figure 5-6, in which plates 1 and 2 are rigidly connected to the GV3 slider and the rear of the seat pan, respectively. Plate 2 is connected to plate 1 through a ball bearing to provide the kinematic pitch motion of the seat pan associated with the passive suspension linkage. Excessive rotation of plate 2 is limited by the stop pin when it moves through the controlled slot of plate 1, thereby limiting the pitch motion of the seat pan.

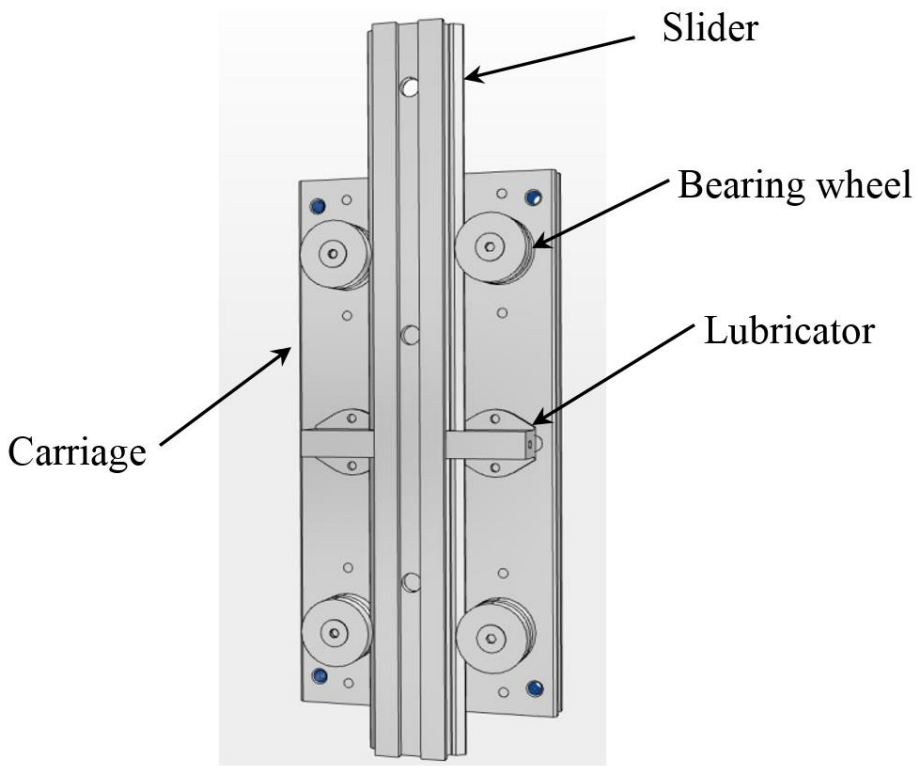

Figure 5-5: A picture of the linear slider mechanism diagram ([195])

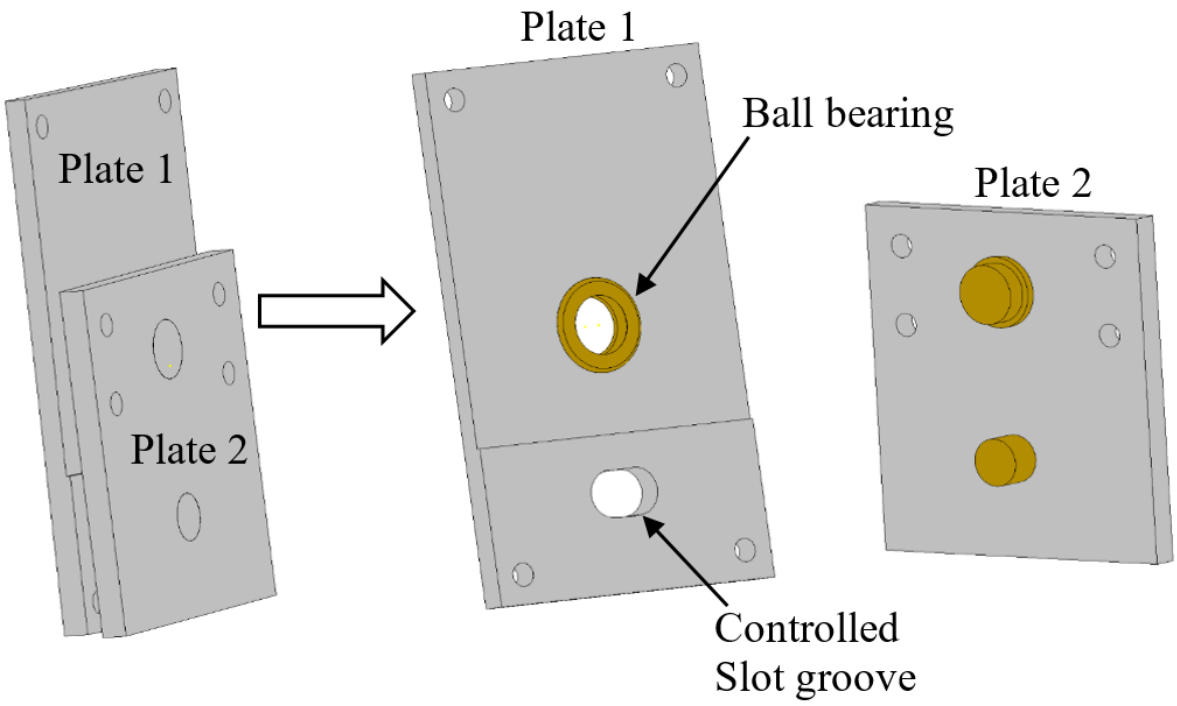

Figure 5-6: Assembly of the slider connection mechanism

5.3 Hardware-in-the-loop (HIL) simulation

To assess the efficiency and the performance of the developed active seat suspension, reliable and repeatable experimental tests in a real vehicle over distinct and extremes road conditions are essential. However, this is challenging, expensive and time-consuming. As an alternative, hardware-in-the-loop (HIL) can be used as a comparable efficient technical approach for field tests [196]. This consists of two systems, a hardware system, such as a component under development and control units as well as software systems, such as simulation models [197]. In the literature, this technology has been extensively utilised in the evaluation and modification of vehicle suspension systems, including semi-active and active devices [136,197]. Commonly, the simulation model corresponding to the vehicle motion has been a quarter vehicle model (QvM), because it is simple and provides sufficient information to analyse the vertical motion of a vehicle. The modified vehicle suspension is physically characterised and is excited using virtual road profile signals from the simulated model, which can be easily and accurately obtained. Moreover, HIL has also been used in the modification of semi-active or active seat suspensions [59,85,97].

The application of HIL technology for a modified seat suspension is more complicated than with a modified vehicle suspension, as it has to be excited by the resulting motion of the vehicle body (chassis or sprung mass) and hence, the motion of platform, on which the modified seat is mounted, has to mimic the simulated motion of the vehicle chassis over the various frequency ranges of interest and different road conditions. Many experimental studies found in the literature have involved hypothesising that the dynamic response of the vibration platform used to drive the modified seat suspension accurately mimics the resulting dynamic response from the simulated model. However, this is an incorrect assumption as the actual dynamic response of the platform and the resulting output from a simulated model are different owing to system friction, bandwidth limitations and time delays relating to the computation of the controlled signals. Hence, the accuracy of the experimental validation tests will be affected particularly when the control scheme of the modified seat suspension employs the dynamic response of the platform or in the case of analysing the parameter uncertainties of the vehicle suspension. Consequently, to have reliable and accurate experimental tests, this issue has to be taken into account and accordingly, in the following sections the MAST is developed to mimic the dynamic response of the vehicle chassis (sprung mass) using the principle of HIL simulation and the well-known QvM.

5.3.1 QvM Quarter vehicle model

For simplicity, a QvM was used to simulate the dynamic response of the vehicle motion in the vertical direction as shown in Figure 5-7 (a), in which m_s and m_{us} denote the unsprung (tyre axle assembly) and sprung masses (vehicle chassis), respectively while x_s and x_{us} are the corresponding displacements in the vertical direction and $x_r$is the road input displacement. The vehicle suspension is represented by the linear elements of a damper c_s and a spring stiffness k_s while the tyre is represented by only a stiffness k_t and its damping is neglected [198]. The equations of motion of the QvM in the vertical direction are given as follows:

$$m_s\ddot{x}_s = -c_s\,(\dot{x}_s - \dot{x}_{us}) - \; k_s\,(x_s - x_{us}) \qquad \textbf{(5-1)}$$

$$m_{us}\ddot{x}_{us} = c_s\,(\dot{x}_s - \dot{x}_{us}) + \; k_s\,(x_s - x_{us}) - k_t\,(x_{us} - x_r) \qquad \textbf{(5-2)}$$

Using a Laplace transform and assuming zero initial conditions, the continuous transfer function from the road excitation displacement to the vehicle chassis (sprung mass) displacement, in terms of the system parameters is expressed mathematically as follows:

$$G_s(s) = \frac{X_s(s)}{X_r(s)} = \frac{k_t(c_s s + k_s)}{m_s m_{us} s^4 + c_s(m_s + m_{us})s^3 + (k_s m_s + k_s m_{us} + k_t m_s)s^2 + k_t c_s s + k_t k_s} \quad \textbf{(5-3)}$$

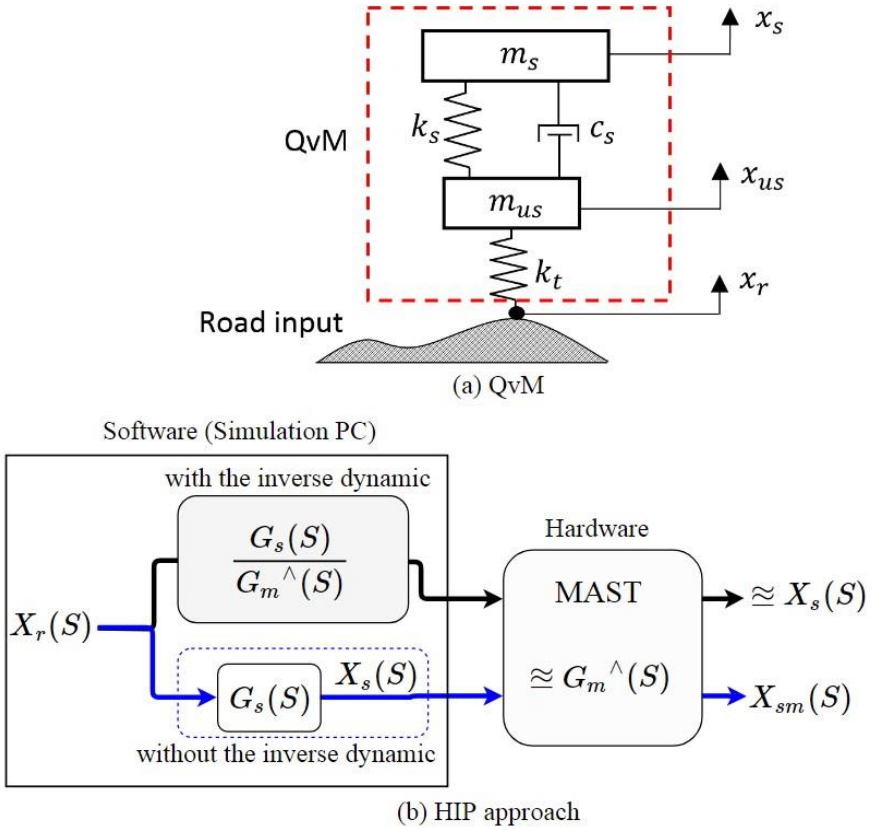

Figure 5-7: A QvM and schematic diagram of the HIL principle

5.3.2 Effect of passive seat-suspension dynamics on the sprung mass response

The sprung mass in the QvM model is influenced by the reaction force between the seat and the sprung masses, and therefore the suspension seat dynamics must be considered. An integrated model of a passive seat suspension and driver model, each with a single DOF together with the QvM is established to study this effect, as shown in Figure 5-8. The Laplace transform of sprung mass displacement is given as:

$$X_s(s) = G_s(s)X_r(s) - F_{se}(s) \quad \textbf{(5-4)}$$

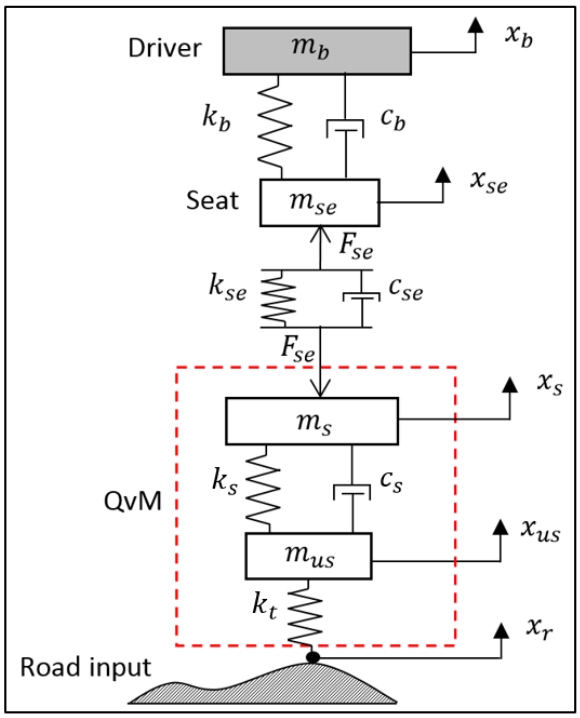

m_b	Mass of a seated driver
k_b	Driver body stiffness
c_b	Driver body damping coefficient
x_b	Vertical displacement of a seated driver
m_{se}	Seat mass
k_{se}	Seat suspension spring
c_{se}	Seat suspension damper
x_{se}	Vertical displacement of the seat
m_s	Sprung mass
k_s	Vehicle suspension spring
c_s	Vehicle suspension damper
x_s	Vertical displacement of the sprung mass
m_{us}	Usprung mass
k_t	Tyre stiffness
x_{us}	Vertical displacement of the tyre
x_r	Road surface
F_{se}	Seat suspension force

Figure 5-8: A QvM with a 1 DOF passive seat suspension and 1 DOF driver model

where F_{se} is the resulting seat suspension force given as:

$$F_{se}(s) = B_1\big(X_s(s) - X_{se}(s)\big) \quad \textbf{(5-5)}$$

$$B_1 = c_{se}s + k_{se} \quad \textbf{(5-6)}$$

After some manipulation, the transfer function from the road displacement to the sprung mass displacement is given as:

$$G_s1(s) = \frac{X_s(s)}{X_r(s)} = \frac{a_1s^5 + a_2s^4 + a_3s^3 + a_4s^2 + a_5s}{b_1s^8 + b_2s^7 + b_3s^6 + b_4s^5 + b_5s^4 + b_6s^3 + b_7s^2 + b_8s + b_9} \quad \textbf{(5-7)}$$

Where the coefficients a's and b's in terms of the system parameters are as follows:

$$a1 = c_sk_tm_bm_{se}$$

$$a_2 = (c_s c_b k_t + c_s c_{se} k_t + k_s k_t m_{se}) m_b + c_b c_s k_t m_{se}$$

$$a_3 = (k_s c_b k_t + c_s k_b k_t + c_s k_{se} k_t + c_{se} k_s k_t) m_b + c_b c_s c_{se} k_t + c_b k_s k_t m_{se} + c_s k_b k_t m_{se}$$

$$a_4 = (c_s k_{se} k_t + c_{se} k_s k_t) k_b + c_b k_s k_{se} k_t$$

$$a_5 = k_b k_s k_{se} k_t$$

$$b_1 = m_b m_s m_{se} m_{us}$$

$$b_2 = (c_b m_s m_{us} + c_s m_s m_{se} + c_s m_{se} m_{us} + c_{se} m_s m_{us} + c_{se} m_{se} m_{us}) m_b + c_b m_s m_{se} m_{us}$$

$$\begin{aligned} b_3 = (&c_b c_s m_s + c_b c_s m_{us} + c_b c_{se} m_{us} + c_s c_{se} m_s + c_s c_{se} m_{se} + c_s c_{se} m_{us} + k_b m_s m_{us} + k_s m_s m_{se} \\ &+ k_t m_s m_{se} + k_s m_{se} m_{us} + k_{se} m_s m_{us} + k_{se} m_{se} m_{us}) m_b + c_b c_s m_s m_{se} \\ &+ c_b c_s m_{se} m_{us} + c_b c_{se} m_s m_{us} + c_b c_{se} m_{se} m_{us} + k_b m_s m_{se} m_{us} \end{aligned}$$

$$\begin{aligned} b_4 = (&c_b c_s c_{se} + c_b k_s m_s + c_s k_b m_s + c_b k_t m_s + c_b k_s m_{us} + c_s k_b m_{us} + c_b k_{se} m_{us} + c_{se} k_b m_{us} \\ &+ c_s k_{se} m_s + c_{se} k_s m_s + c_s k_{se} m_{se} + c_{se} k_s m_{se} + c_s k_t m_{se} + c_{se} k_t m_s + c_{se} k_t m_{se} \\ &+ c_s k_{se} m_{us} + c_{se} k_s m_{us}) m_b + c_s c_b c_{se} (m_s + m_{se} + m_{us}) + m_s m_{se} (c_b k_s + c_s k_b) \\ &+ c_b k_s m_{se} m_{us} + c_b k_{se} m_s m_{us} + c_s k_b m_{se} m_{us} + c_{se} k_b m_s m_{us} + c_b k_{se} m_{se} m_{us} \\ &+ c_{se} k_b m_{se} m_{us} \end{aligned}$$

$$\begin{aligned} b_5 = (&c_b c_s k_{se} + c_b c_{se} k_s + c_s c_{se} k_b + c_b c_s k_t + c_b c_{se} k_t + c_s c_{se} k_t + k_b k_s m_s + k_b k_t m_s \\ &+ k_b k_s m_{us} + k_b k_{se} m_{us} + k_s k_{se} m_s + k_s k_{se} m_{se} + k_s k_t m_{se} + k_{se} k_t m_s \\ &+ k_{se} k_t m_{se} + k_s k_{se} m_{us}) m_b + (c_b c_s k_{se} + c_b c_{se} k_s + c_s c_{se} k_b + c_b c_{se} k_t) m_s \\ &+ (c_b c_s k_{se} + c_b c_{se} k_s + c_s c_{se} k_b + c_b c_s k_t + c_b c_{se} k_t) m_{se} \\ &+ (c_b c_s k_{se} + c_b c_{se} k_s + c_s c_{se} k_b + c_b c_s k_t + c_b c_{se} k_t) m_{us} + m_s m_{se} (k_b k_s + k_b k_t) \\ &+ m_{se} m_{us} (k_b k_s + k_b k_{se}) + k_b k_{se} m_s m_{us} \end{aligned}$$

$$\begin{aligned} b_6 = (&c_b k_s k_{se} + c_s k_b k_{se} + c_{se} k_b k_s + c_b k_s k_t + c_s k_b k_t + c_b k_{se} k_t + c_{se} k_b k_t + c_s k_{se} k_t \\ &+ c_{se} k_s k_t) m_b + c_b c_s c_{se} k_t \\ &+ (c_b k_s k_{se} + c_s k_b k_{se} + c_{se} k_b k_s + c_b k_s k_t + c_{se} k_b k_t)(m_s + m_{se}) \\ &+ (c_b k_s k_t + c_s k_b k_t) m_{se} + (c_b k_s k_{se} + c_s k_b k_{se} + c_{se} k_b k_s) m_{us} \end{aligned}$$

$$\begin{aligned} b_7 = (&k_b k_s k_{se} + k_b k_s k_t + k_b k_{se} k_t + k_s k_{se} k_t) m_b + (c_b c_s k_{se} + c_b c_{se} k_s + c_s c_{se} k_b) k_t \\ &+ (k_b k_s k_{se} + k_b k_{se} k_t) m_s + (k_b k_s k_{se} + k_b k_s k_t + k_b k_{se} k_t) m_{se} + m_{us} k_b k_s k_{se} \end{aligned}$$

$$b_8 = (c_s k_{se} k_t + c_{se} k_s k_t) k_b + c_b k_s k_{se} k_t$$

$$b_9 = a_5$$

To show the effect of the passive seat suspension on the dynamic response of the sprung mass, the frequency response of the sprung mass (vehicle body) subject to road displacement inputs

are compared for different body masses (driver's weight), as shown in Figure 5-9. This figure illustrates that the vehicle body frequency response, with and without the suspension seat dynamics are very similar over the frequency of interest regardless of changes in the driver's weight. This indicates the very small insignificant effects of the passive seat suspension reaction force (F_{se}) on the dynamic response of the sprung mass (vehicle body). Thus, for simulation purpose in the HIL model, the QvM that neglect the passive seat suspension is sufficient. In the case of an active seat suspension, the demand active force required to attenuate vibration at the seat is also acts on the sprung mass (vehicle body). In practice, this force is significantly less than the passive seat suspension force, will have an insignificant effect on the sprung mass motion and therefore can also be excluded from the simulation model. Due to this fact, the terminology of HIL used in this research is inaccurate.

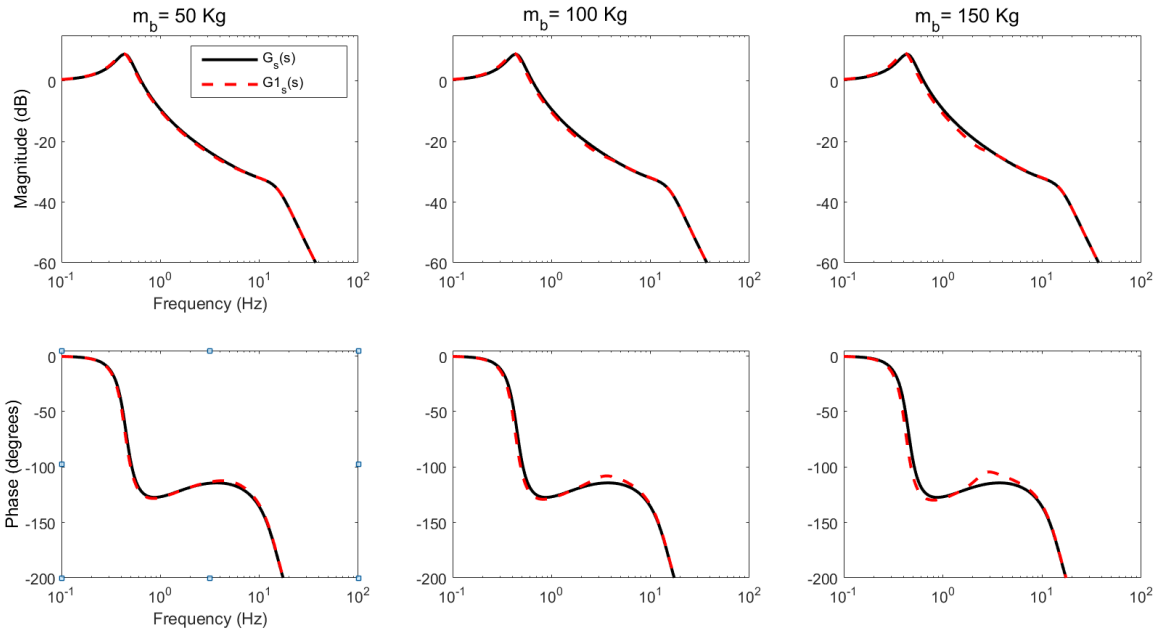

Figure 5-9: Sprung mass frequency responses of the QvM with and without including the seat suspension dynamic force

5.3.3 MAST dynamic response

As stated previously, it is essential to compensate for the limited bandwidth dynamics of the MAST platform. Accordingly, as a first step, the frequency response of the MAST in the vertical direction over a low-frequency range has to be defined experimentally. Hence, the MAST was excited by sinusoidal displacements over a frequency range of 0.5-30 Hz and

different amplitudes. Figure 5-10 (a) shows the magnitude and phase frequency responses of the measured displacement of the MAST and the demand using different excitation amplitudes. It can be seen that the MAST displacement response is linear over the test frequency range. However, the MAST displacement follows the command signal only over a narrow band frequency range of less than 2 Hz. In fact, the dynamic displacement response of the MAST is clearly compromised at higher frequencies, specifically, around the wheel-hoop frequency of the QvM (15 Hz). This is mainly due to the hydraulic system dynamics, friction and time delays with the hydraulic controller. The dynamic displacement response of the MAST over the tested frequency range can be mathematically estimated over the frequency range of interest using the System Identification Toolbox in MATLAB, as given by the continuous transfer function $\widehat{G_m}(s)$ in Eqn. (5-8). The order of this $\widehat{G_m}(s)$ is selected based on that of the transfer function (s), as is explained in the following section. The measured displacement frequency responses of the MAST presented Figure 5-10 (a) are averaged, and the result is compared to the simulated one, as shown in Figure 5-10 (b). This figure demonstrates that there is a respectable agreement between the measured displacement of the MAST and the estimated one over the desired frequency range.

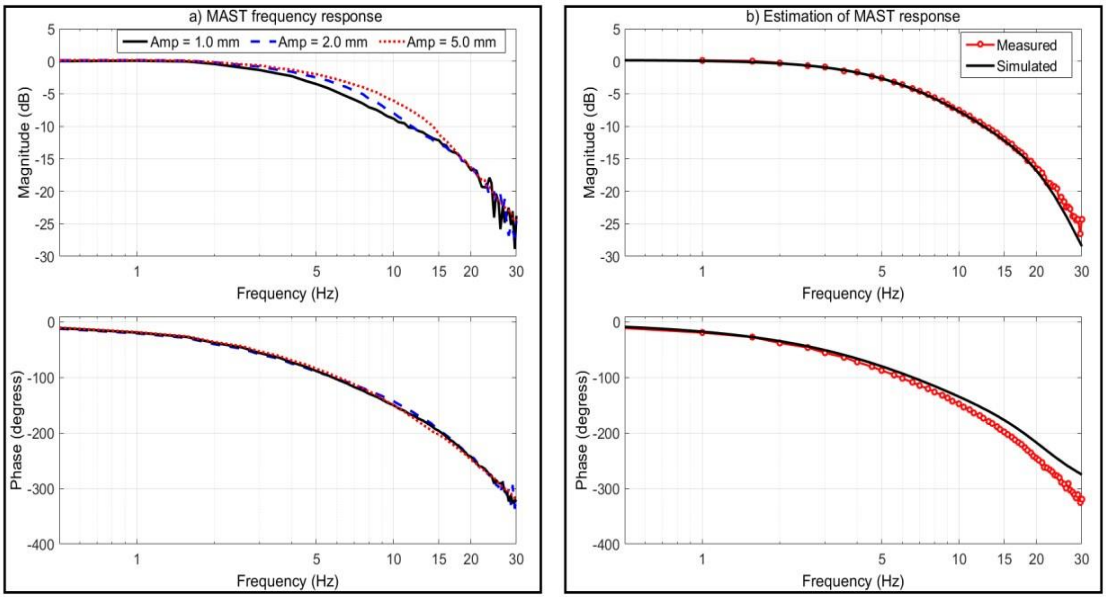

Figure 5-10: Displacement frequency responses of the MAST: (a) MAST frequency response using different excitation amplitudes; and (b) comparison between the measured and simulated displacement frequency responses of the MAST

$$\widehat{G_m}(s) = \frac{12700s + 4.109 \times 10^7}{s^4 + 215.9s^3 + 32270s^2 + 1.962 \times 10^6 s + 4.109 \times 10^7} \quad \textbf{(5-8)}$$

5.3.4 Inverse dynamic response of the MAST

In order for the dynamic response of the MAST to mimic that of the sprung mass in the simulated QvM, the inverse transfer function of its estimated dynamic response has to be included in the HIL simulation, as illustrated in Figure 7-b. However, this inverse transfer function cannot be obtained mathematically as the order of the poles will be lower than the zeros. Alternatively, this can be overcome by multiplying the sprung mass transfer (G_s) by the inverse transfer function of the estimated dynamic response of the MAST $\left(\frac{1}{\widehat{G_m}(s)}\right)$, and this explains the reason behind the selection of the poles order in the estimated transfer function of the of the MAST $\widehat{G_m}(s)$ dynamics.

5.4 Results & Discussion

5.4.1 Frequency analysis

This subsection presents the outcomes of experimental investigation studies regarding the simulated QvM parameter uncertainties associated with the damping coefficient c_s, stiffness rate k_s and sprung mass m_s with the nominal values of these parameters presented in Table 5-4. Accordingly, three main tests were performed in which, one of the QvM parameters was changed with assumed minimum and maximum values while the other two parameters were fixed. In each test, the experimental displacement frequency responses of the MAST when it is excited from the simulated QvM with and without inverse dynamics compensation are compared with that of the sprung mass (vehicle chassis) from the simulated QvM, as shown in Figures 5.11 to 5.13. These figures reveal that including the inverse dynamics of the MAST into the simulated QvM is essential for ensuring acceptable and accurate simulation of the MAST as a QvM (sprung mass motion) over the frequency range of interest.

Table 5-4: QvM parameters

Parameter	Value	Unit
m_s	250.0	kg
m_{us}	20.0	kg
c_s	1500.0	N.s/m
k_s	10.0	kN/m
k_t	180.0	kN/m

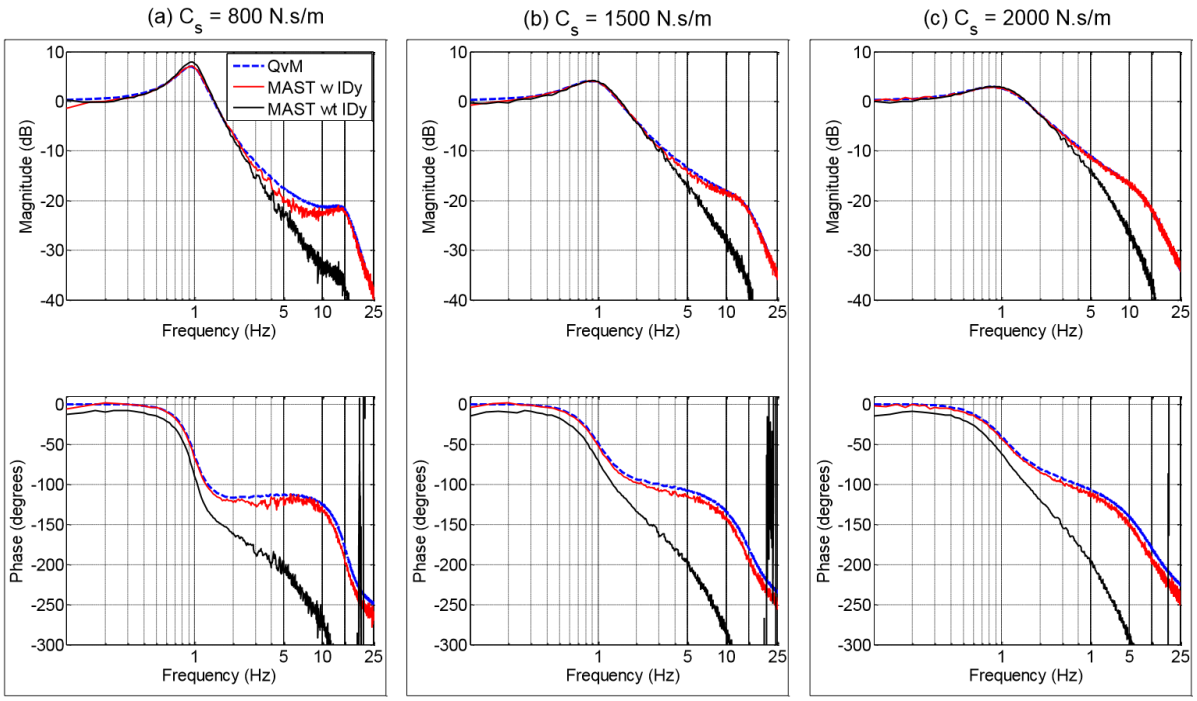

Figure 5-11: Comparison between displacement frequency responses of the MAST for various damping coefficients of the QvM with and without including the inverse dynamics of the MAST

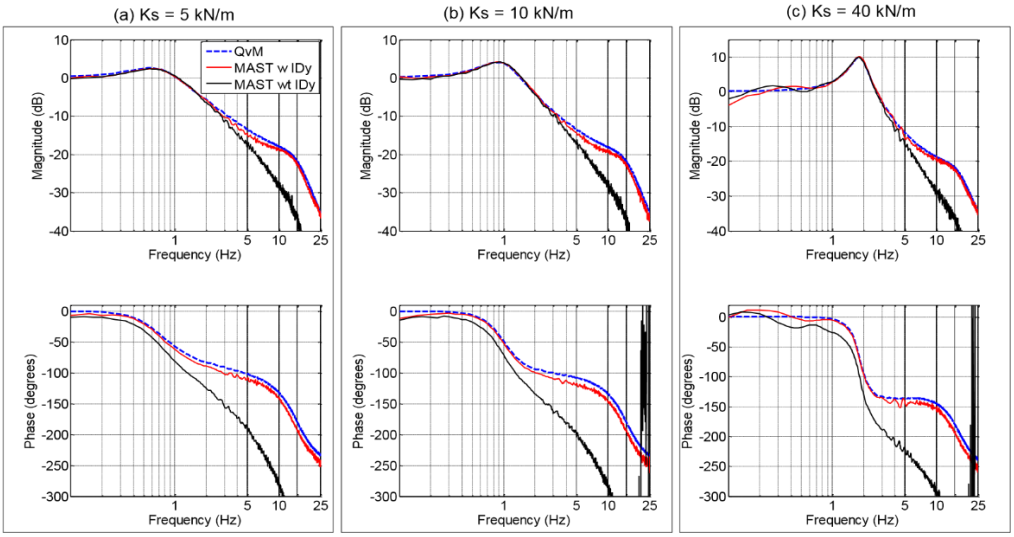

Figure 5-12: Comparison between the displacement frequency responses of the MAST for uncertainties in the suspension stiffness of the QvM with and without including the inverse dynamics of the MAST

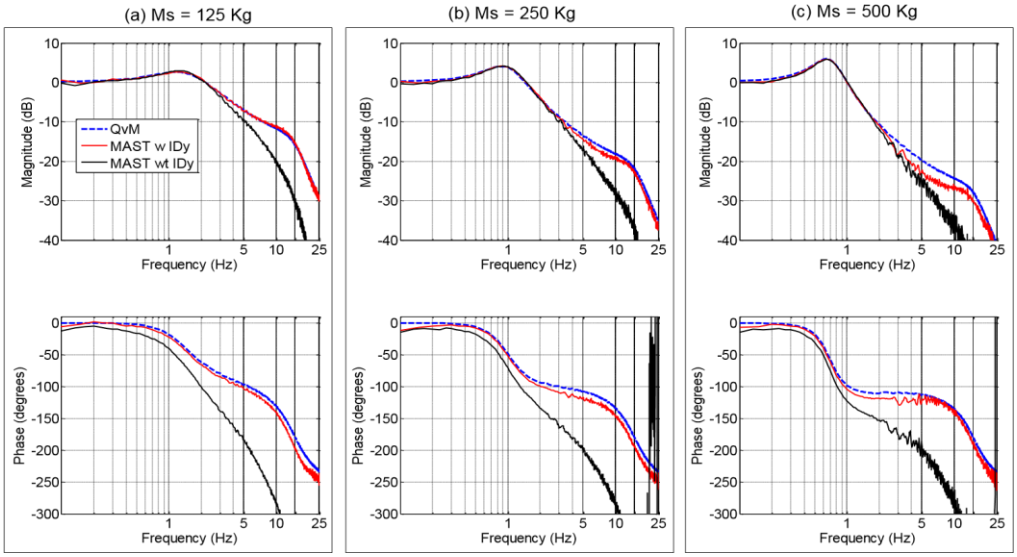

Figure 5-13: Comparison between the displacement frequency responses of the MAST for uncertainties in the sprung mass of the QvM with and without including the inverse dynamics of the MAST

5.4.2 Time response

The MAST time response was also measured experimentally with and without inverse dynamics compensation when subject to random road and bump profiles. Figure 5-14 shows

a comparison between the time responses of the simulated sprung mass (vehicle chassis) and the measured responses of the MAST, in terms of its displacement and acceleration. The results prove once more that the MAST time responses are highly comparable with the responses of the sprung mass in the simulated QvM.

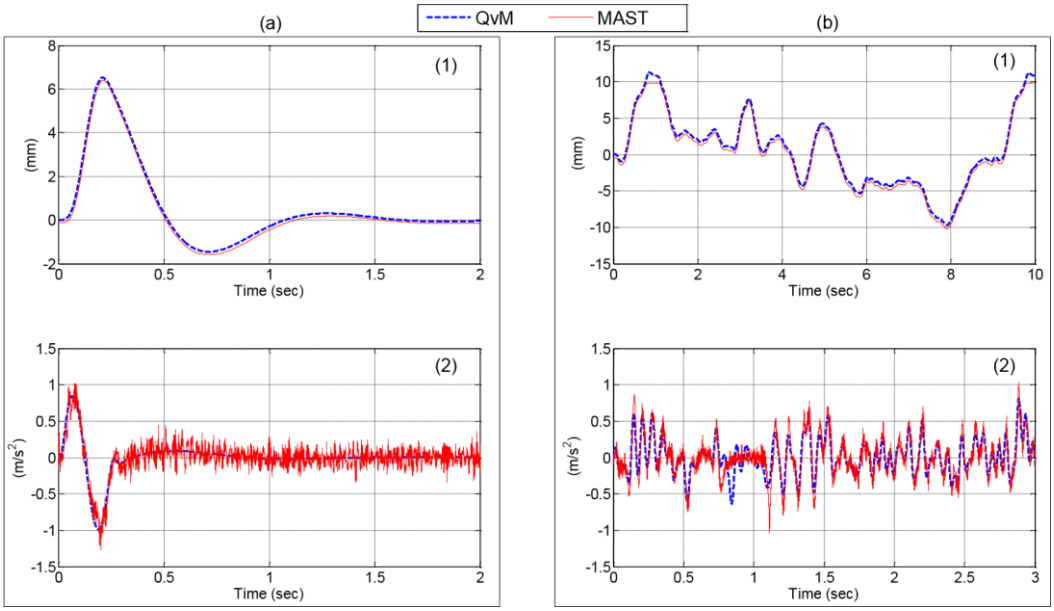

Figure 5-14: Comparison between the simulated time responses of the sprung mass of the QvM with inverse dynamics of the MAST and measured time responses of the MAST under road disturbance profiles of a) bump and b) random; (1) displacement and (2) acceleration

5.5 Conclusions

In this chapter, the experimental apparatus and setup required to investigate the performance of an active seat suspension were introduced and explained. Moreover, the modifications of an existing active seat suspension were highlighted. Further, the dynamic response, of the MAST rig, in the vertical direction over a low-frequency range was characterised and estimated through experimental tests. Also, the MAST was developed and validated to mimic the sprung mass motion of the QvM using the principle of HIL simulation, and the inverse estimated dynamics of the MAST. The experimental results reveal that the MAST is suitable for use as a vibration platform to examine the performance of an active seat suspension and its control algorithm experimentally.

Chapter 6
An Active Seat Suspension with Preview Control

This chapter presents the development of a control strategy that utilises preview information from the vehicle suspension. The aim is to employ this on an active seat suspension to improve the ride comfort of the driver's seat when the vehicle is exposed to vertical vibration from road irregularities. The control force is assumed to be a linear function of this preview information with optimum gains that are obtained by minimising the SEAT factor using a genetic algorithm (GA) and considering the physical limitations of the seat suspension travel and actuator saturation. The proposed controller is evaluated and compared to a passive system using both simulation and experimental tests in both the frequency and time domains including different working conditions and road profiles.

6.1 Introduction

Based on the literature reviewed in Chapter 2, most of active vibration control strategies, even those utilising preview information, assessed gained their potential for improving the suspension's performance through theoretical investigations alone. However, their practical implementation is challenging as some are based on using states that are difficult or costly to obtain. Whilst some have argued that these states could be estimated using an observer, this requires an accurate plant model. To the best of this researcher's knowledge, the concept of using preview information from a vehicle suspension to control an active seat suspension has not been previously investigated. Accordingly, these issues motivate to develop a control strategy for an active seat suspension that employing inexpensive and accessible preview information from the vehicle suspension.

6.2 Control strategy

In order to address the concept of the proposed control strategy for an active seat suspension, an integrated mathematical model is required. Because the seat suspension is secondarily influenced by road irregularities after these have been filtered by the vehicle suspension system [191], this model should include both the vehicle and seat suspension systems. For simplicity, the vehicle is represented by the well-known 2 DOF quarter vehicle model (QvM), which is able to provide satisfactory information regarding the heave motion of the vehicle. The seat suspension system is characterised by a 1DOF lumped mass-spring-damper system. However, to retain the simplicity of the model, the driver body model is ignored in this analysis, while its weight is basically included within the seat's mass. Figure 6-1 shows the integrated model including an active actuator fixed in parallel with the passive seat suspension in which, x_{se}, x_s and x_{us} denote the vertical motion of the combined seat and driver mass (m_{se}), the sprung mass (m_s) and the unsprung mass (m_{se}), respectively, while x_r refers to the road excitation displacement. The stiffness and damping of the passive seat suspension are k_{se} and c_{se}, respectively, while k_s and c_s are those of the vehicle suspension. The tyre dynamics are characterised only by a stiffness k_t, as the tyre damping is much smaller compared to that of the suspension and hence, can be neglected [149]. Assuming linear characteristics for both the seat and vehicle suspension elements, the equations of motion in the vertical direction are derived as:

$$m_{se}\ddot{x}_{se} = -\,c_{se}\,(\dot{x}_{se} - \dot{x}_s) - \,k_{se}\,(x_{se} - x_s) + \,F_a \qquad \textbf{(6-1)}$$

$$m_s\ddot{x}_s = \,c_{se}\,(\dot{x}_{se} - \dot{x}_s) + \,k_{se}\,(x_{se} - x_s) - \,c_s\,(\dot{x}_s - \dot{x}_{us}) - \,k_s\,(x_s - x_{us}) - \,F_a \qquad \textbf{(6-2)}$$

$$m_{us}\ddot{x}_{us} = \,c_s\,(\dot{x}_s - \dot{x}_{us}) + \,k_s\,(x_s - x_{us}) - \,k_t\,(x_{us} - x_r) \qquad \textbf{(6-3)}$$

where, F_a denotes the actuator control force.

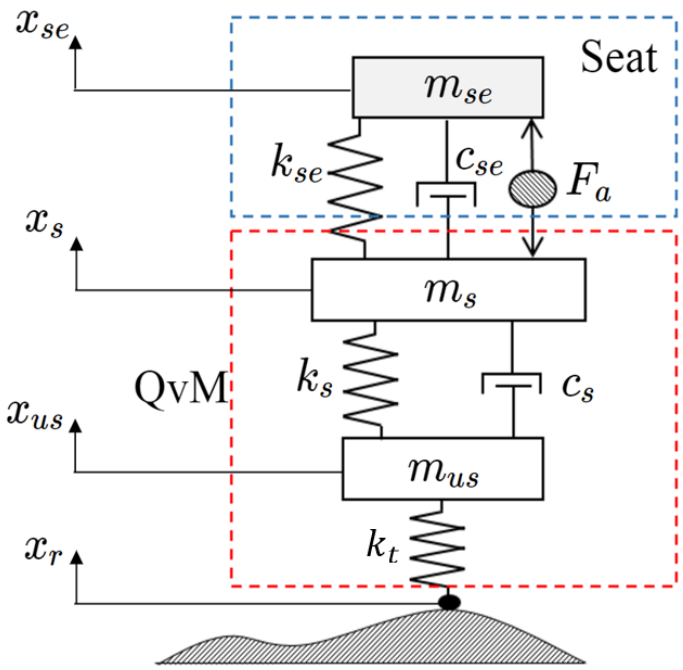

m_{se}	Seat mass
k_{se}	Seat suspension spring
c_{se}	Seat suspension damper
x_{se}	Vertical displacement of the seat
m_s	Sprung mass
k_s	Vehicle suspension spring
c_s	Vehicle suspension damper
x_s	Vertical displacement of the sprung mass
m_{us}	Usprung mass
k_t	Tyre stiffness
x_{us}	Vertical displacement of the tyre
x_r	Road surface
F_a	Active control force

Figure 6-1: A QvM with a 1 DOF active seat suspension system

6.2.1 Control Force

The control strategy for the active seat suspension is used to generate the desired control force based on the system's states. This plays an important role in the performance of active seat suspension in attenuating vibration and hence, improving ride comfort. Thus, intensive attention should be paid to the selection of such a control strategy, especially regarding the practical implementation and cost issues. That is, with the development of any control strategy the number of sensors and their cost need to be taken into consideration as well as the accessibility of the system's states that are employed in the control scheme. In this case, the developed control strategy is based on using available and cost-effective preview information from the vehicle suspension. The control force is assumed to be a linear combination of the displacement and velocity states of the vehicle suspension as given by the following equation:

$$F_a = q_1 \dot{x}_{rel} + q_2 x_{rel} \quad \textbf{(6-4)}$$

$$\dot{x}_{rel} = (\dot{x}_s - \dot{x}_{us}) \quad \text{and} \quad x_{rel} = (x_s - x_{us}) \quad \textbf{(6-5)}$$

where x_{rel} and $\dot{x}_{rel}$ denote the relative displacement and velocity between the sprung and unsprung masses in the QvM.

The gains q_1 and q_2 , values in Eqn. (6-4), can be obtained by minimising an objective function that is associated with improving the vibration attenuation level of the seat suspension. This can be achieved by reducing the seat vertical acceleration and thus improving ride comfort. Based on the discussion given in chapter 3, this can be assessed using the SEAT factor.

Commonly, reducing the seat vertical acceleration produces a large seat stroke (seat suspension travel) which is physically limited [149,199,200]. Moreover, in practical terms the actuator force capacity is also limited, and consequently, these aspects should be considered in the optimisation problem as hard constraints. Referring to the available test rig which has been described in the previous chapter, the maximum allowable seat stroke ($x_{se,max}$) and the actuator force are set to be 45 mm and 1500.0 N, respectively. Thus, the resulting optimisation problem is formulated as follows:

Given: A QvM with a 1 DOF passive seat suspension.

Find: q_1 and q_2

To minimise: $f = SEAT\ factor$ **(6-6)**

Subject to: $g(1) = (x_{se} - x_s)_{max} - (x_{se} - x_s)_{min} \leq x_{se,max}$

$g(2) = |F_a| \leq 1500\ (N)$

where, $g(1)$ and $g(2)$ denote the constraints of the seat stroke and actuator force, respectively. To solve the above constrained optimisation problem in a more convenient way, it is modified to an unconstrained one using a penalty function [201], as well as the original objective function given in Eqn. (6-6) being squared and weighted by an arbitrary number (1,000) so that small changes in the design variables values (optimum gains) can be captured. Thus, the fitness function of the unconstrained optimisation problem is expressed by:

$$J = 1000 * f^2 + PG \quad \textbf{(6-7)}$$

where, PG is a penalty function given by:

$$PG = \begin{Bmatrix} 0 \ ; \ g(1)\ and\ g(2) \leq 0 \\ 1 \times 10^{12} \ ; otherwise \end{Bmatrix} \quad \textbf{(6-8)}$$

Because the size of the above optimisation problem is small (only two design variables), the GA technique that has been previously discussed in chapter 2 is used here to solve for the optimum gains q_1 and q_2 of the preview information control.

6.2.2 Identifying the passive seat characteristics

In order to obtain some realistic dynamic responses from the simulation model, the passive seat suspension elements including the damping coefficient c_{se} and stiffness rate k_{se} were experimentally determined using the experimental rig test and the HIL simulation of the QvM, as explained in chapter 5. The MAST was excited using a swept sinusoidal displacement signal over a frequency range of 1-20 Hz with a step frequency of 0.5 Hz and an amplitude of 10.0 mm. The resulting seat pan and MAST accelerations were measured using a sampling frequency of 10 kHz and filtered using a low-pass filter with a cut-off frequency of 250 Hz, hence, obtaining the measured acceleration transmissibility acceleration of the passive seat suspension, as presented in Figure 6-2. As shown in this figure, the seat and dummy were approximated by a second order continuous function system with a reasonable agreement over the frequency range of interest (< 10Hz). Also, a dominant natural frequency of the (seat and dummy) system was observed around 4 Hz, from which the estimated stiffness and damping of the passive seat were determined as 48.75 kN/m and 1847.0 N.s/m, respectively. Moreover, it reveals that the seat and dummy system has additional higher modes above 10 Hz due to the multi-body nature of the dummy being excited.

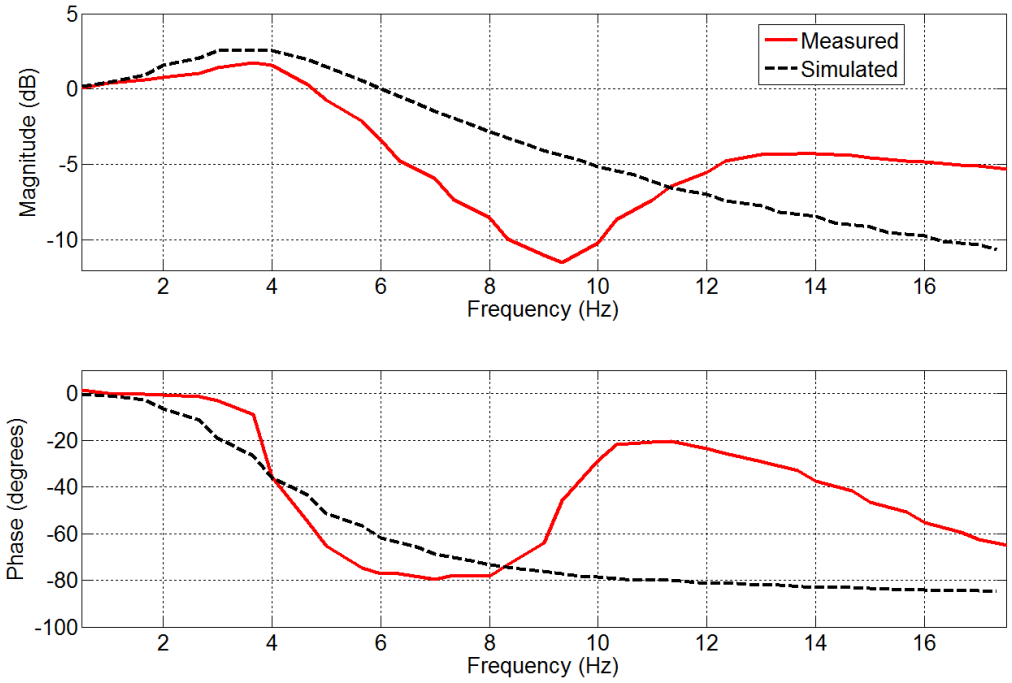

Figure 6-2: Comparison between the measured and simulated frequency responses of the seat acceleration using a 1 DOF passive seat suspension model

Once the characteristics of the passive seat suspension have been identified, the integrated model was modelled using Simulink and the MATLAB GA optimisation toolbox was used to solve the optimisation problem off-line with a random road of class E (very poor) road roughness, as given in Chapter 3, and a vehicle forward speed of 60 km/h. The simulated vehicle suspension parameters, GA parameters and the obtained optimum gains are listed in Table 6-1.

After obtaining the optimum gains, the proposed control strategy was investigated experimentally. As mentioned previously, the preview information used in the control strategy are both the displacement and velocity of the vehicle suspension from the QvM. This is based on the fact that the MAST was able to mimic the motion of the sprung mass of the QvM using the HIL technique as explained in the previous chapter. The measured states of the MAST and the simulated states of the unsprung mass (wheel), together with the optimum gains, were used to generate the demand control force through the two linear actuators mounted on the active seat. Figure 6-3 shows a block diagram of the MAST HIL and the proposed controlled active seat suspension in which the control force requires two states from the vehicle suspension. These states are the sprung and unsprung mass relative displacement (x_{rel}) and velocity ($\dot{x}_{rel}$). The vertical motion of the MAST which represents the sprung mass

motion in the QvM, was measured using a position transducer (LVDT) within the MAST hydraulic actuators. The unsprung mass motion was estimated 'virtually' from the simulated QvM and the suspension displacement is obtained by subtracting these two states while the suspension displacement is differentiated to determine the suspension velocity. Subsequently, the suspension displacement and velocity are fed to the control algorithm model in Simulink to generate the demand control force. In practice, these two states can be easily acquired using inexpensive commercial position transducers.

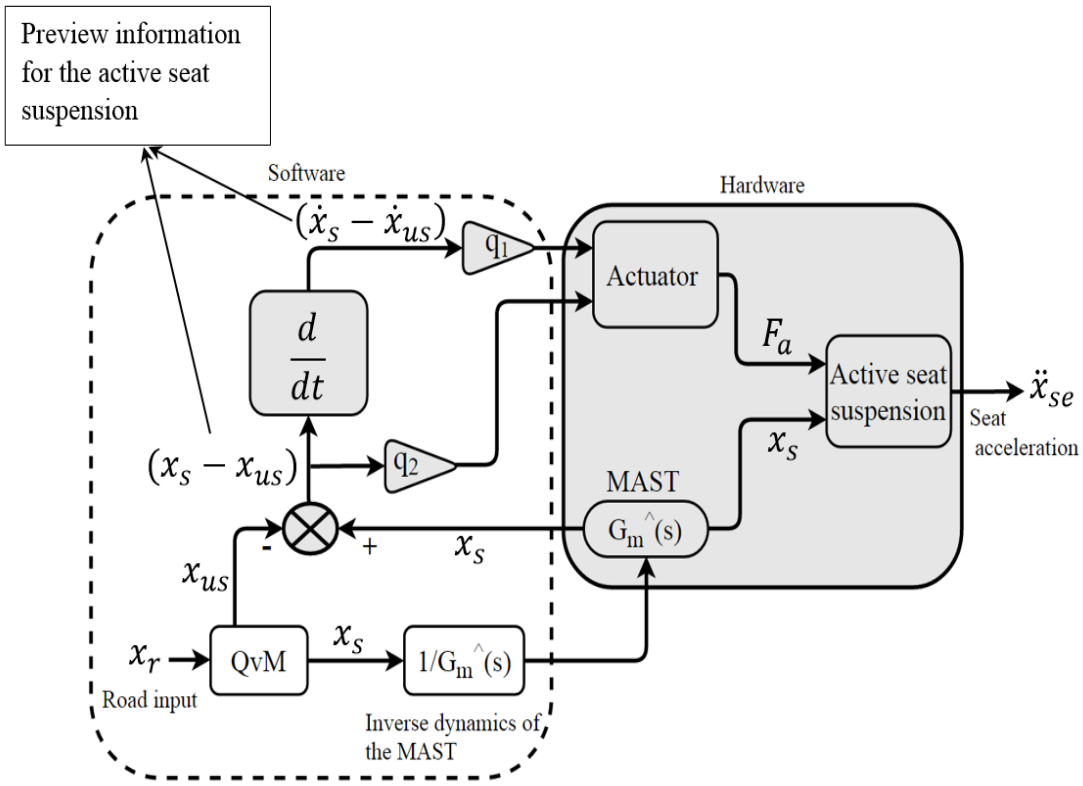

Figure 6-3: Block diagram of the HIL and the preview information control

Table 6-1: QvM and GA simulation parameters and optimum gains values

QvM parameters		
Parameter	Value	Unit
$\boldsymbol{M_s}$ (Sprung mass)	250	Kg
$\boldsymbol{M_{us}}$ (Unsprung mass)	20	Kg
$\boldsymbol{C_s}$ (Suspension damper coefficient)	1500	N.s/m
$\boldsymbol{k_s}$ (Suspension stiffness)	10	kN/m
$\boldsymbol{k_t}$ (Tyre stiffness)	180	kN/m
Optimum gains		
$\boldsymbol{q_1}$	-64.1	N.s/m
$\boldsymbol{q_2}$	5.35	kN/m
GA parameters		
No. of population	40	
No. of generation	6000	
Crossover probability	0.4	
Mutation probability	0.001	

6.3 Performance validation

6.3.1 Frequency domain testing

To validate the performance of the proposed control strategy, the acceleration transmissibility of the active seat was measured and compared to the passive seat, as shown in Figure 6-4. This figure reveals that the active seat suspension significantly attenuates the transmitted vibration at the seat when compared with the passive suspension, with a maximum reduction level of 10 dB, achieved at around 10 Hz. In addition, the acceleration transmissibilities of the passive and active systems obtained from the numerical simulation, using the integrated QvM and seat models, are shown Figure 6-5. These results prove once again the effectiveness of the developed control strategy in suppressing the seat vibration both in simulation and

experimental tests. Whilst the experimental and numerical results for both the passive and active systems have very comparable behaviours, there are differences between simulation and experiment, mainly due to the system non-linearities and a multi-body experimental dummy that is not considered in the simulated model.

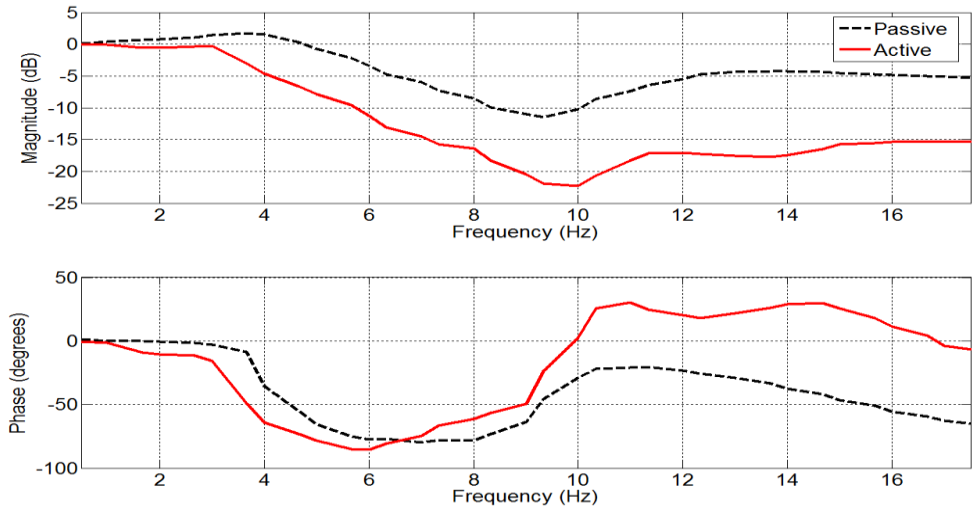

Figure 6-4: Seat acceleration transmissibility for the passive and active seat suspension using preview information control in experimental test

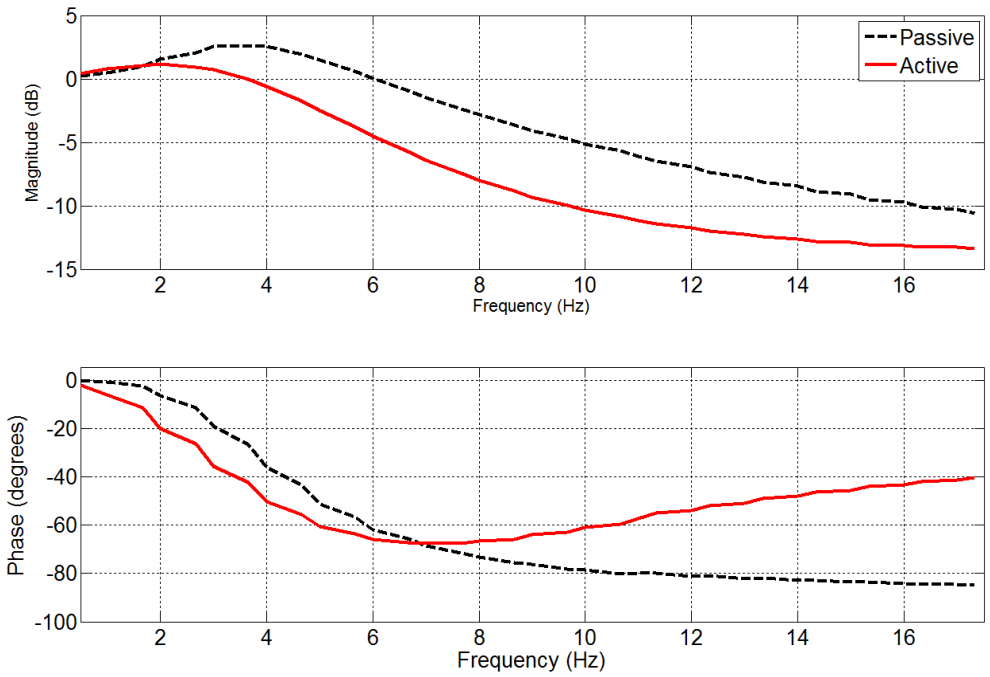

Figure 6-5: Seat acceleration transmissibility for the passive and active seat suspension using preview information control in the simulation test

6.3.2 Time domain

The aim of this section is to evaluate the active seat suspension under different road excitations, including bump and random road profiles, at a range of forward vehicle speeds. For the random road excitation case, the assessment was carried out by comparing the measured and simulated results of the passive and active SEAT factors as well as the frequency weighted RMS acceleration values. In addition, a health risk assessment based on ISO 2631-1, is also presented. In the case of the bump excitation, the evaluation was performed through simulation of the seat acceleration and seat suspension displacements.

6.3.2.1 Random response

Based on the fact that the vehicle forward speed influences the energy content of the transmitted vibration to the vehicle body in the case of a random road disturbance, three vehicle speeds were examined (40, 60 and 100 km/h). In addition, due to the random nature of the road profile the simulation was carried out 100 times for each vehicle speed, each with a time duration of 10 seconds. The experimental tests were repeated three times and an average is taken. To avoid excessive MAST accelerations at high frequency, the reference road roughness $\Phi(\Omega_0)$ used in both the simulation and experiments was set as $16 \times 10^{-6}\ m^3$.

Figure 6-6 shows the measured passive and active time responses in terms of the seat acceleration and seat suspension displacement as well as the road profiles. It is clear that the seat vibration attenuation achieved by the active seat is superior to the passive system. However, this improvement in the seat vibration isolation performance is achieved at the cost of increasing seat suspension displacements. Nonetheless, this increase is within the allowable seat suspension stroke.

The power spectrum densities (PSD) of the passive and active acceleration time responses are presented in Figure 6-7. At low frequencies (< 3 Hz), the active and passive seat suspensions show very similar behaviour for low and medium vehicle speeds. At higher frequencies above 3 Hz, the active seat delivers a substantial reduction in the transmitted vibration PSD, thus demonstrating the effectiveness of both the controller and active system.

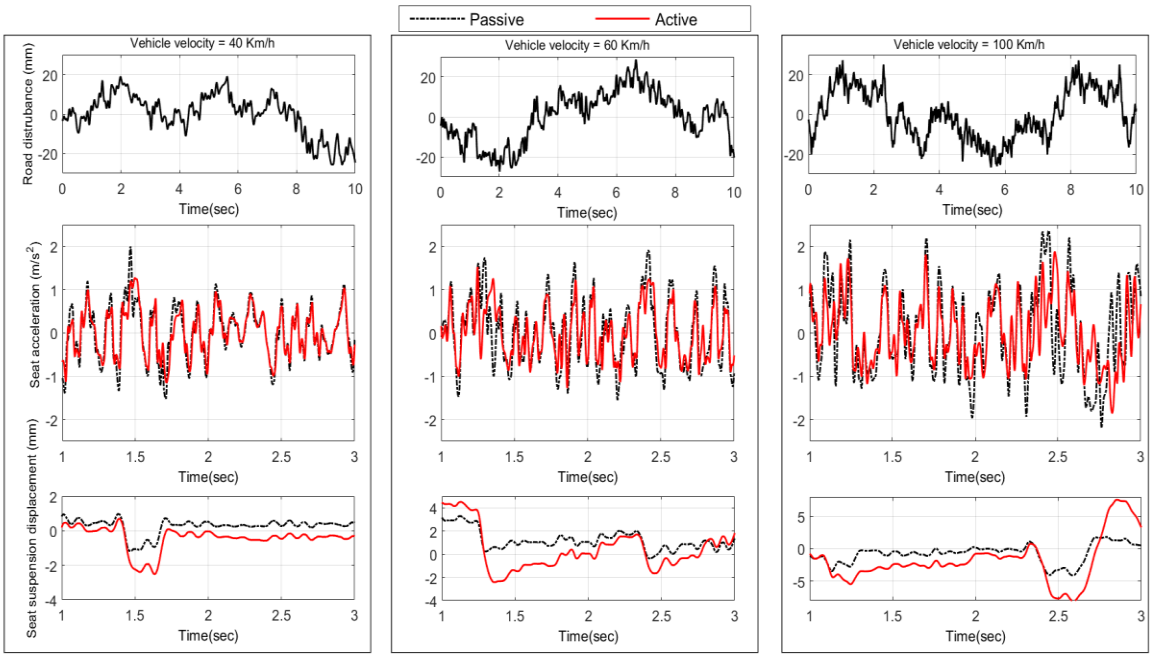

Figure 6-6: Measured time responses for the passive and active seat suspension with preview information control under random road excitation and different vehicle speeds

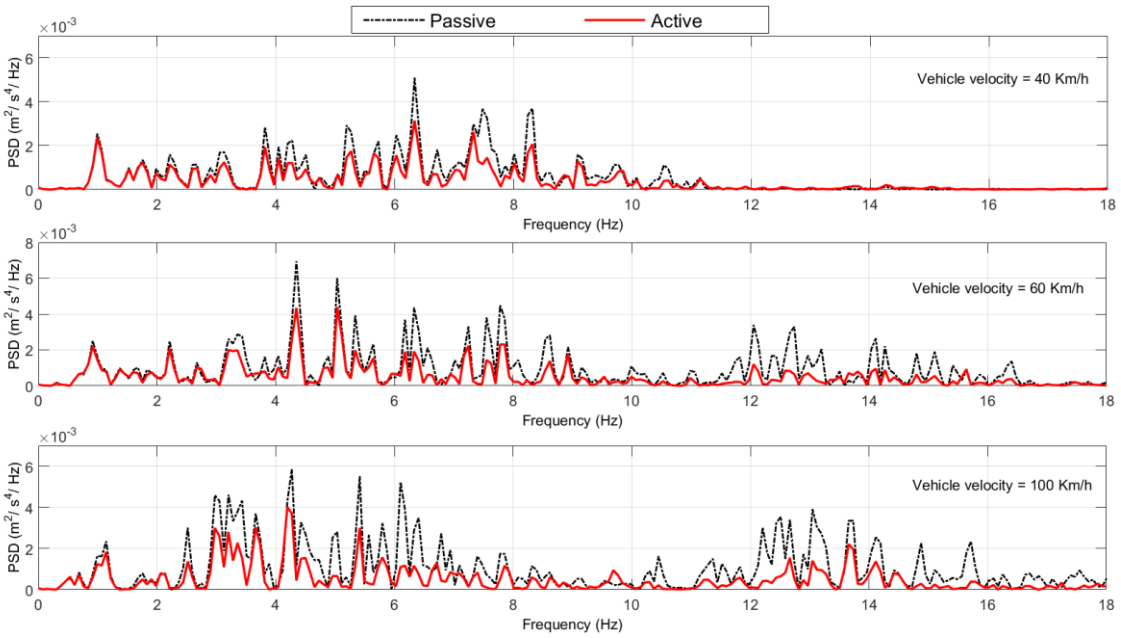

Figure 6-7: PSDs of the seat acceleration for the passive and active seat suspensions with preview information control in the experimental test

Figure 6-8 presents the measured and simulated SEAT factors for both the passive and active seat suspensions at different vehicle speeds. It is notable that the measured and simulated SEAT factors of the active seat are lower than those of the passive system at all the tested

vehicle speeds. Moreover, the maximum percentage improvements when compared with the passive system were 37.5 % and 30.2 % for the simulated and measured systems, respectively. The measured and predicted frequency weighted RMS seat acceleration values of the active and passive seat suspensions are shown in Figure 6-9. It can be seen that for both sets of results the active system has lower weighted RMS seat acceleration values than that of the passive system regardless of the vehicle speed. The proposed active system delivers improvements of more than 30 % and 20 % for the simulated and measured systems respectively, in the weighted RMS seat acceleration when compared with the passive system.

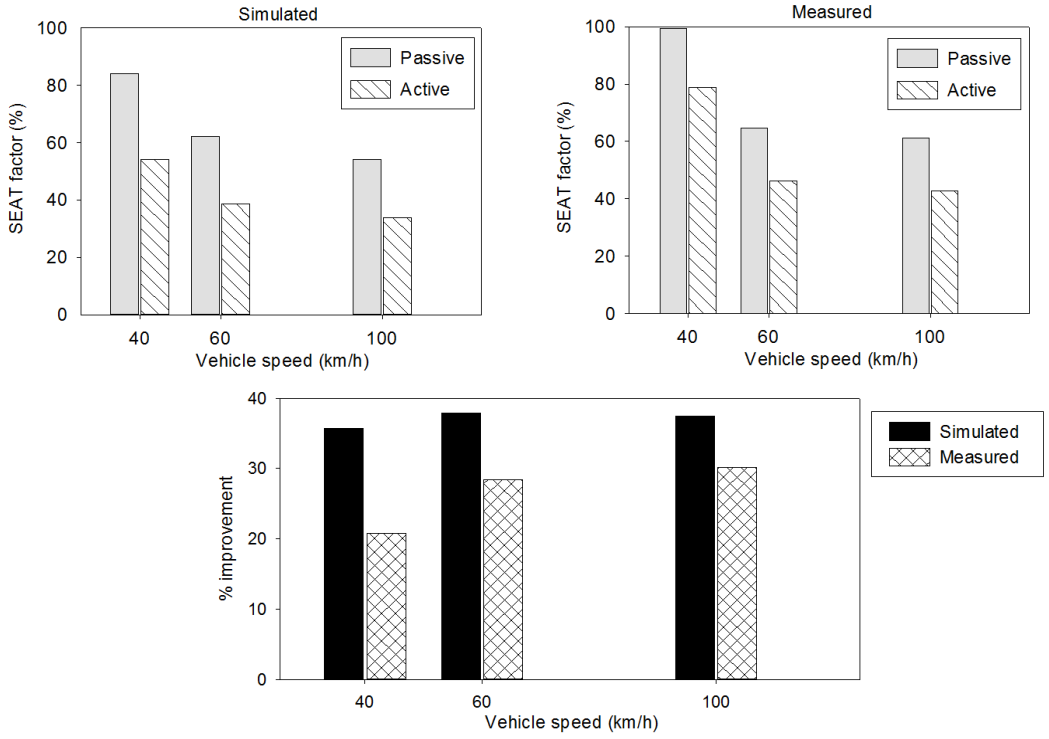

Figure 6-8: Measured and simulated SEAT factor values for the passive and active seat suspension with preview information control and percentage improvements at different vehicle speeds

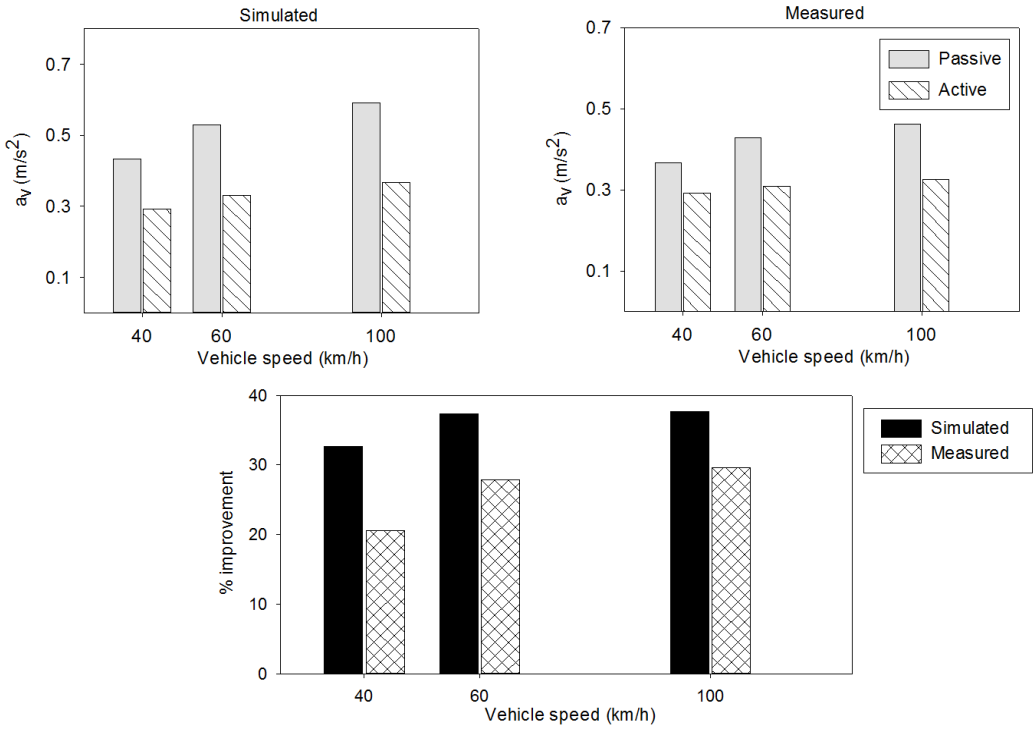

Figure 6-9: Measured and simulated weighted RMS seat acceleration (a_v) for the passive and active seat suspension with preview information control and percentage improvements at different vehicle speeds

Figure 6-10 shows the frequency-weighted RMS acceleration of the active and passive seat suspensions regarding the TLVs, as suggested by the standard ISO 2631-1 at different vehicle speeds. Clearly the proposed active seat suspension operates better than the passive alternative in reducing the weighted RMS seat acceleration over a broadband frequency range especially over the human body sensitive frequency (HBSF) range (4-8 Hz), in which the passive system exceeds the 8h working daily exposure limit. In summary, the active system offers a more comfortable and safer working environment than the passive system.

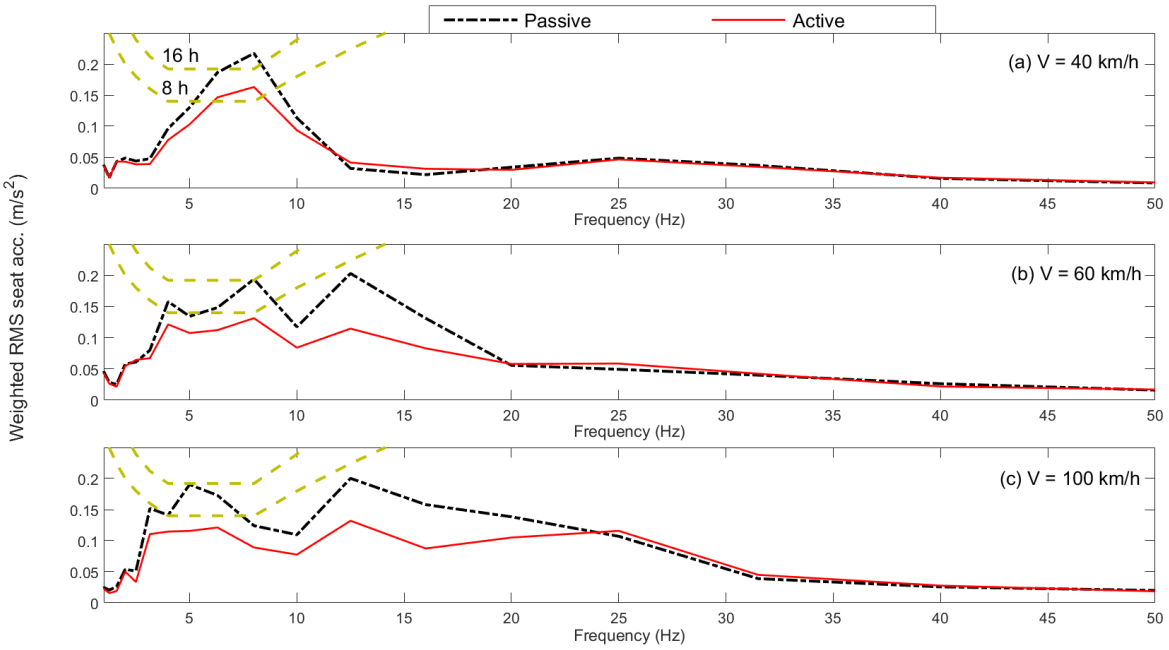

Figure 6-10: Health risk assessment, according to ISO 2631-1, for the passive and active seat suspension with preview information control at different vehicle speeds in the experimental test

6.3.2.2 Bump response

Figure 6-11 shows the simulated time responses of the passive and active seat suspensions under a bump road profile as given by Eqn. (3-17) at different vehicle forward speeds. The RMS values of both the seat acceleration and the seat suspension displacement are listed in Table 6-2. These results reveal that the active seat decreases the seat acceleration more effectively than the passive suspension irrespective of the vehicle forward speed. Nevertheless, this is at the expense of increasing the seat suspension displacement. Moreover, the attenuation performance of the active seat suspension at higher forward vehicle forward speeds is also improved, whereas the seat suspension displacement is decreased compared with that at lower vehicle speeds. These results prove once again that the controller is able to improve the ride quality of the seat without exceeding the allowable limit of the seat suspension travel.

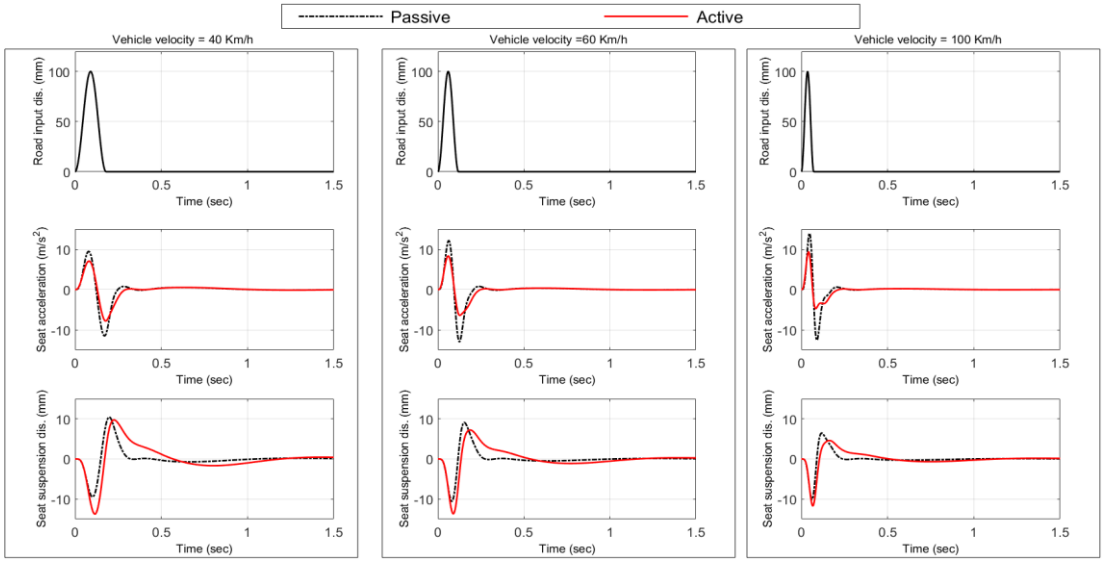

Figure 6-11: Time responses for the passive and active seat suspension with preview information control under a bump road excitation and different vehicle speeds in the simulation test

Table 6-2: Comparison between the performance of the passive and the active seat suspension with preview information control under a bump road profile

Vehicle speed (Km/h)	Bump road profile (Simulated)					
	Seat acceleration RMS (m/s2)		% Improvement	Seat suspension displacement RMS (mm)		% Increase
	Passive	Active		Passive	Active	
40	1.34	1.02	31.40	1.37	1.92	40.20
60	1.37	0.92	32.90	1.22	1.53	25.40
100	1.24	0.75	39.50	0.96	1.06	10.40

6.4 Conclusions

This chapter has presented the development of a novel, simple and inexpensive control strategy for an active seat suspension system based on using measurable and available preview information from the vehicle suspension to attenuate the harmful vertical vibration

over low-frequency range (1-20 Hz) transmitted to a driver as a result of road excitation. The effectiveness of this control strategy has been validated through numerical simulation involving a quarter vehicle model (QvM) and experimental laboratory tests in both the frequency and time domains including different working conditions and road profiles. Both sets of results have demonstrated the effectiveness of the active controller in attenuating the transmitted vibration at the seat. Based on the experimental measurements, an attenuation of more than 10 dB in the frequency domain and a 20 % improvement in the SEAT factor have been achieved with this active seat suspension when compared with the passive alternative regardless of the vehicle speed. In general, this approach offers a viable, practical and cost-effective active seat controller that reduces driver fatigue and provides a safer and comfortable working environment. Further modifications of the developed control approach will be presented in the next chapter.

Chapter 7
An Experimental Study of Active Seat Suspension Controllers with Vehicle Suspension Feedforward and Feedback States

In the previous chapter, the concept of using measurable preview information from the vehicle suspension for controlling an active suspension was presented and its effectiveness in suppressing vertical vibration at the seat was confirmed through both simulation and experimental tests. This chapter involves the development and testing of simple and practical control strategies for the active seat suspension, which employ such preview information together with measurable feedback system states, whilst at the same time satisfying the physical limitations associated with both the seat suspension stroke and control force capacity. Initially, the integrated mathematical model used previously is modified to include the effects of driver body dynamics. Then, the characteristics of the passive seat suspension and the driver body models are estimated through experimental tests. The control force of each control strategy is derived using the same linear approach presented in the previous chapter, and then, the strategies are implemented in real time using the experimental test rig described in chapter 5. Laboratory experimental tests are carried out to evaluate the effectiveness of these strategies in improving ride comfort, according to the ISO 2631-1 standard, in both the frequency and time domains, with a range of different vehicle speeds and two road profiles: random and bump.

7.1 Modification of the integrated model

The integrated model used in chapter 6 was simple and neglected the driver body dynamics. Hence, to make the application more realistic and retain the simplicity, this model has been modified by including the driver body dynamics as a 1 DOF linear lumped spring-damper-mass system as shown in Figure 7-1. The displacement of the driver body mass m_b in the

vertical direction is x_b, whilst k_b and c_b denote the spring stiffness and damper coefficient of the driver body model. Thus, the governing equations of motion in the vertical direction are given as follows:

$$m_b\ddot{x}_b = -c_b(\dot{x}_b - \dot{x}_{se}) - k_b(x_b - x_{se}) \quad \textbf{(7-1)}$$

$$m_{se}\ddot{x}_{se} = c_b(\dot{x}_b - \dot{x}_{se}) + k_b(x_b - x_{se}) - c_{se}(\dot{x}_{se} - \dot{x}_s) - k_{se}(x_{se} - x_s) + F_a \quad \textbf{(7-2)}$$

$$m_s\ddot{x}_s = c_{se}(\dot{x}_{se} - \dot{x}_s) + k_{se}(x_{se} - x_s) - c_s(\dot{x}_s - \dot{x}_{us}) - k_s(x_s - x_{us}) - F_a \quad \textbf{(7-3)}$$

$$m_{us}\ddot{x}_{us} = c_s(\dot{x}_s - \dot{x}_{us}) + k_s(x_s - x_{us}) - k_t(x_{us} - x_r) \quad \textbf{(7-4)}$$

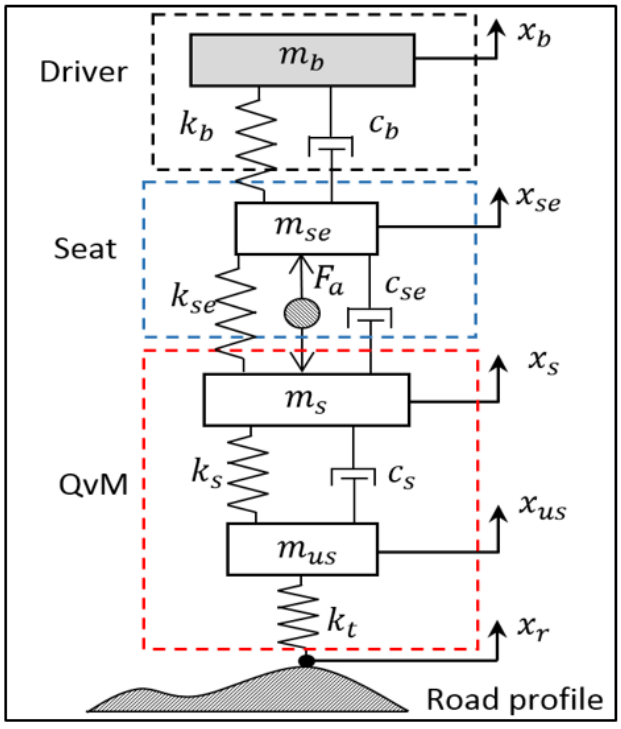

m_b	Mass of a seated driver
k_b	Driver body stiffness
c_b	Driver body damping coefficient
x_b	Vertical displacement of a seated driver
m_{se}	Seat mass
k_{se}	Seat suspension spring
c_{se}	Seat suspension damper
x_{se}	Vertical displacement of the seat
m_s	Sprung mass
k_s	Vehicle suspension spring
c_s	Vehicle suspension damper
x_s	Vertical displacement of the sprung mass
m_{us}	Usprung mass
k_t	Tyre stiffness
x_{us}	Vertical displacement of the tyre
x_r	Road surface
F_a	Active control force

Figure 7-1: QvM, a 1 DOF active seat suspension and 1 DOF driver model

7.2 Active seat suspension control strategies

As mentioned in the previous chapters, the availability and cost of the required states to control an active seat suspension significantly affect the practical implementation of such a system. Not only this, but it also impacts on the complexity of the control strategy itself. Based on these facts, five simple control strategies are designed to attenuate the vertical vibration at the driver's seat. The control force is expressed as a linear function of the preview information from the vehicle suspension combined with the feedback system states with optimum gains, as presented in Table 7-1.

Table 7-1: Actuator force controller algorithms

Control strategy	Control force (Fa)
A1	$F_a = q_1 (\dot{x}_s - \dot{x}_{us}) + q_2 (x_s - x_{us})$
A2	$F_a = q_3 (\dot{x}_s - \dot{x}_{us}) + q_4 (x_s - x_{us}) + r_1 \ddot{x}_s$
A3	$F_a = q_5 (\dot{x}_s - \dot{x}_{us}) + q_6 (x_s - x_{us}) + r_2 \ddot{x}_{se}$
A4	$F_a = q_7 (\dot{x}_s - \dot{x}_{us}) + q_8 (x_s - x_{us}) + r_3 \ddot{x}_s + r_4 \ddot{x}_{se}$
A5	$F_a = q_9 (\dot{x}_s - \dot{x}_{us}) + q_{10} (x_s - x_{us}) + r_5 (\dot{x}_{se} - \dot{x}_s) + r_6 (x_{se} - x_s)$

All of the controllers, A1 to A5, use preview information from the vehicle suspension in terms of the displacement $(x_s - x_{us})$ and velocity $(\dot{x}_s - \dot{x}_{us})$ of the vehicle suspension. Controller A1 requires preview information alone while A2 employs the preview information and the acceleration of the vehicle body (the sprung mass in the QvM). A3 utilises the preview information together with the acceleration of the seat, whereas both the seat and the sprung mass acceleration states are used in the controller A4. The last controller, A5, uses the preview information as well as the feedback states of the seat suspension's displacement and velocity, $(x_{se} - x_s)$ and $(\dot{x}_{se} - \dot{x}_s)$, respectively.

The parameters gains ($q's$) and ($r's$) in Table 7-1, refer to the gains of the feed-forward (preview information) and feedback states for each control strategy, respectively. These are determined

using the same optimisation process given previously in chapter 6 as well as the same constraints regarding the seat suspension stroke and actuator force saturation.

7.3 Identifying the passive seat characteristics

The integrated model shown in Figure 7-1 was modelled using Simulink and the MATLAB GA optimisation toolbox was utilised to solve the optimisation problem. To make the application more realistic, the characteristics of the passive seat suspension (m_{se}, k_{se} and c_{se}) , as well as the driver (k_b and c_b), were estimated based on laboratory tests using the experimental rig, including the passive seat suspension and the dummy, as presented in chapter 5. The MAST was excited by a swept sinusoidal displacement signal with an amplitude of 10.0 mm and a frequency range of 1-20 Hz. The resulting vertical seat pan and MAST accelerations were measured using a sampling frequency of 10 kHz and filtered using a low pass filter with a cut-off frequency of 250 Hz. Hence, the measured vertical acceleration transmissibility from the MAST to the passive seat suspension was obtained and subsequently, the simulated values of the passive seat suspension, as well as the driver's body model, were acquired by fitting this transmissibility with that obtained from the simulated model, as depicted in Figure 7-2. It can be seen that there is a reasonable match between the measured and the simulated seat acceleration transmissibilities over the frequency range of interest (<12 Hz). However, it was found that there was a compromise between fitting either the magnitude or the phase frequency responses. A fundamental natural frequency of the passive seat suspension and the dummy was observed at a frequency of 3.5 Hz, together with additional passive seat suspension and dummy higher order dynamics above 12 Hz, which were not predicted by the simplified model.

The estimated parameters of the passive seat suspension and the dummy are listed in Table 7-2 while the GA parameters are given in Table 7-3, and the calculated optimum controller gains for each controller strategy are listed in Table 7-4.

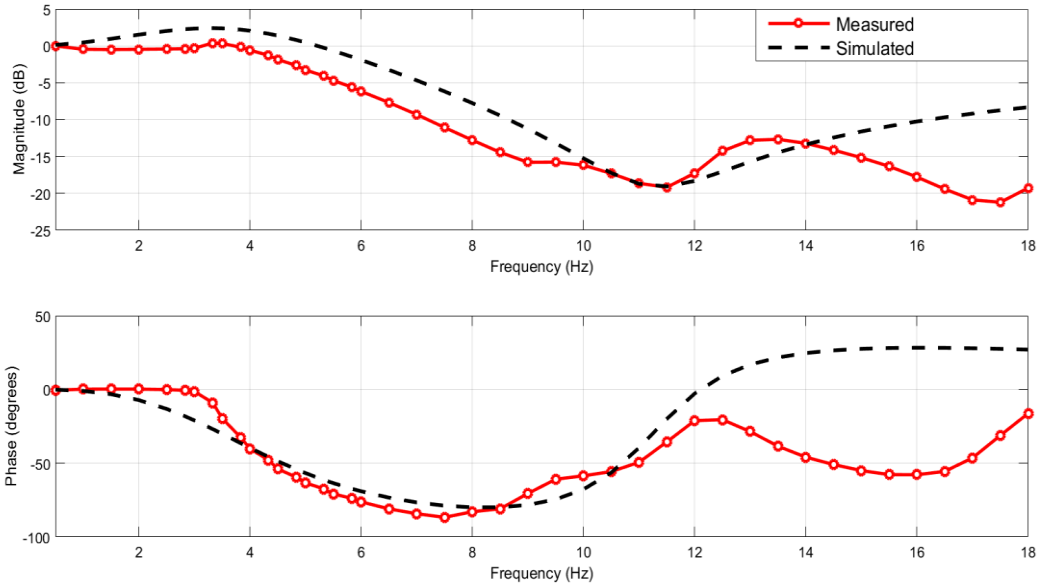

Figure 7-2: Comparison between the measured and simulated seat acceleration transmissibility for the passive seat suspension with a 1 DOF driver model

Table 7-2: QvM and estimated parameters of the passive seat suspension and the dummy

Parameter	Value	Unit
m_{se}	5.0	Kg
m_b	55.25	Kg
c_{se}	2.10	kN.s/m
k_{se}	42.0	kN/m
c_b	0.90	kN.s/m
k_b	280.0	kN

Table 7-3: GA parameters

No. of population	40
No. of generation	1000
Crossover probability	0.2
Mutation probability	0.01

Table 7-4 : Optimum gains of the active seat suspension controller strategies

Gain	Value	Unit
q_1	-93.0	N.s/m
q_2	20.512	kN/m
q_3	-40.0	N.s/m
q_4	21.0	kN/m
q_5	-10.0	N.s/m
q_6	21.0	kN/m
q_7	-50.0	N.s/m
q_8	19.5	kN/m
q_9	-55.0	N.s/m
q_{10}	24.0	kN/m
r_1	1.0	N.s²/m
r_2	1.0	N.s²/m
r_3	0.3	N.s²/m
r_4	0.8	N.s²/m
r_5	-4.0	N.s/m
r_6	20.0	kN/m

7.4 Experimental tests

Once the optimum gains of each active controlled seat suspension strategy had been obtained, these strategies were then implemented in real time using the experimental test rig and the principle of the HIL approach defined in chapter 5, in both the frequency and time domains.

Figure 7-3 shows a block diagram of the MAST HIL and the control strategies as well as the experimental setup for testing the active seat suspension. The following sections present the assessment of these strategies through experimental laboratory tests, in both the frequency and time domains with different road disturbances.

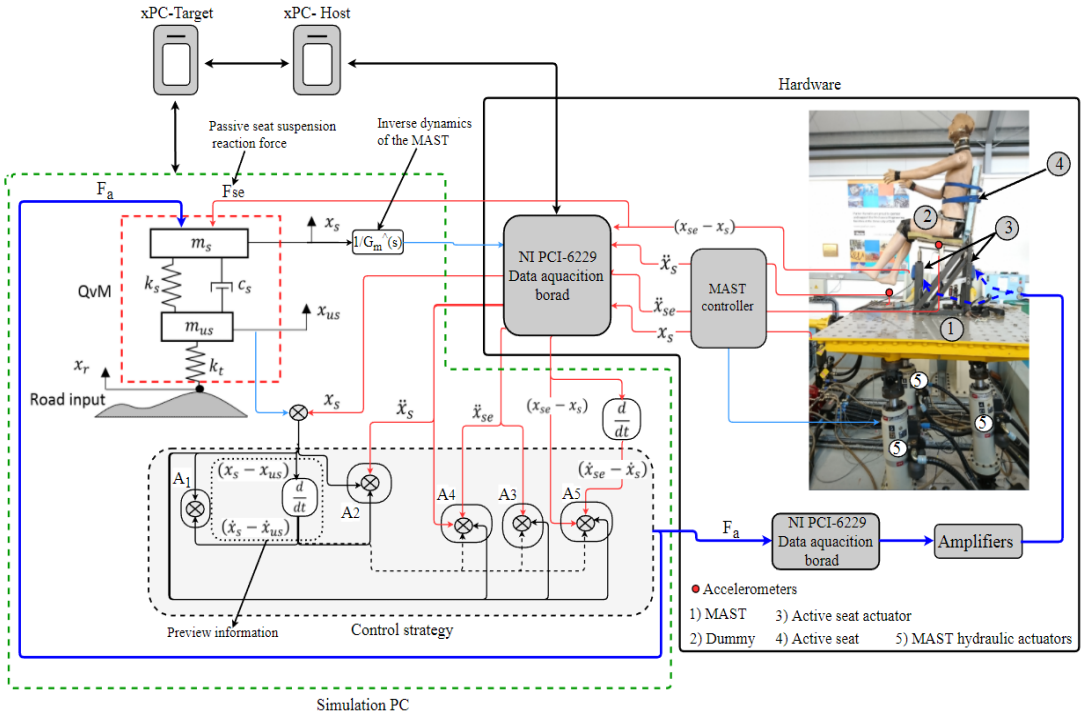

Figure 7-3: General experimental setup and HIL simulation for the active seat suspensions using the preview information- feedback controllers: A1, A2, A3, A4 and A5

7.4.1 Frequency domain testing

The performance of the proposed control strategies (A1-A5) was estimated from the acceleration transmissibility of the active seat with respect to the MAST using both experimental tests and simulation, as shown in Figure 7-4. It can be observed from both the experimental and simulation results that for all five controllers the vibration attenuation of the active seat suspension is superior to the passive seat, all be it with different reduction levels depending on the frequency range. Interestingly, the simplest controller A1 demonstrates the best performance over the low-frequency range (3.5-4.5 Hz), although its performance deteriorates at higher frequencies, where the dummy dynamics are more dominant. This may be due to the open loop nature of this controller that uses only feedforward signals, which do not respond to the dummy and the seat dynamics. This phenomenon is also observed in the experimental performance of the feedforward controller A2, although it is not shown in the

simulation as the linear and lumped mass nature of the dynamic system neglects this behaviour.

Controller A3 combines the feedforward vehicle suspension states with the vertical acceleration of the seat in order to generate the control force. This provides superior vibration attenuation when compared with the A1 and A2 controllers, especially over the HBSF range (4-8 Hz). This indicates the importance of feedback states in the suppression of vibration over a broadband frequency range.

The controller A4 performs less well over a low-frequency range less than 5 Hz, whilst its performance is superior above 5 Hz. Likewise, in simulation, the controller A5 shows the best performance across a wide frequency range, but this was not backed up by the experimental results, especially at a low-frequency range (4-5.8 Hz). Moreover, it amplifies the vibration around the fundamental natural frequency of the seat (f_n= 3.33 Hz). This is mainly due to system non-linearities as well as friction and noise, which in real life compromise the feedback signals and result in an incorrect control force that introduces a disturbance to the seat instead of attenuating the vibration. In conclusion, the controller A4 delivers the best performance in vibration attenuation over the whole frequency range of interest, with a minimum and maximum reduction level of 10 and 19.5 dB over the HBSF.

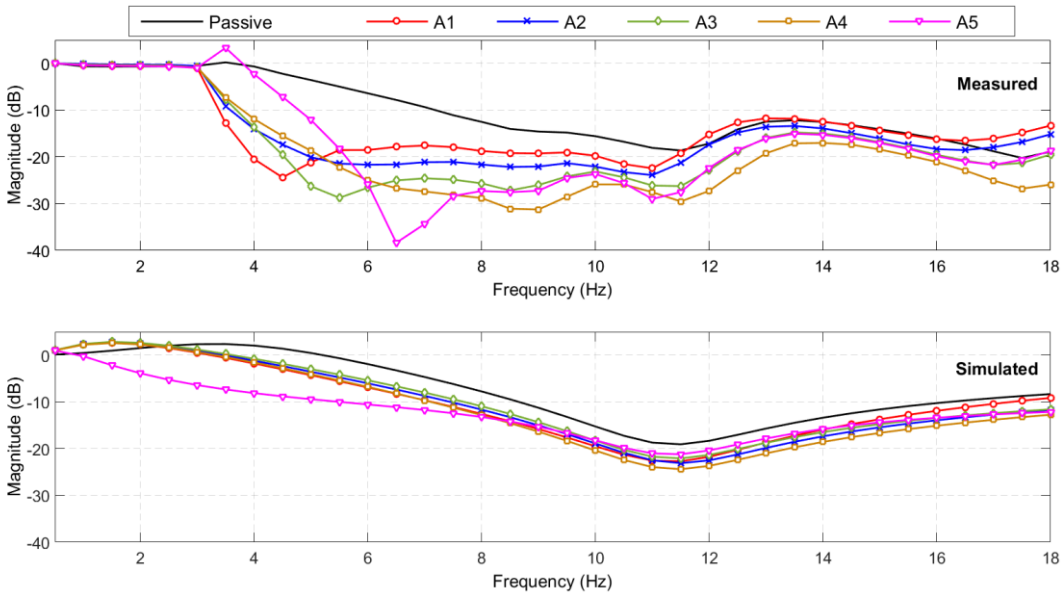

Figure 7-4: Measured and simulated seat acceleration transmissibility for the passive and active seat suspensions using preview information –feedback control approaches

7.4.2 Time domain testing

To investigate the effectiveness of the proposed strategies in the time domain, two common road disturbances were used to excite the QvM including random and bump road profiles. Subsection 2.2.1 presents the experimental evaluation of controlled active seat suspensions when subject to a random road profile at different vehicle speeds. The assessment was carried out by comparing the passive and active SEAT factors and the weighted-frequency RMS seat acceleration in terms of their percentage improvements, according to ISO 2631-1. Furthermore, a health risk assessment, based on the daily working TLVs, is presented. In subsection 2.2.2, the performance is investigated when the QvM was excited by a single bump road input and compared to the passive system.

7.4.2.1 Random road profile

A random road profile was generated according to the ISO 8608 presented in chapter 3, with five different vehicle speeds (20, 40, 60, 80 and 100 km/h) over a period of 12 seconds as shown in Figure 7-5. To avoid extremely large MAST acceleration inputs at high frequencies that could damage the active seat suspension, the road roughness was set as $\Phi(\Omega_0) = 40 \times 10^{-6}\ m^3$.

The measured seat acceleration and seat suspension travel time responses of the active seat suspension with the controllers (A1 to A5) as well as the demand control force are shown in Figures 7.6 to 7.10 parts (a), (b) and (d). It can be observed that all the proposed controllers perform better than the passive suspension in reducing the seat vertical acceleration while maintaining a reasonable seat suspension travel and the demand control force.

The power spectrum densities (PSD) of the active seat suspension using the different proposed controllers (A1 to A5) were compared with the passive seat suspension in Figures 7.6 to 7.10 part (c). Generally, the active seat suspension utilising any of these proposed controllers has lower PSDs, when compared with the passive system over a wide frequency range, especially in the range of 4-8Hz where humans are most sensitive. However, at a low frequency below 4 Hz, the active seat suspension performs less well, especially controllers A1 and A2 that only use the vehicle suspension feedforward signals.

The SEAT factors of the passive and active seat suspensions at a range of vehicle speeds are shown in Figure 7-11. It can be seen that all the proposed active controllers have SEAT factor values less than the passive system, regardless of the vehicle speed. Specifically, the active seat, when using controller A4, provides the best improvement in the SEAT factor reduction, followed by the controller A3, with a percentage improvement of at least 25 % at all vehicle speeds, when compared with the passive system.

The frequency-weighted RMS seat acceleration is also presented Figure 7-11. It is notable that all the active seat suspension controllers provide superior lower frequency-weighted RMS seat acceleration, when compared with the passive seat suspension, across the range vehicle speeds. Also, at intermediate and high vehicle speeds the passive seat system exceeds the "not uncomfortable'' range in terms of ride comfort level, according to the ISO 2631-1 standard. In summary, these results prove the capability and the robustness of the active seat suspensions using the controllers A3 and A4.

Figure 7-12 presents the frequency-weighted RMS acceleration of the active and passive seat suspensions with respect to the TLVs, as suggested by the ISO 2631-1, over the range of vehicle speeds. It can be seen that the active seat suspension, employing any of the proposed controllers, performs better than the passive system, especially over the HBSF range in which the passive system exceeds the 16 h working daily exposure limit. This indicates that, in a practical application, the active seat suspensions provide a less tiring and potentially safer working environment for drivers working long hours.

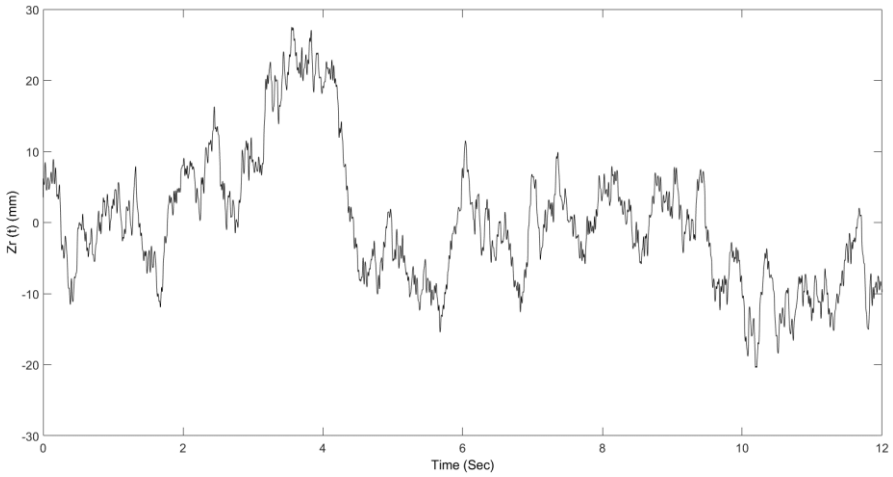

Figure 7-5: Random road profile at a vehicle speed of 60 km/h

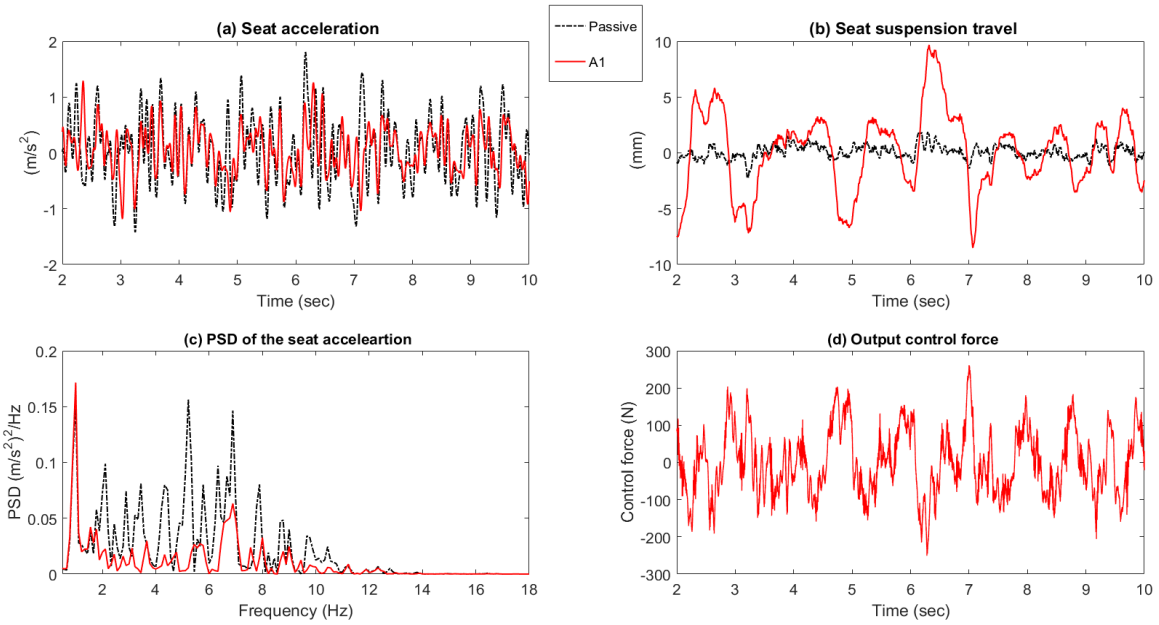

Figure 7-6: Time responses and PSD of the seat acceleration for the passive system and active seat suspension with controller A1

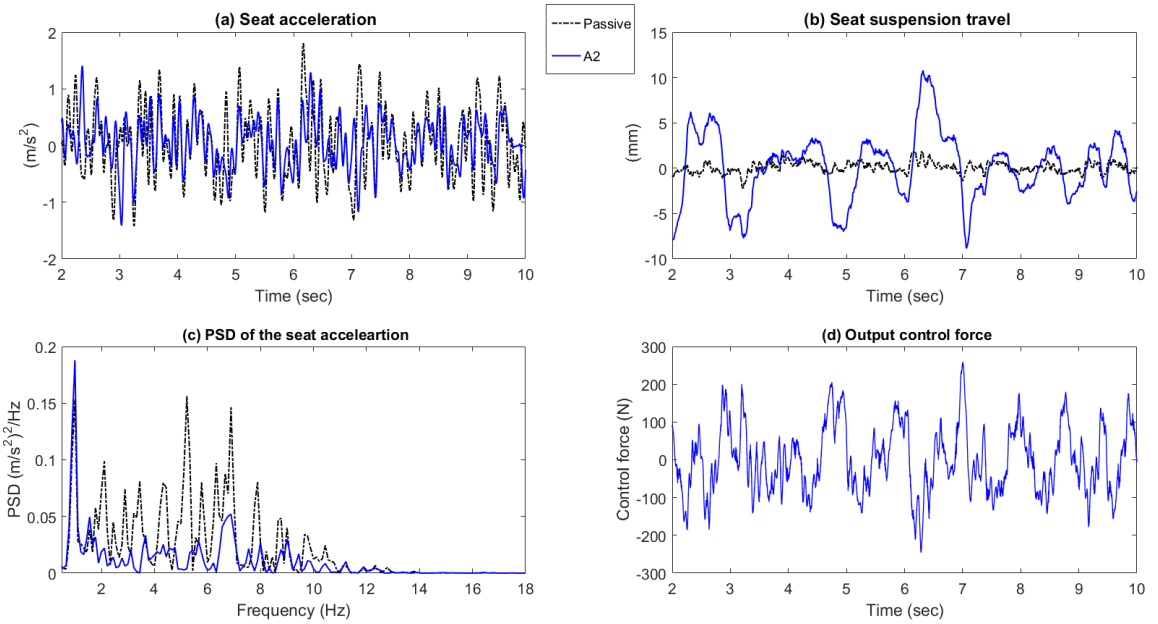

Figure 7-7: Time responses and PSD of the seat acceleration for the passive system and active seat suspension with controller A2

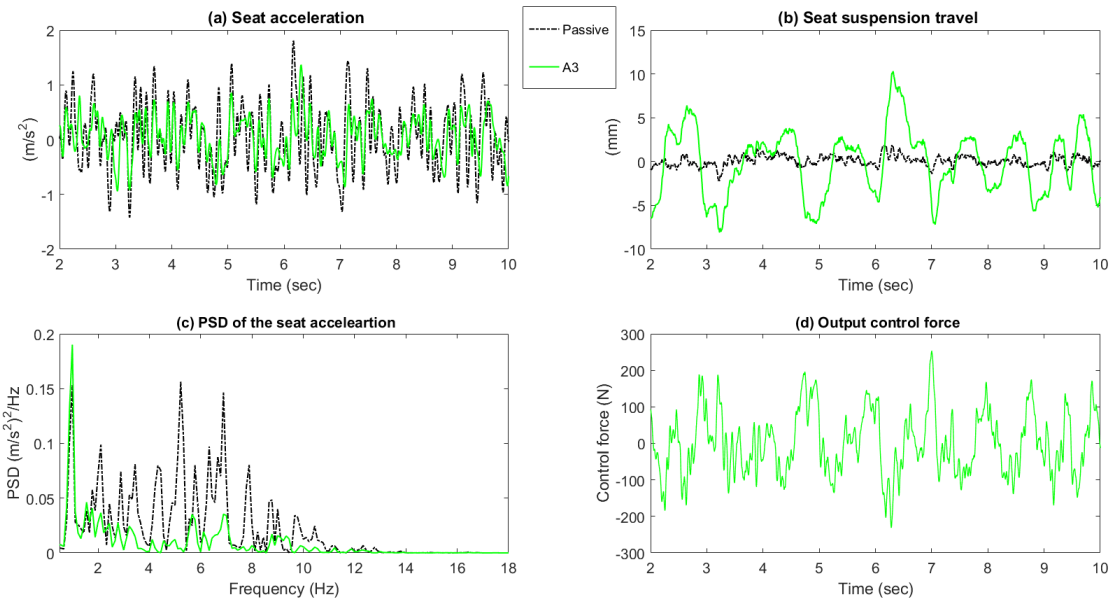

Figure 7-8: Time responses and PSD of the seat acceleration for the passive system and active seat suspension with controller A3

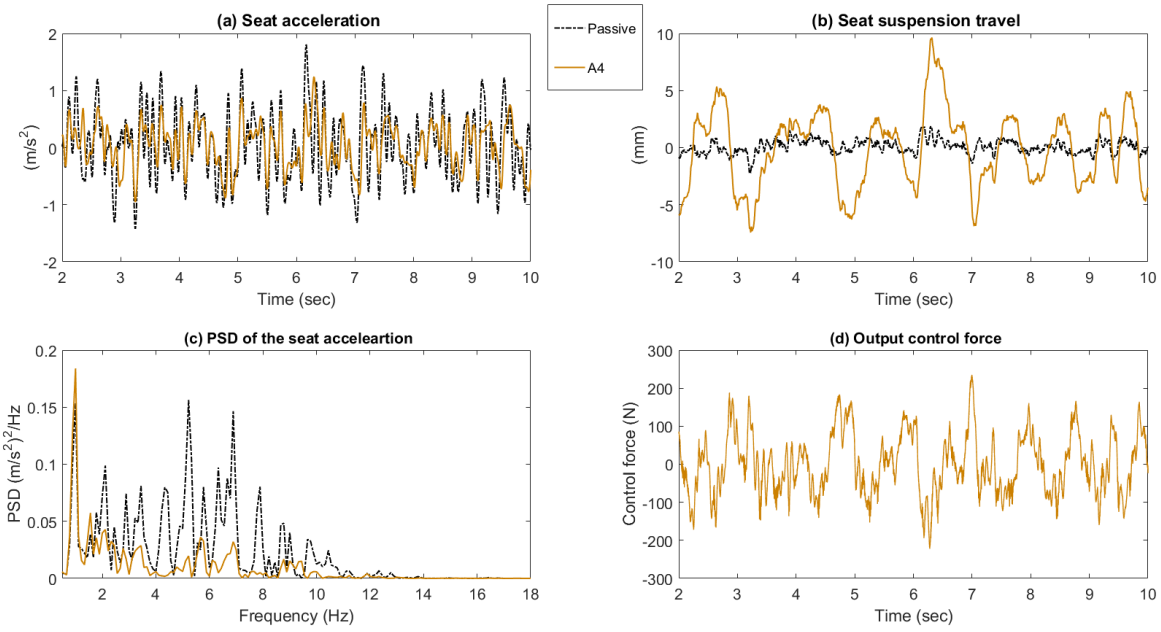

Figure 7-9: Time responses and PSD of the seat acceleration for the passive system and active seat suspension with controller A4

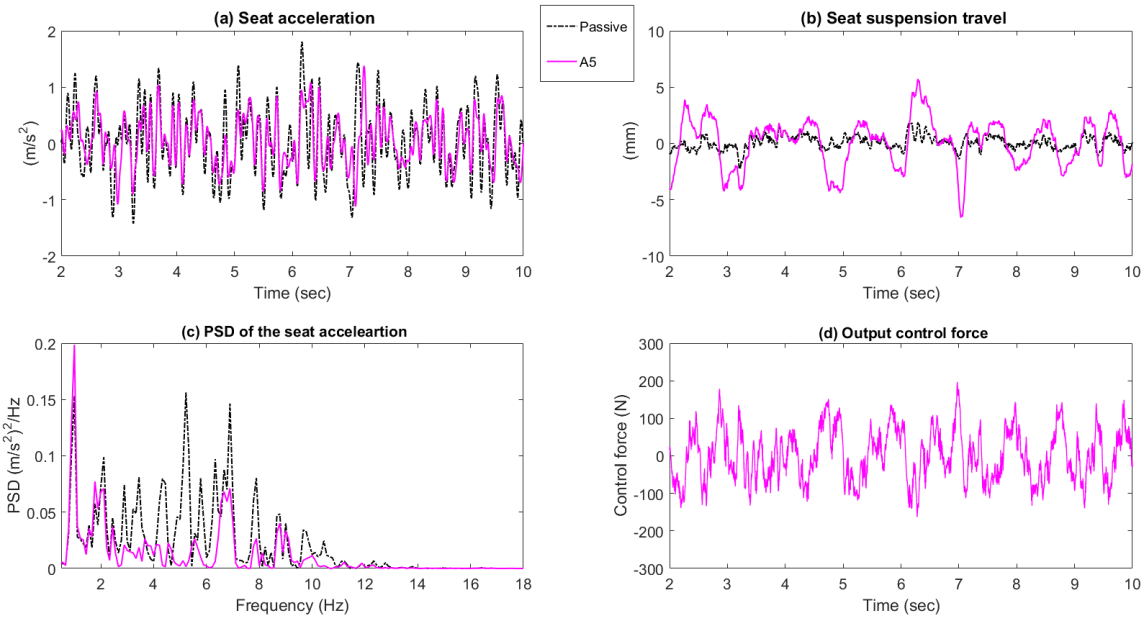

Figure 7-10: Time responses and PSD of the seat acceleration for the passive system and active seat suspension with controller A5

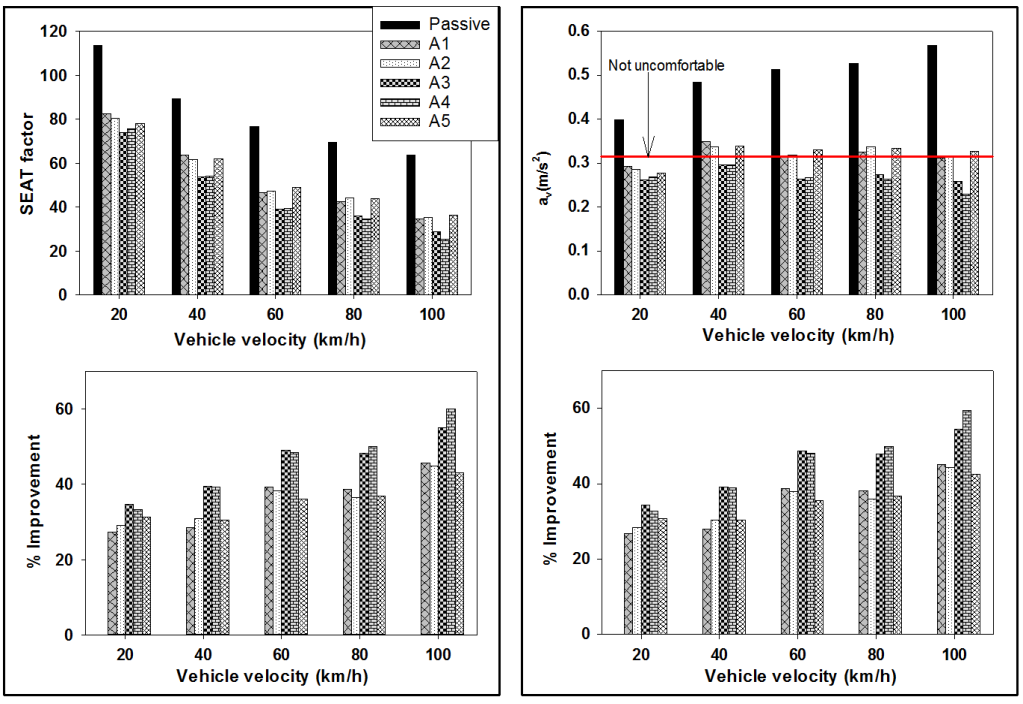

Figure 7-11: Performance assessment for the active seat suspensions using preview information –feedback control approaches under different vehicle speeds

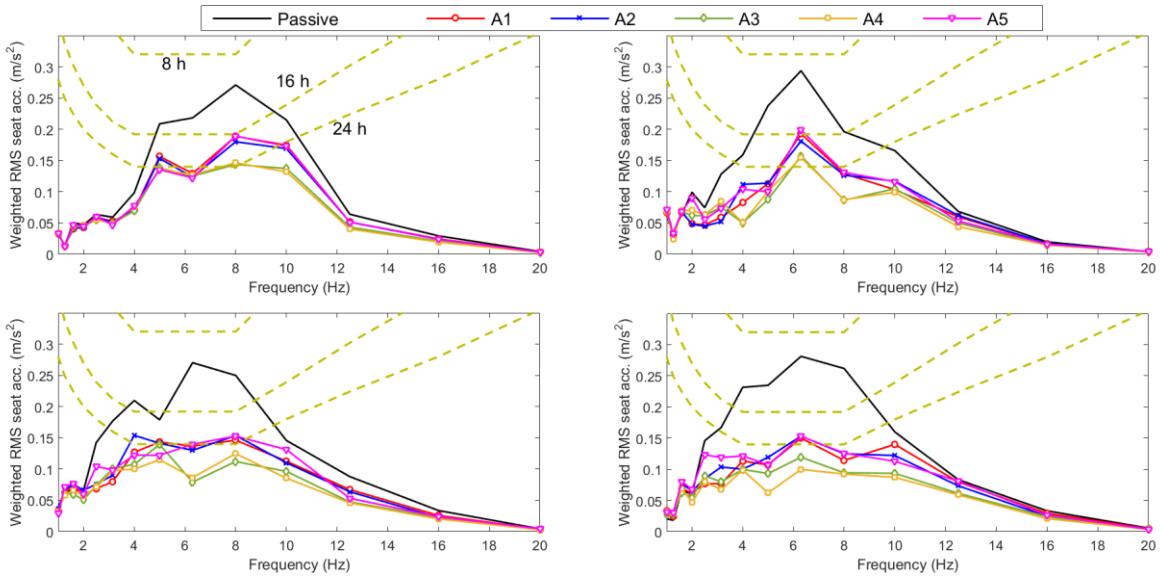

Figure 7-12: Health risk assessment, according to ISO 2631-1, for the passive and active seat suspensions using preview information –feedback control approaches under different vehicle speeds

7.4.3 Bump road profile

In addition to the random road, the performance of the controllers was also examined when subject to a single bump road input at a vehicle speed of 25 km/h, as shown Figure 7-13 (a). This was generated using the formula (Eqn. 3-17) where the values of a and l are 30.0 mm and 2.0 m, respectively.

The measured time responses of the controlled active suspensions in terms of the seat acceleration and seat suspension stroke are compared with those of the passive system in Figure 7-13(b) and Figure 7-14. It can be seen that all the proposed active controllers efficiently reduce the seat acceleration when compared with the passive system. In addition, it was observed that the controllers as well as the passive system change the static position, especially controller A1 as shown in Figure 22b. This is due to the presence of coulomb friction and results in a small random offset following each test. In summary, the controller A1 delivers the best reduction in seat acceleration followed by the controller A2 when compared with the other controllers as presented in Table 7-5. Although the controllers (A3 to A5) show the best performance in simulation tests, this was not backed up by the experimental results. Again, this is attributed to the effects of unmodelled higher-order system dynamics and nonlinearties.

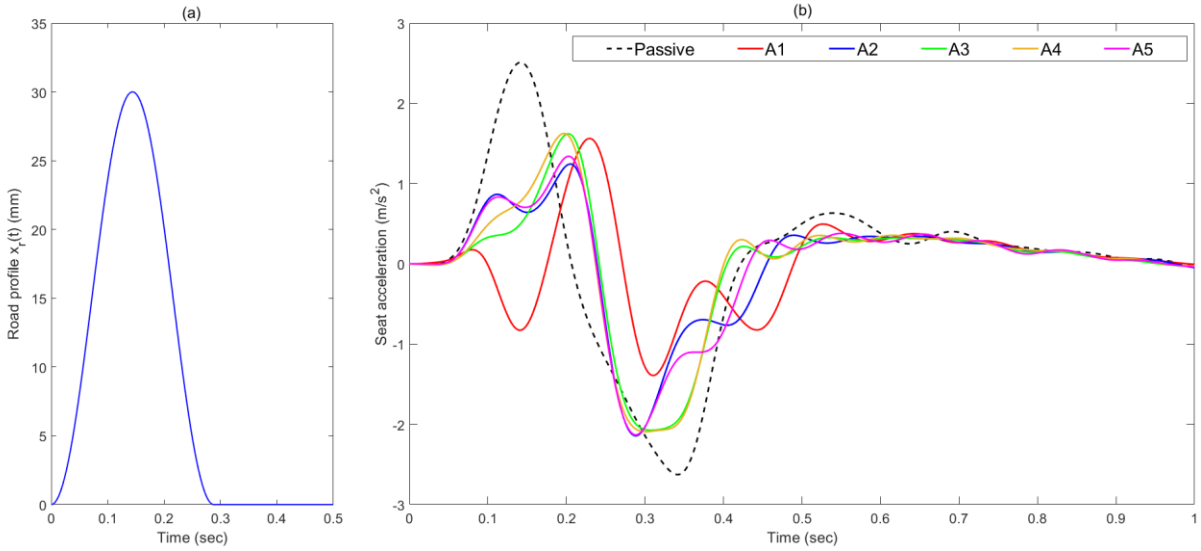

Figure 7-13: Bump road profile and the measured seat acceleration for the passive and active seat suspensions using preview-feedback control approaches: (a) Road profile and (b) Seat acceleration.

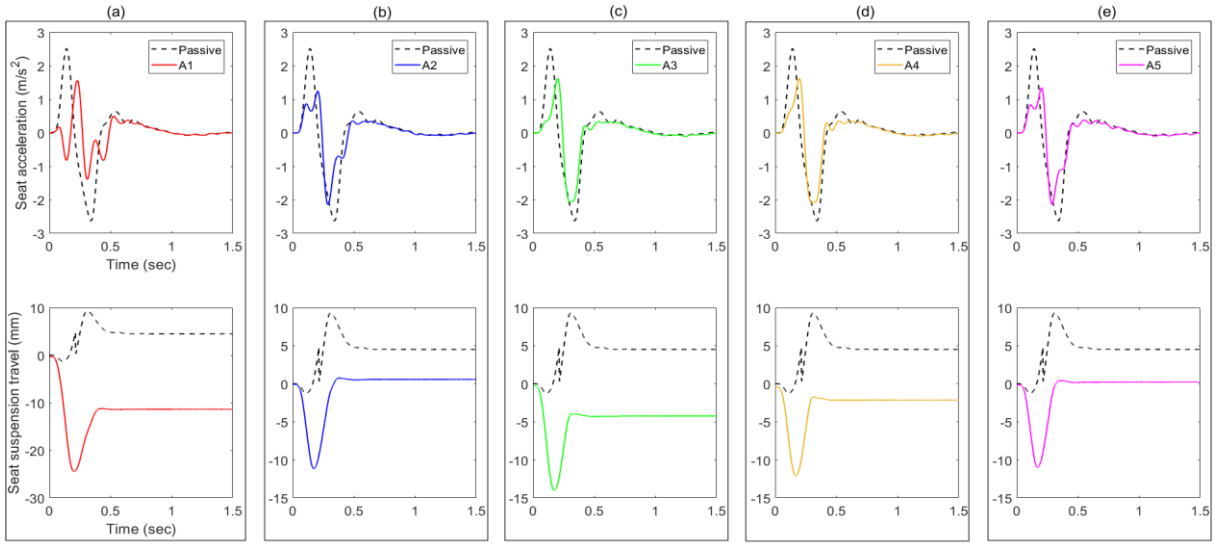

Figure 7-14: Passive and active seat suspension performance when subject to a bump road input: (a) A1, (b) A2, (c) A3, (d) A4 and (e) A5

Table 7-5: Time response characteristics of the active seat suspensions under a bump road profile

Seat system	Seat acceleration RMS (m/s2)	Maximum seat suspension travel (mm)
Passive	0.866	9.302
A1	0.461	24.472
A2	0.566	11.170
A3	0.630	14.038
A4	0.658	12.132
A5	0.593	10.993

7.5 Conclusions

This chapter has presented the development of simple and cost-effective control strategies for an active seat suspension system that to reduce the vertical broadband vibration (1-20 Hz) transmitted to a driver as a result of road excitation. These control strategies employ feedforward preview information from the vehicle suspension as well as inexpensive and measurable feedback states. The performance of these controllers in attenuating the vertical seat vibration has been confirmed through experimental laboratory tests using the principle of HIL technology, QvM and an active seat suspension. The experimental results reveal that the proposed controllers are effective in reducing the vertical seat acceleration over the HBSF range by up to 19.5 dB, when compared with a passive seat suspension. In addition, an improvement in both the SEAT factor and the weighted RMS seat acceleration of at least 25 % was accomplished by the controllers A3 and A4 at the full range of vehicle speeds. In conclusion, the controller A4 that employs both feedforward suspension states and easily measured feedback seat and vehicle chassis states has the best performance and provides a

practical system. This improves ride comfort and reduces the potential danger of long-term health damage for vehicle drivers.

Despite the superior performance demonstrated by the preview controller, there is an inherent drawback involved within the linear controller approach. That is, since the demand control force is linearly dependent on the system states, the physical constraints of limited seat suspension travel and actuator force cannot always be satisfied. This issue will be addressed in detail in the next chapter.

Chapter 8
An Active Seat Suspension with Optimum Fuzzy Logic Control Using Preview Information

In the previous chapters, it was shown that the application of preview information from the vehicle suspension states in linear controller for an active seat suspension is effective in attenuating low-frequency vertical vibration. However, the linear control approach is unable always to guarantee satisfactory performance in terms of seat suspension stroke and actuator force demand. To overcome this shortcoming, this chapter presents the design of two novel fuzzy logic (FL) controllers that can ensure the satisfaction of these constraints independent of the operating conditions. The first FL controller applies similar preview information as in the linear control approach, whilst the second uses the same preview information together with measurable and inexpensive feedback states from the seat suspension.

This chapter is divided into two main parts. The first deals with the theoretical design and performance evaluation of the proposed FLCs through numerical simulations in the frequency and time domains. The second part outlines the experimental implementation and performance assessment of these controllers using the prototype active seat suspension as described in chapter 5.

Part I- Theoretical study

8.1 Introduction

In the previous two chapters, the concept of applying available and inexpensive preview information from the vehicle suspension using a linear based controller for an active seat suspension was intensively investigated through both numerical simulations and experimental tests. Both sets of results demonstrated that this approach can significantly improve the ride comfort quality over the frequency range of interest (1-20 Hz).

For the sake of simplicity, the demand control force was assumed to be a linear function of the measurable preview information with optimum gains based on ride quality and taking into account the physical constraints of the seat suspension travel and the actuator force capacity. In this controller, the force is linearly dependent on the system states and thus, the satisfaction of the physical constraints cannot always be ensured over a range of road surfaces and vehicle speeds. That is, the system is not entirely sufficient in terms of stability, reliability and practical implementation. To deal with these practical challenges, a fuzzy logic controller (FLC) can be a viable alternative through which these hard constraints can be handled [202].

Two optimal FLCs for an active seat suspension, namely feedforward (FF-FLC) and feedforward-feedback (FFFB-FLC), are developed here. These controllers employ similar preview information (feedforward) that was used for the linear control approach as well as measurable and low-cost system feedback states from the seat suspension. The physical constraints related to both the limited seat suspension travel and actuator force capacity are also considered in the design process. The FF-FLC utilises preview information from the vehicle suspension in terms of the displacement and velocity of the vehicle suspension as input variables. The FFFB-FLC uses the same preview information together with available and inexpensive feedback measurements from the seat suspension, namely the seat suspension's travel and velocity. To design an FLC some fundamental aspects of its structure are explained.

8.2 Fuzzy logic controller

Fuzzy logic control (FLC) is based on the theory of 'Fuzzy logic', which was first proposed by Lotfy Zadeh [203]. It involves assigning an input to an output based on the operation of the human brain using a set of logical rules [124]. Due to the simplicity and flexibility in the design of an FLC they have been widely applied in many fields, such as aircraft, automated highway systems and automobiles, including engine transmissions, active steering and suspension etc. [202].

Generally, an FLC is composed of four parts, as presented in Figure 8-1:

1) A fuzzification interface, which converts the controller inputs (crisp values) to linguistic variables (fuzzy sets) that can be used in the inference mechanism. The linguistic variables are represented by membership functions (MF) in the universal discourse;

2) A rule-base (RB), which is a set of linguistic (IF-Then) rules that store the knowledge of how to control the process;
3) An inference mechanism or inference engine, which utilises the linguistic inputs and the rule base to produce the control decision (linguistic outputs);
4) A defuzzification interface that converts the linguistic outputs from the inference engine into crisp outputs.

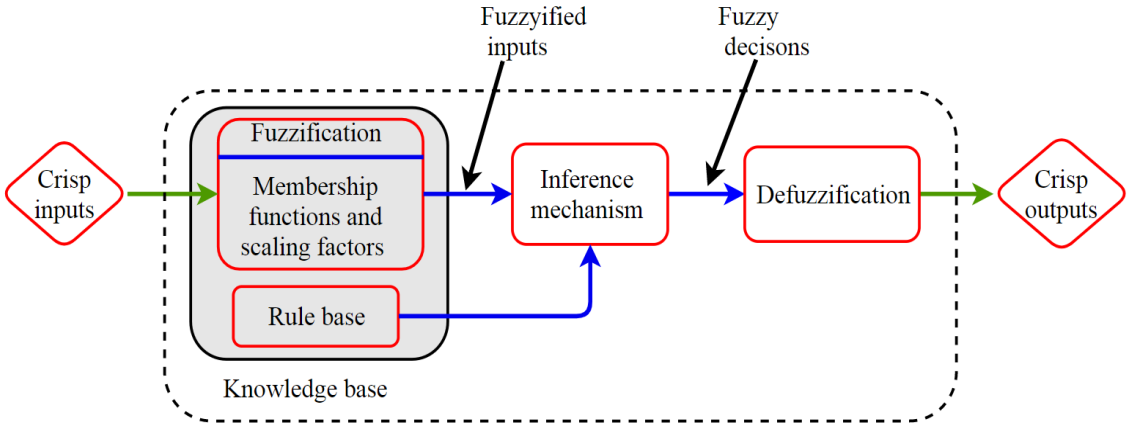

Figure 8-1: FLC structure adapted from [202,204]

Many studies have been conducted in controlling active suspension systems using FLCs. For example, Guclu [205] simulated three active suspension systems using FLCs and a nonlinear full vehicle model. The input variables were the error in the suspension travel and its time change, while the output was the actuator force. Gaussian MFs were used and their parameters were tuned by trial and error, while the rule base (RB) was heuristically established. A similar FLC study was conducted by Sharkawy [206] where the input variables were the suspension travel and suspension velocity. Rao and Prahlad [207] developed an FLC for active vehicle suspensions using the suspension deflection and suspension velocity as the input variables, whilst the rate of change of the control force was the output. The type of the MFs used was bell-shaped and their parameters were altered by trial and error. The rule base was developed based on the Macvicar-Whelan lookup-table.

Moon and Kwon [208] designed a three input, two output FLC for an active vehicle suspension based on a half-vehicle model. The input variables were the sprung mass acceleration and the front and rear suspension displacements, whilst the outputs were the desired control force at the front and rear suspensions. The RB comprised three sub-rule bases that were individually

developed for each input. The MFs for both the input and output variables were triangular and their parameters were tuned using a genetic algorithm (GA). Hurel *et al*. [209] proposed an FLC controller with two-inputs and one output for a vehicle active suspension using a linear QvM. The scaling factors for both the input and output variables were adjusted, under fixed triangular MFs, while a heuristic fuzzy RB was constructed using Particle Swarming Optimisation (PSO). Taskin *et al*. [210] proposed an FLC controller for active vehicle suspensions that improved ride comfort without degrading the suspension deflection using a QvM simulation model. The FLC was composed of three inputs and one output with triangular MFs. The inputs were the suspension deflection, the vertical velocity of the sprung mass and a combination of these two inputs. The 27 rules were able to be reduced by eliminating some that were not physically viable, hence, improving the computational time. The output results of that study showed that this FLC active suspension improved the ride comfort without degrading the suspension travel limits compared with a passive system. Subsequently, this FLC was experimentally examined on a quarter vehicle test rig [211]. It was found to perform well in reducing vertical acceleration, while maintaining the suspension travel and actuator force within their available limits. Montazeri-Gh and Soleymani [181] developed an optimised FLC for an active vehicle suspension that employs measurable feedback signals using a mutli-objective optimisation with GA, based on human sensitivity to vertical vibration. However, only the parameters of the MFs were optimised while the RB was hypothetical. Kaldas *et al*. [212] proposed a semi-active suspension system with an FLC to improve ride comfort considering road holding using a full vehicle model. The inputs of the FLC were the vertical velocity and acceleration of the vehicle, while the output was the controller force. Triangular MFs were used for both the inputs and output of the FLC. Their numbers and parameters, as well as the scaling factors and the RB, were obtained using a discrete optimisation approach with a GA. The simulation results, using a real road profile, showed that the semi-active FLC improves ride comfort and vehicle stability better than both optimum passive and LQR semi-active systems. Kaldas *et al*. [213] modified that particular FLC by utilising the preview information from the road profile. The FLC consisted of two sub-FLCs, the first of which was similar to that in [212], whilst the second sub-FLC used a look-ahead preview at each wheel as inputs. Overall, the structure of each sub-FLC, including the

RB, MFs and scaling factors, was constructed using a discrete optimisation approach with a GA.

Despite the aforementioned benefits of FLC, the structural design process is not systematic, particularly about the construction of the knowledge base that corresponds to the fuzzification and RB formulations. Moreover, there is no a standard approach to select the number and type of inputs as well as their MFs, including the type and number. Also, the RB depends on experts' knowledge about the system behaviour, which is influenced by the type and number of both the input and output variables as well as their corresponding scaling factors. It is challenging and expensive to hypotheses the RB for a complicated system such as for an active seat suspension [172,214]. A trial and error approach has been widely used to tune either the parameters of the MFs or the scaling factors, but this is time consuming as well as being an inefficient way of finding a global optimum solution [215].

To address this, further research led to the application of evolutionary optimisation algorithms such as (GA) [133,212,216,217] and PSO [172,209,218]. Rajeswari and Lakshmi [219] employed both GA and PSO techniques to optimise the scaling factors, MFs and RB of an FLC for an active suspension system. The simulation results showed that PSO is more effective in obtaining the optimum FLC structure when compared with the GA. Moreover, as explained previously in section 2.7.2 the PSO requires fewer functions evaluations compared with GA and hence, this make it more efficient to deal with large-scale problems, such as the construction of the FLC structure. Hence, the PSO technique is used in this chapter to optimise the structure of an FLC, as explained in the following subsections.

To the knowledge of the author, FLC has not been previously applied to an active seat system in which preview information from the vehicle suspension is used to control an actuator force. Hence, it is difficult and time consuming to construct these rules based on experts' knowledge about the system behaviour, and consequently, an optimisation approach is required. As long as the RB, MFs, and scaling factors are the most essential components of an FLC, the optimisation process of an FLC can be mainly classified into three groups [216]:

1) Adjusting only the parameters of the membership functions and/or scaling factors under a hypothesised RB [220] and the references in [216].

2) Constructing the RB under assumed MFs;

3) Constructing both the MFs and the RB. This can be separated into two sub groups, i.e. constructing the MFs and RB simultaneously [216,221] or sequentially. However, the sequential optimisation approach is more efficient at tuning the structure of an FCL as well as reducing the size of the optimisation problem when compared with the simultaneous alternative [204]. Thus, in this thesis, the structure of the FLC is sequentially optimised as will be explained in more details in the following sections.

8.3 Control strategies

The mathematical model used in the design and evaluation process of each FLC is the same as the integrated model that was presented in the previous chapter. As stated earlier, the FF-FLC is based on employing only preview information from the vehicle suspension. It consists of two inputs, namely the relative displacement and velocity across the vehicle suspension, while the output is the control force, as shown in Figure 8-2. In addition to the feedforward (preview information) states, the FFFB-FLC also uses the feedback states of the seat suspension's travel and velocity. Thus, the overall number of inputs is four, while the output is the control force. The required number of rules of the FLC depends on the number of input and output variables as well as the number of their MFs. For example, suppose that each input variable of the FFFB-FLC consists of five MFs, then a total of (5^4 = 625) rules are necessary to establish its RB and hence, this increases not only the optimisation process time, but also the computational time and controller complexity. Instead, the FFFB-FLC is assumed to be composed of two sub-FLCs [213], as illustrated in Figure 8-3. The first sub-FLC, namely PFF-FLC, uses the preview feedforward signals from the vehicle suspension (preview information), namely the relative displacement and velocity of the vehicle suspension, as the two input variables and generates the sub-control force F_{a2} as an output. The second sub-FLC, namely FB-FLC, utilises feedback signals from the seat suspension states, the relative displacement and relative velocity of the seat suspension as the input variables, while the output is the sub-control force F_{a1}. The overall control force is the sum of these two forces. In this way, each sub-FLC has its own RB comprising just 25 rules and the total number of the logic rules is reduced by more than 90 % (50 rules) compared with the conventional method. In sum, using the sub-FLCs approach

decreases the computational time and reduces the RB size without reducing the overall number of input variables.

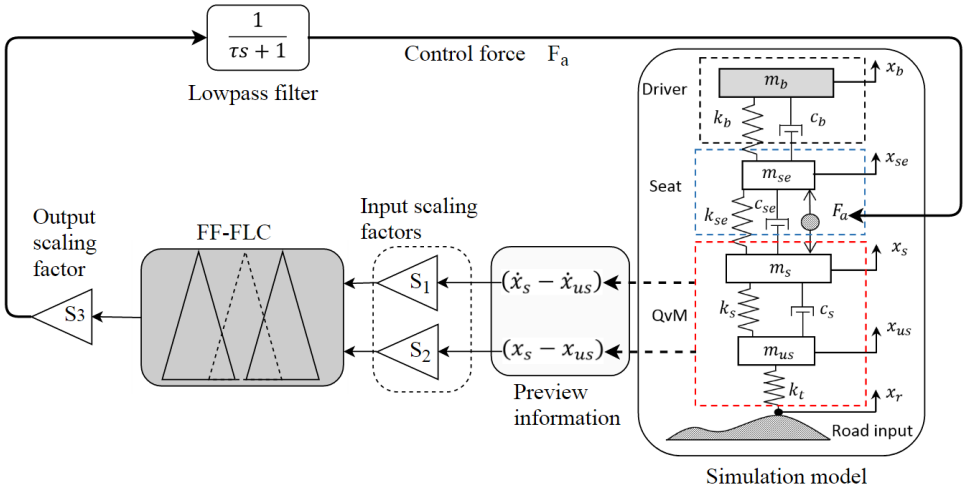

Figure 8-2: Architecture of the FF-FLC

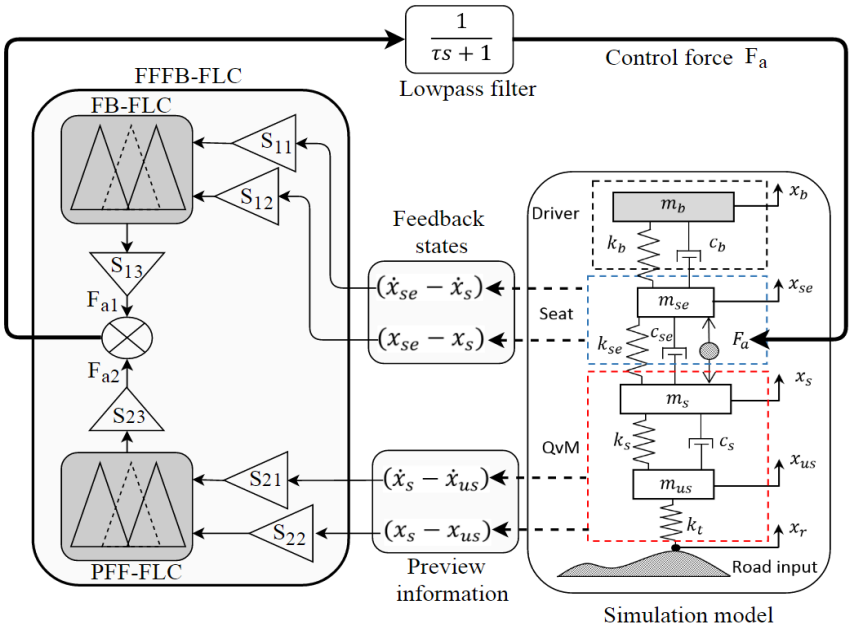

Figure 8-3: Architecture of the FFFB-FLC

8.4 Optimisation process

In this section, the process of optimising the FLC structure is explained in detail. As described briefly, the optimisation process is sequentially performed, whereby the RB and the scaling factors of the input and output variables of each proposed controller are firstly optimised

under assumed MFs. The optimum FLC knowledge base is accomplished through two stages, as shown in Figure 8-4 (a). In the first stage, the optimum RB and scaling factors of the input and output variables are obtained using assumed MFs. These are used in stage 2 to tune the parameters of the assumed MFs for both the input and output variables. Because the output of the FLC corresponds to the actuator force, the output scaling factor is limited, based on the assumed saturated limit of this force, which in this case is 1,500 N. This guarantees that the required control force will always be within the limit of the actuator force, which is essential from a stability point of view as well as ensuring the practical implementation of the controller. The FFFB-FLC controller, which is composed of two sub-FLCs where each output scaling factor has its own value is designed such that the sum of the two output scaling factors is set so that the maximum allowable force is not exceeded.

Moreover, to emulate the dynamics of the active force actuator and also reduce the effect of road induced high frequency content in the preview signal, the output force of each FLC is filtered by a low-pass filter with a cut-off frequency of $f_c = 100$ Hz.

Whilst there are different types of MFs that can be used, triangular ones are selected in this study for both the input and output variables, as they are simple, their parameters can be easily adjusted and they provide the best output results compared to other MF types [222]. It is assumed that each input variable consists of five linguistic degrees (NB: negative big, NS: negative small, ZE: zero, PS: positive small and PB: positive big), whilst the output fuzzy function has seven (NB: negative big, NM: negative medium, NS: negative small, ZE: zero, PS: positive small, PM: positive medium and PB big), as shown in Figure 8-4 (b). Consequently, a total of 25 rules are required to establish the RB. When the crisp values of inputs are both zeros, there is no actuator force and hence this rule was excluded from the optimisation process, which reduces the total rules number to 24. The rules and the scaling factors are encoded using the PSO technique. For example, in the case of FF-FLC, the number of the design variables in stage 1 is equal to 27 and consequently, each particle in the PSO algorithm has a position vector of size 27. The first 24 positions are assigned integers from 1 to the number of the linguistic degrees of the output variable (in this study it is 7). That is, these numbers represent the linguistic degrees of the output variable, for example, a particle with a position vector of **[***351657535415 455252622622***]** has the RB given in Table 8-1. The remaining three particles' positions represent the two input and output scaling factors, respectively.

Table 8-1: Example of the RB encoding method

$(\dot{x}_s - \dot{x}_{us})$ / $(x_s - x_{us})$	NB	NS	ZE	PS	PB
NB	NS	PS	NB	PM	PS
NS	PB	PS	NS	PS	PS
ZE	NB	PS	ZE (fixed)	ZE	PS
PS	PS	NM	PS	NM	PM
PB	NM	NM	PM	NM	NM

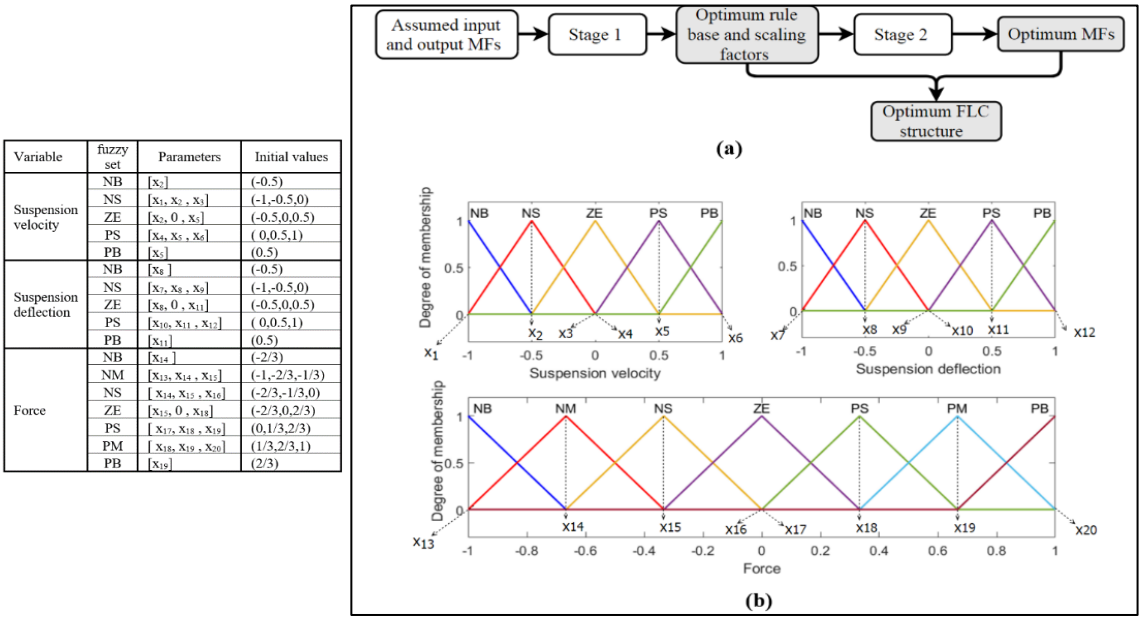

Variable	fuzzy set	Parameters	Initial values
Suspension velocity	NB	$[x_2]$	(-0.5)
	NS	$[x_1, x_2, x_3]$	(-1,-0.5,0)
	ZE	$[x_2, 0, x_5]$	(-0.5,0,0.5)
	PS	$[x_4, x_5, x_6]$	(0,0.5,1)
	PB	$[x_5]$	(0.5)
Suspension deflection	NB	$[x_8]$	(-0.5)
	NS	$[x_7, x_8, x_9]$	(-1,-0.5,0)
	ZE	$[x_8, 0, x_{11}]$	(-0.5,0,0.5)
	PS	$[x_{10}, x_{11}, x_{12}]$	(0,0.5,1)
	PB	$[x_{11}]$	(0.5)
Force	NB	$[x_{14}]$	(-2/3)
	NM	$[x_{13}, x_{14}, x_{15}]$	(-1,-2/3,-1/3)
	NS	$[x_{14}, x_{15}, x_{16}]$	(-2/3,-1/3,0)
	ZE	$[x_{12}, 0, x_{18}]$	(-2/3,0,2/3)
	PS	$[x_{17}, x_{18}, x_{19}]$	(0,1/3,2/3)
	PM	$[x_{18}, x_{19}, x_{20}]$	(1/3,2/3,1)
	PB	$[x_{19}]$	(2/3)

Figure 8-4: (a) Optimisation process of the FLC structure and (b) Input and output MF adjusting parameters

After constructing the scaling factors and the optimum RB in stage 1 using the assumed MFs that are shown in Figure 8-4 (b), the parameters of these MFs are adjusted in stage 2 using the optimum scaling factors and RB. However, to tune these parameters, the following assumptions have been applied [213]:

(1) The MF's are symmetrical about the zero value and the apex of the ZE membership function is fixed at zero to make sure that the resulting output is always zero when the inputs are zeros;

(2) The apexes of the first and last membership functions are fixed at -1 and 1, respectively;

(3) In order to represent any input variable with no more than two fuzzy sets, the base vertices of a membership function are identical to the apexes of its neighbourhood membership functions. This also ensures that the input value of unity has only one fuzzy set;

(4) The input and output universes of discourse are normalised to be within the range of [-1 and 1], while the optimum scaling factors are utilised to provide proper values for the variables.

Based on the above assumptions, the MFs of each input variable have six parameters, while the output has eight, as illustrated in Figure 8-4 (b). Thus, the total number of design variables for the FF-FLC and FFFB-FLC in stage 2 are 20 and 40, respectively. For example, the optimisation problem for the FF-FLC in stage 2 can be summarised as follows:

$$
\begin{aligned}
&\textbf{\textit{Find:}} && x_i \quad i = 1, \ldots, 20 \\
&\textbf{\textit{To minimise:}} && fittness\ function = SEAT\ factor \\
&\textbf{\textit{Subject to:}} && \begin{cases} x_{i+1} > x_i \quad ; i = [\,1\ 2\ 4\ 5\ 7\ 8\ 10\ 11\ 13\ 14\ 15\ 17\ 18\ 19] \\ -1 \le x_j \le 0 \quad ; j = [\,1\ 2\ 3\ 7\ 8\ 9\ 13\ 14\ 15\ 16] \\ 0 \le x_j \le 1 \quad ; j = [4\ 5\ 6\ 10\ 11\ 12\ 17\ 18\ 19\ 20] \end{cases}
\end{aligned}
\tag{3-17}
$$

The optimisation problem, including the fitness function, constraints, simulated model parameters and road disturbance, are the same as those used in Chapter 7. Thus, the two stages of the optimisation problem can be written in the standard form, as presented in Table 8-2.

Table 8-2: Summary of the optimisation process

	Stage 1	Stage 2
Given	Simulation model Assumed input and output MFs (Figure 8-4 (b)) Random road profile class E and a vehicle speed of 60 km/h	Simulation model Assumed input and output MFs (Figure 8-4 (b)) Random road profile class E and a vehicle speed of 60 km/h Optimum RB and scaling factors (from stage 1)
Find	Optimum RB and scaling factors	Optimum parameters of input and output MFs
To minimise	SEAT factor (Chapter 3)	
Subject to	$g(1) = (x_{se} - x_s)_{max} - (x_{se} - x_s)_{min} \leq x_{se,max}$ $g(2) = \lvert F_a \rvert \leq 1500\ (N)$	

The system was modelled using Simulink and the optimisation problem for each case was coded in MATLAB, being solved off-line using the PSO and Fuzzy Logic toolboxes. The inference method used was a Mamdani-type, because it provided a natural and interpretable RB with a simple structure [223]. Whilst the centre of gravity (COG) method was utilised in the defuzzification process due to it being consistent as well providing a continuous and smooth output response [224]. The detailed structure specification of each FLC used in the optimisation process is presented in Table 8-3. In the optimisation process, the default MATLAB setting parameters of the PSO algorithm were used as listed in Table 8-4, with a swarm size of 14. These are in line with the recommendations described in section 2.7.2.

Table 8-3: Structure specification of optimised FLCs

Parameter		FLC type		
		FF-FLC	FFFB-FLC	
			FB-FLC	PFF-FLC
No. of scaling factors	Input	2	2	2
	Output	1	1	1
Type of MFs fuzzy sets	Input	Triangle	Triangle	Triangle
	Output	Triangle	Triangle	Triangle
No. of MFs fuzzy sets	Input	5	5	5
	Output	7	7	7
RB size		24 rules	24 rules	24 rules
Inference mechanism		Mamdani	Mamdani	Mamdani
Defuzzification method		COG	COG	COG

Having solved the aforementioned optimisation problems for each FLC, the resulting optimum controller map is presented in Figures 8.6 and 8.7, respectively, while the optimum input and output scaling factors of each FLC are listed in Table 8-5.

Table 8-4: Parameters of the PSO algorithm

Parameter	Description	Value
w	Inertia weight	[0.1- 1.1]
c_1	Cognitive factor	1.49
c_2	Social factor	1.49

Table 8-5: Optimum parameters of the proposed FLCs

Parameter	Value	unit
S_1	0.0213	s/m
S_2	0.255	1/m
S_3	1500	N
S_{11}	0.8681	s/m
S_{12}	0.5714	1/m
S_{13}	750.0	N
S_{21}	0.050	m/s
S_{22}	14.925	1/m
S_{23}	750.0	N

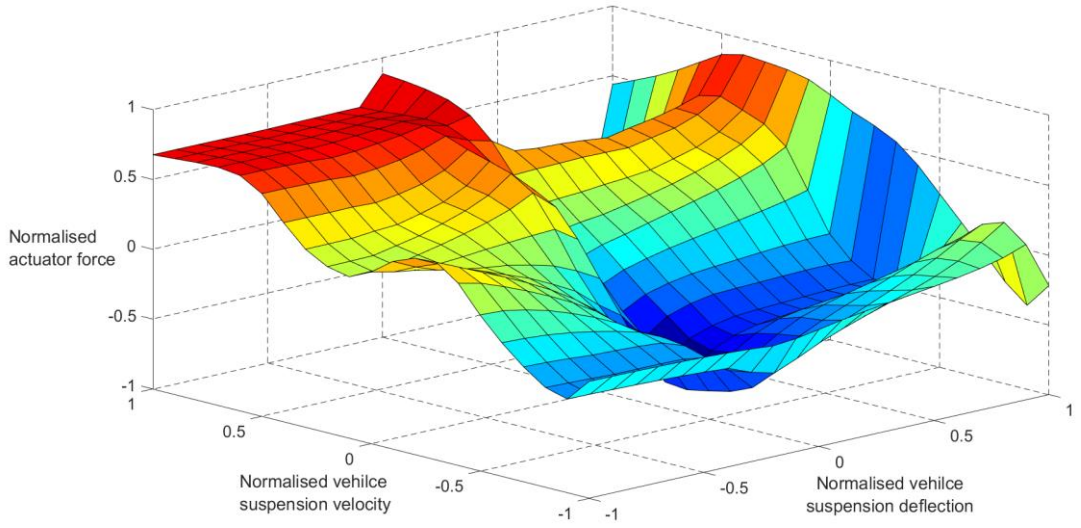

Figure 8-5: Optimised control force map of the FF-FLC

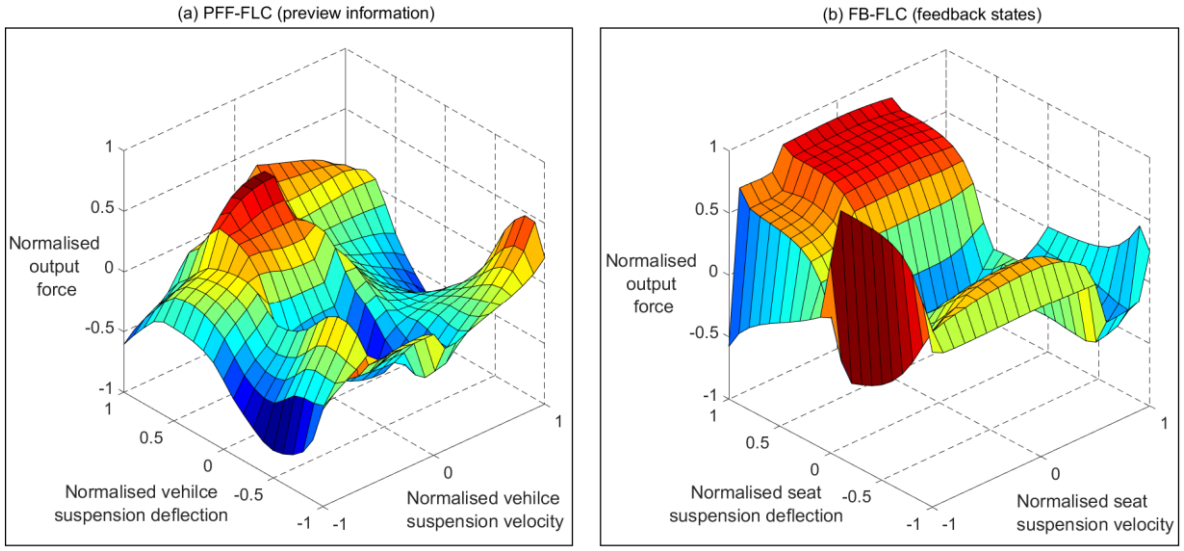

Figure 8-6: Optimised control force map of the FFFB-FLC

8.5 Simulation analysis

In this section, the effectiveness of the proposed controllers to improve the ride comfort is assessed in both the frequency and time domains. In the frequency domain, evaluation was established in terms of the acceleration transmissibility of the active seat suspensions with respect to the vehicle sprung mass over the frequency range (1-20 Hz).

In the time domain, two typical road profiles were used to excite the QvM, namely random and single bump profiles. For both road inputs, the assessment was performed by comparing the time responses of the active seat controllers against the passive system in terms of seat acceleration and seat suspension travel.

For the random road input, further comparisons in terms of the actuator force and power spectrum densities (PSDs) of the seat acceleration are performed. In addition, the percentage improvements in the SEAT and weighted-frequency RMS seat acceleration over a range of vehicle speeds as well as a health risk assessment, according to the daily working TLVs, are also presented. Moreover, the robustness of the proposed controllers to a change in the driver's weight as well as vehicle speed is also considered.

8.5.1 Frequency domain testing

To show the performance of the control strategies in attenuating transmitted energy at the vehicle's seat, the simulated acceleration transmissibilities of the active seat controllers are compared with the passive system over a low-frequency range, as illustrated in Figure 8-7. These results reveal that all of the proposed controllers significantly reduce the transmitted vertical vibration to the driver compared with the passive system, in particular, over the HBSF range (4-8 Hz). However, the FF-FLC and FFFB-FLC amplify the seat acceleration transmissibility around the sprung mass resonance frequency (1 Hz). Overall, the FFFB linear and FFFB-FL controllers show similar behaviours and they provide superior performance compared with the FF-FLC and passive systems over a broadband frequency range, especially over the HBSF range (4-8 Hz). However, the linear controller FFFB performs better than the FLC especially over low-frequency range, less than 6 Hz. These results show the benefit of combining both feedback states with preview information from the vehicle suspension, in attenuating vibration.

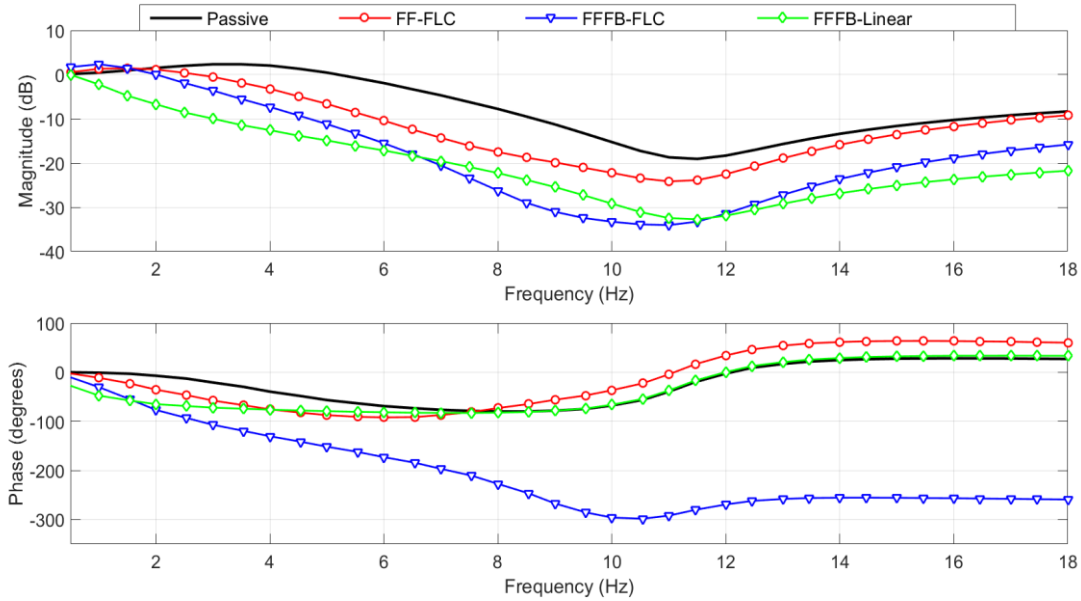

Figure 8-7: Comparison between the simulated seat acceleration transmissibility for the passive and active seat suspensions using the FLC and linear control approaches

8.5.2 Time domain

8.5.2.1 Random road

In this subsection, the analysis is carried out by exciting the vehicle QvM with a random road profile that has a road roughness of class E (very poor), according to ISO 8608, under different vehicle speeds. Figure 8-8 shows an example of the road profile at a vehicle speed of 100 km/h. The simulated time responses of the active and passive seat suspensions over a range of vehicle speeds, in terms of seat acceleration and seat suspension travel are presented Figures 8.10 and 8.11 in, respectively. It can be seen that all of the controllers efficiently suppress seat acceleration compared with the passive system notwithstanding the vehicle speed. Moreover, the FFFB-Linear shows the best performance followed by the FFFB-FLC and FF-FLC at all vehicle speeds. Nevertheless, this enhancement in reducing the seat acceleration results in increasing seat suspension stroke compared with the passive system. Whilst, the resulting seat stroke and demand control force when employing the FFFB-Linear controller are within their allowable limits at vehicle speeds of 40 and 60 km/h, they exceed these limits at vehicle speeds of 80 and 100 km/h, as illustrated in Figures 8.11 and 8.12. This indicates that this type of controller cannot always ensure the satisfaction of system constraints over different driving

conditions and thus, it is inadequate for practical implementation. Conversely, both FL controllers guarantee that the resulting seat suspension travel and the demand control force are within their permissible limits regardless of the vehicle speed, which clearly shows the advantage of using an FLC.

Figure 8-12 shows the PSDs of the seat acceleration of the active and passive seat suspensions at a range of vehicle speeds. It can be seen that the active seat controllers have lower PSDs when compared with the passive suspension over a broadband frequency range, particularly over the HBSF range (4-8Hz), irrespective of the vehicle speed. However, their performance deteriorates at lower frequencies, especially around the sprung mass mode ($f_n = 1$ Hz). Overall, the FFFB-FLC demonstrates the best performance over a broadband frequency range.

Figure 8-13 presents the SEAT factor and the weighted RMS seat acceleration of the active system using the proposed controllers and the passive system at different vehicle speeds. Notably, the SEAT factor and weighted RMS seat acceleration values for the active seat suspensions are lower than those for the passive seat suspension, regardless of the vehicle speed and hence, this improves the ride comfort of the driver. In general, the FF-FLC and FFFB-FLC active suspension attenuate at least 30 % and 45 % of the transmitted vibration at the seat when compared with the passive system, regardless of the vehicle speed. Also, the FF-FLC and FFFB-FLC improve the weighted RMS acceleration by approximately 30% and 40% more than the passive system over the tested vehicle speeds. Moreover, over the full range of vehicle speeds, the proposed active seat controllers maintain the comfort level, according to the vibration environments proposed by ISO 2631-1 provided in Chapter 3, within the 'a little uncomfortable' range, while the passive seat suspension often strays into the 'uncomfortable' range.

Figure 8-14 shows the frequency-weighted RMS acceleration of the active and passive seat suspensions with respect to the TLVs given in Chapter 3, across the range of vehicle speeds. It is observed that both of the proposed controllers perform better than the passive system which in most cases exceeds the 8 hour working daily exposure limit, especially over the HBSF range and the FFFB-FLC provides the best performance. This indicates that employing any of the proposed controllers in a vehicle active seat suspension delivers a potentially safer and more comfortable working environment for drivers working long hours.

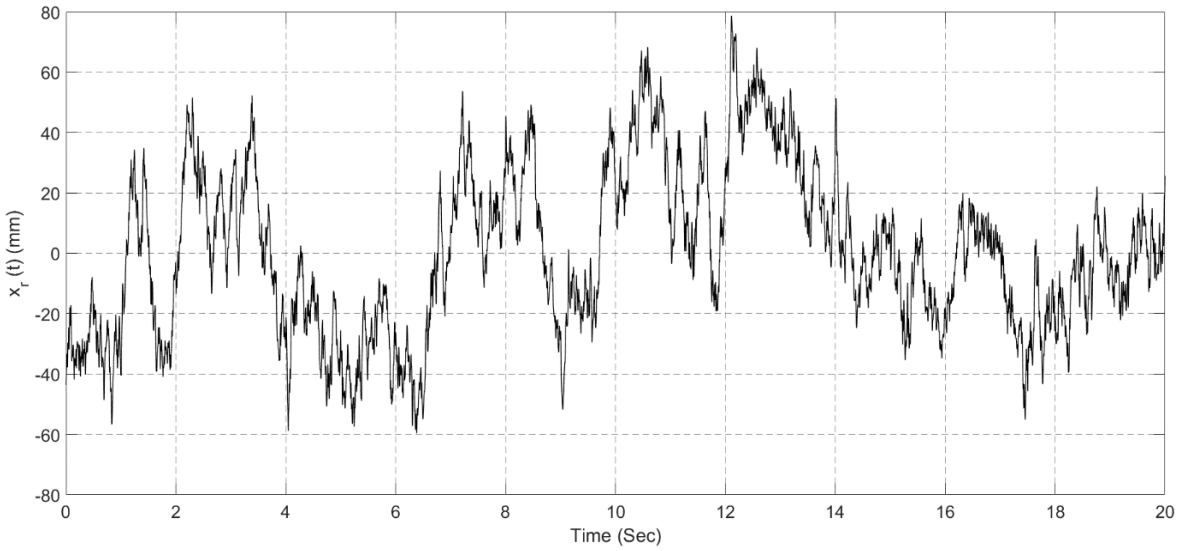

Figure 8-8: Random road profile at a vehicle speed of 100 km/h

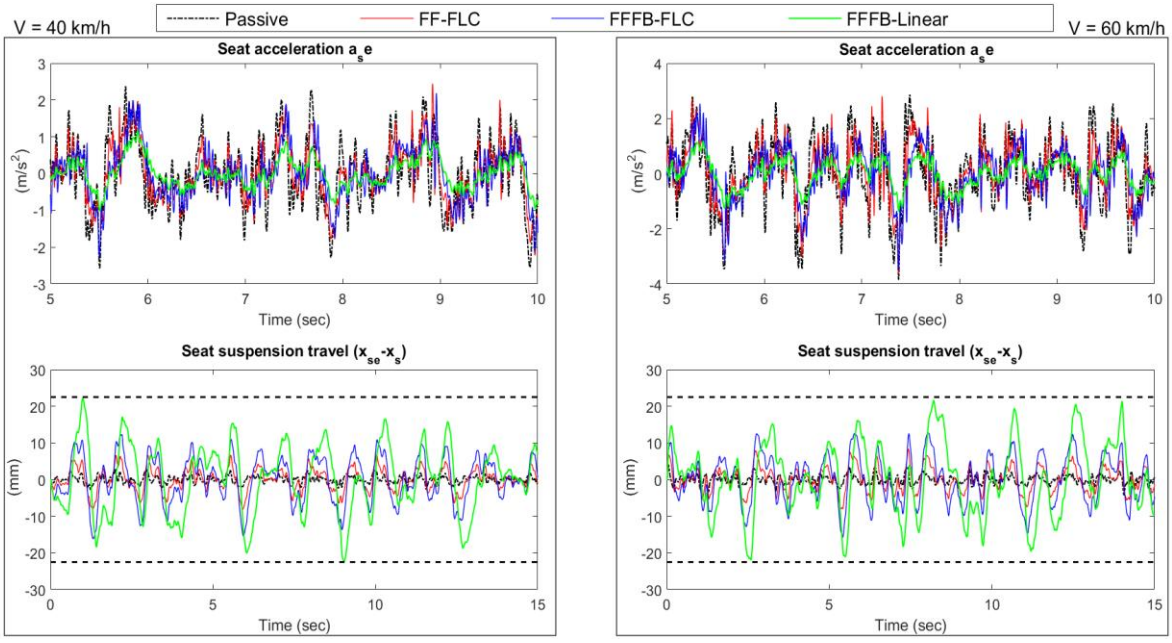

Figure 8-9: Time responses for the passive and active seat suspensions using FLC and linear control approaches under random road input at vehicle speeds of 40 and 60 km/h

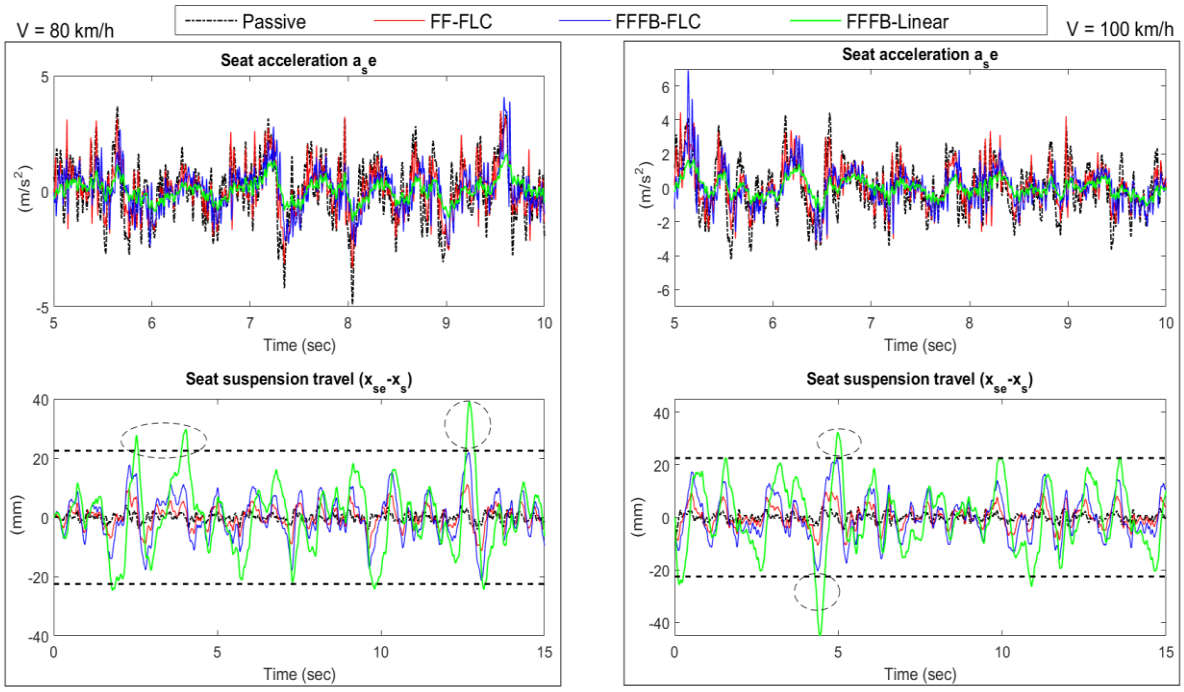

Figure 8-10: Time responses for the passive and active seat suspensions using FLC and linear control approaches under random road input at vehicle speeds of 80 and 100 km/h

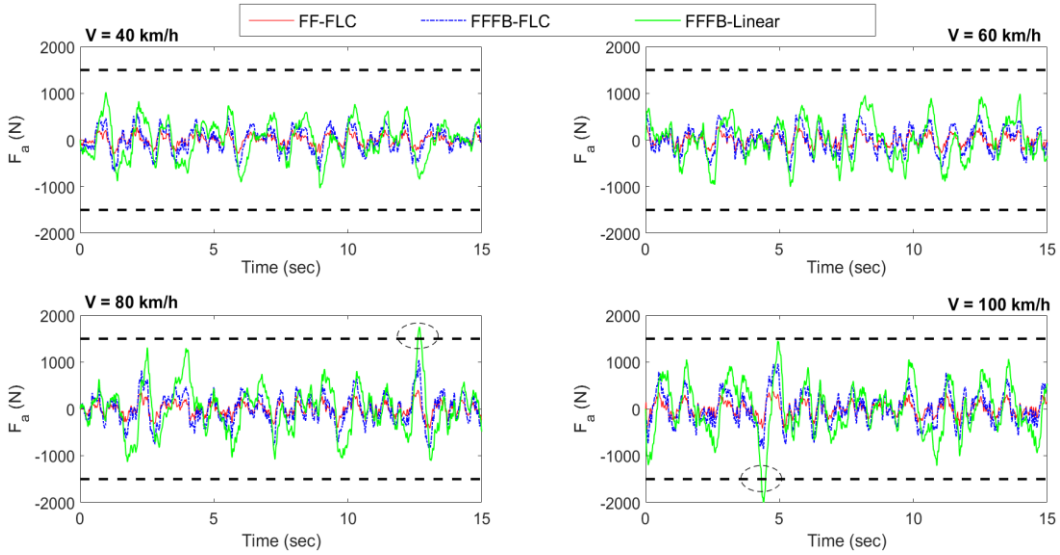

Figure 8-11: Time responses of the control force for the passive and active seat suspensions using FLC and linear control approaches under random road input at different vehicle speeds

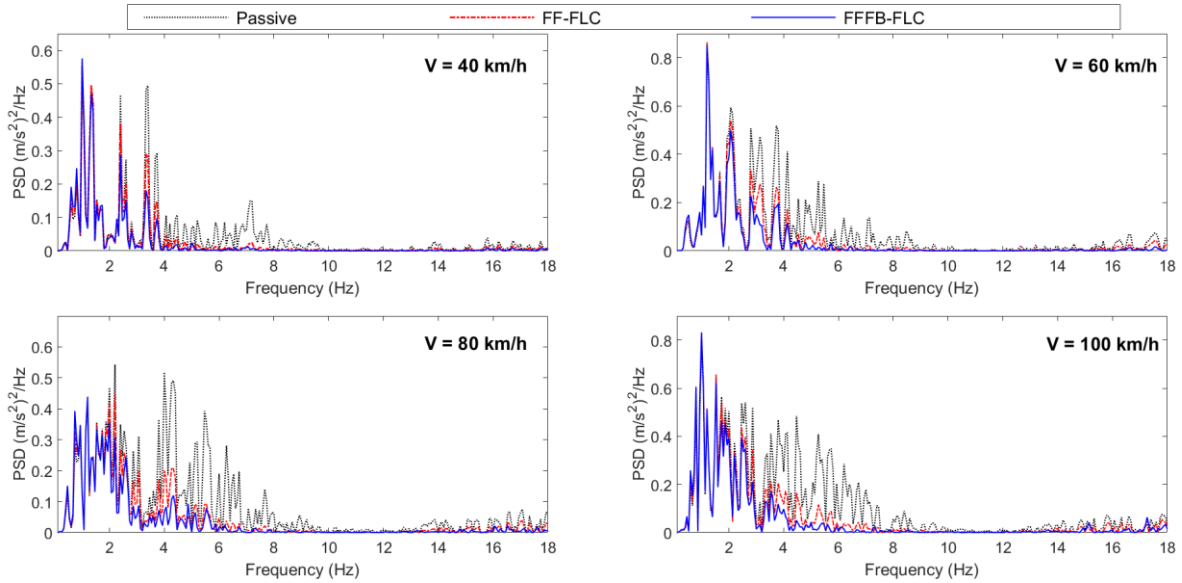

Figure 8-12: PSDs of the seat acceleration for the passive and active seat suspensions with FLC approaches in simulation test at different vehicle speeds

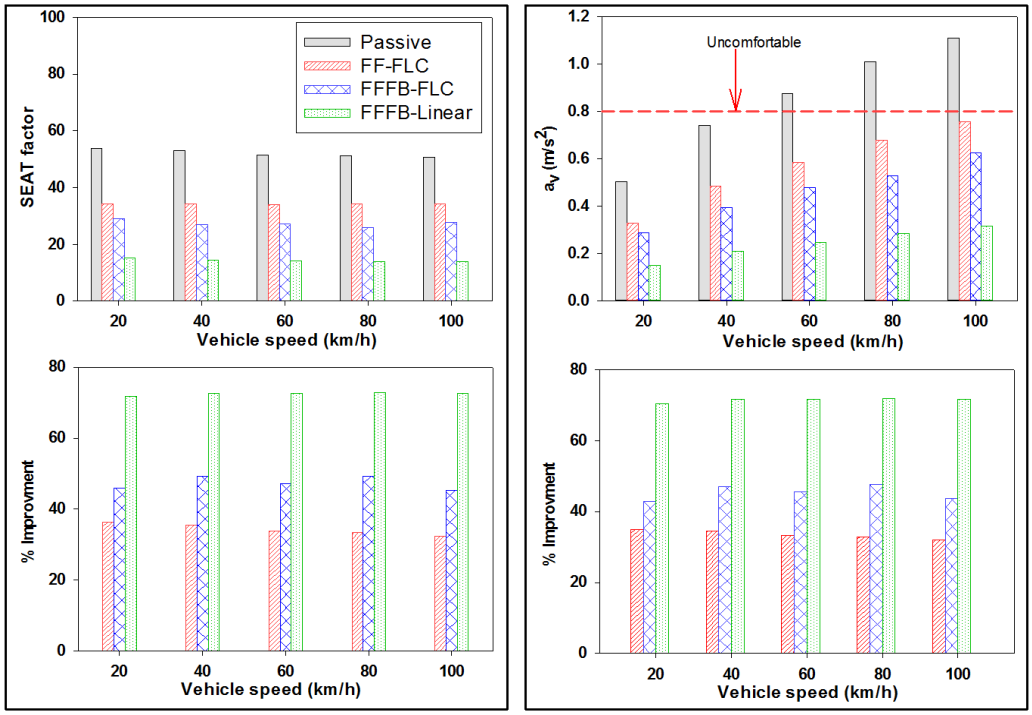

Figure 8-13: SEAT factor and weighted RMS seat acceleration of the proposed controllers and percentage improvements at different vehicle speeds

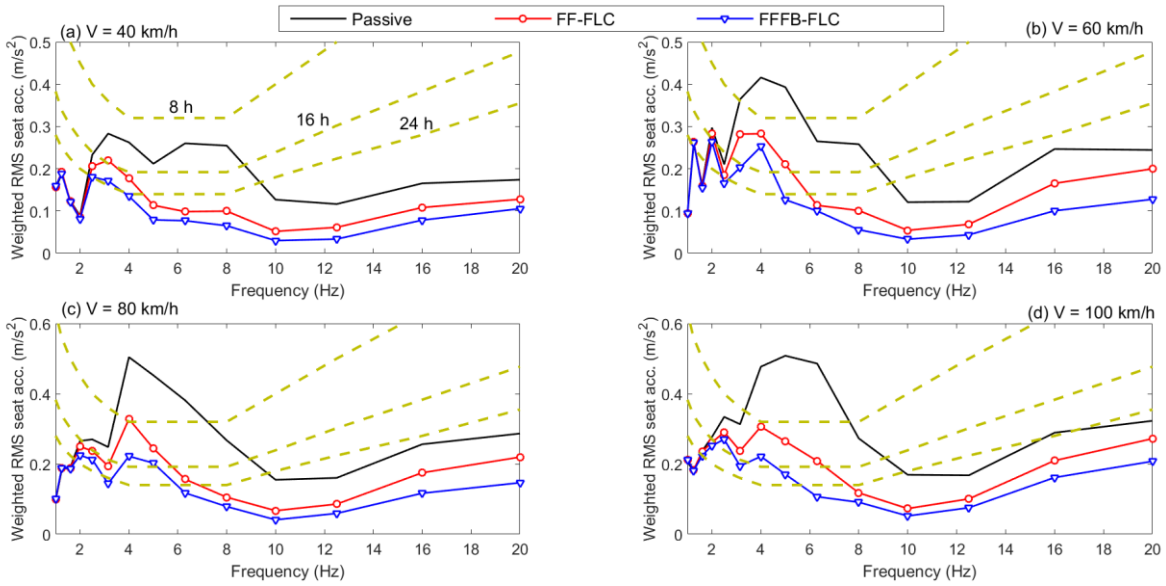

Figure 8-14: Health risk assessment, according to ISO 2631-1, for the passive and active seat suspension with FLC approaches at different vehicle speeds

8.5.2.2 Parameter Uncertainties

One critical feature of an active seat suspension is its robustness to uncertainties in the system parameters and working conditions [225]. The driver's weight and the vehicle speed are very common system parameters that vary with use. Consequently, the sensitivity of the proposed active controlled seat suspensions to these factors was evaluated in terms of the SEAT factor and the weighted RMS seat acceleration. Taking into account the nature of a random road profile, the simulations were repeated ten times for 15 seconds and the average values were taken. Figure 8-15 (a) shows the sensitivity maps of the SEAT factor for the passive and the proposed active controlled seat suspensions subject to changes in the driver's weight and the vehicle speed. It is notable that the isolation of the transmitted vibration of the passive seat suspension is sensitive to both parameter variations. Not surprisingly, light drivers are exposed to more vibration energy than heavy ones, regardless of the vehicle speed. Conversely, both of the proposed controllers are less sensitive to a variation in the either the driver's weight or vehicle speed. The robustness of the active seat controlled by the FFFB-FLC is significantly better than with the FF-FLC.

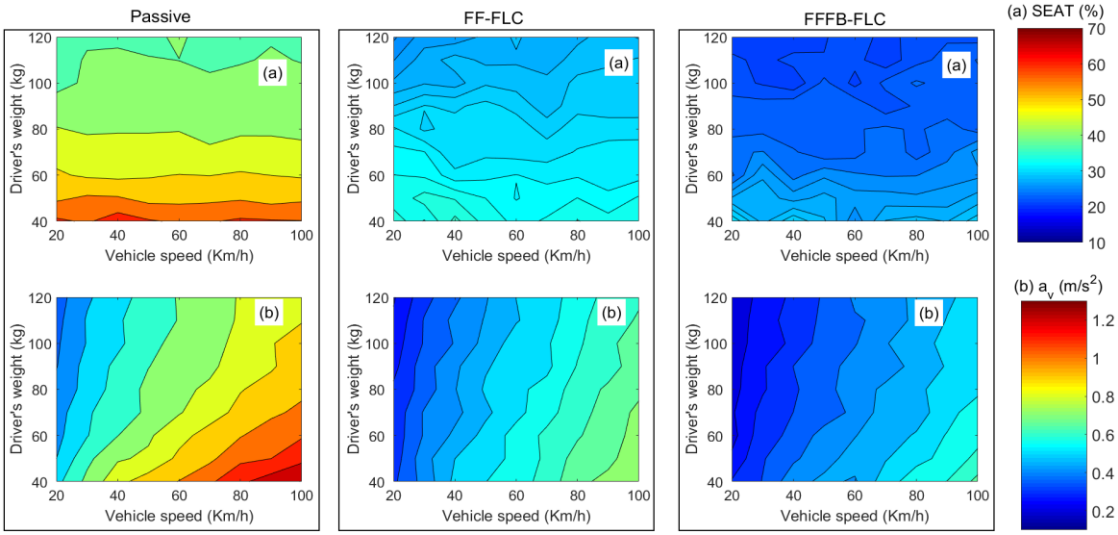

Figure 8-15: Simulated SEAT factor and weighted RMS seat acceleration sensitivity maps for the passive and active seat suspensions with FLC approaches for different driver weights and vehicle speeds

The sensitivity maps of the weighted RMS seat acceleration are presented in Figure 8-15 (b). Once again, the passive seat suspension ride comfort level is significantly more sensitive to parameter changes and light drivers are subject to the most discomfort when driving at high speeds. Conversely, the comfort levels of the proposed active controlled seat suspensions were only slightly affected by these variations and overall, the robustness of the FFFB-FLC is better than that of the FF-FLC.

8.5.2.3 Bump road input

The performance of the controllers has also been assessed in simulation using a single bump road input represented by Eqn. (3-15), as described in chapter 3. Figure 8-16 shows the bump road profile used in this study where the bump height a was assumed as to be 3 cm. The simulated time responses of the passive and active controlled seat suspensions in terms of the seat acceleration and seat travel are presented in Figure 8-17. It can be clearly observed that the controllers perform better than the passive system in reducing the seat acceleration with a reasonable increase in the seat travel. Moreover, the FFFB-FLC active seat suspension demonstrated the best reduction in both the RMS and maximum seat acceleration, when

compared with the passive system and FF-FLC, for which the peak and the RMS value of the seat acceleration are reduced by more than 45 %, as presented in Table 8-6. These results reveal once again that using feedforward preview information together with the feedback seat's states provides the best improvement in the ride quality.

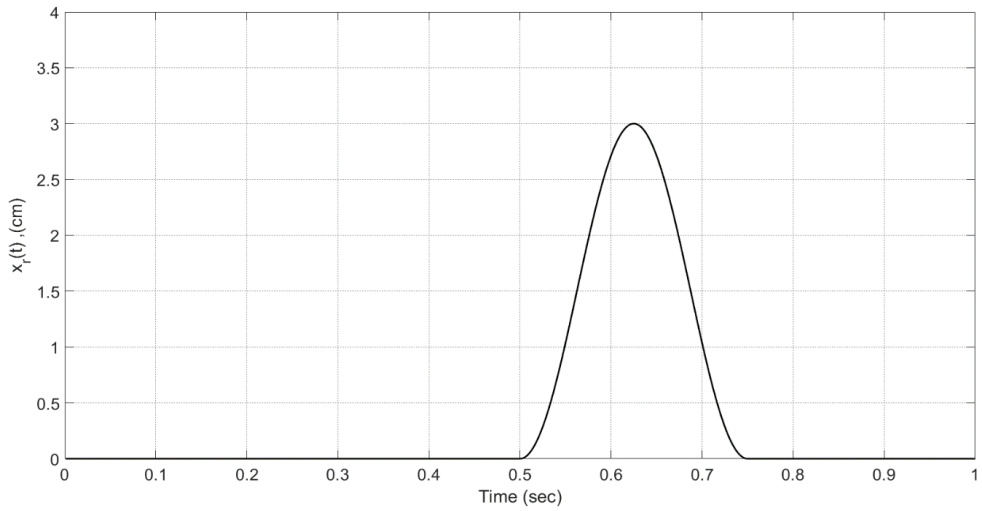

Figure 8-16: Bump road profile

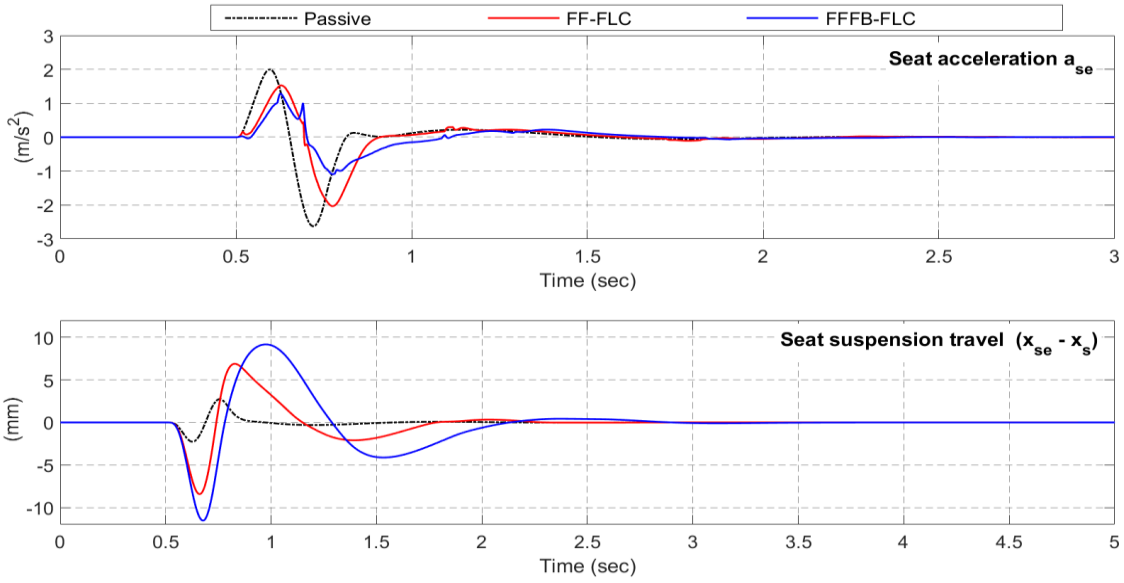

Figure 8-17: Simulated time responses for the passive and active seat suspensions using FLC approaches under a bump road profile

Table 8-6: Simulated time response characteristics of the proposed controllers under a bump road profile

Seat acceleration				Seat suspension deflection			
Index	**Passive**	**FF-FLC**	**FFFB-FLC**	**Index**	**Passive**	**FF-FLC**	**FFFB-FLC**
RMS (m/s^2)	0.2716	0.2265	0.1487	RMS (mm)	0.305	1.23	2.02
Peak (m/s^2)	2.630	2.033	1.285	Peak (mm)	2.74	8.43	11.53

Part II- Experimental Validation

This part focuses on validating and examining the performance of the FLCs for an active seat suspension in real time through experimental tests using the experimental QvM rig and the HIL approach described in chapter 5. These strategies are modelled in Simulink/MATLAB and their assessment is carried out in the same manner as presented previously in chapter 7, in both the frequency and time domains with different road disturbances and at a range of vehicle speeds.

8.6 Frequency domain

To obtain the frequency responses of the proposed controller experimentally, a sinewave excitation signal as explained previously in chapter 5, was used to excite the MAST. Figure 8-18 compares the measured seat acceleration transmissibility of the active seat suspension using the proposed FLCs with that of the passive seat suspension over the frequency range of interest. It can be seen that the controllers significantly attenuate the transmitted vertical vibration to the driver when compared with the passive system, especially over the HBSF range. In agreement with the simulation results, the FFFB-FLC demonstrates the best performance compared with the FF-FLC and passive system over a wide frequency range, in particular, over the HBSF range. However, at a higher frequency range greater than 14 Hz it

performs less well than that of the FF-FLC and this might be related to the effect of the dummy dynamics, which are more dominant over this frequency range and have not been considered in the simulation model.

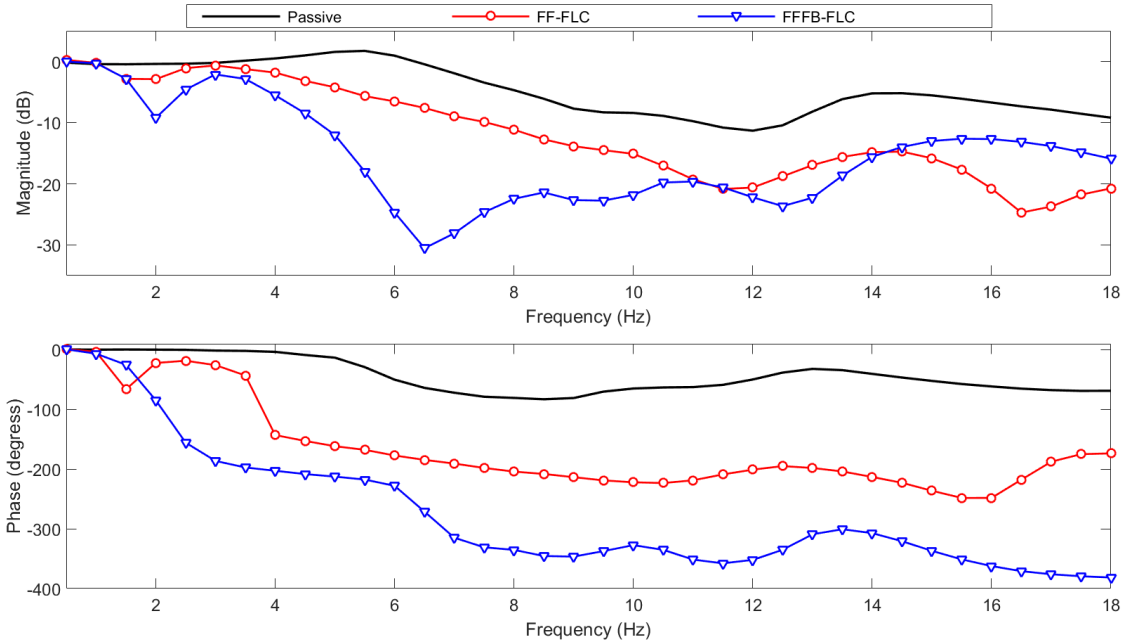

Figure 8-18: Comparison between the seat acceleration transmissibility for the passive and active seat suspensions with FLC approaches in experimental test

8.7 Time domain

8.7.1 Random input

In this subsection, a random road profile similar to that used in chapter 7 at a range of different vehicle speeds is used to excite the QvM. Figures 8.20 and 8.21 show the measured time responses of the active and passive seat suspensions in terms of the seat acceleration and seat suspension travel. It can be observed that the seat acceleration of both the FF-FLC and FFFB-FLC are lower than that of the passive system, especially at a low vehicle speed, whilst the FFFB-FLC shows the best performance. As expected, this reduction in the seat acceleration level is matched by an increase in the seat suspension travel, but this does not exceed the allowable limit.

Figure 8-21 demonstrates that the controllers result in a lower seat acceleration PSD when compared with the passive system, especially over the HBSF range (4-8 Hz) and at low vehicle speed. However, at a frequency range below 4 Hz, their performance deteriorates, especially the FF-FLC at high vehicle speed. These results are in agreement with those previously obtained using the linear control approach, as presented in Chapter 7.

The SEAT factor and the frequency-weighted RMS seat acceleration of passive and active seat suspensions are presented in Figure 8-22. The FLCs provide lower SEAT factor and frequency-weighted RMS seat acceleration than the passive system over the whole vehicle speed range, particularly at low and intermediate vehicle speeds. Once again, the FFBL-FLC shows the best performance compared with the FF-FLC, with almost a 30 % improvement in both the SEAT factor and the frequency-weighted RMS seat acceleration at a vehicle speed of 40 km/h.

This performance is reduced at higher vehicle speeds and becomes similar to that of the FF-FLC. This is may be caused by the dummy dynamics, which are more dominant at these vehicle speeds, and hence, influence the quality of the feedback signals. In addition, this may be related to the fact that the seated dummy is not sufficiently secured to the seat and at high vehicle speeds, there are more possibilities for the dummy to leave the seat, which consequently leads to deteriorating the accuracy of the feedback states from the seat suspension.

Figure 8-23 demonstrates the frequency-weighted RMS acceleration of the active and passive seat suspensions with respect to the TLVs, as suggested by the ISO 2631-1, over the whole range of vehicle speeds. It can be seen that the active seat suspension, employing any of the developed FLCs, performs better than the passive system, especially over the HBSF range in which the lattermost system exceeds the 16 hour working daily exposure limit. However, their performance deteriorates over a low-frequency range below 4 Hz, especially at higher vehicle speeds. In general, the FFFB-FLC delivers the best performance when compared to that of the FF-FLC.

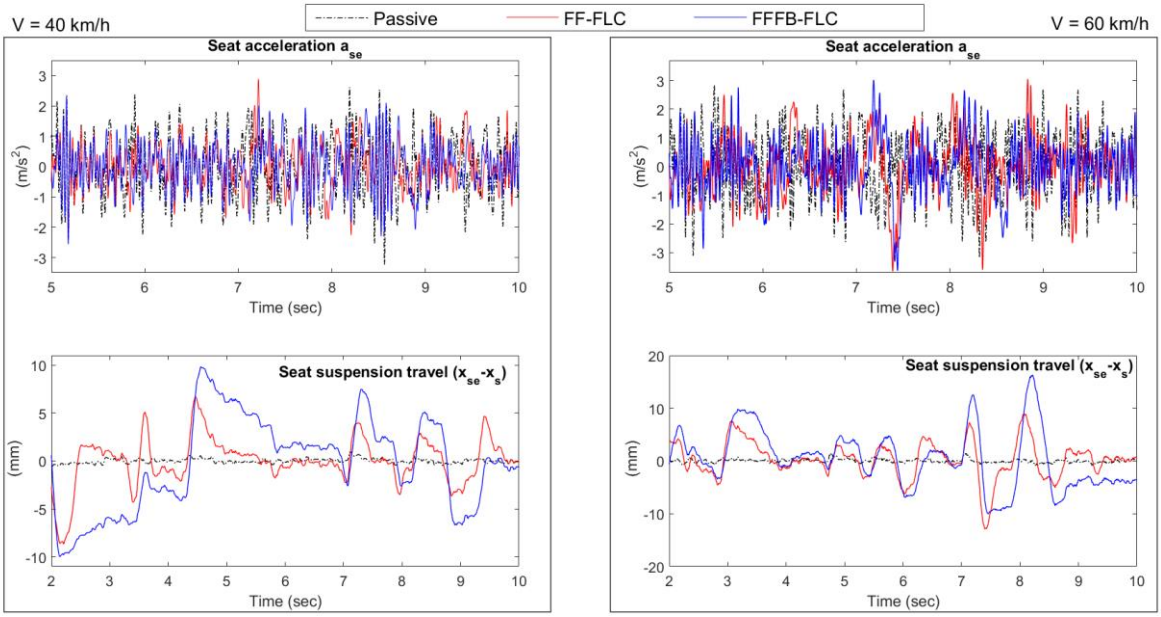

Figure 8-19: Time responses for the passive and active seat suspensions with FLC approaches in the experimental test at vehicle speeds of 40 and 60 km/h

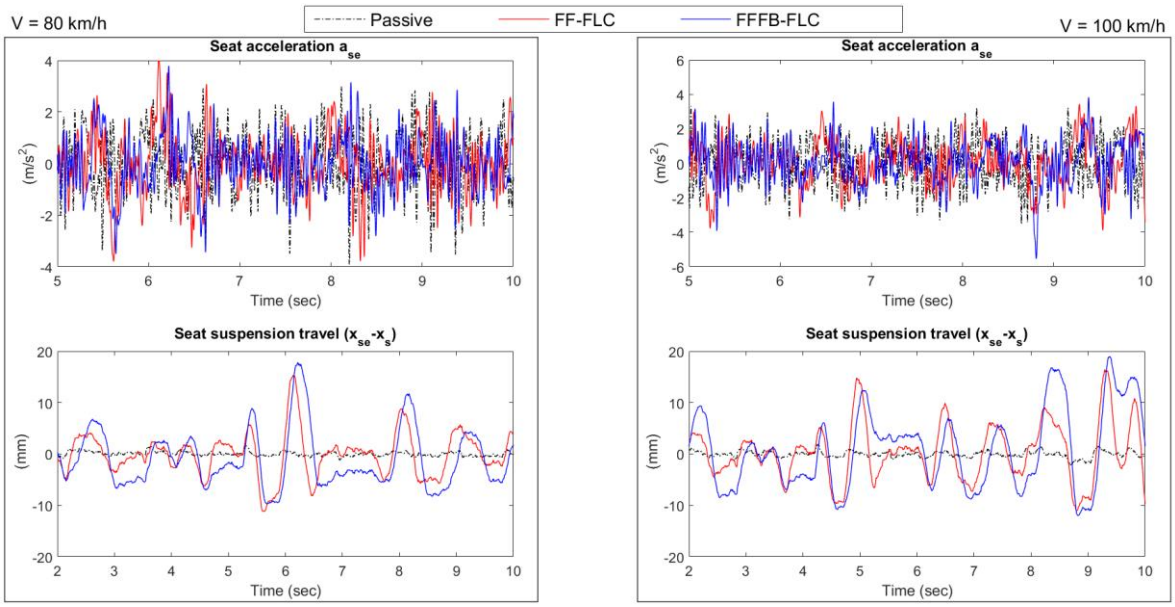

Figure 8-20: Time responses for the passive and active seat suspensions with FLC approaches in the experimental test at vehicle speeds of 80 and 100 km/h

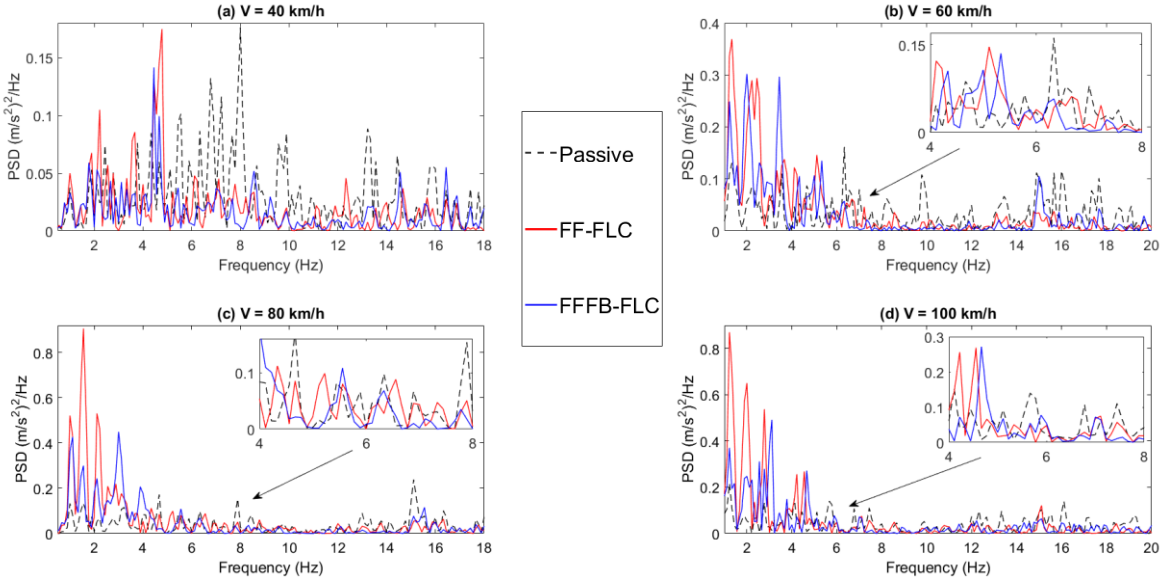

Figure 8-21: PSDs of the seat acceleration for the passive and active seat suspensions with FLC approaches in the experimental test at different vehicle speeds

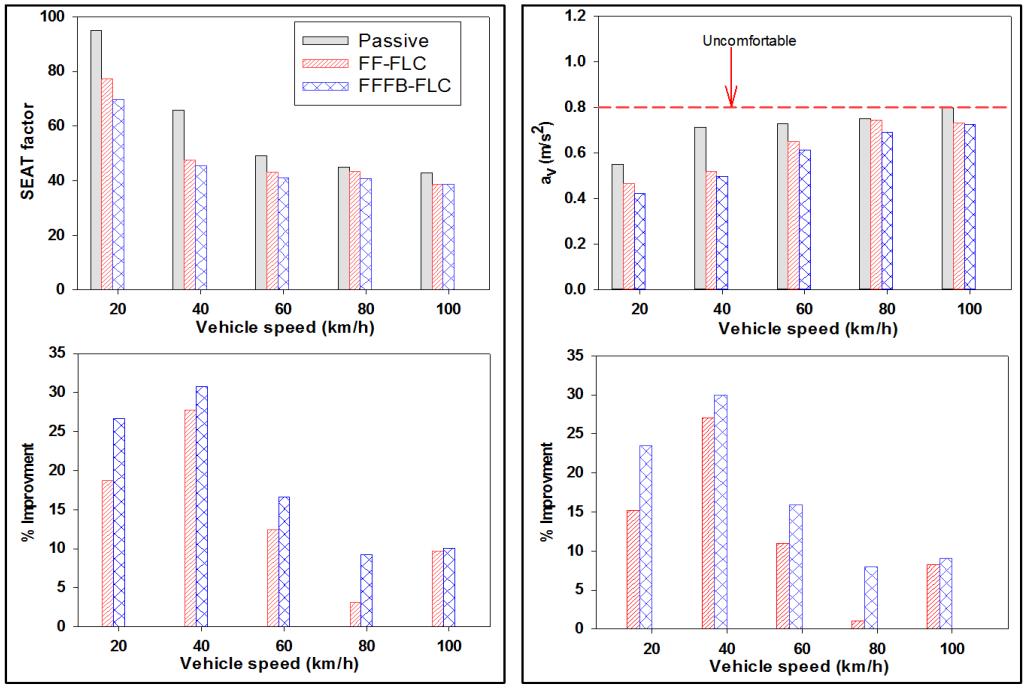

Figure 8-22: Experimental SEAT factor and weighted RMS seat acceleration values for the passive and active seat suspensions with FLC approaches at different vehicle speeds

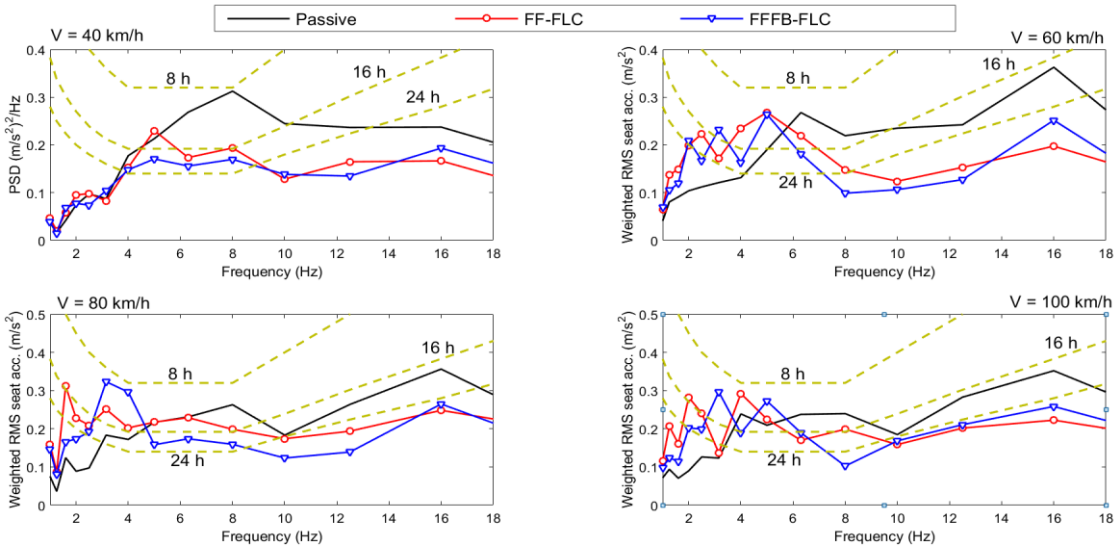

Figure 8-23: Health risk assessment, according to ISO 2631-1, for the passive and active seat suspensions with FLC approaches in experimental test at different vehicle speed and FLC active

8.7.2 Bump road profile

The performance of the controllers was also experimentally evaluated when the QvM was subject to the same single bump road that was previously presented in Chapter 7. Figure 8-24 shows the time responses of the FLC active suspensions and the passive system in terms of the seat acceleration and seat suspension travel. It can be seen that the FLC active seat suspensions perform better than the passive system, particularly with the FF-FLC, which is in agreement with the results obtained in the previous chapter when using the linear control approach. Also, the passive system as well as the FL controllers, change the static position, especially the FF-FLC. However, the measured performance of the FFFB-FLC is less good than the previously presented simulation results as a result of the friction effects and nonlinearities present within the experimental prototype system as well as the dummy dynamics. This indicates the importance of considering these aspects in order to compensate for their effects and thus, accurately validate the effectiveness of the controllers.

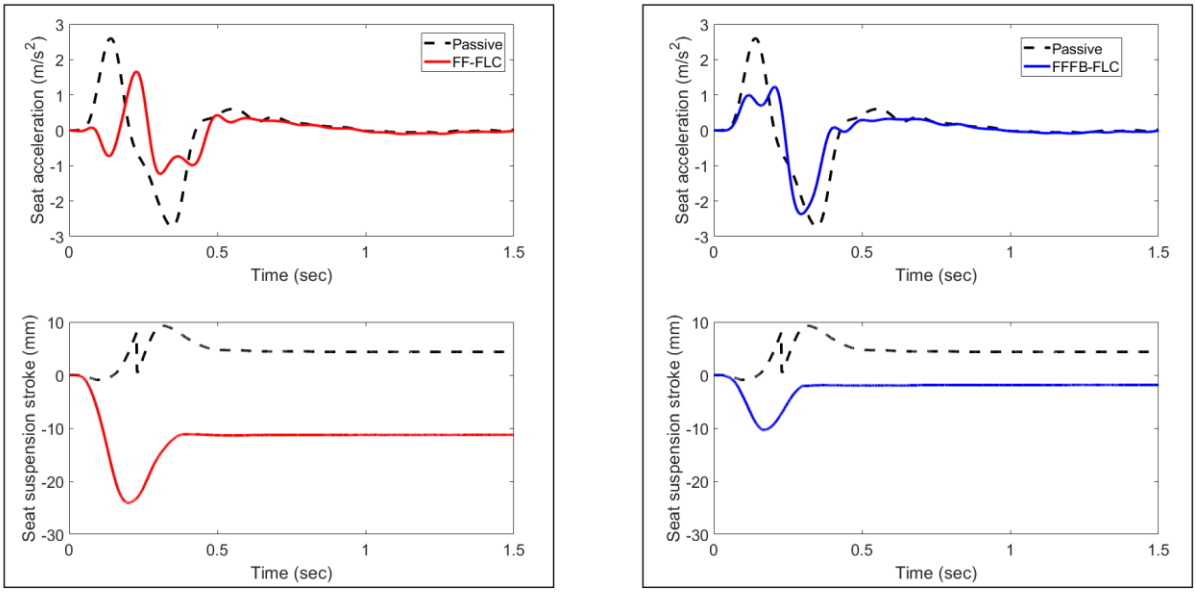

Figure 8-24: Measured time responses for the passive and active seat suspensions with FLC approaches under a bump road profile

8.8 Conclusions

This chapter has demonstrated the design of two novel, simple, practical and cost-effective optimal FLCs for an active seat suspension system. These controllers utilise the preview information from the vehicle suspension as well as inexpensive and measurable feedback seat states. In addition, they ensure that the seat suspension travel as well as the demand control force are within their allowable limits over a variety of operating conditions, which cannot be guaranteed with a linear controller approach. The simulation results have shown that the proposed FLCs significantly attenuate the vertical seat acceleration over the HBSF range and hence, improve the ride quality. Moreover, they are more robust to both the driver's weight and vehicle speed, when compared with a passive system. In addition, the performance of these controllers was confirmed experimentally when subjected to random road disturbances. In conclusion, the controller FFFB-FLC, which employs both feedforward preview information of the vehicle's suspension and feedback seat states, has the best performance, providing a robust, practical and cost-effective system that improves ride quality as well as reducing the potential danger of vehicle driver fatigue.

In the next chapter, the principle of a feedforward controller (preview information) is applied to a full, four wheel vehicle model.

Chapter 9
The Application of Preview Control within a Full Vehicle Model

9.1 Introduction

The effectiveness of applying the suspension preview information from the QvM to control an active seat suspension to attenuate low-frequency vertical vibration has been confirmed through both experimental and simulation tests in the preceding chapters. However, in reality, a road vehicle will be subjected to disturbances from all four wheels, and therefore the concept of preview enhanced control should be applied to a full vehicle model. Different preview scenarios can be established depending on which suspension or suspensions are used to acquire this preview information. Accordingly, three preview control strategies are hypothesised namely: front-left suspension (FLS), front axle (FA) and four wheels (4W). The foremost utilises suspension displacement and velocity preview information from the vehicle suspension nearest to the driver's seat whilst the FA uses similar preview information, but from both the front-left and front-right suspensions. The 4W controller employs similar preview information from all the vehicle suspensions.

To cope with the friction non-linearities involved within the dampers of the vehicle suspensions as well as the constraints of the active actuator displacement and force capabilities, an FLC is selected. This chapter presents the development of three optimal FLCs namely, front-left suspension (FLS-FLC), front axle (FA-FLC) and four wheels (4W-FLC). The optimal structure of each (FLC) including the MFs, scaling factors and RB is sequentially optimised in the same manner as previously described in chapter 8, using the PSO algorithm. These strategies are evaluated through simulation according to the ISO 2631-1 standard, using different road disturbances across a range of forward vehicle speeds. Finally, to reduce the implementation cost of the 4W-FLC, a practical alternative is developed that requires less measured preview information.

9.2 Integrated model

The vehicle and seat simulation model used in this chapter consists of a full linear vehicle model, a passive seat suspension and a driver's body model, as shown in Figure 9-1. The full vehicle model is the seven degrees of freedom model presented in [226]. The vehicle body mass M_s (sprung mass) is assumed to be a rigid body with bounce, pitch and roll motions, denoted by x_s, θ and ϕ, respectively. Each wheel of the front and rear axles, represented by the unsprung masses m_{11}, m_{12}, m_{21} and m_{22}, has a single degree of freedom in the vertical direction, denoted by x_{11}, x_{12}, x_{21} and x_{22}, respectively, while the road disturbances at these wheels are represented by x_{r11}, x_{r12}, x_{r21} and x_{r22}. For simplicity, this model involves only the driver's seat, with a linear lumped mass-spring-damper of one degree of freedom in the vertical direction, denoted by x_{se}. Moreover, the driver's body is represented by one DOF in the vertical direction, denoted by x_b. The tyre springs and suspension spring elements of the front and rear axles are presumed to be linear. Assuming small pitch and roll angles, the dynamic equations of the integrated model are given as follows:

1) Vehicle body motion:

a) Bounce

$$M_s\ddot{x}_s = -\left[\sum_{i,j=1,2} F_{sij} + f\left(V_{sij}\right)\right] + F_{se} - F_a \tag{9-1}$$

where, F_{sij} is the suspension dynamic force at each vehicle suspension, given by:

$$F_{sij} = k_{sij}\left(x_{sij} - x_{ij}\right) + c_{sij}\left(\dot{x}_{sij} - \dot{x}_{ij}\right), \quad i = 1,2 \;\&\; j = 1,2 \tag{9-2}$$

while $f\left(V_{sij}\right)$ is the dry friction force of the suspension damper at each wheel, F_{se} is the seat suspension force and F_a is the controller force.

b) Pitch

$$\begin{aligned} I_{sy}\ddot{\theta} = {} & L_f\left(F_{s11} + F_{s12} + f(V_{s11}) + f(V_{s12})\right) \\ & - L_r\left(F_{s21} + F_{s22} + f(V_{s21}) + f(V_{s22})\right) \\ & - R_x(F_{se} - F_a) \end{aligned} \tag{9-3}$$

c) Roll

$$I_{sx}\ddot{\phi} = b\left(F_{s12} + F_{s22} + f(V_{s12}) + f(V_{s22})\right) - a\left(F_{s11} + F_{s21} + f(V_{s11}) + f(V_{s21})\right) + R_y(F_{se} - F_a) \quad \textbf{(9-4)}$$

2) Unsprung masses

$$m_{ij}\ddot{x}_{ij} = F_{sij} + f\left(V_{sij}\right) - k_{tij}\left(x_{ij} - x_{rij}\right) \qquad i,j = 1\ \&\ 2 \quad \textbf{(9-5)}$$

3) Seat suspension

$$F_{se} = k_{se}(x_{se} - x_s) + c_{se}(\dot{x}_{se} - \dot{x}_s) \quad \textbf{(9-6)}$$

$$m_{se}\ddot{x}_{se} = -F_{se} + F_a - k_b(x_{se} - x_b) + c_b(\dot{x}_{se} - \dot{x}_b) \quad \textbf{(9-7)}$$

4) Driver's body

$$m_b\ddot{x}_b = k_b(x_{se} - x_b) + c_b(\dot{x}_{se} - \dot{x}_b) \quad \textbf{(9-8)}$$

Each of the vehicle suspension dampers includes a non-linear dry friction force $f(V_s)$ that depends on the velocity across the suspension V_s and a viscous band ε (Guclu, 2005), as presented in Figure 9-2.

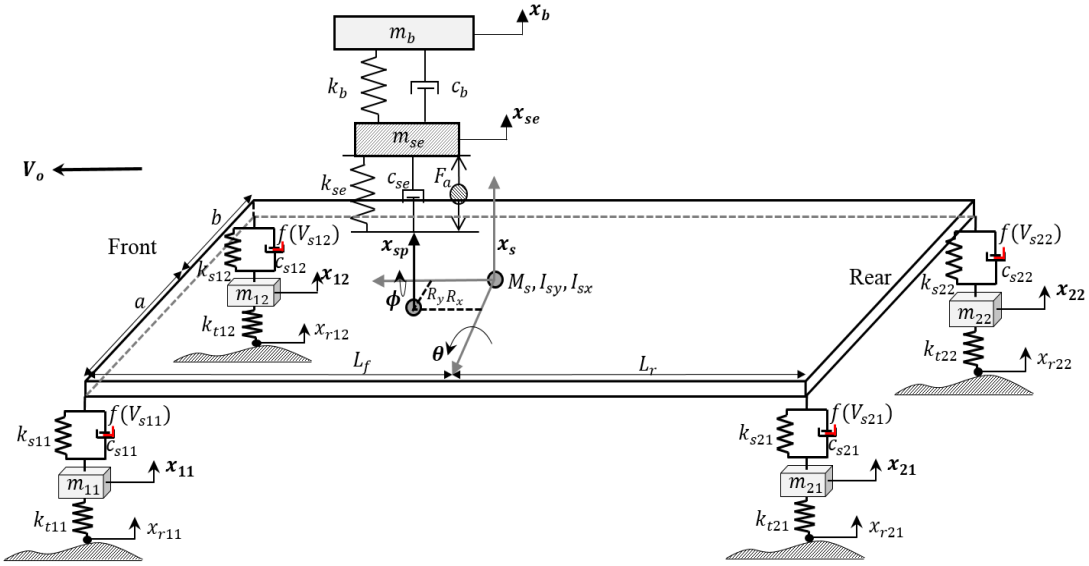

Figure 9-1: Full vehicle model with a 1 DOF active seat suspension and 1 DOF driver model (adapted from [226])

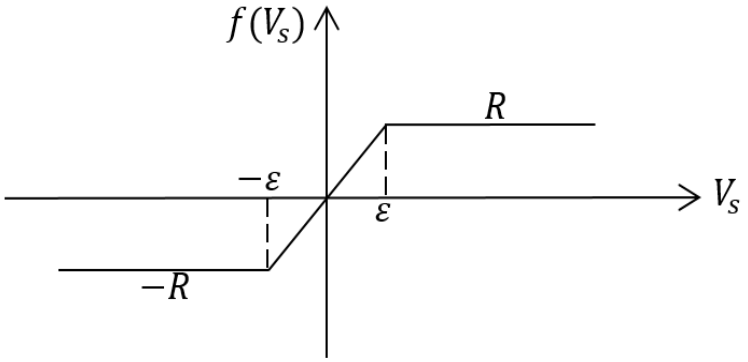

Figure 9-2: Dry friction model of the vehicle suspension damper [226]

9.3 Control strategies

The proposed FLCs are designed in the same manner as previously described in chapter 8, with the QvM. Put simply, the output of each proposed FLC is the control force and the total number of inputs for each is different. For instance, the FLS-FLC has only two inputs as presented in Figure 9-3 whilst the FA-FLC requires four inputs, namely the displacements and velocities of the front left and right suspensions. Conversely, the number of inputs to the 4W-FLC is eight.

Recalling the sub-FLCs approach described in chapter 8, the FA-FLC is assumed to consist of two sub-FLCs, namely, FA1-FLC and FA2-FLC. The former using the preview information from the front-left vehicle suspension, in terms of the displacement and velocity across the suspension, as the two input variables, generating the sub-control force F_{a1}. Whilst the latter utilises similar preview information, but from the front-right suspension and produces the sub-control force F_{a2} as an output, with the resultant control force being the sum of these forces, as shown in Figure 9-4. Similarly, the 4W-FLC has four sub-FLCs, each corresponding to a vehicle suspension, as illustrated in Figure 9-5. Moreover, each sub-FLC has its own RB, thereby decreasing the computational time and reducing the overall RB size.

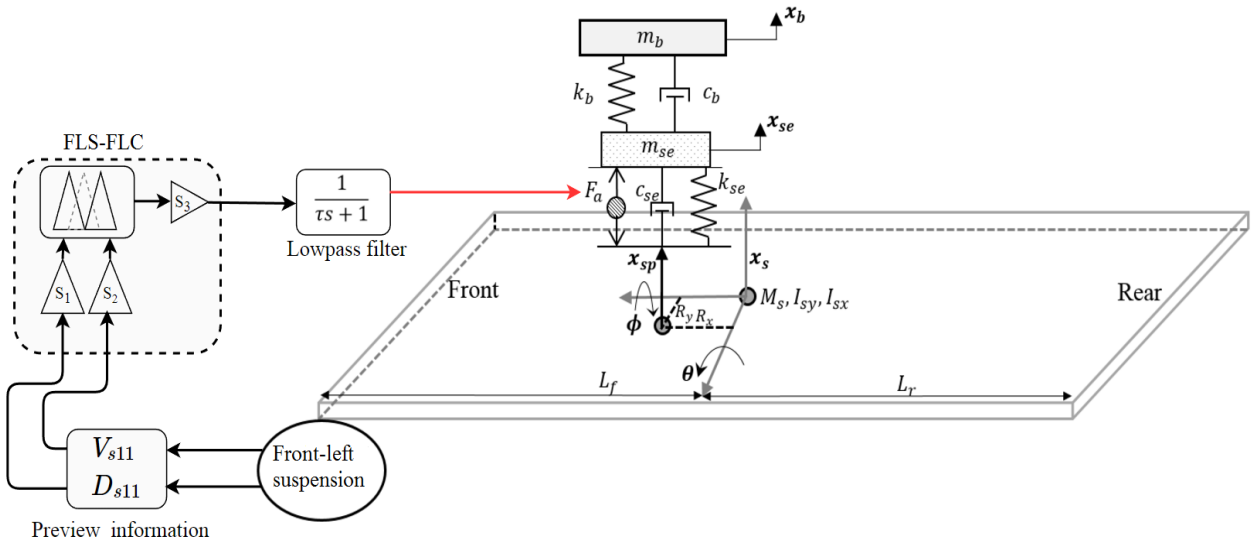

Figure 9-3: Architecture of the FLS–FLC

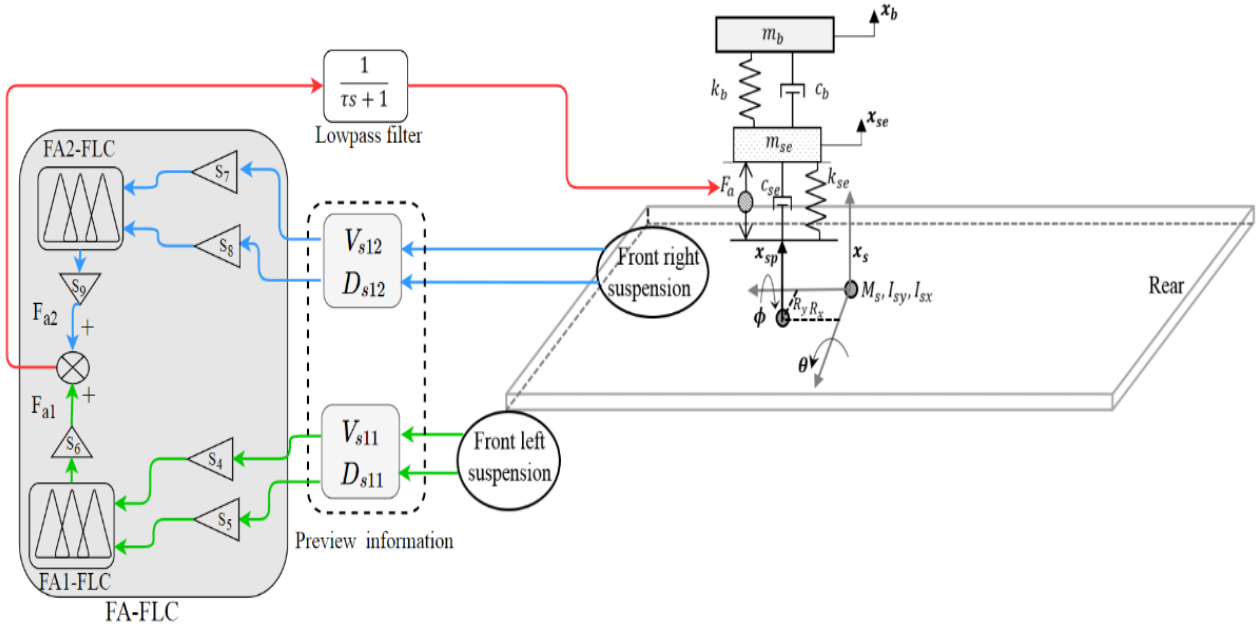

Figure 9-4: Architecture of the FA–FLC

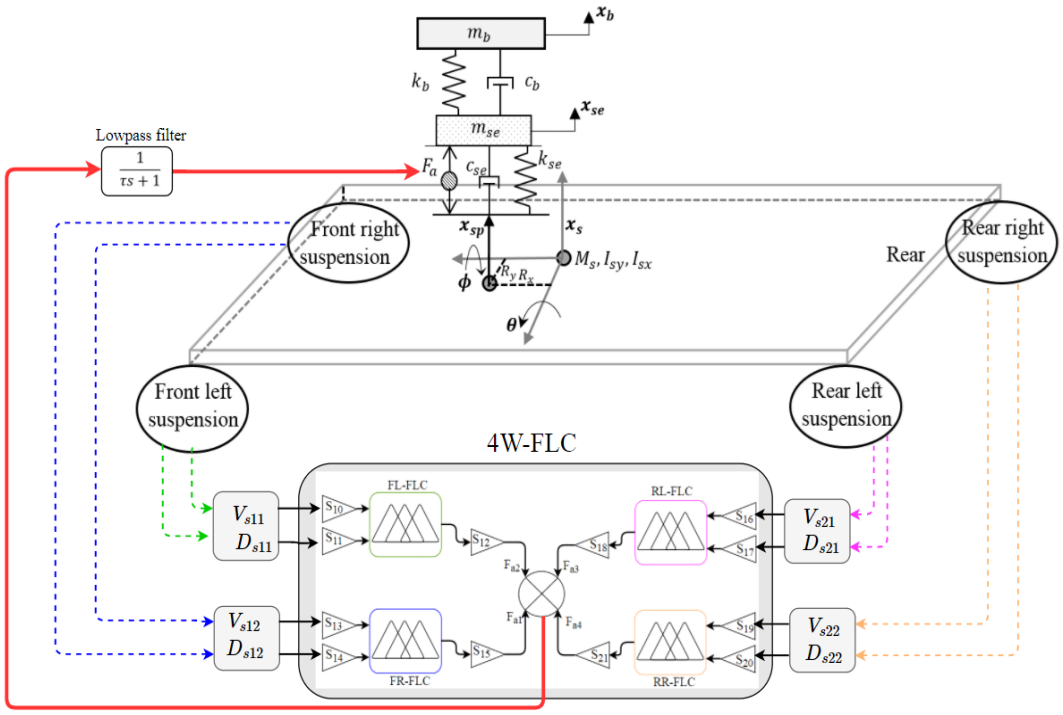

Figure 9-5: Architecture of the 4W-FLC

9.4 Optimisation process

Recalling the optimisation process of the FF-FLC defined in the chapter 8, the structure for each FLC is optimised here also through two stages, using the same fitness function and constraints, except that the simulated model used here is for the full vehicle model. In addition, the type and the number of MFs for both the input and output variables of the FLS-FLC or any sub-FLCs are the same as those used previously in chapter 8 with the QvM. Hence, the RB in each of these FLCs is composed of 25 rules. Moreover, in the same manner as was described in the previous chapter the output force of each FLC is filtered by a low-pass filter with a cut-off frequency of $f_c = 100$ Hz. This simulates the force actuator dynamics and also helps to reduce high frequency excitation of the active seat.

The integrated model was modelled in Simulink and the optimisation problem for each stage was formulated in MATLAB, being solved off-line. Also, the road used in the optimisation process is of class E (very poor) according to the ISO 8606 standard with a forward vehicle speed of 60 km/h. To make the study more realistic the full vehicle model was assumed to be excited at the left and right front wheels with different random disturbances. Moreover, the

coherence characteristics between the left and right front wheels were used, which indicated a low correlation in the amplitude and phase as the spatial frequency increases [227]. The disturbances at the rear wheels were similar to those at the front, with a time delay dependent upon the vehicle wheelbase and the forward vehicle speed.

The parameters of the full vehicle model are listed in Table 9-1 whilst the characteristics of the passive seat suspension as well as the driver's body are those used in the previous chapter. After solving the optimisation problem, the optimised scaling factors for each FLC is presented in Table 9-2 while the resulting optimum demand control force maps are presented in Figures 9.6 to 9.8.

Table 9-1: Parameters of the full vehicle model [191]

Parameter	Value	Unit
M_s	1200.0	Kg
$m_{ij}\ \ i,j = 1\ and\ 2$	20.0	Kg
I_{sy}	2100.0	Kg.m2
I_{sx}	460.0	Kg.m2
$K_{sij}\ \ (i,j = 1\ and\ 2)$	10.0	kN/m
$c_{sij}\ \ (i,j = 1\ and\ 2)$	2000.0	N.s/m
$K_{tij}\ \ (i,j = 1\ and\ 2)$	180.0	kN/m
L_f	1.011	m
L_r	1.803	m
a	0.761	kN.s/m
b	0.761	kN/m
R_x	0.3	m
R_y	0.25	m
R	22.0	N
ε	0.0012	m/s

Table 9-2 Optimised input and output scaling factors

Control strategy	Parameter	Value	Unit
FLS-FLC	S_1	1.362	s/m
	S_2	0.024	m^{-1}
	S_3	1349.600	N
FA-FLC	S_4	2.857	s/m
	S_5	0.010	m^{-1}
	S_6	1265.400	N
	S_7	2.141	s/m
	S_8	0.010	m^{-1}
	S_9	191.250	N
4W-FLC	S_{10}	12.407	s/m
	S_{11}	0.042	m^{-1}
	S_{12}	461.386	N
	S_{13}	13.210	s/m
	S_{14}	0.125	m^{-1}
	S_{15}	118.149	N
	S_{16}	34.014	s/m
	S_{17}	0.003	m^{-1}
	S_{18}	1.000	N
	S_{19}	2.669	s/m
	S_{20}	0.018	m^{-1}
	S_{21}	919.455	N

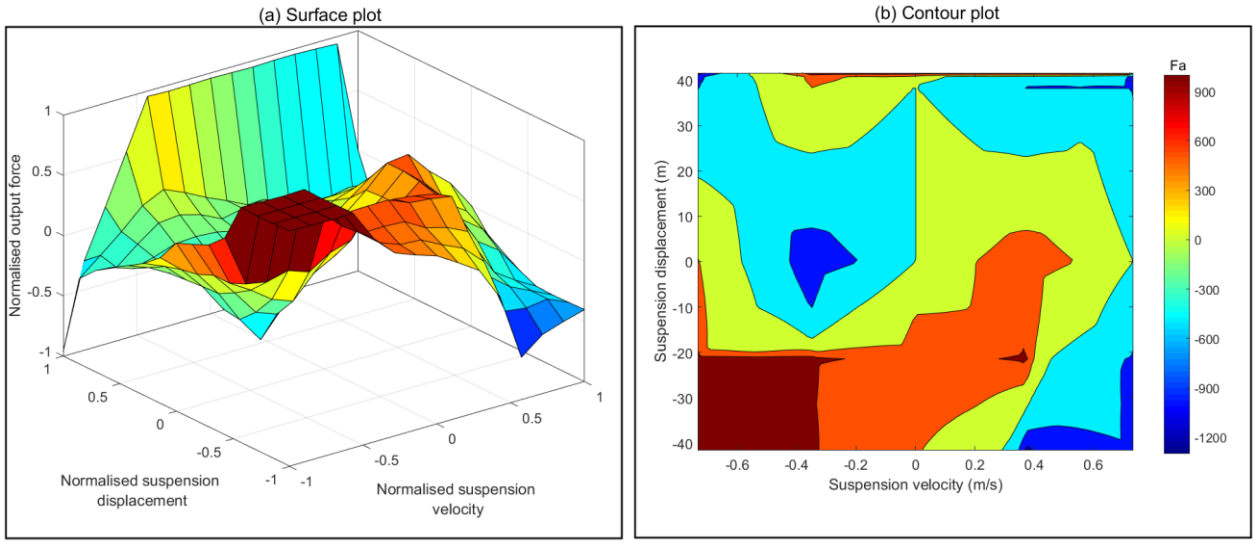

Figure 9-6: Optimised demand control force map of the FLS –FLC

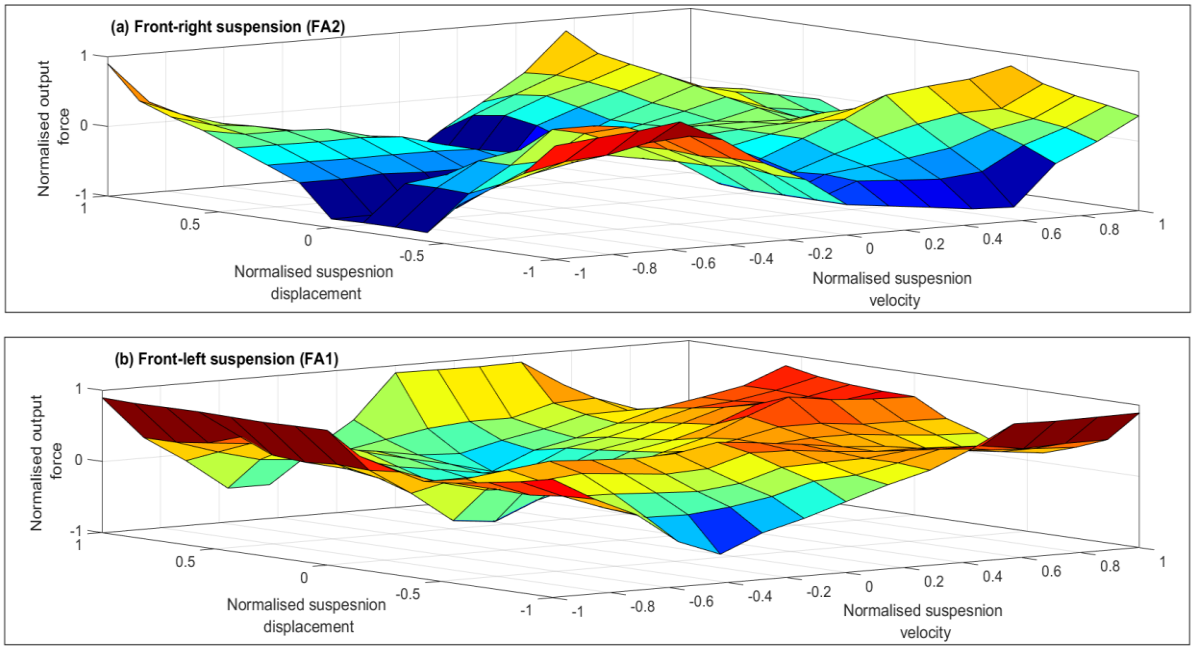

Figure 9-7: Optimised demand control force map of the FA –FLC

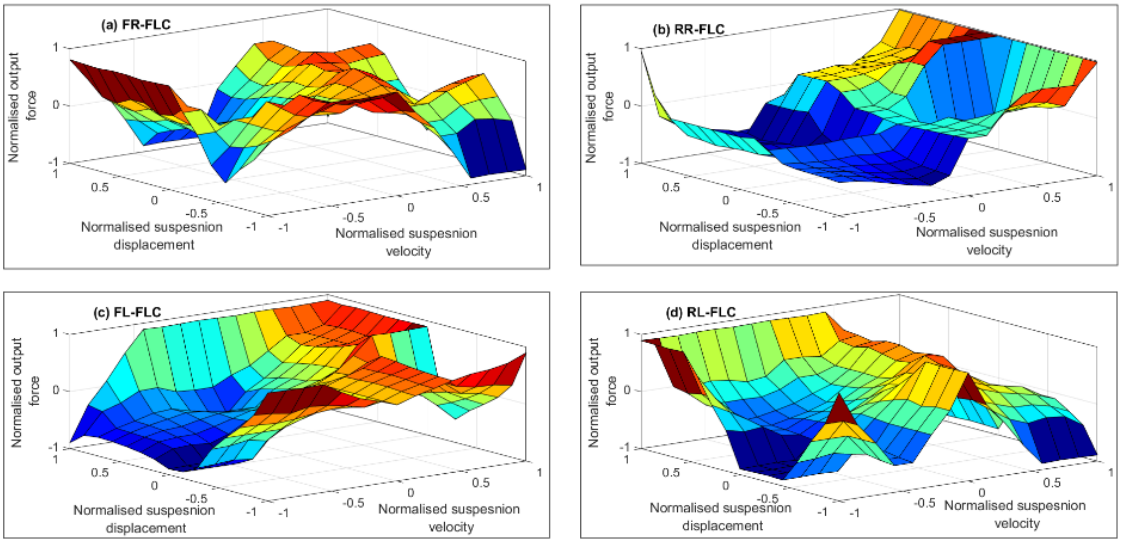

Figure 9-8: Optimised demand control force map of the 4W–FLC

9.5 Simulation analysis

In this section, the effectiveness of the proposed active controlled seat suspensions in improving the ride comfort is evaluated using two typical road disturbances, i.e., random and bump profiles.

9.5.1 Random road

In this analysis, the full vehicle model was excited with a random road profile of class E (very poor), according to the ISO 8608 standard, at a range of forward vehicle speeds. Figure 9-9 shows an example of this road profile at the front left and right wheels, with a vehicle speed of 60 km/h. The resulting time responses of the active and passive seat suspensions, in terms of the seat acceleration, seat suspension travel and the demand control force, are shown in Figures 9.10 to 9.12. It can be seen that the controllers more effectively reduce the seat acceleration when compared with the passive system, with the 4W-FLC delivering the best performance followed by the FA-FLC and the FLS-FLC, respectively. However, this improvement in the ride quality comes at the expense of increased the seat suspension travel, although this and the actuator force constraints are satisfied.

It can be observed from Figures 9.13 and 9.14 that the active seat suspensions provide lower PSD acceleration, when compared with the passive system over a broadband frequency range, especially over the HBSF range (4-8 Hz). However, this performance deteriorates at lower

frequencies during high forward vehicle speeds. In general, the 4W-FLC demonstrates the best performance over a broadband frequency range, irrespective of the vehicle speed followed by the FA-FLC and the FLS-FLC.

Due to the random nature of the road surface the simulations for obtaining the SEAT factor and the weighted RMS seat acceleration were performed 10 times for each vehicle speed over a time period of 20 seconds. Figures 9.15 (a) and (b) show that the proposed active seat suspensions significantly attenuate the vibration at the seat as well as reducing the weighted RMS seat acceleration when compared with the passive seat suspension. At high speed the active systems perform less well, although they are as good as the passive system throughout the speed range. Moreover, at low speed the performance of the FA-FLC is better than that of the FLS-FLC whilst at high speed they perform similarly. The reduction in the performance at high vehicle speeds, especially of the FLS-FLC and FA-FLC, indicates that the preview information obtained from the front suspensions becomes insignificant because the delay time between front suspensions and the seat becomes shorter. This phenomenon has also been observed in studies that applied a wheelbase preview controller to a vehicle active suspension [154,156]. This can be overcome by using a high bandwidth actuator but this at the expense of increasing system cost. However, the attenuation performance of the passive system at high speeds could be sufficient without additional active control.

Nevertheless, this is at the expense of increasing the seat suspension displacement

In general, the 4W-FLC provides the best vibration isolation performance in which the transmitted vibration and the weighted RMS seat acceleration is reduced by at least 15 % with respect to the passive seat suspension regardless of the vehicle speed, as shown in Figures 9.15 (c) and (d).

Figures 9.16 and 9.17 present the frequency-weighted RMS acceleration of the active and passive seat suspensions with respect to the threshold limit values (TLVs), as suggested by the American Conference of Governmental Industrial Hygienists (ACGIH), over a whole range of vehicle speeds. It can be seen that the active seat suspension, using any of the developed controllers, delivers a lower frequency-weighted RMS seat acceleration over the HBSF range, whereas the passive system often exceeds the 16 hour working daily exposure limit. Once again, the 4W-FLC provides the best performance regardless of the vehicle speeds.

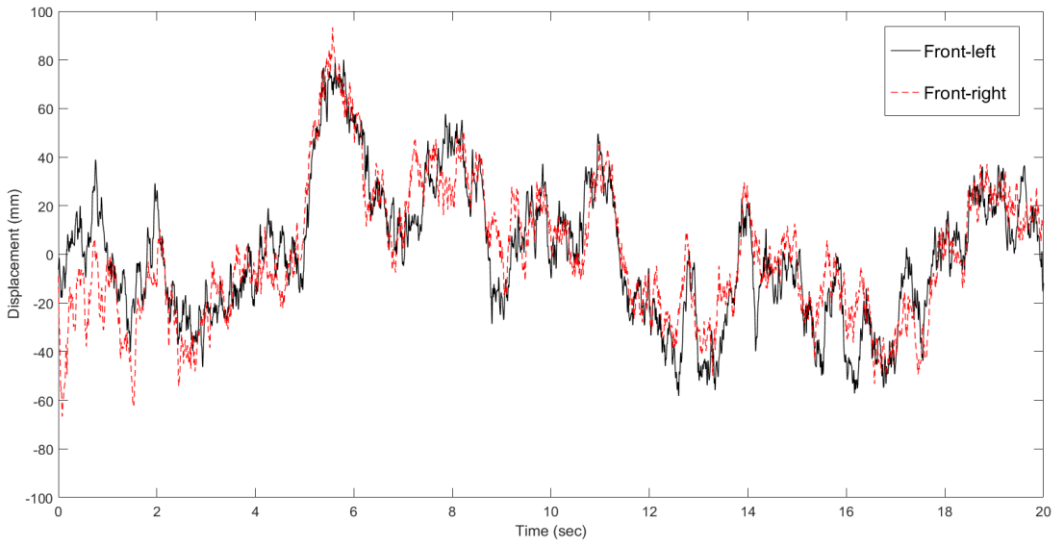

Figure 9-9: An example of random road profiles at the front left and right wheels with a vehicle speed of 60 km/h

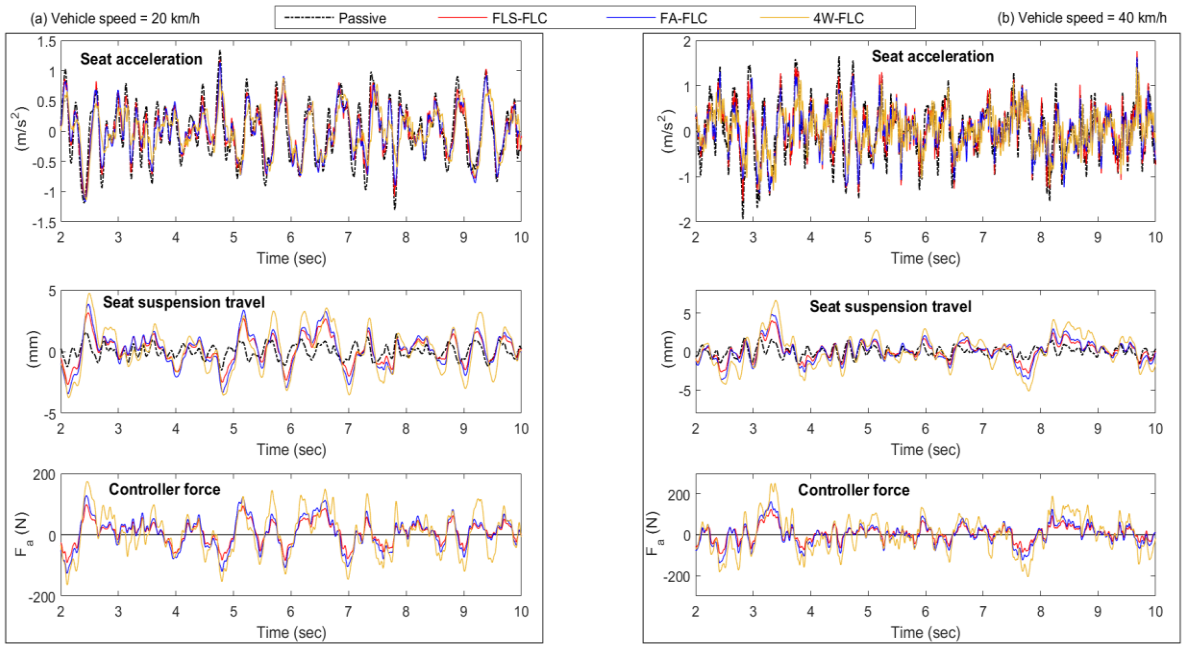

Figure 9-10: Time responses of the passive and active seat suspensions at vehicle speeds of 20 and 40 km/h

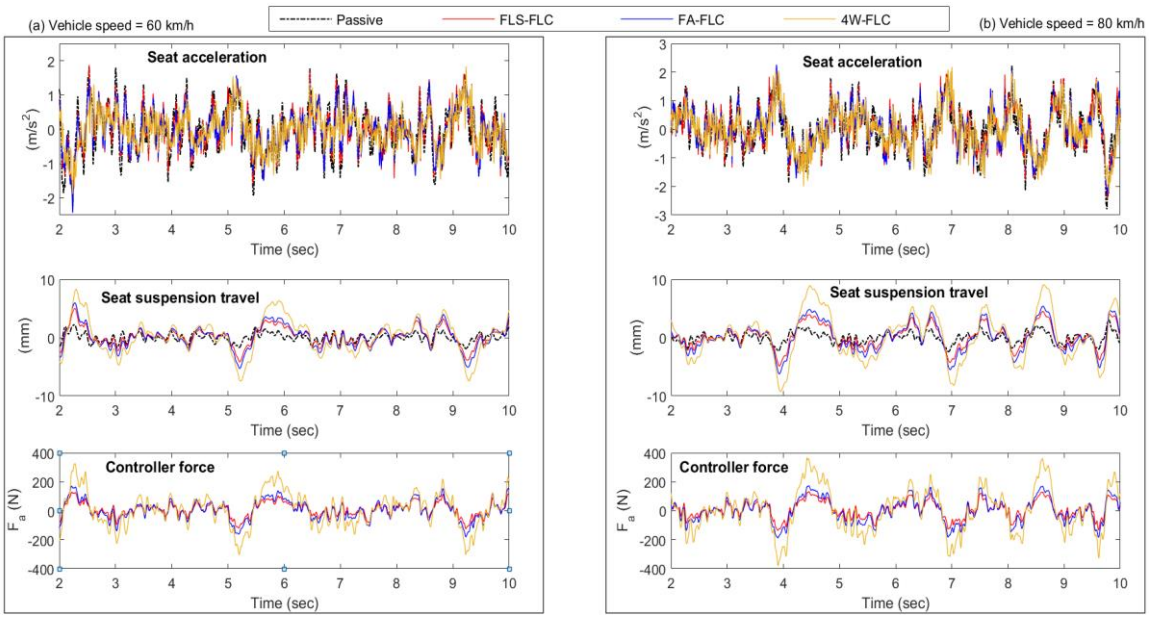

Figure 9-11: Time responses for the passive and active seat suspensions with preview information control at vehicle speeds of 60 and 80 km/h

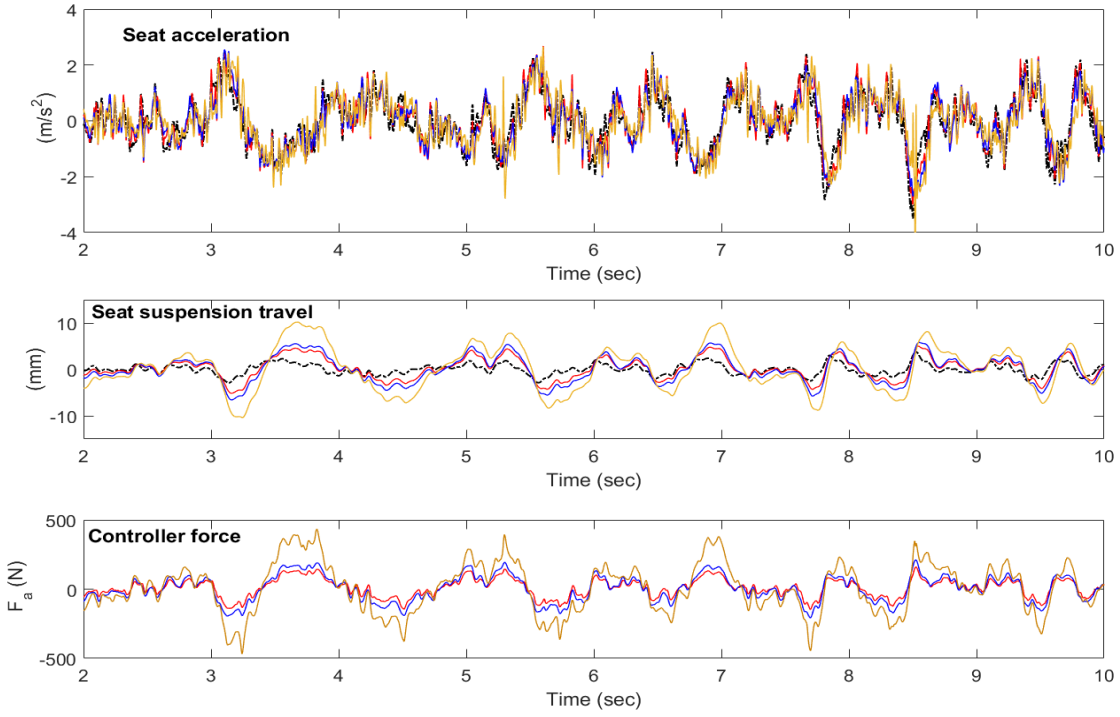

Figure 9-12: Time responses for the passive and active seat suspensions with preview information control at a vehicle speed of 100 km/h

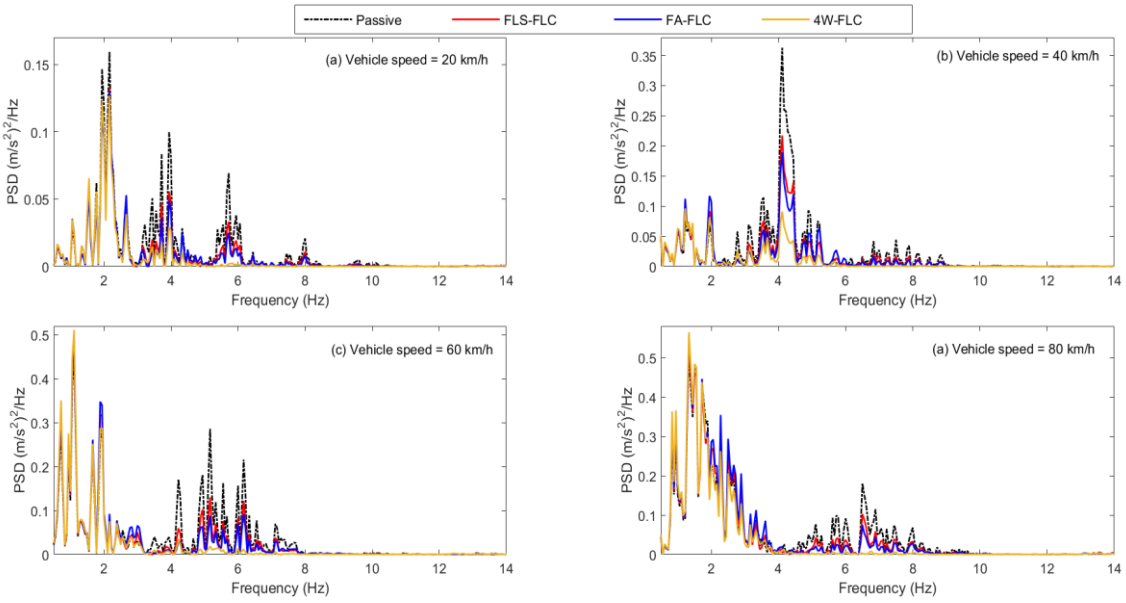

Figure 9-13: PSDs of the seat acceleration for the passive and active seat suspensions with preview information control at different vehicle speeds

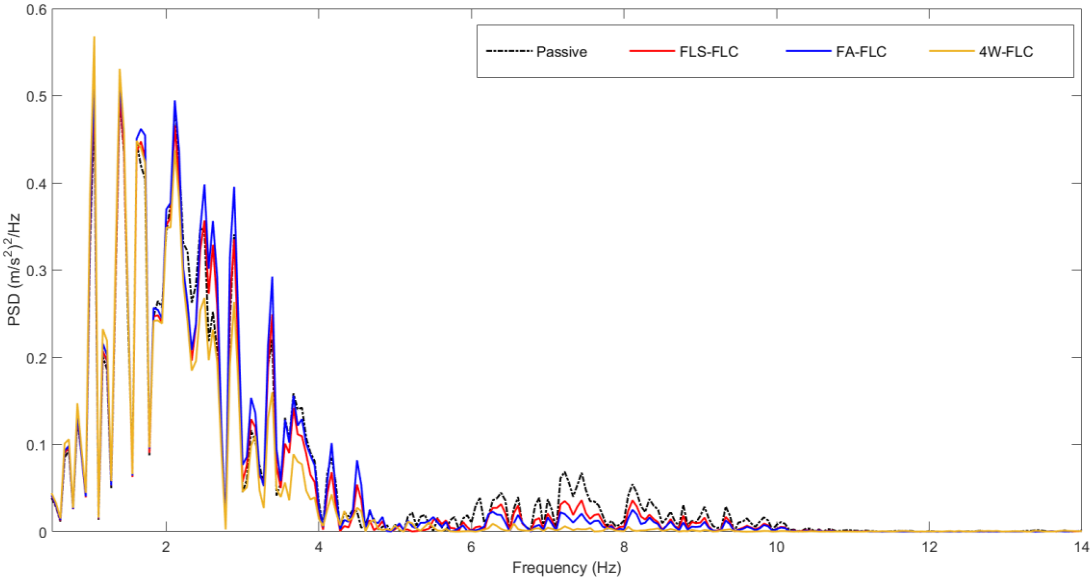

Figure 9-14: PSDs of the seat acceleration for the passive and active seat suspensions with preview information control at a vehicle speed of 100 km/h

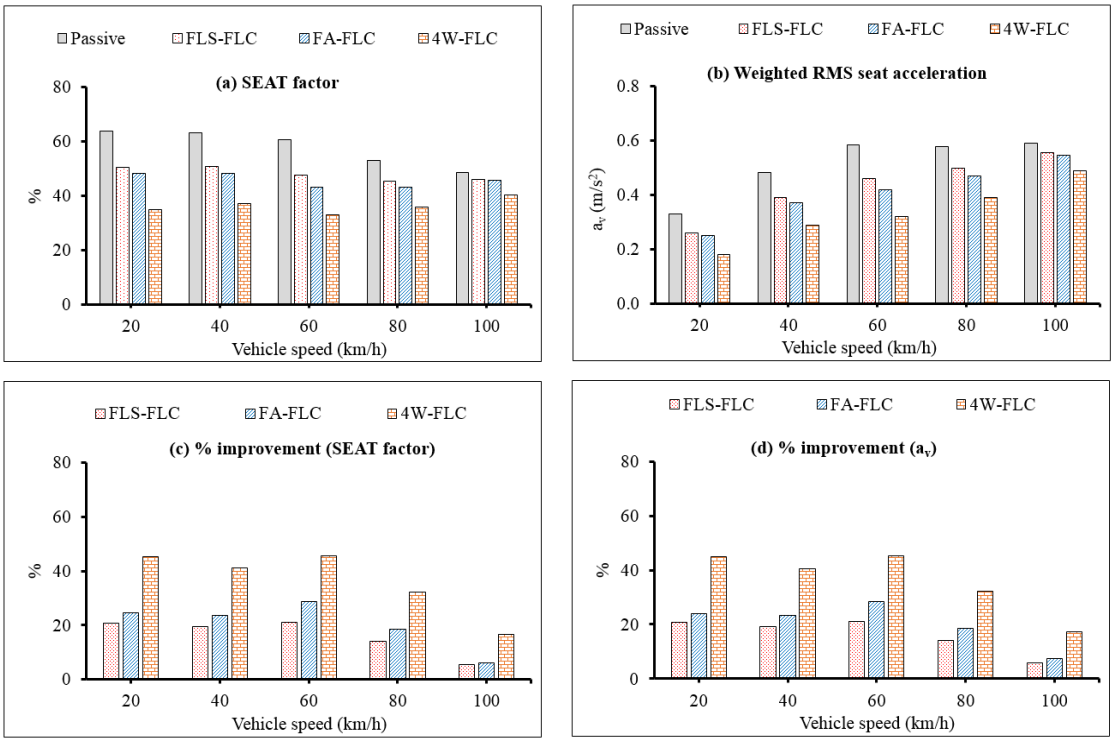

Figure 9-15: SEAT factor and weighted RMS seat acceleration of the proposed controllers and percentage improvements at different vehicle speeds

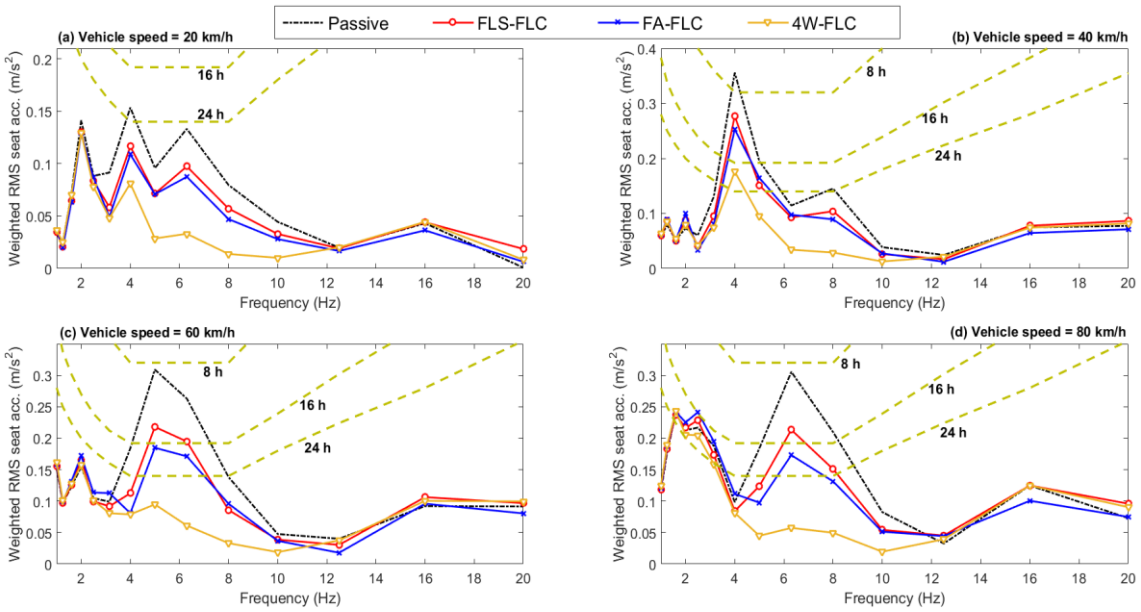

Figure 9-16: Health risk assessment, according to the ISO 2631-1 standard, for the passive and active seat suspensions with preview information control over different vehicle speeds

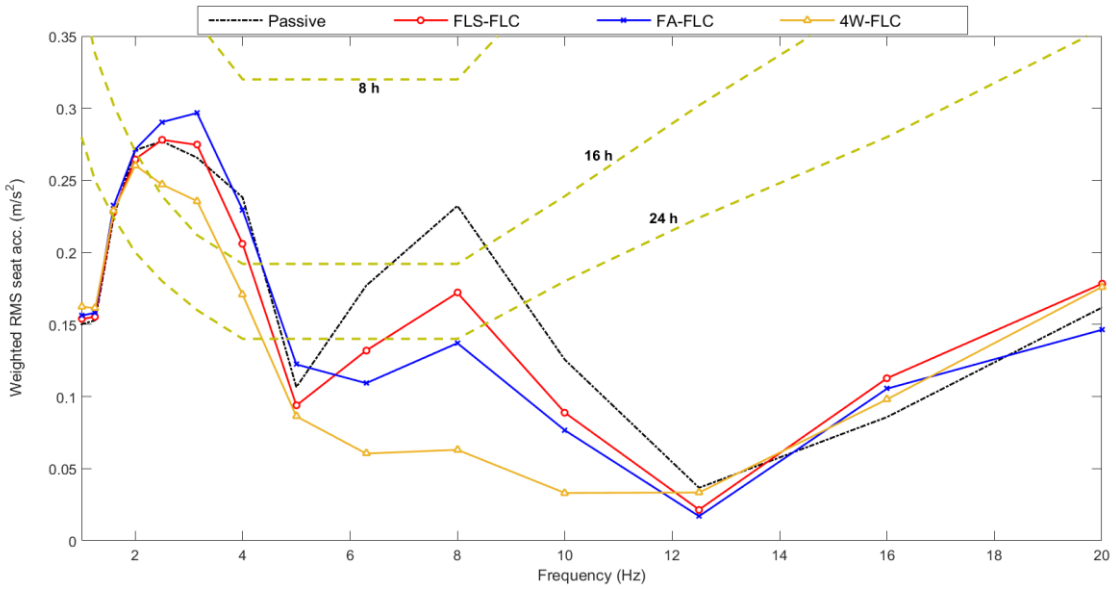

Figure 9-17: Health risk assessment, according to the ISO 2631-1 standard, for the passive and active seat suspensions with preview information control at a vehicle speed of 100 km/h

Whilst the 4W-FLC is shown to be the best preview based controller for use in an active seat suspension, its real implementation is somewhat costly, as it requires instrumentation at each corner of the car. This can be partially overcome in a new controller, denoted as the 'practical four wheel' (P4W) FLC, which is similar to the 4W-FLC, but uses fewer states. Specifically, this controller employs the same optimum sub-fuzzy logic controllers as the 4W-FLC. However, it requires only the states from the front suspensions, as the required states from rear suspensions are hypothesised as a time delayed version of the measured states at the front, as illustrated in Figure 9-18.

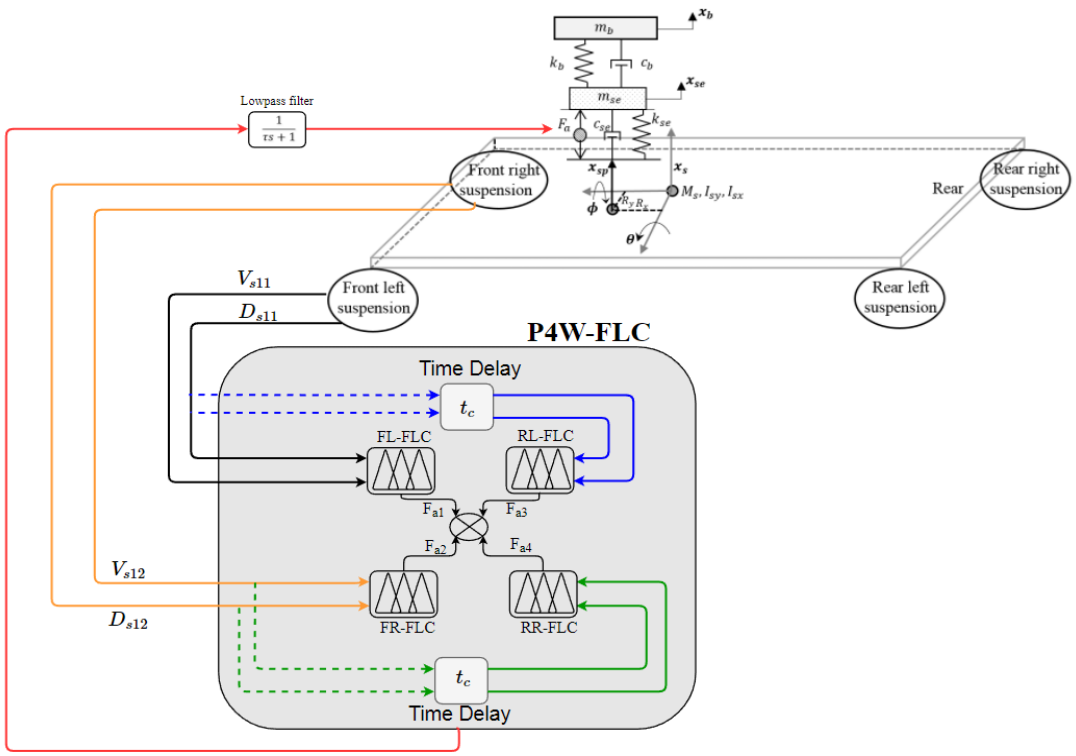

Figure 9-18: Architecture of the P4W–FLC

Figures 9.19 and 9.20 compare the seat acceleration PSD of the P4W-FLC and 4W-FLC active seats to those of the passive system at a range of vehicle speeds. Clearly, the P4W-FLC is almost identical to the 4W-FLC regardless of the vehicle speed. Moreover, as shown in Figure 9-21 the P4W-FLC provides very similar vibration attenuation performance and weighted RMS seat acceleration to the 4W-FLC at the full range of vehicle speeds. Moreover, the P4W-FLC delivers very similar frequency-weighted RMS seat acceleration values to the 4W-FLC irrespective to the vehicle speed, as illustrated, in Figure 9-22.

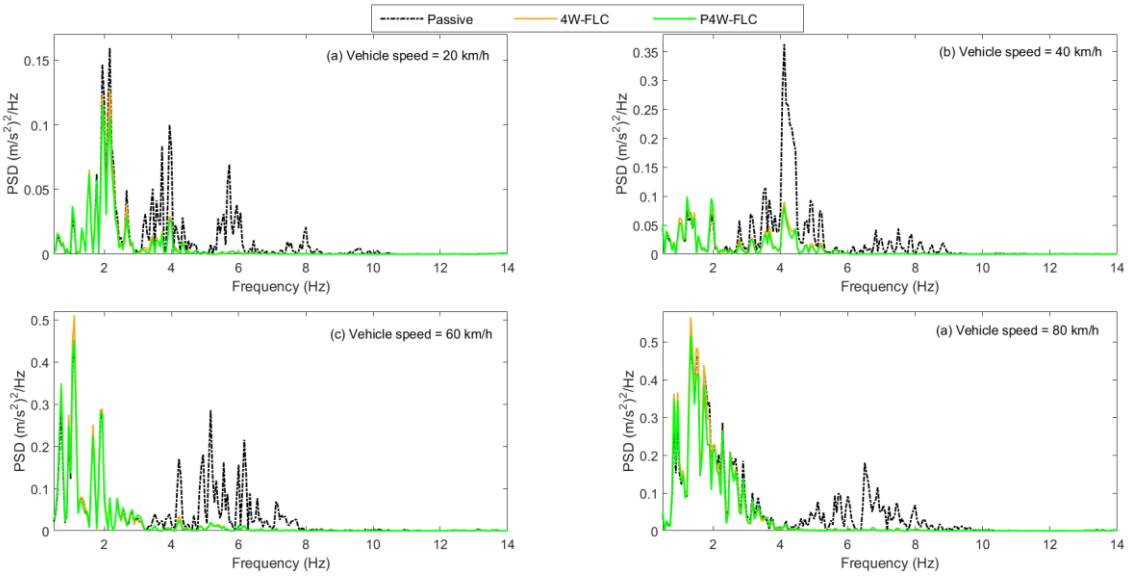

Figure 9-19: PSDs of the seat acceleration for the passive and active seat suspensions using the 4W-FLC and P4W-FLC approaches at different vehicle speeds

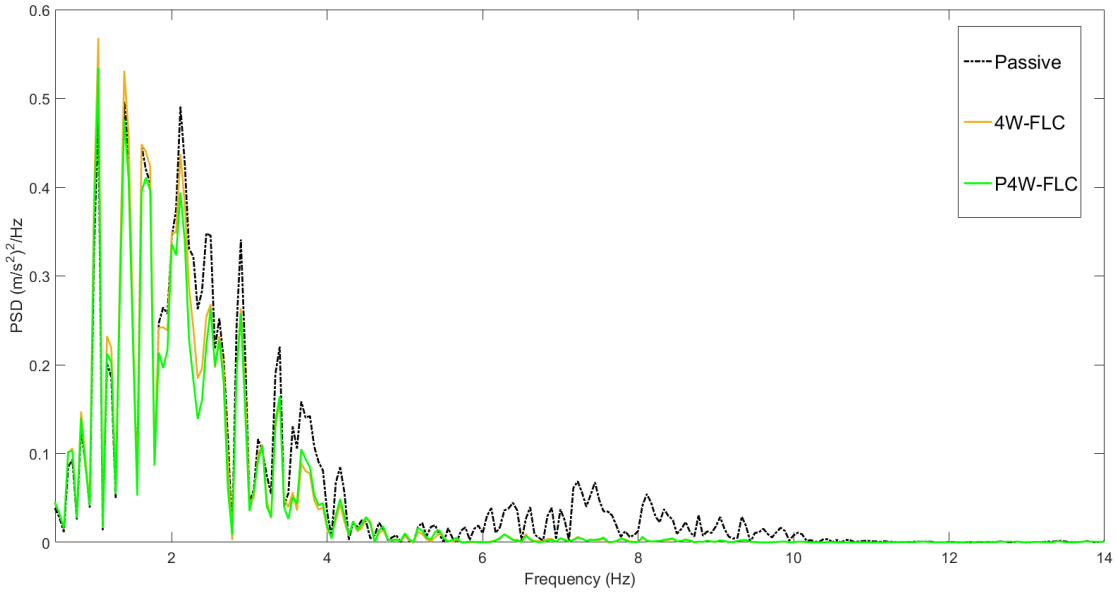

Figure 9-20: PSDs of the seat acceleration for the passive and active seat suspensions using the 4W-FLC and P4W-FLC approaches at a vehicle speed of 100 km/h

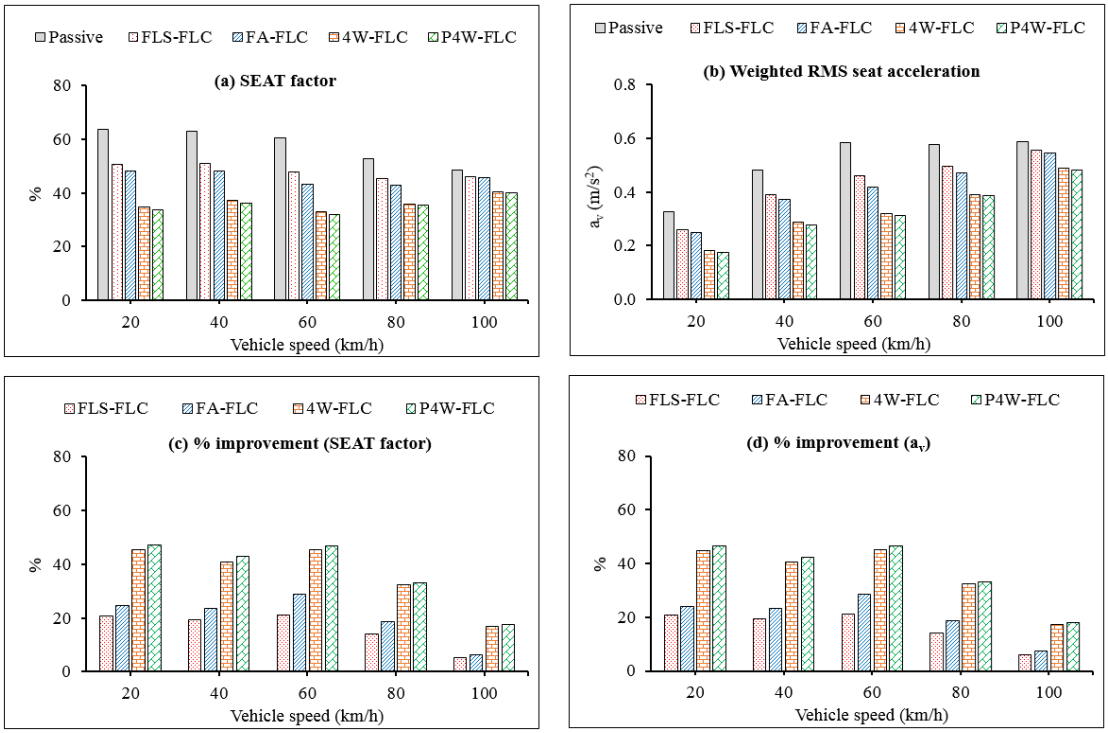

Figure 9-21: Performance evaluation in terms of the SEAT factor and weighted RMS seat acceleration values and percentage improvements for the active seat suspensions with preview information control using at different vehicle speeds

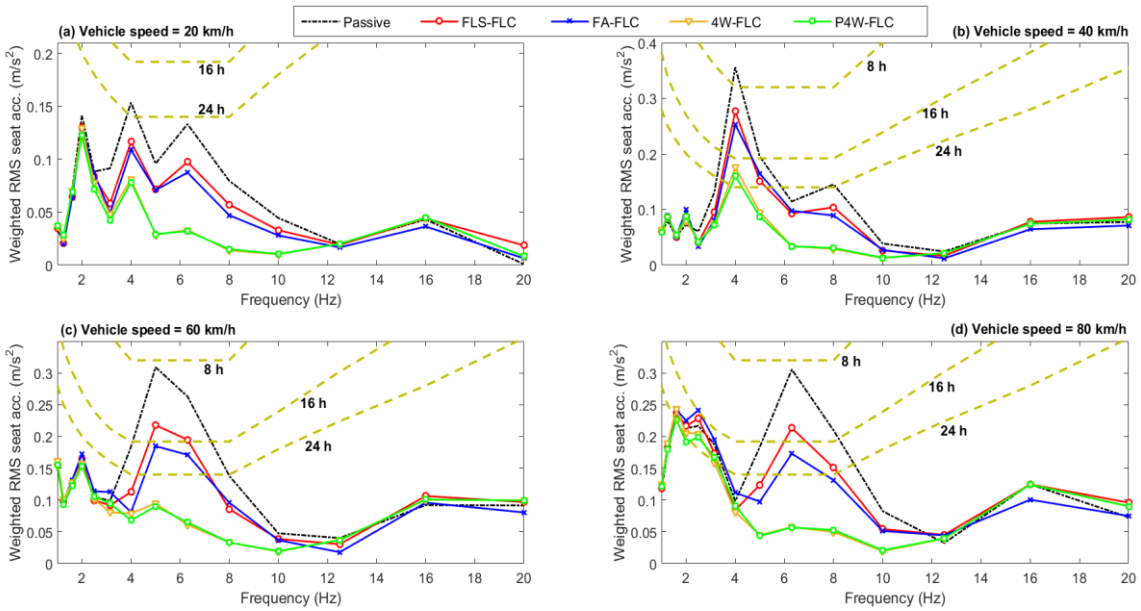

Figure 9-22: Health risk assessment, according to the ISO 2631-1 standard, of the passive and proposed active seat suspensions over different vehicle speeds

9.5.2 Bump road input

Figure 9-23 shows the bump road profile used to excite the full vehicle model. Figures 9.24 (a) and (b) show the superior ability of the proposed controllers in reducing the seat acceleration when compared with the passive system, without exceeding the seat suspension travel limit. Once again, the 4W-FLC and P4W-FLC show very similar results, reducing the RMS value of seat acceleration from 1.15 m/s² with the passive system to 0.91 m/s² and 0.88 m/s², respectively, as presented in Table 9-3.

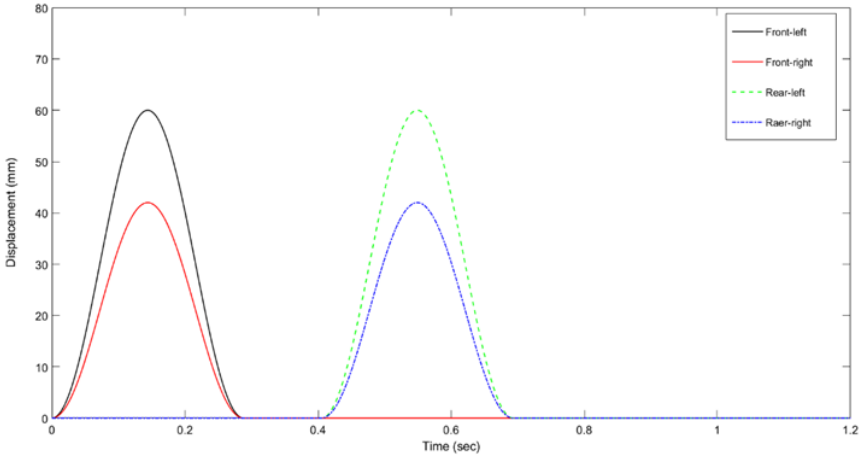

Figure 9-23: Bump road profile for a full vehicle model

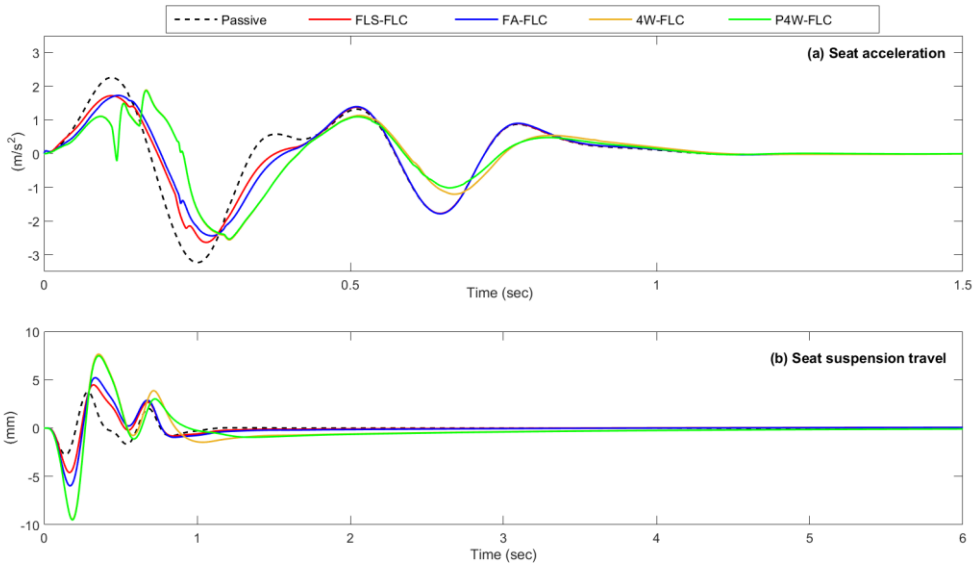

Figure 9-24: Time responses for the passive and active seat suspensions with preview information control under a bump road profile: (a) Seat acceleration and (b) seat suspension travel

Table 9-3: Time response characteristics of the proposed controllers under a bump road profile

System	Seat acceleration		Seat suspension travel	
	RMS (m/s2)	Peak (m/s2)	RMS (mm)	Peak (mm)
Passive	1.15	3.23	1.38	3.75
FLS-FLC	1.00	2.64	2.02	4.64
FA-FLC	0.99	2.44	2.52	6.04
4W-FLC	0.91	2.56	3.84	9.43
P4W-FLC	0.88	2.53	3.71	9.49

9.6 Conclusions

This chapter has presented the application of the preview information enhanced controller for an active seat suspension in a full vehicle model. Three novel and cost-effective FL controllers have been developed that employ inexpensive and available preview information from the vehicle suspensions, while satisfying the physical system constraints at a range of different operational conditions. The simulation results indicate that the controllers significantly improve ride comfort compared with the passive system and the 4W-FLC shows the best performance regardless of the vehicle speed. Interestingly, the P4W-FLC performs very similarly to the 4W-FLC and requires fewer measured system states, thus being a practical and cost-effective system that improves ride comfort and reduces driver fatigue.

Chapter 10
Conclusions and Future Work

10.1 Conclusions

1) This thesis was aimed at improving the ride comfort of vehicle drivers through the application of an active seat suspension system that attenuates harmful low frequency vertical vibration at the driver's seat over the frequency range of 1-20 Hz. One main feature of this system is the novel control strategy that utilises preview information from the vehicle suspension in terms of the suspension displacement and velocity and which takes into account the practical limitations associated with both the seat suspension travel and actuator force. For simplicity, the demand control force was derived firstly based upon a linear control approach using a linear QvM and was then practically examined using a prototype active seat suspension and the HIL simulation technique. The results of the experimental and simulation studies over different operating conditions have shown that this strategy significantly improves the ride comfort compared with a passive alternative, specifically, over the HBSF range 4-8 Hz. Moreover, laboratory results verify that the vibration attenuation performance over a whole range of vehicle speeds can be further improved by combining both the preview information (feedforward) states with the acceleration states (feedback) of both the vehicle and seat.

2) Despite the complexity involved in the design of a Fuzzy Logic Controller (FLC), it shows some advantages over the linear control approach. Its capability to satisfy ensure the physical constraints of the seat suspension stroke and actuator force independent of the operating

conditions as well as handling nonlinearities involved in the suspension system make superior to a traditional PID controller.

3) Once again, the simulation and experimental results reveal that the application of the vehicle suspension preview information with FLCs provides a significant improvement in the ride quality. Moreover, the FFFB-FLC that uses the preview information together with the displacement and velocity of the seat suspension feedback states provides the best performance and most robust control strategy when compared with the passive system. Whilst it requires four input variables its rule base (RB) size was reduced using the sub-FLCs technique, thereby limiting the controller complexity and computational time.

4) In general, there was a good agreement between the simulation and experimental results in the case of random road profiles. However, this was not achieved with a bump road profile mainly due to the presence of friction within the experimental prototype system which dominates at the low frequency range. Also, the dummy dynamics and system nonlinearities, which have not been included in the simulation model, influence these results. Moreover, this has a significant impact on the accuracy of the feedback states from the seat suspension.

5) To apply the preview enhanced controller for an active seat suspension in a full vehicle model, three FLCs which employ preview information from either the front-left suspension (FLS-FLC), the front-left and front-right suspensions (FA-FLC) or all the vehicle suspensions (4W-FLC) were developed and examined. The simulation results have demonstrated that the performance of these strategies surpasses that of the passive system, although their performance is not so good at high vehicle speeds. The preview controller that uses information from all suspensions provides the best performance regardless of the vehicle speed. In conclusion, this novel controller for an active seat suspension provides an efficient, robust and cost-effective control strategy for road going or off-road vehicles.

10.2 Recommendations for future work

Based on the work that has been undertaken for this thesis the following topics are recommended for future work.

- The application of the preview information for the active seat suspension amplifies vibration at the low frequency range, below the vehicle bounce natural frequency. Hence this issue needs to be investigated and overcome. It could be achieved by using a high-pass filter of the suspension preview information at this frequency range taking into account the effect of this filter on the controller dynamics.
- The linear simulation models can be further modified by considering nonlinearities associated with the vehicle suspension components (spring and/or damper), seat suspension and actuator. Besides, the driver's body model could be replaced with a higher DOF model.
- The presence of friction in the prototype active seat suspension has a significant impact on the accuracy of the experimental results, especially at the low frequency range or when using a bump road profile. This effect could be reduced by replacing the prototype active seat suspension with a commercial active seat with low friction.
- The preview controller could be extended to attenuate the pitch vibration which is known to contribute to discomfort.
- It is worth investigating the benefits of applying this concept to compensate for the time delay associated with the actuator or measurements as well as the effects of measurement noise which is important to assess if low-cost components would be acceptable.

- The fuzzy type of the FLC used in this work was the Mamdani fuzzy system with a triangle MFs type. Other fuzzy systems, such as a Takgai-Sugeno (T-S) or Interval Type 2-Fuzzy logic controller with different MFs type, such as trapezoid or Gaussian could be investigated in order to further improve the performance and robustness of the active seat suspension. Moreover, adaptive FLC strategies that consider parameter uncertainties could be researched.
- The effectiveness of applying the preview information to a full vehicle model has been confirmed through numerical simulation, but this still needs to be validated by experimental as well as real field tests. This could be performed primarily through laboratory tests by modifying a HIL simulation to mimic the vehicle body dynamics of the full vehicle model. Later, it could be implemented for an active seat suspension in a real vehicle.
- The concept of preview information has been applied to an active seat suspension. It would be worthwhile investigating the application of this strategy to a semi-active seat suspension or adaptive seat suspension which reduces cost and power consumption.
- It may be useful to investigate the application of the developed preview information control for a cab suspension system or seat suspension, practically for heavy or off-road vehicle.

References

[1] Li, H., 2012, "Robust Control Design for Vehicle Active Suspension Systems with Uncertainty," Ph.D., University of Portsmouth.

[2] Liu, Y., Waters, T. P., and Brennan, M. J., 2005, "A Comparison of Semi-Active Damping Control Strategies for Vibration Isolation of Harmonic Disturbances," J. Sound Vib., **280**(1), pp. 21–39.

[3] Tseng, H. E., and Hrovat, D., 2015, "State of the Art Survey: Active and Semi-Active Suspension Control," Veh. Syst. Dyn., **53**(7), pp. 1034–1062.

[4] Bovenzi, M., and Hulshof, C. T. J., 1998, "An Updated Review of Epidemiologic Studies on the Relationship between Exposure to Whole-Body Vibration and Low Back Pain," J. Sound Vib., **215**(4), pp. 595–611.

[5] Caffaro, F., Cremasco, M. M., Preti, C., and Cavallo, E., 2016, "Ergonomic Analysis of the Effects of a Telehandler's Active Suspended Cab on Whole Body Vibration Level and Operator Comfort," Int. J. Ind. Ergon., **53**, pp. 19–26.

[6] Meng, X., Tao, X., Wang, W., Zhang, C., Cheng, B., Wang, B., Zhou, C., Jin, X., Zeng, C., and Cavanaugh, J., 2015, *Effects of Sinusoidal Whole Body Vibration Frequency on Drivers' Muscle Responses*, SAE Technical Paper.

[7] Stayner, 2001, *Whole-Body Vibration and Shock Extension of a Study of Overtravel of Seat Suspensions*.

[8] Wikström, B.-O., Kjellberg, A., and Landström, U., 1994, "Health Effects of Long-Term Occupational Exposure to Whole-Body Vibration: A Review," Int. J. Ind. Ergon., **14**(4), pp. 273–292.

[9] Palmer, K. T., Griffin, M. J., Bendall, H., Pannett, B., and Coggon, D., 2000, "Prevalence and Pattern of Occupational Exposure to Whole Body Vibration in Great Britain: Findings from a National Survey," Occup. Environ. Med., **57**(4), pp. 229–236.

[10] Bovenzi, M., Rui, F., Negro, C., D'Agostin, F., Angotzi, G., Bianchi, S., Bramanti, L., Festa, G., Gatti, S., Pinto, I., and others, 2006, "An Epidemiological Study of Low Back Pain in Professional Drivers," J. Sound Vib., **298**(3), pp. 514–539.

[11] BS 6841, 1987, *BRITISH STANDARDS INSTITUTION, 1987, BS 6841, Measurement and Evaluation of Human Exposure to Whole-Body Mechanical Vibration and Repeated Shock*.

[12] Okunribido, O. O., Magnusson, M., and Pope, M., "Delivery Drivers and Low-Back Pain: A Study of the Exposures to Posture Demands, Manual Materials Handling and Whole-Body Vibration," Int. J. Ind. Ergon., **36**(3), pp. 265–274.

[13] Smith, D. R., and Leggat, P. A., 2005, "Whole-Body Vibration," Prof. Saf., **50**(7), p. 35.

[14] Palmer, K. T., Griffin, M. J., Syddall, H. E., Pannett, B., Cooper, C., and Coggon, D., 2003, "The Relative Importance of Whole Body Vibration and Occupational Lifting as Risk Factors for Low-Back Pain," Occup. Environ. Med., **60**(10), pp. 715–721.

[15] Donati, P., 2008, *Workplace Exposure to Vibration in Europe: An Expert Review*, Office for Official Publications of.

[16] Bovenzi, M., 2010, "A Longitudinal Study of Low Back Pain and Daily Vibration Exposure in Professional Drivers," Ind. Health, **48**(5), pp. 584–595.

[17] Bovenzi, M., and Betta, A., 1994, "Low-Back Disorders in Agricultural Tractor Drivers Exposed to Whole-Body Vibration and Postural Stress," Appl. Ergon., **25**(4), pp. 231–241.

[18] Hulshof, C., and van Zanten, B. V., 1987, "Whole-Body Vibration and Low-Back Pain," Int. Arch. Occup. Environ. Health, **59**(3), pp. 205–220.

[19] Seidel, H., 1993, "Selected Health Risks Caused by Long-Term, Whole-Body Vibration," Am. J. Ind. Med., **23**(4), pp. 589–604.

[20] Funakoshi, M., Taoda, K., Tsujimura, H., and Nishiyama, K., 2004, "Measurement of Whole-Body Vibration in Taxi Drivers," J. Occup. Health, **46**(2), pp. 119–124.

[21] JC, C., WR, C., WP, C., JT, D., and LM, R., 2003, "Predictors of Whole-Body Vibration Levels among Urban Taxi Drivers," Ergonomics.

[22] Raanaas, R. K., and Anderson, D., 2008, "A Questionnaire Survey of Norwegian Taxi Drivers' Musculoskeletal Health, and Work-Related Risk Factors," Int. J. Ind. Ergon., **38**(3), pp. 280–290.

[23] Paddan, G. S., and Griffin, M. J., 2002, "Evaluation of Whole-Body Vibration in Vehicles," J. Sound Vib., **253**(1), pp. 195–213.

[24] ISO 2631-1, 1997, *ISO 2631-1:1997 - Mechanical Vibration and Shock -- Evaluation of Human Exposure to Whole-Body Vibration -- Part 1: General Requirements*.

[25] Griffin, M., 1990, *Handbook of Human Vibration Academic Press London 1990*.

[26] Goswami, D. Y., 2004, *The CRC Handbook of Mechanical Engineering*, CRC press.

[27] Anna, D. H., 2011, *The Occupational Environment: Its Evaluation, Control and Management*, American Industrial Hygiene Association.

[28] Liang, C.-C., and Chiang, C.-F., 2006, "A Study on Biodynamic Models of Seated Human Subjects Exposed to Vertical Vibration," Int. J. Ind. Ergon., **36**(10), pp. 869–890.

[29] Smith, S. D., 2000, "Modeling Differences in the Vibration Response Characteristics of the Human Body," J. Biomech., **33**(11), pp. 1513–1516.

[30] Mansfield, N. J., 2005, "Impedance Methods (Apparent Mass, Driving Point Mechanical Impedance and Absorbed Power) for Assessment of the Biomechanical Response of the Seated Person to Whole-Body Vibration," Ind. Health, **43**(3), pp. 378–389.

[31] Mansfield, N. J., 2004, *Human Response to Vibration*, CRC press.

[32] Kumbhar, P., Xu, P., and Yang, J., 2013, *Evaluation of Human Body Response for Different Vehicle Seats Using a Multibody Biodynamic Model*, SAE Technical Paper.

[33] Kitazaki, S., and Griffin, M. J., 1997, "Resonance Behaviour of the Seated Human Body and Effects of Posture," J. Biomech., **31**(2), pp. 143–149.

[34] Broch, J. T., 1980, *Mechanical Vibration and Shock Measurements*, Brüel & Kj\a er.

[35] Rakheja, S., Dong, R. G., Patra, S., Boileau, P.-É., Marcotte, P., and Warren, C., 2010, "Biodynamics of the Human Body under Whole-Body Vibration: Synthesis of the Reported Data," Int. J. Ind. Ergon., **40**(6), pp. 710–732.

[36] Cho, Y., and Yoon, Y.-S., 2001, "Biomechanical Model of Human on Seat with Backrest for Evaluating Ride Quality," Int. J. Ind. Ergon., **27**(5), pp. 331–345.

[37] Emanuele. Guglielmino, 2008, *Semi-Active Suspension Control Improved Vehicle Ride and Road Friendliness*, Springer, Dordrecht.

[38] Wong, J. Y., 1993, *Theory of Ground Vehicles.*, JWiley, New York, N.Y. ; Chichester.

[39] Hillis, A. J., 2005, "Adaptive Control of Active Engine Mounts," Ph.D., University of Bristol.

[40] Basri, B., and Griffin, M. J., 2014, "The Application of SEAT Values for Predicting How Compliant Seats with Backrests Influence Vibration Discomfort," Appl. Ergon., **45**(6), pp. 1461–1474.

[41] Griffin, M. J., 1978, "The Evaluation of Vehicle Vibration and Seats," Appl. Ergon., **9**(1), pp. 15–21.

[42] Hostens, I., Deprez, K., and Ramon, H., 2004, "An Improved Design of Air Suspension for Seats of Mobile Agricultural Machines," J. Sound Vib., **276**(1), pp. 141–156.

[43] Hostens, I., and Ramon, H., 2003, "Descriptive Analysis of Combine Cabin Vibrations and Their Effect on the Human Body," J. Sound Vib., **266**(3), pp. 453–464.

[44] Lewis, C. H., and Griffin, M. J., 2002, "Evaluating the Vibration Isolation of Soft Seat Cushions Using an Active Anthropodynamic Dummy," J. Sound Vib., **253**(1), pp. 295–311.

[45] Maciejewski, I., 2012, "Control System Design of Active Seat Suspensions," J. Sound Vib., **331**(6), pp. 1291–1309.

[46] van der Westhuizen, A., and van Niekerk, J. L., 2006, "Verification of Seat Effective Amplitude Transmissibility (SEAT) Value as a Reliable Metric to Predict Dynamic Seat Comfort," J. Sound Vib., **295**(3), pp. 1060–1075.

[47] Van Niekerk, J. L., Pielemeier, W. J., and Greenberg, J. A., 2003, "The Use of Seat Effective Amplitude Transmissibility (SEAT) Values to Predict Dynamic Seat Comfort," J. Sound Vib., **260**(5), pp. 867–888.

[48] Magid, E. B., Coermann, R. R., and Ziegenruecker, G. H., 1960, "Human Tolerance to Whole Body Sinusoidal Vibration. Short-Time, One-Minute and Three-Minute Studies," Aerosp. Med., **31**, pp. 915–924.

[49] Corbridge, C., and Grifftn, M. J., 1986, "Vibration and Comfort: Vertical and Lateral Motion in the Range 0· 5 to 5· 0 Hz," Ergonomics, **29**(2), pp. 249–272.

[50] Corbridge, C., 1987, "Vibration in Vehicles: Its Effect on Comfort," University of Southampton.

[51] BURDORF, A., and SWUSTE, P., 1993, "The Effect of Seat Suspension on Exposure to Whole-Body Vibration of Professional Drivers," Ann. Occup. Hyg., **37**(1), pp. 45–55.

[52] Paddan, G. S., and Griffin, M. J., 2002, "Effect of Seating on Exposures to Whole-Body Vibration in Vehicles," J. Sound Vib., **253**(1), pp. 215–241.

[53] Thamsuwan, O., Blood, R. P., Lewis, C., Rynell, P. W., and Johnson, P. W., 2012, "Whole Body Vibration Exposure and Seat Effective Amplitude Transmissibility of Air Suspension Seat in Different Bus Designs," *Proceedings of the Human Factors and Ergonomics Society Annual Meeting*, SAGE Publications, pp. 1218–1222.

[54] Johanning, E., Fischer, S., Christ, E., Göres, B., and Landsbergis, P., 2002, "Whole-Body Vibration Exposure Study in US Railroad Locomotives—an Ergonomic Risk Assessment," AIHA J., **63**(4), pp. 439–446.

[55] Blood, R. P., Ploger, J. D., and Johnson, P. W., 2010, "Whole Body Vibration Exposures in Forklift Operators: Comparison of a Mechanical and Air Suspension Seat," Ergonomics, **53**(11), pp. 1385–1394.

[56] Blood, R. P., Ploger, J. D., Yost, M. G., Ching, R. P., and Johnson, P. W., 2010, "Whole Body Vibration Exposures in Metropolitan Bus Drivers: A Comparison of Three Seats," J. Sound Vib., **329**(1), pp. 109–120.

[57] Blood, R. P., Yost, M. G., Camp, J. E., and Ching, R. P., 2015, "Whole-Body Vibration Exposure Intervention among Professional Bus and Truck Drivers: A Laboratory Evaluation of Seat-Suspension Designs," J. Occup. Environ. Hyg., **12**(6), pp. 351–362.

[58] Wang, F., Davies, H., Du, B., and Johnson, P. W., 2016, "Comparing the Whole Body Vibration Exposures across Three Truck Seats," *Proceedings of the Human Factors and Ergonomics Society Annual Meeting*, SAGE Publications Sage CA: Los Angeles, CA, pp. 933–936.

[59] Wu, X., and Griffin, M. J., 1997, "A Semi-Active Control Policy to Reduce the Occurrence and Severity of End-Stop Impacts in a Suspension Seat with an Electrorheological Fluid Damper," J. Sound Vib., **203**(5), pp. 781–793.

[60] Wu, X., and Griffin, M. J., 1998, "The Influence of End-Stop Buffer Characteristics on the Severity of Suspension Seat End-Stop Impacts," J. Sound Vib., **215**(4), pp. 989–996.

[61] Rebelle, J., 2004, "Methodology to Improve the Performance of the End-Stop Buffers of Suspension Seats," Veh. Syst. Dyn., **42**(4), pp. 211–233.

[62] Zhou, N., and Liu, K., 2010, "A Tunable High-Static–low-Dynamic Stiffness Vibration Isolator," J. Sound Vib., **329**(9), pp. 1254–1273.

[63] Carrella, A., Brennan, M. J., Waters, T. P., and Lopes, V., 2012, "Force and Displacement Transmissibility of a Nonlinear Isolator with High-Static-Low-Dynamic-Stiffness," Int. J. Mech. Sci., **55**(1), pp. 22–29.

[64] Carrella, A., Brennan, M. J., and Waters, T. P., 2007, "Static Analysis of a Passive Vibration Isolator with Quasi-Zero-Stiffness Characteristic," J. Sound Vib., **301**(3), pp. 678–689.

[65] Sun, X., Xu, J., Jing, X., and Cheng, L., 2014, "Beneficial Performance of a Quasi-Zero-Stiffness Vibration Isolator with Time-Delayed Active Control," Int. J. Mech. Sci., **82**, pp. 32–40.

[66] Le, T. D., and Ahn, K. K., 2011, "A Vibration Isolation System in Low Frequency Excitation Region Using Negative Stiffness Structure for Vehicle Seat," J. Sound Vib., **330**(26), pp. 6311–6335.

[67] Valeev, A., 2018, "Dynamics of a Group of Quasi-Zero Stiffness Vibration Isolators with Slightly Different Parameters," J. Low Freq. Noise Vib. Act. Control, p. 1461348418756022.

[68] Sergio M. Savaresi, 2010, *Semi-Active Suspension Control Design for Vehicles*, Elsevier Science, Burlington.

[69] Eamcharoenying, P., 2015, "Hybrid Numerical-Experimental Testing of Active and Semi-Active Suspensions," Ph.D., University of Bath.

[70] Jalili, N., 2002, "A Comparative Study and Analysis of Semi-Active Vibration-Control Systems," J. Vib. Acoust., **124**(4), pp. 593–605.

[71] Koch, G., 2011, "Adaptive Control of Mechatronic Vehicle Suspension Systems," PhD, Tech. Univ. M¨unchen, M ¨unchen.

[72] Braun, S. G., Ewins, D., Rao, S. S., and Leissa, A., 2002, "Encyclopedia of Vibration: Volumes 1, 2, and 3," Appl. Mech. Rev., **55**(3), p. B45.

[73] Jalili, N., 2002, "A Comparative Study and Analysis of Semi-Active Vibration-Control Systems," J. Vib. Acoust., **124**(4), pp. 593–605.

[74] Sarami, S., 2009, "Development and Evaluation of a Semi-Active Suspension System for Full Suspension Tractors," PhD, TU, Fachbereich Konstruktion von Maschinensystemen.

[75] Choi, S. B., Choi, J. H., Lee, Y. S., and Han, M. S., 2003, "Vibration Control of an ER Seat Suspension for a Commercial Vehicle," J. Dyn. Syst. Meas. Control, **125**(1), pp. 60–68.

[76] Tiemessen, I. J., Hulshof, C. T., and Frings-Dresen, M. H., 2007, "An Overview of Strategies to Reduce Whole-Body Vibration Exposure on Drivers: A Systematic Review," Int. J. Ind. Ergon., **37**(3), pp. 245–256.

[77] TEK SEATING, "Grammer Maximo Evolution Active Seat" [Online]. Available: http://tekseating.co.uk/agricultural-tractor-seats/grammer-maximo-evolution-active-seat. [Accessed: 15-Oct-2017].

[78] Bose Ride system, "Driver Suspension System for Heavy-Duty Trucking | Bose Ride®" [Online]. Available: http://www.boseride.com/seat-suspension-system. [Accessed: 15-Oct-2017].

[79] Gutierrez Soto, M., and Adeli, H., 2017, "Recent Advances in Control Algorithms for Smart Structures and Machines," Expert Syst., **34**(2).

[80] Simons, S. J., 2007, *Concepts of Chemical Engineering 4 Chemists*, Royal Society of Chemistry.

[81] Karnopp, D., Crosby, M. J., and Harwood, R. A., 1974, "Vibration Control Using Semi-Active Force Generators," J. Eng. Ind., **96**(2), pp. 619–626.

[82] Li, H., and Goodall, R. M., 1999, "Linear and Non-Linear Skyhook Damping Control Laws for Active Railway Suspensions," Control Eng. Pract., **7**(7), pp. 843–850.

[83] Priyandoko, G., Mailah, M., and Jamaluddin, H., 2009, "Vehicle Active Suspension System Using Skyhook Adaptive Neuro Active Force Control," Mech. Syst. Signal Process., **23**(3), pp. 855–868.

[84] Ahmadian, M., and Pare, C. A., 2000, "A Quarter-Car Experimental Analysis of Alternative Semiactive Control Methods," J. Intell. Mater. Syst. Struct., **11**(8), pp. 604–612.

[85] Choi, S.-B., Nam, M.-H., and Lee, B.-K., 2000, "Vibration Control of a MR Seat Damper for Commercial Vehicles," J. Intell. Mater. Syst. Struct., **11**(12), pp. 936–944.

[86] Lee, Y., and Jeon, D., 2002, "A Study on the Vibration Attenuation of a Driver Seat Using an MR Fluid Damper," J. Intell. Mater. Syst. Struct., **13**(7–8), pp. 437–441.

[87] Ahmadian, M., Song, X., and Southward, S. C., 2004, "No-Jerk Skyhook Control Methods for Semiactive Suspensions," J. Vib. Acoust., **126**(4), pp. 580–584.

[88] Liu, Y., 2004, "Semi-Active Damping Control for Vibration Isolation of Base Disturbances," University of Southampton.

[89] Alanoly, J., and Sankar, S., 1987, "A New Concept in Semi-Active Vibration Isolation," J. Mech. Transm. Autom. Des., **109**(2), pp. 242–247.

[90] Shen, Y., Golnaraghi, M. F., and Heppler, G. R., 2006, "Semi-Active Vibration Control Schemes for Suspension Systems Using Magnetorheological Dampers," J. Vib. Control, **12**(1), pp. 3–24.

[91] Savaresi, S. M., Silani, E., and Bittanti, S., 2005, "Acceleration-Driven-Damper (ADD): An Optimal Control Algorithm for Comfort-Oriented Semiactive Suspensions," J. Dyn. Syst. Meas. Control, **127**(2), pp. 218–229.

[92] BalaMurugan, L., and Jancirani, J., 2012, "An Investigation on Semi-Active Suspension Damper and Control Strategies for Vehicle Ride Comfort and Road Holding," Proc. Inst. Mech. Eng. Part J. Syst. Control Eng., p. 0959651812447520.

[93] Kirk, D. E., 2012, *Optimal Control Theory: An Introduction*, Courier Corporation.

[94] Fuller, C. C., Elliott, S., and Nelson, P. A., 1996, *Active Control of Vibration*, Academic Press.

[95] Hrovat, D., 1997, "Survey of Advanced Suspension Developments and Related Optimal Control Applications," Automatica, **33**(10), pp. 1781–1817.

[96] Hrovat, D., 1993, "Applications of Optimal Control to Advanced Automotive Suspension Design," Trans.-Am. Soc. Mech. Eng. J. Dyn. Syst. Meas. CONTROL, **115**, pp. 328–328.

[97] Kawana, M., and Shimogo, T., 1998, "Active Suspension of Truck Seat," Shock Vib., **5**(1), pp. 35–41.

[98] Wilson, D. A., Sharp, R. S., and Hassan, S. A., 1986, "The Application of Linear Optimal Control Theory to the Design of Active Automotive Suspensions," Veh. Syst. Dyn., **15**(2), pp. 105–118.

[99] Choi, S.-B., and Han, Y.-M., 2007, "Vibration Control of Electrorheological Seat Suspension with Human-Body Model Using Sliding Mode Control," J. Sound Vib., **303**(1), pp. 391–404.

[100] Ghasemalizadeh, O., Taheri, S., Singh, A., and Goryca, J., 2014, "Semi-Active Suspension Control Using Modern Methodology: Comprehensive Comparison Study," ArXiv Prepr. ArXiv14113305.

[101] Yao, H. J., Fu, J., Yu, M., and Peng, Y. X., 2013, "Semi-Active Control of Seat Suspension with MR Damper," *Journal of Physics: Conference Series*, IOP Publishing, p. 012054.

[102] Gu, Z., Zhao, Y., Gu, Z., Fei, S., and Tian, E., 2014, "Robust Control of Automotive Active Seat-Suspension System Subject to Actuator Saturation," J. Dyn. Syst. Meas. Control Trans. ASME, **136**(4).

[103] Lauwerys, C., Swevers, J., and Sas, P., 2005, "Robust Linear Control of an Active Suspension on a Quarter Car Test-Rig," Control Eng. Pract., **13**(5), pp. 577–586.

[104] Sezgin, A., Hacioglu, Y., and Yagiz, N., 2016, "Sliding Mode Control for Active Suspension System with Actuator Delay," World Acad. Sci. Eng. Technol. Int. J. Mech. Aerosp. Ind. Mechatron. Manuf. Eng., **10**(8), pp. 1356–1360.

[105] Van der Sande, T. P. J., Gysen, B. L. J., Besselink, I. J. M., Paulides, J. J. H., Lomonova, E. A., and Nijmeijer, H., 2013, "Robust Control of an Electromagnetic Active Suspension System: Simulations and Measurements," Mechatronics, **23**(2), pp. 204–212.

[106] Yagiz, N., Yuksek, I., and Sivrioglu, S., 2000, "Robust Control of Active Suspensions for a Full Vehicle Model Using Sliding Mode Control.," JSME Int. J. Ser. C Mech. Syst. Mach. Elem. Manuf., **43**(2), pp. 253–258.

[107] Méndez Cubillos, X. C., and de Souza, L. C. G., 2010, "Using of H-Infinity Control Method in Attitude Control System of Rigid-Flexible Satellite," Math. Probl. Eng., **2009**.

[108] Cao, J., Liu, H., Li, P., and Brown, D. J., 2008, "State of the Art in Vehicle Active Suspension Adaptive Control Systems Based on Intelligent Methodologies," IEEE Trans. Intell. Transp. Syst., **9**(3), pp. 392–405.

[109] Alkhatib, R., and Golnaraghi, M. F., 2003, "Active Structural Vibration Control: A Review," Shock Vib. Dig., **35**(5), p. 367.

[110] Landau, I. D., Lozano, R., M'Saad, M., and Karimi, A., 2011, "Introduction to Adaptive Control," *Adaptive Control*, Springer, pp. 1–33.

[111] \AAström, K. J., and Wittenmark, B., 2013, *Adaptive Control*, Courier Corporation.

[112] Smith, E. H., 2013, *Mechanical Engineer's Reference Book*, Butterworth-Heinemann.

[113] Maleki, N., Sedigh, A. K., and Labibi, B., 2006, "Robust Model Reference Adaptive Control of Active Suspension System," *Control and Automation, 2006. MED '06. 14th Mediterranean Conference On*, pp. 1–6.

[114] Sunwoo, M., Cheok, K. C., and Huang, N. J., 1991, "Model Reference Adaptive Control for Vehicle Active Suspension Systems," IEEE Trans. Ind. Electron., **38**(3), pp. 217–222.

[115] Yu, F., and Crolla, D. A., 1998, "An Optimal Self-Tuning Controller for an Active Suspension," Veh. Syst. Dyn., **29**(1), pp. 51–65.

[116] Cho, Y., Song, B. S., and Yi, K., 1999, "A Road-Adaptive Control Law for Semi-Active Suspensions," J. Mech. Sci. Technol., **13**(10), pp. 667–676.

[117] El Majdoub, K., Ghani, D., Giri, F., and Chaoui, F. Z., 2015, "Adaptive Semi-Active Suspension of Quarter-Vehicle with Magnetorheological Damper," J. Dyn. Syst. Meas. Control, **137**(2), p. 021010.

[118] Nguyen, L., Hong, K.-S., and Park, S., 2010, "Road-Frequency Adaptive Control for Semi-Active Suspension Systems," Int. J. Control Autom. Syst., **8**(5), pp. 1029–1038.

[119] Song, X., Ahmadian, M., Southward, S., and Miller, L. R., 2005, "An Adaptive Semiactive Control Algorithm for Magnetorheological Suspension Systems," J. Vib. Acoust., **127**(5), pp. 493–502.

[120] Yi, K., and Song, B. S., 1999, "A New Adaptive Sky-Hook Control of Vehicle Semi-Active Suspensions," Proc. Inst. Mech. Eng. Part J. Automob. Eng., **213**(3), pp. 293–303.

[121] Gan, Z., 2015, "Adaptive Control of an Active Seat for Occupant Vibration Reduction."

[122] Wu, J.-D., and Chen, R.-J., 2004, "Application of an Active Controller for Reducing Small-Amplitude Vertical Vibration in a Vehicle Seat," J. Sound Vib., **274**(3), pp. 939–951.

[123] Levine, W. S., 1996, *The Control Handbook*, CRC press.

[124] Lagaros, N. D., 2012, *Design Optimization of Active and Passive Structural Control Systems*, IGI Global.

[125] Avdagic, Z., Besic, I., Buza, E., and Omanovic, S., 2013, "Comparation of Controllers Based on Fuzzy Logic and Artificial Neural Networks for Reducing Vibration of the Driver's Seat," *Industrial Electronics Society, IECON 2013-39th Annual Conference of the IEEE*, IEEE, pp. 3382–3387.

[126] Nguyen, S. D., Nguyen, Q. H., and Choi, S.-B., 2015, "A Hybrid Clustering Based Fuzzy Structure for Vibration Control–Part 2: An Application to Semi-Active Vehicle Seat-Suspension System," Mech. Syst. Signal Process., **56**, pp. 288–301.

[127] Sathishkumar, P., Jancirani, J., and John, D., 2014, "Reducing the Seat Vibration of Vehicle by Semi Active Force Control Technique," J. Mech. Sci. Technol., **28**(2), pp. 473–479.

[128] Godjevac, J., 1995, "Comparative Study of Fuzzy Control, Neural Network Control and Neuro-Fuzzy Control," *Fuzzy Set Theory and Advanced Mathematical Applications*, Springer, pp. 291–322.

[129] Al-Holou, N., Lahdhiri, T., Joo, D. S., Weaver, J., and Al-Abbas, F., 2002, "Sliding Mode Neural Network Inference Fuzzy Logic Control for Active Suspension Systems," IEEE Trans. Fuzzy Syst., **10**(2), pp. 234–246.

[130] Demir, O., Keskin, I., and Cetin, S., 2012, "Modeling and Control of a Nonlinear Half-Vehicle Suspension System: A Hybrid Fuzzy Logic Approach," Nonlinear Dyn., **67**(3), pp. 2139–2151.

[131] Du, H., Lam, J., and Sze, K. Y., 2003, "Non-Fragile Output Feedback H∞ Vehicle Suspension Control Using Genetic Algorithm," Eng. Appl. Artif. Intell., **16**(7), pp. 667–680.

[132] Eski, I., and Yıldırım, Ş., 2009, "Vibration Control of Vehicle Active Suspension System Using a New Robust Neural Network Control System," Simul. Model. Pract. Theory, **17**(5), pp. 778–793.

[133] Kuo, Y.-P., and Li, T. S. S., 1999, "GA-Based Fuzzy PI/PD Controller for Automotive Active Suspension System," IEEE Trans. Ind. Electron., **46**(6), pp. 1051–1056.

[134] Li, H., Yu, J., Hilton, C., and Liu, H., 2013, "Adaptive Sliding-Mode Control for Nonlinear Active Suspension Vehicle Systems Using T–S Fuzzy Approach," IEEE Trans. Ind. Electron., **60**(8), pp. 3328–3338.

[135] Li, H., Liu, H., Gao, H., and Shi, P., 2012, "Reliable Fuzzy Control for Active Suspension Systems with Actuator Delay and Fault," IEEE Trans. Fuzzy Syst., **20**(2), pp. 342–357.

[136] Priyandoko, G., Mailah, M., and Jamaluddin, H., 2009, "Vehicle Active Suspension System Using Skyhook Adaptive Neuro Active Force Control," Mech. Syst. Signal Process., **23**(3), pp. 855–868.

[137] Ahmad Akbari Alvanagh, 2008, "Multi-Objective H∞/GH2 Preview Control of Active Vehicle Suspensions," PhD, TECHNISCHE UNIVERSITAT M ¨ UNCHEN ¨ Lehrstuhl f ¨ur Regelungstechnik.

[138] Arunachalam, K., Jawahar, P. M., and Tamilporai, P., 2003, *Active Suspension System with Preview Control-A Review*, SAE Technical Paper.

[139] Sarami, S., 2009, "Development and Evaluation of a Semi-Active Suspension System for Full Suspension Tractors," TU, Fachbereich Konstruktion von Maschinensystemen.

[140] Bender, E. K., 1968, "Optimum Linear Preview Control with Application to Vehicle Suspension," J. Basic Eng., **90**(2), pp. 213–221.

[141] Thompson, A. G., Davis, B. R., and Pearce, C. E. M., 1980, "An Optimal Linear Active Suspension with Finite Road Preview."

[142] HAĆ, A., 1992, "Optimal Linear Preview Control of Active Vehicle Suspension," Veh. Syst. Dyn., **21**(1), pp. 167–195.

[143] Soliman, A. M. A., and Crolla, D. A., 1996, "Preview Control for a Semi–active Suspension System," Int. J. Veh. Des., **17**(4), pp. 384–397.

[144] Kim, H.-J., Yang, H. S., and Park, Y.-P., 2002, "Improving the Vehicle Performance with Active Suspension Using Road-Sensing Algorithm," Comput. Struct., **80**(18), pp. 1569–1577.

[145] El Madany, M., Abduljabbar, Z., and Foda, M., 2003, "Optimal Preview Control of Active Suspensions with Integral Constraint," Modal Anal., **9**(12), pp. 1377–1400.

[146] Langlois, R. G., Hanna, D. M., and Anderson, R. J., 1992, "Implementing Preview Control on an Off-Road Vehicle with Active Suspension," Veh. Syst. Dyn., **20**(sup1), pp. 340–353.

[147] Nagiri, S., Doi, S. 'ichi, Shoh-no, S., and Hiraiwa, N., 1992, *Improvement of Ride Comfort by Preview Vehicle-Suspension System*, SAE Technical Paper.

[148] Akbari, A., Koch, G., Pellegrini, E., Spirk, S., and Lohmann, B., 2010, "Multi-Objective Preview Control of Active Vehicle Suspensions: Experimental Results," IEEE, pp. 497–502.

[149] Li, P., Lam, J., and Cheung, K. C., 2014, "Multi-Objective Control for Active Vehicle Suspension with Wheelbase Preview," J. Sound Vib., **333**(21), pp. 5269–5282.

[150] Louam, N., Wilson, D. A., and Sharp, R. S., 1988, "Optimal Control of a Vehicle Suspension Incorporating the Time Delay between Front and Rear Wheel Inputs," Veh. Syst. Dyn., **17**(6), pp. 317–336.

[151] Pilbeam, C., and Sharp, R. S., 1993, "On the Preview Control of Limited Bandwidth Vehicle Suspensions," Proc. Inst. Mech. Eng. Part J. Automob. Eng., **207**(3), pp. 185–193.

[152] Roh, H.-S., and Park, Y., 1998, "Observer-Based Wheelbase Preview Control of Active Vehicle Suspensions," J. Mech. Sci. Technol., **12**(5), pp. 782–791.

[153] Kitching, K. J., Cebon, D., and Cole, D. J., 1999, "An Experimental Investigation of Preview Control," Veh. Syst. Dyn., **32**(6), pp. 459–478.

[154] ElMadany, M. M., Al Bassam, B. A., and Fayed, A. A., 2011, "Preview Control of Slow-Active Suspension Systems," J. Vib. Control, **17**(2), pp. 245–258.

[155] ElMadany, M. M., 2012, "Control and Evaluation of Slow-Active Suspensions with Preview for a Full Car," Math. Probl. Eng., **2012**.

[156] Sharp, R. S., and Peng, H., 2011, "Vehicle Dynamics Applications of Optimal Control Theory," Veh. Syst. Dyn., **49**(7), pp. 1073–1111.

[157] Bergh, F. van den, 2006, "An Analysis of Particle Swarm Optimizers Thesis," Ph.D., University of Pretoria etd.

[158] Elbeltagi, E., Hegazy, T., and Grierson, D., 2005, "Comparison among Five Evolutionary-Based Optimization Algorithms," Adv. Eng. Inform., **19**(1), pp. 43–53.

[159] Holland, J. H., 1975, *Adaptation in Natural and Artificial Systems*, Ann Arbor, MI: University of Michigan Press.

[160] J. Zhang, M. Yi, C. Xu, and Z. Jiang, 2009, "Prediction of the Mechanical Properties of Ceramic Die Material with Artificial Neural Network and Genetic Algorithm," *2009 IEEE International Conference on Intelligent Computing and Intelligent Systems*, pp. 603–607.

[161] J. C. Cassa, G. Floridia, A. R. Souza, and R. T. Oliveira, 1999, "Prediction of Cement Paste Mechanical Behaviour from Chemical Composition Using Genetic Algorithms and Artificial Neural Networks," *Intelligent Processing and Manufacturing of Materials, 1999. IPMM '99. Proceedings of the Second International Conference On*, pp. 291–298 vol.1.

[162] S. Wang, and X. Dong, 2009, "Predicting China's Energy Consumption Using Artificial Neural Networks and Genetic Algorithms," *2009 International Conference on Business Intelligence and Financial Engineering*, pp. 8–11.

[163] Hassan, R., Cohanim, B., De Weck, O., and Venter, G., 2005, "A Comparison of Particle Swarm Optimization and the Genetic Algorithm," *46th AIAA/ASME/ASCE/AHS/ASC Structures, Structural Dynamics and Materials Conference*, p. 1897.

[164] Gündoğdu, Ö., 2007, "Optimal Seat and Suspension Design for a Quarter Car with Driver Model Using Genetic Algorithms," Int. J. Ind. Ergon., **37**(4), pp. 327–332.

[165] Baumal, A. E., McPhee, J. J., and Calamai, P. H., 1998, "Application of Genetic Algorithms to the Design Optimization of an Active Vehicle Suspension System," Comput. Methods Appl. Mech. Eng., **163**(1), pp. 87–94.

[166] Elbeltagi, E., Hegazy, T., and Grierson, D., 2005, "Comparison among Five Evolutionary-Based Optimization Algorithms," Adv. Eng. Inform., **19**(1), pp. 43–53.

[167] Gad, S., Metered, H., Bassuiny, A., and Ghany, A. A., 2015, "Multi-Objective Genetic Algorithm Fractional-Order PID Controller for Semi-Active Magnetorheologically Damped Seat Suspension," J. Vib. Control, pp. 1248–1266.

[168] Zalzala, A. M., and Fleming, P. J., 1997, *Genetic Algorithms in Engineering Systems*, Iet.

[169] Gen, M., and Cheng, R., 2000, *Genetic Algorithms and Engineering Optimization*, John Wiley & Sons.

[170] J. Kennedy, and R.C. Eberhart, 1995, "Particle Swarm Optimization," *Proceedings IEEE International Conference on Neural Networks, IV (1995)*, pp. 1942–1948.

[171] Shi, Y., and others, 2001, "Particle Swarm Optimization: Developments, Applications and Resources," *Evolutionary Computation, 2001. Proceedings of the 2001 Congress On*, IEEE, pp. 81–86.

[172] Chiou, J.-S., Tsai, S.-H., and Liu, M.-T., 2012, "A PSO-Based Adaptive Fuzzy PID-Controllers," Simul. Model. Pract. Theory, **26**, pp. 49–59.

[173] Lazinica, A., 2009, *Particle Swarm Optimization*, InTech Kirchengasse.

[174] Shi, Y., and Eberhart, R., 1998, "A Modified Particle Swarm Optimizer," *Evolutionary Computation Proceedings, 1998. IEEE World Congress on Computational Intelligence., The 1998 IEEE International Conference On*, IEEE, pp. 69–73.

[175] Kennedy, J., 2011, "Particle Swarm Optimization," *Encyclopedia of Machine Learning*, Springer, pp. 760–766.

[176] Bingül, Z., and Karahan, O., 2011, "A Fuzzy Logic Controller Tuned with PSO for 2 DOF Robot Trajectory Control," Expert Syst. Appl., **38**(1), pp. 1017–1031.

[177] Sun, W., Li, J., Zhao, Y., and Gao, H., 2011, "Vibration Control for Active Seat Suspension Systems via Dynamic Output Feedback with Limited Frequency Characteristic," Mechatronics, **21**(1), pp. 250–260.

[178] Crosby, M. J., and Karnopp, D. C., 1973, "The Active Damper-a New Concept for Shock and Vibration Control," Shock Vib. Bull., **43**(4), pp. 119–133.

[179] Thong, Y. K., Woolfson, M. S., Crowe, J. A., Hayes-Gill, B. R., and Jones, D. A., 2004, "Numerical Double Integration of Acceleration Measurements in Noise," Measurement, **36**(1), pp. 73–92.

[180] Savaresi, S. M., Poussot-Vassal, C., Spelta, C., Sename, O., and Dugard, L., 2010, *Semi-Active Suspension Control Design for Vehicles*, Elsevier.

[181] Montazeri-Gh, M., and Soleymani, M., 2008, "Genetic Optimization of a Fuzzy Active Suspension System Based on Human Sensitivity to the Transmitted Vibrations," Proc. Inst. Mech. Eng. Part J. Automob. Eng., **222**(10), pp. 1769–1780.

[182] Crespo, J. A., 2009, "Measurements of Vibrations in Wooden Floors Induced by Walking," Eng. Acoust. LTH Swed. 2009, pp. 1–48.

[183] ACGIH, "American Conference of Governmental Industrial Hygienists (2005). Whole-Body Vibration. In: Threshold Limit Values, TLVs and Biological Exposure Indices for 2005," Cincinnati, Ohio., pp. 126–133.

[184] Paschold, H. W., 2008, "Whole-Body Vibration," Prof. Saf., **53**(6), p. 52.

[185] Finucane, E., 2010, *Definitions, Conversions, and Calculations for Occupational Safety and Health Professionals*, CRC Press.

[186] Wang, Y. H., and Shih, M. C., 2011, "Design of a Genetic-Algorithm-Based Self-Tuning Sliding Fuzzy Controller for an Active Suspension System," Proc. Inst. Mech. Eng. Part J. Syst. Control Eng., **225**(3), pp. 367–383.

[187] GERGER, O., 2013, "DESIGN, CONTROL AND OPTIMIZATION OF VEHICLE SUSPENSIONS WITH INERTERS," MIDDLE EAST TECHNICAL UNIVERSITY.

[188] Tyan, F., Hong, Y.-F., Tu, S.-H., and Jeng, W. S., 2009, "Generation of Random Road Profiles," J. Adv. Eng., **4**(2), pp. 1373–1378.

[189] Li, H., 2012, "Robust Control Design for Vehicle Active Suspension Systems with Uncertainty," PhD, University of Portsmouth.

[190] D'Amato, F. J., and Viassolo, D. E., 2000, "Fuzzy Control for Active Suspensions," Mechatronics, **10**(8), pp. 897–920.

[191] Du, H., Li, W., and Zhang, N., 2012, "Integrated Seat and Suspension Control for a Quarter Car with Driver Model," IEEE Trans. Veh. Technol., **61**(9), pp. 3893–3908.

[192] Dong, X., Yu, M., Liao, C., and Chen, W., 2010, "Comparative Research on Semi-Active Control Strategies for Magneto-Rheological Suspension," Nonlinear Dyn., **59**(3), pp. 433–453.

[193] Gizatullin, A. O., and Edge, K. A., 2007, "Adaptive Control for a Multi-Axis Hydraulic Test Rig," Proc. Inst. Mech. Eng. Part J. Syst. Control Eng., **221**(2), pp. 183–198.

[194] "PTMC," Cent. Power Transm. Motion Control [Online]. Available: https://www.google.co.uk/?gws_rd=ssl#q=multi-axis+simulation+table+the+center+for+power+transmission+bath+. [Accessed: 11-Jul-2017].

[195] HepcoMotion, "GV3 - Configurator - HepcoMotion" [Online]. Available: https://b2b.partcommunity.com/3d-cad-models/gv3-configurator-hepcomotion/?info=hepcomotion%2F07_gv3%2F07_01_gv3_configurator_asmtab.prj. [Accessed: 14-May-2017].

[196] Hanselmann, H., 1993, *Hardware-in-the Loop Simulation as a Standard Approach for Development, Customization, and Production Test of ECU's*, SAE Technical Paper.

[197] Jorge de-J, L.-S., Morales-Menendez, R., and Ramirez-Mendoza, R. A., 2015, "Evaluation of On–off Semi-Active Vehicle Suspension Systems by Using the Hardware-in-the-Loop Approach and the Software-in-the-Loop Approach," Proc. Inst. Mech. Eng. Part J. Automob. Eng., **229**(1), pp. 52–69.

[198] Hać, A., 1985, "Suspension Optimization of a 2-DOF Vehicle Model Using a Stochastic Optimal Control Technique," J. Sound Vib., **100**(3), pp. 343–357.

[199] Baumal, A. E., McPhee, J. J., and Calamai, P. H., 1998, "Application of Genetic Algorithms to the Design Optimization of an Active Vehicle Suspension System," Comput. Methods Appl. Mech. Eng., **163**(1), pp. 87–94.

[200] Maciejewski, I., Meyer, L., and Krzyzynski, T., 2009, "Modelling and Multi-Criteria Optimisation of Passive Seat Suspension Vibro-Isolating Properties," J. Sound Vib., **324**(3), pp. 520–538.

[201] Shirahatti, A., Prasad, P. S. S., Panzade, P., and Kulkarni, M. M., 2008, "Optimal Design of Passenger Car Suspension for Ride and Road Holding," J. Braz. Soc. Mech. Sci. Eng., **30**(1), pp. 66–76.

[202] Kevin M. Passino, 1998, *Fuzzy Control*, Addison-Wesley, Menlo Park, Calif. ; Harlow.

[203] Zadeh, L. A., 1965, "Fuzzy Sets," Inf. Control, **8**(3), pp. 338–353.

[204] Chiou, Y.-C., and Lan, L. W., 2005, "Genetic Fuzzy Logic Controller: An Iterative Evolution Algorithm with New Encoding Method," Fuzzy Sets Syst., **152**(3), pp. 617–635.

[205] Guclu, R., 2005, "Fuzzy Logic Control of Seat Vibrations of a Non-Linear Full Vehicle Model," Nonlinear Dyn., **40**(1), pp. 21–34.

[206] Sharkawy, A. B., 2005, "Fuzzy and Adaptive Fuzzy Control for the Automobiles' Active Suspension System," Veh. Syst. Dyn., **43**(11), pp. 795–806.

[207] Rao, M. V. C., and Prahlad, V., 1997, "A Tunable Fuzzy Logic Controller for Vehicle-Active Suspension Systems," Fuzzy Sets Syst., **85**(1), pp. 11–21.

[208] MOON, S. Y., and KWON, W. H., 1998, "Genetic-Based Fuzzy Control for Half-Car Active Suspension Systems," Int. J. Syst. Sci., **29**(7), pp. 699–710.

[209] Hurel, J., Mandow, A., and García-Cerezo, A., 2012, "Tuning a Fuzzy Controller by Particle Swarm Optimization for an Active Suspension System," *IECON 2012-38th Annual Conference on IEEE Industrial Electronics Society*, IEEE, pp. 2524–2529.

[210] Taskin, Y., Hacioglu, Y., and Yagiz, N., 2007, "The Use of Fuzzy-Logic Control to Improve the Ride Comfort of Vehicles," Strojniski Vestn., **53**(4), pp. 233–240.

[211] Taskin, Y., Hacioglu, Y., and Yagiz, N., 2016, "Experimental Evaluation of a Fuzzy Logic Controller on a Quarter Car Test Rig," J. Braz. Soc. Mech. Sci. Eng., pp. 1–13.

[212] Kaldas, M. M. S., Çalışkan, K., Henze, R., and Küçükay, F., 2013, "Rule Optimized Fuzzy Logic Controller for Full Vehicle Semi-Active Suspension," SAE Int. J. Passeng. Cars - Mech. Syst., **6**(1), pp. 332–344.

[213] Kaldas, M., Caliskan, K., Henze, R., and Küçükay, F., 2014, "Preview Enhanced Rule-Optimized Fuzzy Logic Damper Controller," SAE Int. J. Passeng. Cars - Mech. Syst., **7**(2), pp. 804–815.

[214] Lin, J., and Lian, R.-J., 2011, "Intelligent Control of Active Suspension Systems," IEEE Trans. Ind. Electron., **58**(2), pp. 618–628.

[215] Pishkenari, H. N., Mahboobi, S. H., and Alasty, A., 2011, "Optimum Synthesis of Fuzzy Logic Controller for Trajectory Tracking by Differential Evolution," Sci. Iran., **18**(2), pp. 261–267.

[216] Chiou, J.-S., and Liu, M.-T., 2009, "Using Fuzzy Logic Controller and Evolutionary Genetic Algorithm for Automotive Active Suspension System," Int. J. Automot. Technol., **10**(6), p. 703.

[217] Hashiyama, T., Furuhashi, T., and Uchikawa, Y., 1995, "A Study on Finding Fuzzy Rules for Semi-Active Suspension Controllers with Genetic Algorithm," *Evolutionary Computation, 1995., IEEE International Conference On*, IEEE, p. 279.

[218] Cao, J., Li, P., Liu, H., and Brown, D., 2008, "Adaptive Fuzzy Controller for Vehicle Active Suspensions with Particle Swarm Optimization," *Seventh International Symposium on Instrumentation and Control Technology*, International Society for Optics and Photonics, pp. 712922–712922.

[219] Rajeswari, K., and Lakshmi, P., 2010, "PSO Optimized Fuzzy Logic Controller for Active Suspension System," *Advances in Recent Technologies in Communication and Computing (ARTCom), 2010 International Conference On*, IEEE, pp. 278–283.

[220] Pekgökgöz, R. K., Gürel, M. A., Bilgehan, M., and Kısa, M., 2010, "Active Suspension of Cars Using Fuzzy Logic Controller Optimized by Genetic Algorithm," Int. J. Eng. Appl. Sci., **2**(4), pp. 27–37.

[221] Kim, H.-S., and Roschke, P. N., 2006, "Design of Fuzzy Logic Controller for Smart Base Isolation System Using Genetic Algorithm," Eng. Struct., **28**(1), pp. 84–96.

[222] Zhao, J., and Bose, B. K., 2002, "Evaluation of Membership Functions for Fuzzy Logic Controlled Induction Motor Drive," *IECON 02 [Industrial Electronics Society, IEEE 2002 28th Annual Conference of The]*, IEEE, pp. 229–234.

[223] Kaur, A., and Kaur, A., 2012, "Comparison of Fuzzy Logic and Neuro-Fuzzy Algorithms for Air Conditioning System," Int. J. Soft Comput. Eng., **2**(1), pp. 417–20.

[224] Pham, D. T., and Castellani, M., 2002, "Action Aggregation and Defuzzification in Mamdani-Type Fuzzy Systems," Proc. Inst. Mech. Eng. Part C J. Mech. Eng. Sci., **216**(7), pp. 747–759.

[225] Maciejewski, I., Meyer, L., and Krzyzynski, T., 2010, "The Vibration Damping Effectiveness of an Active Seat Suspension System and Its Robustness to Varying Mass Loading," J. Sound Vib., **329**(19), pp. 3898–3914.

[226] Bouazara, M., Richard, M. J., and Rakheja, S., 2006, "Safety and Comfort Analysis of a 3-D Vehicle Model with Optimal Non-Linear Active Seat Suspension," J. Terramechanics, **43**(2), pp. 97–118.

[227] Hongbin, R., Sizhong, C., and Zhicheng, W., 2011, "Model of Excitation of Random Road Profile in Time Domain for a Vehicle with Four Wheels," *Mechatronic Science, Electric Engineering and Computer (MEC), 2011 International Conference On*, IEEE, pp. 2332–2335.